Structure and Dynamics of Water in Bulk and at Molecular and Nanoscopic Interfaces: A Molecular Dynamics Simulation Study

By

Dibyendu Bandyopadhyay

(CHEM01201004007)

BHABHA ATOMIC RESEARCH CENTRE, MUMBAI

A thesis submitted to the
Board of Studies in Chemical Sciences
In partial fulfillment of requirements
for the Degree of
DOCTOR OF PHILOSOPHY
of
HOMI BHABHA NATIONAL INSTITUTE

December 2015

Homi Bhabha National Institute

Recommendations of the Viva Voce Committee

As members of the Viva Voce Committee, we certify that we have read the dissertation prepared by Shri Dibyendu Bandyopadhyay entitled "**Structure and Dynamics of Water in Bulk and at Molecular and Nanoscopic Interfaces: A Molecular Dynamics Simulation Study**" and recommend that it may be accepted as fulfilling the thesis requirement for the award of Degree of Doctor of Philosophy.

Chairman - Dr. A. K. Arya	**Date:** 28/10/16
Guide / Convener - Dr. N. Choudhury Niharendu Choudhury	**Date:** 28/10/2016
Co-guide/Member - Dr. Swapan K. Ghosh Swapankumar Ghosh	**Date:** 28-10-2016
Examiner - Prof. B. L. Tembe	**Date:** 28/10/16
Member 1- Dr. C. N. Patra	**Date:** 28-10-16
Member 2- Dr. P. A. Hassan	**Date:** 28/10/2016
Member 3- Dr. A. K. Samanta	**Date:** 28/10/2016

Final approval and acceptance of this thesis is contingent upon the candidate's submission of the final copies of the thesis to HBNI.

We hereby certify that we have read this thesis prepared under our direction and recommend that it may be accepted as fulfilling the thesis requirement.

Date: 28-10-2016
Place: Mumbai

Swapankumar Ghosh
Co-guide

Niharendu Choudhury
Guide

STATEMENT BY AUTHOR

This dissertation has been submitted in partial fulfillment of requirements for an advanced degree at Homi Bhabha National Institute (HBNI) and is deposited in the Library to be made available to borrowers under rules of the HBNI.

Brief quotations from this dissertation are allowable without special permission, provided that accurate acknowledgement of source is made. Requests for permission for extended quotation from or reproduction of this manuscript in whole or in part may be granted by the Competent Authority of HBNI when in his or her judgment the proposed use of the material is in the interests of scholarship. In all other instances, however, permission must be obtained from the author.

Dibyendu Bandyopadhyay

Dibyendu Bandyopadhyay

DECLARATION

I, hereby declare that the investigation presented in the thesis has been carried out by me. The work is original and has not been submitted earlier as a whole or in part for a degree / diploma at this or any other Institution / University.

Dibyendu Bandyopadhyay

Dibyendu Bandyopadhyay

List of Publications arising from the thesis

Journals

(1) Properties of Heavy Water in the Temperature Range T = 223 K to 373 K from Molecular Dynamics Simulation Using the Simple Point Charge/Heavy Water (SPC/HW) Model.

Bandyopadhyay, D.; Mohan, S.; Ghosh, S. K.; Choudhury, N. *J. Chem. Eng. Data*, **2012**, *57*, 1751−1758.

(2) Characterizing hydrophobicity at the nanoscale: A molecular dynamics simulation study.

Bandyopadhyay, D.; Choudhury, N. *J. Chem. Phys.,* **2012**, *136*, 224505.

(3) Comparison of Orders, Structures and Anomalies of water: A Molecular Dynamics Simulation study.

Bandyopadhyay, D.; Mohan, S.; Ghosh, S. K.; Choudhury, N. *AIP Conf. Proc***.** doi. 10.1063/1.4791175, 2013, 1512. 590-591.

(4) Correlation of Structural Order, Anomalous Density and Hydrogen Bonding Network of Liquid Water.

Bandyopadhyay, D.; Mohan, S.; Ghosh, S. K.; Choudhury, N. *J. Phys. Chem. B* **2013**, *117*, 8831−8843.

(5) Molecular Dynamics Simulation of Aqueous Urea Solution: Is Urea a Structure Breaker? **Bandyopadhyay, D**.; Mohan, S.; Ghosh, S. K.; Choudhury, N. *J. Phys. Chem. B*, **2014**, *118*, 11757−11768.

(6) Effects of Concentration on Like-Charge Pairing of Guanidinium Ions and on the Structure of Water: An All-Atom Molecular Dynamics Simulation Study. **Bandyopadhyay, D**.; Mohan, S.; Bhanja, K.; Ghosh S. K.; Choudhury, N. *J. Phys. Chem. B,* **2015**, 119, 11262–11274.

(7) Effects of solute-water dispersion interaction on the solvation and dewetting of a fullerene in coarse-grained Water: A Molecular Dynamics Simulation Study. **Bandyopadhyay, D**.; Pantawane, S.; Choudhury, N. (To be communicated)

Dibyendu Bandyopadhyay

Dibyendu Bandyopadhyay

DEDICATED
TO
MA & BABA

Acknowledgement

Standing near the shore after a long six years voyage, I commence to contemplate about my PhD expedition in theoretical computational chemistry. In the very beginning, I would like to thank Almighty for the kindness by fulfilling me in such an extent in every aspects of my life by simply overlooking the fact that I don't worthy for all these. Herby, I gracefully accept that I am a person with limited capabilities both as a student and a person. Thus, I owe to everyone who directly or indirectly helped me during this journey. Expression of the gratitude by words about my own feeling is not possible because I am highly indebted and no word is simply sufficient to articulate my emotion towards each and every one of them.

First and foremost, I would like to thank my PhD guides Dr. N. Choudhury and Dr. S. K. Ghosh without whom it would never ever be possible for me to even begin this work. I express my sincere gratitude to them for offering me the opportunity to work in their research group. I am deeply indebted to them for their inspiration, never ending guidance, infinite patience, unconditional help and extraordinary trust on me in difficult phases of my life.

I am also thankful to Dr. Sadhana Mohan (Head, Heavy Water Division) and Mr. Kalyan Bhanja for their guidance and enthusiastic support during my PhD. I am deeply grateful to Dr. Sushama Mishra, S. K. Das, S. K. Bhattacharya, S. Narwaria, G. K. Nath, S. Nayak, Dr. R. Kumar, V. P. Haridas, E. Mohonon, S. Phadol for their continued inspiration during this journey. I express my deep gratitude towards Mr. S. K. Ghosh (former Director, Chemical Engineering Group, BARC) and Dr. (Smt.) S. B. Roy (Associate Director, Chemical Engineering Group, BARC) for all their important supports. I would specially thank Ashok, Rupsha, Sulabh, Venky, Sachin, Krunal, saikat and Golatkar for giving me help, inspiration and encourage all the time. I would like to thank Gaikwad and Sandip for their unconditional help in any problem I have ever encountered after joining BARC. I would like to thank all the members of Theoretical Chemistry Section, Chemistry Group, for their constant help and encouragement and sharing their vast knowledge with me. It is a great pleasure to thank all the members of the doctoral committee Dr. T. Mukherjee (ex-chairman), Dr. A. Arya (chairman), Dr.

A. K. Samanta (member), Dr. C. N. Patra (member), Dr. P. A. Hasan (member), and Dr. B. S. Tomar (Dean-academic, Chemical Sciences) for their guidance and help throughout this journey. There is no word to thank Raghuda & Sukanata for all their help. I would also like to thank Prabhatda, Mondalda, Chattaraj, Sabyada, Arkada, Ashis, Mamu, Sourav, Sanat, Sadhu, Samui, Amruta and Sanwardhini for their help and constant encouragement.

I would like to express my deepest gratitude to my ma (Mrs. Alaka Bandyopadhyay) and my baba (Mr. N. D. Bandyopadhyay) for giving me unconditional support, endless sacrifice, relentless motivation and boundless love. There is no word in the dictionary which can express my parent's devotion in the making of us. I can only say that whatever I am today, is just because of them. Thank you God for blessing me with such wonderful parents.

I would like to extend my gratitude and affection towards my family members (Bappa, Monu, boudi, Rita and full-kaka). I would like to express my deep gratitude to my in laws (Lt Utpal K. Sur & Mrs. Kalyani Sur). Last but not the least I would like to thank my wife (Payel) for all her efforts and sacrifice. Our family life completes a mini-cycle with the arrival of my son (Gobindo) and my two nephews (Gopal, Gourango) whom we adore so much!

There are many others, who have provided support and inspiration in this wonderful reward journey. I should be excused since I cannot list them all here but I am grateful to all of them.

The very fact that I am getting the opportunity to write this acknowledgement as a part of PhD thesis is due to my teacher and my mentor Dr N. Choudhury, who appeared in my life as a ray of light in a room full of darkness and changed my perception not only in the field of science but also in day to day real life. There are no words to put my emotion towards him, I can only say thank you for appearing as guide, philosopher and friend.

Dibyendu Bandyopadhyay

CONTENTS

Page No

SYNOPSIS i

LIST OF FIGURES xii

LIST OF TABLES xx

Chapter 1 Introduction and Computational Methodology 1

1.1 Introduction 2

1.2 Classical Molecular Dynamics 5

1.3 Statistical Mechanical Ensembles & Averages 11

  1.3.1. Time Averaging (Method of Boltzmann) 12

  1.3.2. Ensemble Average 13

  1.3.3. Micro-Canonical Ensemble 14

  1.3.4. Canonical (NVT) Ensemble 14

  1.3.5. Isothermal–Isobaric (*NPT*) Ensemble 16

  1.3.6. Grant Canonical (μ VT) Ensemble 17

1.4 Equilibrium particle Densities and Distribution functions 18

1.5 Time Correlation Functions and Transport Coefficients 23

1.6 Nature and Scope of the Present Work 24

Chapter 2 Structural and Dynamical Correlations in Water and its Density Anomaly 31

2.1 Introduction 32

2.2 Models and methods 37

2.3 Results and Discussion 42

2.3.1 Correlation of Structural Orders, Density anomaly and Hydrogen Bonding Network of Water 42

2.3.2 Correlation of Hydrogen Bonding Network and Dynamics of Water 70

2.4 Summary and Conclusions 76

Chapter 3 Structure, Thermophysical Properties and Dynamics: A Comparative Study of Water and Heavy Water 81

3.1 Introduction 82

3.2 Models and Methods 84

3.3 Results and Discussion 85

3.3.1 Structure and Thermophysical Properties 85

3.3.2 Dynamics 102

3.3.3 Effect of Potential Parameters on the Results 106

3.3.4 Summary and Conclusions 110

Chapter 4 Water at Molecular Lengthscale Interfaces 113

Chapter- 4A Structure and Dynamics of Aqueous Urea Solution: Is Urea a Structure Breaker? 116

4.A.1 Introduction 117

4.A.2 Models and methods 123

4.A.3 Results and Discussion 127

4.A.3.1 Structure 127

4.A.3.2 Dynamics 145

4.A.4 Summary and Conclusions 148

Chapter- 4B Effect of Concentration on Like-Charge Pairing of Guanidinium Ions, Proteins and on the Structure and Dynamics of Water 151

4.B.1 Introduction 152

4.B.2 Models and methods 156

4.B.3 Results and Discussion 161

4.B.3.1 Structure 161

4.B.3.1.a. Ion-pair Formation and its Concentration Dependence 161

4.B.3.1.b. Effect of GdmCl Concentration on Water Structure 171

4.B.3.1.c. An Arginine-rich Peptidein the Aqueous Solution of Gdmcl 186

4.B.3.2 Effect of Gdmcl Concentration on Translational Dynamics of Water 190

4.B.4 Summary and Conclusions 191

Chapter 5 Characterizing Hydrophobicity at the Nanoscale 195

5.1 Introduction 196

5.2 Models and methods 200

5.3 Results and Discussion 203

5.3.1. Hydration characteristics of single plate 203

5.3.2. Interplate dewetting 221

5.4 Summary and Conclusions 224

Chapter 6 **Effect of Temperature, Solvent Density and Hydrophobicity on the Solvation of Fullerene: A Coarse-Grained Description** 226

6.1 Introduction 227

6.2 Models and methods 229

6.3 Results and Discussion 232

6.4 Summary and Conclusions 241

Chapter 7 **Summary and Future Directions** 243

References 251

SYNOPSIS

Most of the chemical and biological processes occurring both in natural systems and in systems engineered by human beings involve many-body systems at finite temperature. The studies of these systems have direct relevance in various fields of science and technology, e.g. chemistry, physics, biology, chemical engineering, oceanology, environmental studies etc. In a many-body system at a finite temperature, manifestation of the properties of the system gets modified from that of a single molecule due to the presence of many-body interactions and its modifications due to thermal fluctuations inherent in such systems. In such a system, both local structural arrangements and instantaneous dynamical activities are strongly coupled and the interplay between the two governs dynamical evolution and hence all the average thermophysical properties of the systems.[1] In order to understand these many-body systems, a new branch of physics, the so called "condensed matter physics" has been emerged.

Substances in condensed matter as encountered in everyday life can usually exist in one of three phases, namely gas, liquid or solid. Investigation of liquid phases of matter poses greater difficulty as compared to the same of the other two phases. This is because, unlike gaseous or solid phase, where many-body problem can be reduced to a few-body problem due to inherent low density of the gases or the presence of long ranged translational symmetry of the crystalline solids respectively.[2] However, in the liquid phase, further simplification of the many-body nature of the problem often become rather difficult. Understanding liquid state of matter therefore requires information not only about detailed nature of interactions among the constituent particles or molecules in the system, but about the additive/non-additive nature of the inter-particle interaction as well. Apart from this, details of the instantaneous short-ranged (local) structural arrangements (motifs) and how these local motifs and therefore the interactions among the constituent particles change due to random thermal fluctuations dictate average bulk properties of the system.

Among many condensed phase systems, liquid water is one of the most widely used, universal substance and it plays a pivotal role in deciding physical, chemical and/or biological activities of a system.[3] As a solvent, water is intriguing since this can simultaneously dissolve polar and non-polar species. Its remarkable ability to dissolve variety of solutes has been attributed to its small molecular size, high dielectric constant, strong electrostatic interactions, high diffusivity, hydrogen bonding ability and its ability to manifest hydrophobic interaction among large lengthscale hydrophobic materials.[4] In biological systems, the behaviour of water is very fascinating since most of the time a biological molecule can manifest its bioactivities only in presence of a certain level of hydration water.[5] Actually, water can dissolve, stabilize, selectively prefer a particular conformer and/or influence biological activities of proteins, nucleic acids, lipids etc. Although it is certain that without water, existence of life cannot be imagined, but the decisive role played by water for the manifestation of life still remains fuzzy.[6] Any chemical, biochemical or biophysical process in an aqueous medium is governed by ever changing microscopic local arrangements of water. Therefore, understanding local structural motif and dynamics of water is a fundamental step towards comprehending various complicated processes and phenomena observed in various chemical, physical and biological processes.

Properties and local structural arrangements of water significantly differ depending on whether it is in bulk or at interfaces. Classifying water in terms of whether it is in bulk or at interfaces will help us in understanding different structural and dynamics aspects of water. In case of interfacial water, manifestation of different properties of water changes according to the lengthscale of the interface.[7] For example, in most of the solutions, when a solute is dissolved in water, creation of a molecular lengthscale interface, the so called solute-solvent interface, is involved; whereas in many other cases such as the one relevant to a colloidal, a micellar or a bio-macromolecular system, formation of a larger length scale interface of nanoscopic or larger dimension is involved.

In order to study the local structure and dynamics of the bulk as well as interfacial water, it is essential to probe the system at the atomistic level. Only a few sophisticated experimental techniques such as X-ray scattering, small-angle neutron scattering, Raman spectroscopy[8], terahertz spectroscopy, various variants of sum frequency generation spectroscopy etc. can be used to get information about local structural arrangements and dynamics of bulk water and water at interfaces. However, in order to interpret the experimental results and to get information at the atomistic level, theoretical modelling and simulation are extremely useful and essential. In fact, in recent years, due to enormous advancement in the development of supercomputing machines, theoretical modeling as well as simulation has emerged as a very powerful tool for investigating structure and dynamics of bulk and interfacial water. Theoretical modeling and simulation can yield information at the atomistic level and provide detailed insight, which is sometimes beyond the scope of even modern, state-of-the-art experimental techniques. Among the different available simulation techniques, molecular dynamics (MD) simulation has the advantage of not only predicting the structure of the fluid at the atomistic scale resolution, but providing information about the dynamical time history and hence the dynamics of the system as well.[9] In fact, MD simulations not only validate theoretical models and help in explaining experimental results but also direct new research by raising many new questions. The main broad objective of the present thesis is to understand structure and dynamics of water in bulk and at interfaces by using extensive atomistic molecular dynamics simulations. Starting from exploring the microscopic details of the local structure of bulk water and its dynamics, the present work proceeds through predicting various properties of heavy water and finally revealing modifications in structure and dynamics of water at molecular as well as nanoscopic interfaces. The present thesis consists of six chapters and a brief discussion of each of these chapters is given below.

In **Chapter 1**, the present thesis starts with a very general introduction about importance and applicability of water and aqueous solutions, microscopic local structure and dynamics of bulk water and how the structure and dynamics get modified at interfaces. As a theoretical tool we have used molecular dynamics simulation throughout these studies. Therefore, a brief introduction about the molecular dynamics simulation methodology has been presented in this chapter.[1,9] As a result of molecular dynamics simulation, we obtain time evolution of the phase-space in terms of trajectories (sets of positions and momenta of all the particles) of the system. From these microscopic variables, various structural, thermodynamic and dynamic properties of the system can be obtained through the application of classical statistical mechanics.[10] Therefore, we present here a brief theoretical description of statistical mechanical *n*-body distribution functions which are used for gauging local structure of a fluid and the time correlation function, which is used for calculating various dynamical quantities. Finally, in the last part of the Chapter 1, the nature and scope of the present thesis is discussed.

Water is known to be an anomalous liquid. There are around 73 different anomalies involving structural, thermodynamic and dynamic properties of water.[11] Out of all these anomalies, density anomaly (temperature of maximum density at 277K) is the most talked-about anomaly of bulk water.[12] A large body of work has been devoted to understand the correlation, if any, between the local structural motif and the density anomaly.[13] However, contradictory predictions and observations about this correlation have made this field ever challenging.[14,15,16] In **Chapter 2** of this thesis, we have therefore explored different structural aspects of liquid water at ambient pressure to understand the origin of its density anomaly. In order to explore structural and dynamic properties of water by using the classical force-field based molecular dynamics simulation, an accurate model of water is necessary. In the course of this work it is found that computed results on various structural parameters and properties as a function of temperature as obtained from different available atomistic models of water are considerably different. This model dependence of the results clearly obstructs further progress in this direction and necessitates investigation on finding a single parameter through which all these results from different models can be correlated. In this work, we have established a new yardstick (average number of hydrogen bonds), which is able to correlate apparently disparate results from all these water models. Further, by introducing a new definition of 1st solvation shell of a water molecule in the bulk water, the competitive effects of thermal expansion and contraction due to angular distortion have been shown to lead to the density anomaly of water along the 1 atm isobar. The present work clearly demonstrates that density anomaly of water at ambient pressure can be explained without invoking the concept of structural and density inhomogeneity of water. Apart from structural and density anomalies, water is known to possess a number of dynamic anomalies as well. As the structural and thermodynamic properties of bulk water are shown to be model dependent, the dynamical properties also show considerable dependence on the details of the water model used in the MD simulation. Therefore, here the objective is to check whether average number of hydrogen bond, which is able to correlate disparate structural properties obtained from different models into a single context, can also correlate disparate results obtained from different water models on the dynamics of bulk water. Although disparate results on temperature dependence of structural and thermodynamic properties obtained from different models are found to be correlated in terms of average number of hydrogen bonds, similar correlation among the results on dynamical properties of water arising from different water models in terms of average number of hydrogen bonds does not exist.[17]

Isotopically substituted water i.e. deuterium oxide (D_2O), commonly known as heavy water is an important material in view of its relevance in nuclear, chemical, medical and pharmaceutical industries. Molecular dynamics simulation is an enviable theoretical tool to calculate various properties of heavy water at ambient as well as extreme conditions of temperatures and pressures.[18] However, the bottleneck in this direction stems from the absence of a suitable atomistic model of heavy water. A three-site SPC/HW heavy water model, to the best of our knowledge, is the only model available for heavy water. Although this model is shown to reproduce properties of heavy water at ambient condition quite accurately, its applicability has never been tested beyond the ambient condition.[19] In **Chapter 3,** we have therefore investigated the applicability of this model at different temperatures in the range of 223K to 360K at ambient pressure by calculating various thermophysical properties and comparing them with the available experimental or literature values.[20] What emanates from this study is that, the SPC/HW model although reproduces experimental data for heavy water at room temperature appreciably well, largely fails at lower range of temperatures. A comparative study of different thermophysical and structural properties of D_2O (SPC/Hw) and H_2O (SPC/E) has also been presented. Finally, the effect of various potential parameters such as molar mass and partial charges on atoms on the results has been estimated and the findings can act as a guide for further development of a new model for heavy water.

So far we have dealt with structure, dynamics and properties of bulk water and heavy water. Interesting modifications of structural, dynamic and thermodynamic properties of water can be observed when water meets interfaces.[21] The interface may arise due to solvation of different solute molecules in water or due to physical contact of water with a large extended solid surface. In the former case a molecular interface is generated and it is interesting to know whether structural integrity of water will be retained in presence of such molecular interfaces. In this connection, structural information of two molecular interfaces namely that of urea-water and guanidinium chloride (GdmCl)-water are extremely important as these two interfaces are relevant to protein denaturation.[22] The **Chapter 4** of this thesis deals with the structural and dynamical aspects of these interfaces and its relevance in elucidating role of water in the underlying mechanism of protein denaturation. This chapter is divided into two parts. In **Part A**, we have investigated the effect of increasing concentration of urea on various structural and dynamical properties of water in the solution.[23] By calculating various order parameters that gauge the structural integrity of water, it has been demonstrated that tetrahedral and hydrogen bonding structure of urea remain unaffected at least up to the concentration of 9M urea. Exploration of the dynamical features of the aqueous urea solution reveals that with increasing concentration of urea, translational diffusivity decreases considerably, whereas the rotational dynamics remains almost unaltered with the increasing urea concentration.

The **Part B** of this chapter has dealt with another molecular interface created due to solvation of guanidinium (Gdm) chloride, another very useful chemical denaturant of protein, in water. Mainly the effect of increasing concentration of guanidinium chloride (GdmCl) on the structural and dynamical properties of water has been thoroughly investigated here. The two major issues, one dealing with the staked ion-pair formation of the Gdm moieties and the other on the influence of guanidinium ion on the tetrahedral and hydrogen bonding structures of water in the aqueous solution of GdmCl, have been investigated. What transpires from this study is that the water structure is not significantly perturbed by the presence of GdmCl. The finding from this study supports the so-called direct mechanism of protein denaturation according to which Gdm moieties of the denaturant directly attacks the similar (arginine) moieties of the protein in parallel-staking orientation. In order to confirm it we have further extended our study[24] by incorporating one polypeptide into the aqueous solution of Gdmcl and confirmed the existence of such staking between the Gdm ion and the arginine moiety of the peptide. We are also able to establish that such parallel staking orientations (of the arginine moieties) can be observed in case of temperature denaturation of an arginine based peptides. Apart from these, various dynamical properties at different concentrations of the GdmCl have also been calculated.

Manifestation of various properties of water at a nanoscopic or larger interface formed by water and a large surface is dramatically different from the same at the molecular level interface. It has a huge significance in terms of bio-macromolecular stability and protein folding if the interface is made up of nanoscopic or larger hydrophobic objects and water. In fact, for a nanoscopic or larger hydrophobic solute in water, a new interaction, the so called hydrophobic interaction originates and it is thought that the hydrophobic interaction is responsible for self-assembly and aggregation/folding of many bio-macromolecules.[7,25] However, measuring hydrophobicity of such a nanoscopic interface using the conventional method of measuring contact angle is rather difficult and therefore defining new order parameters to estimate hydrophobicity at the nanoscale is essential. The **Chapter 5** of this thesis deals with the characterization of hydrophobicity at the nanoscale.[26] For this, we have considered a nanoscopic paraffin like plates in water and hydrophobicity has been tuned by altering the attractive part of the plate-water dispersion interaction. We have calculated different structural parameters and follow their changes as a function of degree of hydrophobicity. In this work, we are able to identify a few order parameters, each one of which can be a promising descriptor to gauge the hydrophobicity at the nanoscale.

In all these investigations as described in **Chapters 2-5**, we were involved in the modelling at the atomistic lengthscale. In many cases, where we deal with extended solid-water interfaces such as nanomaterial-water interfaces, modelling at the atomistic lengthscale may be computationally expensive and therefore use of a coarse-grained (CG) description might be beneficial. In this context, a spherically symmetrical two-lengthscale potential[27-30] has been found to reproduce almost all the anomalies of liquid water. In **Chapter** 6 of this thesis we have used this coarse-grained description to study the hydration behaviour of one of the very important nanomaterial C_{60}. Using molecular dynamics simulation it is demonstrated how solvation characteristic changes with the changes in the degree of attractiveness in the interaction between the atoms of the C_{60} and CG water.

Finally, in **Chapter** 7, a brief summary of the work described so far has been presented. This chapter also describes how the present work can be extended in near future. It will also describe how the knowledge emanated from the present studies can be used in understanding structure and dynamics of fluids at non-aqueous solute-solvent interfaces.

Reference

1. Allen, M. P.; Tildesley, D. J. *Computer Simulation of Liquids*; Oxford University, New York, **1987**.
2. van Gunsteren, W. E.; Berendsen, H. J. C. *Angew. Chem. Int. Ed. Engl,* **1990**, *29,* 992-1023.
3. Franks, F. *Water. A Comprehensive Treatise*; Plenum: New York, **1973**.
4. http://www.cuchd.in/e-library/resource_library/University%20Institutes%20of%20Sciences/ Fundamentals %20of%20Biochemistry/Chap-02.pdf
5. Hilser, V. J. *Nature*, **2011,** *469*(13), 166-167.
6. Karplus, M.; McCammon, J. A. *Nat. Struct. Biol*, **2002,** *9*,646-652.
7. Chandler, D. *Nature*, **2005**, *437*, 640-647.
8. Clark, G. N. I.; Cappa, C. D.; Smith, J. D.; Saykally, R. J.; Head-Gordon, T. *Mol. Phys*, **2010**, *108*, 1415–1433.
9. Frenkel D.; Smit, B. *Understanding Molecular Simulation*, Academic Press, New York, **2002**
10. McQuarrie, D. A. *Statistical Mechanics*, University Science Books, California, **2000**.
11. http://www1.lsbu.ac.uk/water/water_anomalies.html
12. *Debated waters*, Editorial, *Nature Materials*, **2014**, *13*, 663.
13. Errington, J. R.; Debenedetti, P. G. *Nature*, **2001**, *409,* 318−321.
14. Poole P. H. et al. *Nature,* **1992**, *360*, 324–328.
15. Matsumoto, M. *M. Phys. Rev. Lett.*, **2009**, *103,* 017801-1−017801-4.
16. Head-Gordon T.; Johnson, M. E. *Proc. Natl. Acad. Sci. U.S.A.*, **2006**, *103*, 7973− 7977.
17. Bandyopadhyay, D.; Mohan, S.; Ghosh, S. K.; Choudhury, N. *J. Phys. Chem. B,* **2013**, *117,* 8831−8843.
18. Soper A. K.; Benmore, C. J. *Phys. Rev. Lett.,* **2008**, *101*, 065502.
19. J. R. Grigera, *J. Chem. Phys*., **2001**, *114,* 8064−8065.

20. Bandyopadhyay, D.; Mohan, S.; Ghosh, S. K.; Choudhury, N. *Chem. Eng. Data,* **2012**, *57*, 1751−1758.

21. Tanford, C. *J. Am. Chem. Soc*., **1962**, *84* (22), 4240−4247.

22. Vanzi, F.; Madan, B.; Sharp, K. *J. Am. Chem. Soc*., **1998**, *120*, 10748−10753.

23. Bandyopadhyay, D.; Mohan, S.; Ghosh, S. K.; Choudhury, N. *J. Phys. Chem. B,* **2014**, *118*, 11757−11768.

24. Bandyopadhyay, D.; Mohan, S.; Ghosh, S. K.; Choudhury, N. *J. Phys. Chem. B*, **2015**, *119*, 11262−11274.

25. Choudhury, N.; Pettitt, B. M. *J. Am. Chem. Soc*., **2005**, *127*, 3556-3567.

26. Bandyopadhyay D.; Choudhury, N. *J. Chem. Phys*., **2012**, *136*, 224505-1-224505-2.

27. Hemmer, P. C.; Stell, G. *Phys. Rev. Lett*. **1970**, *24*, 1284.

28. Jagla, E. A. *Phys. Rev. E,* **1998**, *58*, 1478.

29. de Oliveira, A. B.; Netz, P. A.; Colla, T.; Barbosa, M. C. *J. Chem. Phys*., **2006**, *125*, 124503.

30. Pant, S.; Gera, T.; Choudhury, N. *J. Chem. Phys*., **2013**, *139*, 244505.

Figure number	Figure Caption	Page Number
Figure 2.1	Average values of (a) the tetrahedral order parameter, q4, (b) the orientational order parameter, Q6, for the second shell water molecules, and (c) the number of hydrogen bonds as a function of temperature for different models of water.	43
Figure 2.2	Average values of (a) the tetrahedral order parameter, q_4, and (b) the orientational order parameter, Q_6, as a function of the average number of hydrogen bonds, $\langle n_{HB} \rangle$, for different models of water.	45
Figure 2.3	Average density of water for different water models as a function of (a) temperature and (b) average number of hydrogen bonds.	46
Figure 2.4	Radial distribution functions of water molecules around a central water molecule at 298K for each model.	48
Figure 2.5	Radial distribution functions of water molecules around a central water molecule at T=TMD for each water model.	49
Figure 2.6	(a)Probability distribution $P(q_4)$ of the tetrahedral order parameter, q_4, For different water models. Static structure factors obtained from (b) in the low temperature region and (c) high temperature region.	51
Figure 2.7	Percentage of water molecules having n hydrogen bonds as a function of temperature and (b) radial distribution functions of water molecules around a central water molecule having n hydrogen bonds, (In the inset, the number of water molecules in the second solvation shell as obtained from the integration of the radial distribution function has been shown as a function of temperature.)	52
Figure 2.8	(a) Average distance r_n of the nth nearest neighbor at a temperature T relative to its distance at T = 223 K from the central molecule (b) Deviation of the tetrahedral order parameter q_4 from an ideal tetrahedral value of 1 (c) Volume of the void space between the first and second solvation shell of a central water molecule.	55
Figure 2.9	Distributions of tetrahedral order parameter, $P(q_4)$ vs temperature.	59
Figure 2.10	Distributions $P(\cos\theta)$ of the cosine of angle θ made by first four neighbors as a function of temperature.	60
Figure 2.11	Distributions $P(\cos\theta)$ of the cosine of angle θ made by (a) two hydrogen-bonded, (b) two non-hydrogen-bonded, and (c) one hydrogen-bonded and the other non-hydrogen-bonded nearest neighbors to the central molecule C_{HB}=n.	62
Figure 2.12	A schematic representation (not to scale) of a central molecule C, which is hydrogen-bonded to three water molecules in the conventional first shell.	64

Figure 2.13 (a) Volumes of the first shell, the second shell, and the void space between the two shells of SPC/E water as a function of temperature (b) Density ρ in g/cc of SPC/E water as a function of temperature. 67

Figure 2.14 Diffusion of bulk water calculated from MSD at different temperature. 71

Figure 2.15 Diffusion of bulk water calculated from MSD comparing by average number of hydrogen bond. 72

Figure 2.16 Time correlation function of dipole moment vector(μ)of water molecule comparing at TMD for Legendre polynomial(*l*=1). 74

Figure 2.17 Time correlation function of dipole moment vector(μ) of water molecule comparing at TMD for Legendre polynomial(*l*=2). 75

Figure 2.18 Time correlation function of OH bond vector(OH)of water molecule comparing at TMD for Legendre polynomial(*l*=1). 75

Figure 2.19 Time correlation function of OH bond vector(OH)of water molecule comparing at TMD for Legendre polynomial(*l*=2). 76

Figure 3.1 Oxygen−oxygen radial distribution functions $g_{OO}(r)$ for heavy water at 1 atm pressure and at different temperatures. 86

Figure 3.2 Values of the oxygen−oxygen radial distribution function, $g_{max}(r_{max})$, at the first peak and those $g_{min}(r_{min})$ at the trough between the first and the second peaks as a function of temperature. 86

Figure 3.3 Oxygen−oxygen radial distribution functions $g_{OO}(r)$ for SPC/E water at 1 atm pressure and at different temperatures. 87

Figure 3.4 Values of the oxygen−oxygen radial distribution function, $g_{max}(r_{max})$, at the first peak and those $g_{min}(r_{min})$ at the trough between the first and the second peaks as a function of temperature. 88

Figure 3.5 Values of average number of hydrogen bonds, $\langle n_{HB} \rangle$, as calculated. from the simulation trajectory for heavy as a function of temperature along P = 1 atm isobar. 91

Figure 3.6 Computed heat of vaporization, ΔH_{vap}, along with the available experimental results for (a) heavy water and (b) SPC/E water at different temperatures along the P = 1 atm isobar. The inset in panel- a shows the potential energy per particle for the same. 93

Figure 3.7 Isobaric heat capacity Cp of (a) heavy water and (b) SPC/E water at different temperatures along the P = 1 atm isobar. 94

Figure 3.8 Isothermal compressibility κ_T of heavy water along P = 1 atm isobar as a function of (a) absolute temperature, T, and (b) T/TMD, where TMD is the temperature of maximum density for this model. 96

Figure 3.9 Plots of (a) static dielectric constant ε_0, (b) finite system Kirkwood factor G_k, and (c) infinite system Kirkwood factor g_k as calculated from the simulation trajectory using a dipole fluctuation formula for heavy water at different temperatures along P = 1 atm. 98

Figure 3.10 Plots of (a) static dielectric constant ε_0, (b) finite system Kirkwood factor G_k, and (c) infinite system Kirkwood factor g_k as calculated from the simulation trajectory using dipole fluctuation formula for SPC/E water at different temperatures along P = 1 atm. 100

Figure 3.11 Plot of thermal expansion coefficient α_P as calculated fromthe simulation trajectory for (a) heavy water and (b) SPC/E water at different temperatures along P = 1 atm using a finite difference formula. 101

Figure 3.12 Diffusion of bulk water calculated from MSD at different temperature. 103

Figure 3.13 Time correlation function of the dipole moment vector (μ) of SPC/HW heavy water at different temperatures for Legendre polynomial of order ($l= 1$). 104

Figure 3.14 Time correlation function of dipole moment vector (μ) of SPC/HW heavy water at different temperatures for the second order Legendre polynomial ($l = 2$). 105

Figure 3.15 Time correlation function of the OD bond vector of SPC/HW heavy water at different temperatures for Legendre polynomial of order ($l = 1$). 105

Figure 3.16 Time correlation function of OD bond vector of SPC/HW molecule comparing at different temperature for Legendre polynomial of order ($l = 2$). 106

Figure 3.17 Scaled density $\rho\sigma^3$ as a function of partial charge on the oxygen atom and as a function of mass of model water scaled by the heavy water mass. 107

Figure 3.18 Average number of hydrogen bonds, $\langle n_{HB} \rangle$, per water molecule as a function of partial charge on the oxygen atom (bottom axis as indicated by a black arrow) and as a function of mass (top axis as indicated by a red arrow) of model water scaled by the heavy water mass. 108

Figure 3.19 Mean square displacement (MSD) of water molecule as a function of mass model water scaled by the heavy water mass. 109

Figure 3.20 Mean square displacement (MSD) of heavy water molecule as a function of partial charge on oxygen of heavy water molecule. 109

Figure 4.a.1 (a) Average tetrahedral order parameter $\langle q_4^w \rangle$ considering all four water neighbors of a reference water molecule as a function of molar concentration of urea (b) distributions $P(q_4^w)$ of tetrahedral order parameters. 128

Figure 4.a.2 Distributions $P(\theta_{HB})$ of the hydrogen bonding angle formed by a reference water molecule and one of its neighbors. (only water has been considered as neighbors). 130

Figure 4.a.3 (a) Average oxygen−oxygen distance of the n^{th} water neighbor from a reference water molecule for first six water neighbors;(b) fluctuations in the above-mentioned quantities. (only water has been considered as neighbors). 131

Figure 4.a.4 Distributions $P(r_n)$ of the distance r_n of the nth water neighbor from a reference water molecule for n = 1−4 are shown in panels a−d. (only water has been considered as neighbors). 132

Figure 4.a.5 Probability P(n,U/W) that the nth neighbor of a reference water molecule is a urea/water site as a function of urea concentration. 134

Figure 4.a.6 Distributions $P(r_n)$ of the distance r_n of the nth water neighbor from a reference water molecule for n = 1−4 are shown in panels a−d. (both water and urea have been considered as neighbors). 135

Figure 4.a.7 (a) Average oxygen−oxygen distance of the n^{th} water neighbor from a reference water molecule for first six water neighbors;(b) fluctuations in the above-mentioned quantities.(both water and urea have been considered as neighbors). 136

Figure 4.a.8 Distributions $P(\theta_{HB})$ of the hydrogen bonding angle formed by a reference water molecule and one of its neighbors.(both water and urea have been considered as neighbors). 137

Figure 4.a.9 (a) Average tetrahedral order parameter $\langle q_4 \rangle$ as a function of molar concentration of urea by considering both urea and water as neighbors. (b)Distributions $P(q_4)$ of tetrahedral order parameter q_4. 138

Figure 4.a.10 (a) Average number of hydrogen bonds $\langle n_{HB} \rangle$ as a function of concentration of urea. (b) Distribution of hydrogen bonds in bulk water. 142

Figure 4.a.11 (a) Distribution $P(\cos\theta)$ of cosine of the triplet angle $\cos\theta$ at different urea concentrations (b)Distributions $P(\cos\theta)$ of the cosine of angle θ made by (i) two hydrogen-bonded (ii) two non-hydrogen bonded, and (iii) one hydrogen-bonded and the other non-hydrogen-bonded nearest neighbors at the central molecule. 144

Figure 4.a.12 Mean squared displacements (MSDs) of (a) urea and (b) water molecules as a function of time at different urea concentrations. 146

Figure 4.a.13 Time correlation function of dipole moment vector (μ) of tip4p/2005 water molecule comparing at different urea concentration for Legendre polynomial (*l*=1). 147

Figure 4.a.14 Time correlation function of dipole moment vector (μ) of tip4p/2005 water molecule comparing at different urea concentration for Legendre polynomial (*l*=2). 147

Figure 4.b.1 (A) Snapshot of a typical configuration of peptide─water system. (B) The arginine residue, shown as a ball-and-stick model. 159

Figure 4.b.2.a Radial distribution functions of the carbon atom of the guanidinium moiety around the same for three different concentrations. In the inset, numbers of Gdm^+ ions in the first and second solvation shells have been shown.(for tip4p/2005) water model. 161

Figure 4.b.2.b Same as Figure 4.b.2.a (for tip3p water model). 162

Figure 4.b.3 Radial distribution functions of O_w of water and chloride ion around the carbon atom of guanidinium moiety. In the inset, numbers of chloride ions and water molecules in the first solvation shell of the Gdm^+ ion are shown. 163

Figure 4.b.4 Effect of total time steps and box size used for simulation on RDF function. 166

Figure 4.b.5 Schematic representation of two molecular planes of guanidinium ions inclined at an angle ϕ. 167

Figure 4.b.6 Distributions $P(\phi)$ of the angles ϕ made by the perpendiculars drawn from two guanidinium molecular planes at three different GdmCl concentrations. 168

Figure 4.b.7 Distributions $P(\phi)$ of the angles ϕ made by the perpendiculars drawn from two guanidinium molecular planes at four different temperatures. 169

Figure 4.b.8 (a) Potential of mean force values (w(r)) among the guanidinium. moieties at three different concentrations of GdmCl salts. (b) Direct solute─solute interaction (c) Solvent-induced contribution to the PMF at different GdmCl concentrations. 170

Figure 4.b.9 Distributions $P(r_n^w)$ of the distances r_n of the n^{th} water neighbor from a reference water molecule for n=1-4 are shown in four different panels (a)-(d). (only water has been considered as adjacent neighbors) . 172

Figure 4.b.10 Same as in Figure 4.b.9 (Sites of Gdm^+, Cl^- and water all species have been considered as adjacent neighbors) . 173

Figure4.b.11.a Average tetrahedral order parameter <q_4>calculated by considering all the four water neighbors of a reference water molecule as a function of molar concentration of Gdmcl and the same calculated by considering all the species (Gdm$^+$, Cl$^-$ of Gdmcl and O$_w$ of water) in solution. (for tip4p/2005 water model). 175

Figure 4.b.11.b Same as in Figure 4.b.11.a (for tip3p water model). 176

Figure 4.b.12.a. Distributions $P(\theta_{HB})$ of the hydrogen-bonding angle formedby a reference water molecule and one of its neighbors. Hydrogen bonding angle θ_{HB} is the angle formed by the line joining the two oxygen atoms and the OH bond vector. In this case, species from GdmCl molecules are not considered to be a probable neighbor. 178

Figure 4.b.12.b. Same as in Figure 4.b.12.a (for tip3p water model). 179

Figure 4.b.13.a. Same as in Figure 4.b.11.a, except, five nearest neighbors (Gdm$^+$, Cl$^-$ of Gdmcl and O$_w$ of water) are chosen to calculate the hydrogen-bonding angle within the first five (distance-wise) neighbors. (for tip4p/2005 water model). 180

Figure 4.b.13.b Same as in Figure 4.b.13.a (for tip3p water model). 181

Figure 4.b.14 Radial distribution functions of O$_w$ of water, nitrogen and carbon atoms of the guanidinium moiety and chloride ions around the O$_w$ of water. 182

Figure 4.b.15 Average number of water–water hydrogen bonds $\langle n_{HB} \rangle$ as a function of concentration of GdmCl at different conditions 183

Figure 4.b.16 Distributions $P(\theta_{HB})$ of the hydrogen-bonding angle calculated by imposing three different conditions. 185

Figure 4.b.17 Radial distribution functions of the carbon atom of the Gdm$^+$ moiety of GdmCl around the C1 carbon atom of the ARG side chain of the protein, carbon atom of the Gdm$^+$ moiety with and without protein . 186

Figure 4.b.18 Radial distribution functions of the carbon atom of the Gdm$^+$ moiety of GdmCl around the carbon atoms of the ARG side chain. In the inset, same plots with longer range are shown. 187

Figure 4.b.19 Distributions $P(\theta)$ of the angles θ made by the perpendiculars drawn from the molecular plane formed by carbon and three nitrogen atoms of Gdm$^+$ moiety in the GdmCl and the molecular plane of the guanidinium moiety of the ARG side chain of the protein. 189

Figure 4.b.20 Mean squared displacements of water, Gdm+ ions and Chloride ions in the Gdmcl-water solutions of different concentrations. 190

Figure 5.1 The normalized single particle density $g_{SO}(z)$ of water oxygen as a function of distance z from the model paraffin plate for different values of λ. 204

Figure 5.2 The normalized single particle density $g_{SO}(z)$ of water oxygen as a function of distance z from the model paraffin plate for different values of λ.(a) Solute-water potential of mean force $W_{SO}(z)$ of a water. molecule as a function of distance z from the model paraffin solute (plate) for values $\lambda = 0, 0.5$, and 1. (b) Solvent induced PMF $\omega_{ind}(z)$ for values of $\lambda = 0, 0.25,0.5, 0.75$, and 1. 206

Figure 5.3 Orientational distribution functions of the (a) dipole moment vector $P\mu(\cos\theta)$ vs. $\cos\theta$ (b) OH bond vector $P_{OH}(\cos\psi)$ vs. $\cos\psi$, and (c) $P_{\perp}(\cos\varphi)$ vs. $\cos\varphi$ of the water molecules for different values of λ. 208

Figure 5.4 Average values of the cosines of the angles made by (a) dipole moment vectors, (b) OH bond vectors, and (c) plane-perpendicular vectors of the water molecules with outward normal to the solute plate as a function of perpendicular distance from the solute plate with different values of λ. 210

Figure 5.5 Histograms of water molecules with n hydrogen bonds $f_3^{HB}$for water in plate-water systems with $\lambda = 0, 0.25, 0.5, 0.75, 1$, and bulk. 212

Figure 5.6 (a) Average coordination number $(\langle n_{CN} \rangle)$ of water, (b) average number of hydrogen bonds $(\langle n_{HB} \rangle)$ per water molecules, and (c) fraction $(\langle n_{HB} \rangle / \langle n_{CN} \rangle)$ of nearest neighbors that are hydrogen bonded as a function of perpendicular distance z from the solute plate for different paraffin-like plates (with different values of λ). 213

Figure.5.7 Local compressibility $\chi_T(z)$ of a slab of water of width 1 Å at different locations along the perpendicular direction of the plate for different values of λ. 214

Figure.5.8 Normalized fluctuations $K_N(z)$ of a slab of water of width 1 Å at different locations along the perpendicular direction of the plate for different values of λ and for bulk water. 215

Figure.5.9 Water-water correlations at different interfaces with different λ values as calculated through intermolecular water (a) oxygen-oxygen pair correlation function $g_{OO}(r)$ and (b) oxygen-hydrogen pair correlation function $g_{OH}(r)$ near the paraffin plate measured in a 1 Å thick slab placed parallel to the interface located at the half density plane of water. 217

Figure.5.10 (a) First shell tetrahedral order parameter, q_4 (Bottom to top:λ= 0.0, 0.25, 0.50, 0.75, 1.00) and (b) second shell orientational order parameter Q_6 for water at different slabs parallel to the surfaces as a function ofdistance from the plate for different plates of varying λ values. In the inset of panel (a), q_4 as a function of λ is shown. 219

Figure.5.11 Normalized one-particle density profile, $\rho(z)/\rho_0$ as a function of perpendicular distance from the plate, z (a) for $\lambda = 1.0$ and (b) for $\lambda = 0.75$ plate-water systems. The red lines in (b) is for plates with interplate distance,r_0= 12 Å and the black line is for the same with r_0=10 Å. 222

Figure.5.12 Normalized one-particle density profile, $\rho(z)/\rho_0$ as a function of perpendicular distance from the plate, z for (a) $\lambda = 0.5$ and for (b) $\lambda = 0.75$ plate-water systems. The red lines are for plates with interplate distance, r_0= 14 Å and the black line is for the same with r_0 = 12 Å. 223

Figure 6.1 Interaction potential between (a)two CG water molecules interacting with core softened model potential and (b) a carbon atom of C60 and the CG water molecule. 231

Figure 6.2 Snapshot of a typical configuration of a box of CG water with a C60 molecule in it. 232

Figure 6.3 Radial distribution of CG water around the C_{60} molecule at four different temperatures and at different densities. 233

Figure 6.4 Radial distribution functions of CG water around the C_{60} molecule at four different temperatures and at four different densities for repulsive solute (λ=0 case). 234

Figure 6.5 Average number $\langle N\rangle_{1st\ shell}$of solvent molecules on the first solvation shell of C_{60} for (a)λ=1 and (b) λ=0. 236

Figure 6.6 Fluctuations in the number of solvent molecules in the first solvation shell of C_{60} for (a)λ=1 and (b) λ=0. 237

Figure 6.7 Distributions of solvent molecules in the first solvation shell of C_{60}. In left panel distribution is shown for λ=1 at (a) T*=0.25 and (b) T*=3.0. In the right panel the same is shown for λ=0 at (c) T*=0.25 and (d) T*=3.0. 238

Figure 6.8 Density distributions $\rho(r)\sigma^3$or the un-normalized $g_{C60\text{-}water}(r)$ of solvent molecules around the solute C_{60}at T*=0.25 and at two different bulk densities ρ*=0.24 and 0.07.Top panel is for λ=1 and the bottom panel is for λ=0. 239

Table number	**Table Caption**	**Page Number**
Table 2.1	Temperature range and TMD of all the water models.	38
Table 3.1	Temperature dependence of the average volume and density of heavy water.	89
Table 3.2	Effect of mass and partial charge on bulk diffusion of water/heavy water model.	110
Table 4.a.1	Composition of different concentrated urea water solution.	126
Table 4.b.1	Composition of different concentrated guanidinium chloride - Water solution.	158
Table 4.b.2	Diffusion coefficient of water, guanidinium and chloride ion in Solution.	191

Chapter 1

Introduction and Computational Methodology

1.1: Introduction

Most of the chemical and biological processes occurring both in natural systems and in systems engineered by human beings involve many-body systems at a finite temperature.[1,2] The studies of these systems have direct relevance in various fields of science and technology, e.g. chemistry[3], physics[4], biology[5], chemical engineering[6], material science[7], oceanology[8], environmental studies[9] etc. In a many-body system at a finite temperature, manifestation of the properties of the system gets modified from that of a single molecule due to the presence of many-body interactions and its modifications due to thermal fluctuations inherent in such systems. In such a system, both local structural arrangements and instantaneous dynamical activities are strongly coupled and the interplay between the two governs dynamical evolution and hence all the average thermo-physical properties of the systems.[10] In order to understand these many-body systems, a new branch of physics, the so called "condensed matter physics" has been emerged.

Matters in condensed phase as encountered in everyday life can usually exist in one of three phases, namely gas, liquid and solid. Investigation of liquid phases of matter poses greater difficulty as compared to the same of the other two phases. This is because, in gaseous and solid phases, many-body problem can be reduced to a few-body problem due to inherent low density of the gases and the presence of long ranged translational symmetry of the crystalline solidsrespectively.[11] However, in the liquid phase, further simplification of the many-body nature of the problem often becomes rather difficult. Understanding liquid state of matter, therefore, requires information not only about detailed nature of interactions among the constituent particles in the system, but also about the additive/non-additive nature of the inter-particle interactions. Apart from this, details of the instantaneous short-ranged (local) structural arrangements (motifs) and how these local motifs and therefore the interactions among the constituent particles changes due to random thermal fluctuations dictate average bulk properties of the system.

Among many condensed phase systems, liquid water is one of the most widely used, universal substance and it plays a pivotal role in many chemical, biological and other processes to decide physical, chemical and/or biological activities of the system.[12,13] As a substance, water is very unique in the sense that it can exists in all three phases under different environmental conditions.[14,15] As a solvent, water is intriguing since this can simultaneously dissolve polar and non-polar species. Its remarkable ability to dissolve variety of solutes has been attributed to its small molecular size, high dielectric constant, strong electrostatic interactions, high diffusivity, hydrogen bonding ability and its ability to manifest hydrophobic interaction among large lengthscale hydrophobic materials.[16,17,18] In biological systems, the behavior of water is very fascinating since most of the time a biomolecule can manifest its bioactivities only in presence of a certain level of hydration water.[19,20] Actually, water can dissolve, stabilize, selectively prefer a particular conformer and/or influence biological activities of proteins, nucleic acids, lipids etc. This is the reason why a minimum percentage of water proportional to the body mass a living being is essential.[21,22,23,24] Although it is certain that without water, existence of life cannot be imagined, but the decisive role played by water for the manifestation of life still remains fuzzy.[25] Any chemical or biochemical process in an aqueous medium is governed by ever changing microscopic local arrangements of water.[26] Therefore, understanding local structural motif and dynamics of water is a fundamental step towards comprehending various complicated processes and phenomena observed in various chemical, physical and biological processes.

Properties and local structural arrangements of water significantly differ depending on whether it is in bulk or at interfaces.[27,28] Classifying water in terms of whether it is in bulk or at interfaces will help us in understanding different structural and dynamics aspects of water. In case of interfacial water, manifestation of different properties of water changes according to the length scale of the interfaces.[29,30] For example, in most of the solutions, creation of a molecular lengthscale interface, the so called solute-solvent interface, is involved; whereas in many other cases such as the one relevant to colloidal, micellar and bio-macro-molecular systems, formation of larger length scale interfaces of nanoscopic or larger dimensions are involved.[31]

In order to study local structure and dynamics of bulk as well as interfacial water, it is essential to probe the system at the atomistic level. Only a few sophisticated experimental techniques such as X-ray[32] and neutron scattering[33], X-ray absorption spectroscopy[34], X-ray emission spectroscopy[35], X-ray standing wave[36], Small-angle scattering[37], Raman spectroscopy[38] etccan be used to get information about local structural arrangements and dynamics of bulk water and the same at the interface can be probed by using variants of sum frequency generation spectroscopy.[39] However, in order to interpret the experimental results and to get information at the atomistic level, theoretical modelling and simulation are extremely useful and essential.[40]In fact, in recent years, due to enormous advancement in the development of supercomputing machines, theoretical modeling as well as simulation has emerged as a very powerful tool for investigating structure and dynamics of bulk and interfacial water. Theoretical modeling and simulation can yield information at the atomistic level and provide detailed insight, which is sometimes beyond the scope of even modern, state-of-the-art experimental techniques.Among the different available simulation techniques, molecular dynamics (MD) simulation has the advantage of not only predicting the structure of the fluid at the atomistic scale resolution, but providing information about the dynamical time history and hence dynamics of the system as well.[41]In fact, MD simulations not only validate theoretical models and help explaining experimental results but directnew research by raising many new questions as well. The main broad objective of the present thesis is to understand structure and dynamics of water in bulk and atinterfaces by using extensive atomistic molecular dynamics simulations. Starting from exploring the microscopic details of the local structure of bulk water and its relation with its anomalous properties as well as dynamics, the present work proceeds through predicting various properties of heavy water and finally revealing modifications in structure and dynamics of water at molecular as well as nanoscopic interfaces.The nature and scope of the present thesis are discussed in details at the end of this Chapter (see Section 1.6). Since the entire work presented in this thesis is based on molecular dynamics simulations, a brief account of this technique has been depicted in the following subsection. The MD simulation provides us the detailed microscopic picture in terms of the trajectory (positions and velocities of all the constituent particles) of the system. In order to obtain average thermo-physical and dynamic properties of the system application of statistical mechanics is essential. Therefore a brief description of the statistical mechanical theory pertaining to liquid structure and dynamics are also presented in the following subsection.

1.2: Classical Molecular Dynamics

B. J. Alder and T. E. Wainright first introduced molecular dynamics (MD) simulation technique in 1957 to study phase transition of a system consisting of hard spheres.[42,43] Later in 1964, A. Rahman first used this powerful technique to understand local structure and dynamics of a condensed phase system of argon atoms interacting with each other with an effective interaction potential.[44] In this path breaking work, transport properties of a system of interacting particles through the introduction of equilibrium auto correlation functions, have been calculated for the first time. With the introduction of high performance supercomputing machines, nowadays, the MD simulation technique has been used in a variety of fields such as Physics, Chemistry, Biology, Chemical Engineering, Material Science, Mechanical Engineering etc. Classical MD simulation is a deterministic method which follows the laws of classical mechanics to depict the time evolution of the phase space of a set of interacting atoms or molecules. For example, by integrating Newton's equations of motion, this method generates a set of coordinates and momenta (velocities) of constituent particles of the system as a function of time. For a simple atomic system Newton's second law of motion can be written as

$$\boldsymbol{F} = m\frac{d^2\boldsymbol{r}}{dt^2} \qquad (1.1)$$

where m is the mass of the atom and **r** is the positional coordinate. By integrating the above equation of motion, from a set of positions and velocities at a particular time step, the consecutive positions and velocities of the next time frames separated by a small time interval δt can be calculated. Various approximate solutions have been used to integrate the above equation of motion. Among these methods, Verlet algorithm, velocity-Verlet algorithm, leap-frog algorithm to name a few. According to the velocity Verlet algorithm, the position **r**(t+δt) and velocity **v**(t+δt) of each particle constituting the system at time (t+δt) can be obtained from position **r**(t), velocity **v**(t) and force (**F**(t)) of the same at time t such that

$$\boldsymbol{r}(t+\delta t) = \boldsymbol{r}(t) + \boldsymbol{v}(t)\delta t + \frac{\boldsymbol{F}(t)}{2m}\delta t^2 \qquad (1.2)$$

$$\boldsymbol{v}(t+\delta t)=\boldsymbol{v}(t)+\frac{\boldsymbol{F}(t+\delta t)+\boldsymbol{F}(t)}{2m}\delta t \qquad (1.3)$$

In order to implement these equations, one needs to have the value of force acting on each constituent particle in the system. Force can be calculated from the negative gradient of the total potential energy of the system i.e.

$$\boldsymbol{F}=-\boldsymbol{\nabla}V(\boldsymbol{r}N) \qquad (1.4)$$

Hereby, $V(\mathbf{r}^N)$ is the potential energy of the system which can be calculated from the position of atoms by using an empirical force field corresponding to the simulation system defined by the user. Thus, once empirical force field is defined, above set of equations can be solved successively to obtain positions and velocities as a function of time, commonly known as trajectory of the system.

In a classical molecular dynamics simulation, the system characteristics are hidden in its potential energy function, commonly known as force field. In an atomistic description, every atom in the system and in some cases lone pair of electrons associated with an atom is considered as an interaction site. Depending on the bonding nature in a molecule such a site-site interaction potential function consists of two distinct types of interactions namely, (a) non-bonded interactions and (b) bonded interactions. By suitably choosing the potential functions for these two types of interactions, total potential energy of the system can be calculated by considering various intra- and inter-molecular interactions among different sites in the system. One of the functional forms for calculating energy of the N-atom molecular system can be expressed as

$$V(\boldsymbol{r}^N) = \sum_{i=1}^{N}\sum_{j=i+1}^{N}\left(4\in_{ij}\left[\left(\frac{\sigma_{ij}}{r_{ij}}\right)^{12}-\left(\frac{\sigma_{ij}}{r_{ij}}\right)^{6}\right]+\frac{q_i q_j}{4\pi\epsilon_0 r_{ij}}\right)+\sum_{bonds} K_b(b-b_0)^2+$$

$$\sum_{angles} K_\theta(\theta-\theta_0)^2+\sum_{dihedrals}\sum_{n=1}^{N} K_\varphi^{(n)}\left[1+\cos(n\varphi-\delta)\right]+\sum_{impropers} K_\omega(\omega-\omega_0)^2$$

(1.5)

Hereby, the total potential $V((r^N)$ is the function of coordinates of the N sites of the systems. The first two terms of the right hand sides of the equation correspond to non-bonded interactions and the rest of the terms are bonded parameters. The very first term of the equation captures the van der Waals (VDW) interaction between two atoms i and j with interatomic distancer_{ij}. The VDW force originates from the interplay of repulsive and attractive forces and yields an energy minimum at a particular interatomic separation. As atoms are brought closer from infinite separation, initially negative term $(1/r^6)$ in the square bracket prevails and hence energy becomes gradually more negative. In case of distance closer to energy minimum the positive part $(1/r^{12})$ of the equation starts to dominate and energy becomes positive rapidly. The parameter $\in_{ij}$ represents the depth of the potential well and σ_{ij} represents the collision diameter or the inter atomic distance at which potential energy becomes zero. The values of these two parameters are basically guided by the nature of the interacting atoms. The second term in the above equation is the non-bonded electrostatics interaction as given by the Coulomb's law due to point charges on different interaction sites of the system. The interacting atoms are separated by distance r_{ij} and pose partial charge q_i and q_j respectively. The third term of the equation is the potential energy for bond vibration or the bond energy and is modeled by using harmonic potential; b represents the bond length at any instant of time and b_0 is the equilibrium bond length and K_b is the force constant of the bond. In a similar fashion, the 4th term in the equation representing energy change during bending motion of molecule is also modeled by using harmonic potential. Hereby, K_θ

represents the force constant and θ and θ_0 are the angles formed by three consecutive atoms and its equilibrium value, respectively. The 5th term provides the potential energy change due to dihedral or torsional motion (dihedral term). Actually, four consecutive atoms in a molecule form a dihedral angle. The angle Φ represents torsion angle, K_{Φ} represents height of rotational energy barrier, n is the multiplicity which illustrates the number of minimum points in the function during a 360^0 rotation of a bond. The phase factor δ decides where the torsion angle goes through the minimum values. The cosine function in this term stands for the periodicity of this function. The 6th term in the equation demonstrates improper dihedral potential involving improper torsion/dihedral angle ω, its equilibrium value ω_0 and force constant K_{ω}.

The parameters of a force field are mainly obtained from experimental or quantum mechanical studies. Transferability of parameters, for example parameters derived for a small molecule of fragments of a big molecule can be used to study another big molecule without much complexity is a noteworthy advantage. In last 30 years, different types of force field have been developed which are extensively used in simulations for many different systems of interests. In our work, we have mostly adopted AMBER[45], CHARMM[46], OPLS[47] force-field for solutes and SPC/E and TIP series of models for water[48,49,50,51,52,53]. The primary requirement of any MD simulation is the modeling of the system by choosing appropriate lengthscale and force-field or model potentials and subsequent creation of initial configuration for the same. Initial velocities of each atom can be provided by using Maxwell-Boltzmann equation by taking care of the average temperature of the system. Before starting the simulation, a suitable boundary condition to mimic the system of interest should be employed. Periodic boundary condition is one such condition which apart from maintaining the number of atoms/particles fixed in the simulation box, creates bulk environment by removing the surface effects. Because of the long-ranged nature of the Coulomb potential, particle mesh Ewald (PME) summation method is used to evaluate the charge-charge interaction correctly.[54,55,56,57] The equation of motion is generally integrated by applying finite difference methods. The basic criteria of a reliable integrator are it should be (a) accurate (follow the true trajectory) (b) stable (energetically conserved) and (c) robust (allow larger time in propagation of system in phase space). There are several algorithms proposed for the integrators in MD simulations. Throughout this work, we have used velocity Verlet[58] and leap-frog[59] algorithm for our simulation purposes. One usual way of avoiding larger computational requirement is to avoid simulating very fast motions like the one due to bond or angle vibration by constraining these bonds or angles to its equilibrium value during the simulation. Here we have used SHAKE[60] and LINCS[61] for constraining bonds.

In general a trajectory obtained by solving the Newtonian equations of motion corresponds to micro canonical or NVE ensemble. Special thermostating methods are to be employed to simulate systems in any other ensemble. Different types of thermostats such as Berendsen temperature coupling[62], Velocity rescaling[63], Nose-Hoover[64] temperature coupling are used to maintain the temperature of the system and different barostats such as Berendsen pressure coupling[62], Parrinello-Rahman[65] method etc. are used to control the pressure of the system. Some of the well-known ensembles used in this thesis work are canonical or NVT ensemble in which the total number of particles, temperature and volume of the system are fixed and isothermal-isobaric (NPT) ensemble in which the total number of particles, temperature and pressure of the system are fixed.[66] There are some mathematical relations relating a particular statistical ensemble and various thermodynamic properties of the system. As outputs of the MD simulation we obtain phase-space trajectory of the system which contains entire time history of the evolution of the system in terms of macroscopic quantities. The extraction of the macroscopic properties of the system from this microscopic description involves application of statistical mechanics.[67] In what follows we shall describe various aspects of statistical mechanics associated with the static and dynamical properties of a many-particle finite-temperature system.

1.3: Statistical Mechanical Ensembles & Averages

The aim of the equilibrium statistical mechanics is to calculate observable properties of a many particle system from its microscopic description. Thermodynamic properties of a system, with some exceptions, are expressible as average of certain functions of the coordinates and/or momenta of the constituent particles of the system. In a state of thermodynamic equilibrium, the average must be independent of time. Let us assume a system consisting of N identical spherical particles and also assume the system is isolated from its surroundings, in which case we know the Hamiltonian H is a constant of motion. Given the initial positions and momenta, positions at any later time can in principle be obtained from the solution of Newtonian equation of motion

$$m\ddot{r}_i = -\nabla U_N(\vec{r}^N) \qquad (1.6)$$

The above equation is a combination of equations. (1.1) and (1.4).

In a conventional MD simulation, we generally deal with positions and momenta of all the N particles of the system. These positions and momenta of the system are continuously changing with the passage of time and these position and momenta can be thought of as coordinates in a multidimensional space, called “phase space”. Let us use the abbreviation Γ for a particular point in phase space and Γ corresponds to N coordinates and N-momenta. Let us assume an instantaneous function $\mathcal{A}(\Gamma)$, which corresponds to some macroscopic property A of the system. As the system evolves Γ changes and thus instantaneous value of the property $\mathcal{A}(\Gamma)$ changes, and thus any observable A can be obtained as average of all the $\mathcal{A}(\Gamma)$ i.e.

$$A = \langle \mathcal{A}(\vec{r}^N, \vec{p}^N) \rangle \qquad (1.7)$$

where the angular brackets denote average value.

1.3.1: Time Averaging (Method of Boltzmann)

In a MD simulation, as we solve Newtonian equation of motion, we generate phase space point Γ as a function of time. It is therefore reasonable to assume that the experimentally measured value of the property, A is actually the time average of $\mathcal{A}(\Gamma)$ taken over a long time interval such that

$$\langle \mathcal{A} \rangle_t = \lim_{\tau_{obs} \to \infty} \frac{1}{\tau} \int_0^{\tau_{obs}} \mathcal{A}\,[\vec{r}^N(t), \vec{p}^N(t)]\, dt \qquad (1.8)$$

The above concept of time averaging is due to Boltzmann. As in practice, we cannot extend the integration up to infinity and we represent a discrete time in MD, it is therefore convenient to express the above averaging procedure as a sum of N_t number of time steps of discrete step length $= \frac{T_{obs}}{N_t}$, viz.

$$A = \langle \mathcal{A} \rangle_t = \frac{1}{N_t} \sum_{\tau=1}^{N_t} \mathcal{A}(\Gamma(\tau)) \qquad (1.9)$$

where$\Gamma(\tau)$ is the phase-space point corresponding to a particular set of N positions and N momenta (where N is number of particles in the system). The definition is correct when the system is “ergodic” which means that after a suitable time of observation the phase trajectory of the system will have passed equal number of times through every points in phase- space.

1.3.2: Ensemble Average:

The same averaging of equation (1.8) can be carried out by averaging over ensemble of systems, each of which is a replica of the original system of interest. This is known as the method of Gibbs. An ensemble is an arbitrary large collection of imaginary systems, all of which are replicas of the system of interest in so far as they are characterised by same mcroscopic parameter like N, V, T, P, µ etc. The systems of ensemble differ from each other in the assignment of coordinates and momenta of the particles of the system. Ensemble is thus represented by a cloud of phase points distributed in space according to some probability density distribution. In Gibbs’ formulation of statistical mechanics the distribution of phase points of the ensemble is described by a phase-space probability density $f^{(N)}(\vec{r}^N, \vec{p}^N, t)$; The quantity $f^{(N)} d\vec{r}^N, d\vec{p}^N$ is the probability that at time t, the actual physical system is in a microscopic state represented by a phase point lying in the infinitesimal phase space element $d\vec{r}^N, d\vec{p}^N$. Given a complete knowledge of the probability density, it would be possible to calculate average values of any functions of the coordinate and momenta. The equilibrium ensemble average of a phase function $\mathcal{A}(\vec{r}^N, \vec{p}^N)$ is given by

$$\langle \mathcal{A} \rangle_e = \iint \mathcal{A}(\vec{r}^N, \vec{p}^N) f_0^{(N)} (\vec{r}^N, \vec{p}^N) d\vec{r}^N, d\vec{p}^N \qquad (1.10)$$

Where $f_0^{(N)}$is normalised in such that

$$\iint f_0^{(N)} (\vec{r}^N, \vec{p}^N) d\vec{r}^N, d\vec{p}^N = 1 \qquad (1.11)$$

Various Monte carlo methods use this averaging procedure but in a much efficient way. The explicit form of the probability density $f_0^{(N)}$ depends on the macroscopic parameters chosen to characterize the ensemble. Here we discuss different types of ensembles.

1.3.3: Micro-Canonical Ensemble

A particularly simple case is one where the systems of the ensemble are assumed to have the same number of particles (*N*), same volume (*V*) and same total energy (*E*) say. An ensemble constructed in this way is called 'micro-canonical' ensemble and clearly is representative of a real system. That can exchange neither matter nor heat with the surroundings. The equilibrium probability density for this ensemble is

$$f_0^{(N)}(\vec{r}^N, \vec{p}^N) = C\ \delta\ (\mathcal{H}_N(\vec{r}^N, \vec{p}^N) - E_0) \qquad (1.12)$$

the $\delta(\ldots)$ is the Dirac delta-function and C normalization constant. The systems of a microcannonical ensemble are therefore distributed on the hyper surface in the phase-space corresponding to total energy E_0. where C^{-1} is the total volume of that hyper-surface. Now if we put this $f_0^{(N)}$ in equation (1.10) with $\mathcal{A}(\vec{r}^N, \vec{p}^N)$as $\mathcal{H}_N(\vec{r}^N, \vec{p}^N)$, we get total internal energy of the system. Thus it is reminiscent of the condition of conservation of total energy under which time average are taken. Indeed time average and micro-canonical ensemble averages are identical if the system is ergodic, which means that after a suitable lapse of time the phase trajectory of the system will have passed equal number of times through every phase-space element lying on the hyper surface defined by equation (1.12).

1.3.4: Canonical (NVT) Ensemble

A canonical ensemble is a collection of systems characterized by the same values of *N*, *V* & *T*; it is therefore also called *NVT*-ensemble. In order to have constant *T* the systems of ensemble are imagined to have been brought into 'Thermal equilibrium' with each other by immersing them into a heat bath of temperature *T*. The canonical equilibrium probability density for *N* identical point is

$$f_0^{(N)}(\vec{r}^N,\vec{p}^N) = \frac{1}{N!}h^{-3N}\frac{\exp[-\beta\mathcal{H}_N(\vec{r}^N,\vec{p}^N)]}{Q_N(V,T)} \qquad (1.13)$$

Where h is plank's constant, the factor *N!* Takes care of in-distinguish ability of the particles; $Q_N(V,T)$ is the normalization factor and is called canonical partition function, defined as

$$Q_N(V,T) = \frac{h^{-3N}}{N!}\iint \exp[-\beta\mathcal{H}_N(\vec{r}^N,\vec{p}^N)]\,d\vec{r}^N, d\vec{p}^N \qquad (1.14)$$

Link between statistical mechanics and Thermodynamics is established via the relation

$$A = -K_B T\, log\, Q_N(V,T) \qquad (1.15)$$

Where *A* is the Helmholtz free energy. For any system of fixed *N, V, T*, A is the thermodynamic potential, which is minimum at equilibrium.

If the Hamiltonian is separated into kinetics and potential terms, i.e.

$$\mathcal{H}_N(\vec{r}^N,\vec{p}^N) = \tfrac{1}{2m}\textstyle\sum_{i=1}^{N}|p_i|^2 + V_N\,(r^N) \qquad (1.16)$$

Putting this in equation (1.13), and integrating over momenta N times we get a factor $(2\pi m K_B T)^{3N/2}$ and $Q_N(V,T)$ is recast into

$$Q_N(V,T) = \frac{\Lambda^{-3N}}{N!} Z_N(V,T) \qquad (1.17)$$

Where $\Lambda = (\frac{h^2}{2\pi m K_B T})^{1/2}$ is known as thermal de Broglie wave length and

$$Z_N(V,T) = \int \exp[-\beta U_N(\vec{r}^N)]\, d\vec{r}^N \qquad (1.18)$$

Is the configuration integral.

In case of ideal or perfect gas $U_N(\vec{r}^N) = 0$ and

$Z_N(V,T) = \int d\vec{r}^N = V^N$ (*v*=total volume)

The canonical partition function of an ideal gas is there for given by

$$Q_N^{id}(V,T) = \frac{\Lambda^{-3N}}{N!} V^N \qquad (1.19)$$

1.3.5: Isothermal–Isobaric (*NPT*) Ensemble

Here systems under this ensemble have same number of particles (N), same P and same T. In the isothermal –isobaric ensemble pressure (not volume) is a fixed parameter. The thermodynamic parameter is now Gibbs free energy G defined as

$$G = A + PV \qquad (1.20)$$

And it is related to statistical mechanics through the relation

$$G = -K_B T\ log\ \Delta_N(P,T) \qquad (1.21)$$

Where isothermal-isobaric partition function $\Delta_N(P,T)$

$$\Delta_N(P,T) = \frac{h^{-3N}}{N!}\iiint \exp[-\beta PV - \beta\mathcal{H}_N(\vec{r}^N,\vec{p}^N)]\; d\vec{r}^N, d\vec{p}^N dV$$

$$= \int \exp(-\beta PV)Q_N(V,T)\, dV$$

$$f_{0,NPT}^{(N)} = \frac{h^{-3N}}{N!}\frac{\mathrm{e}^{-\beta PV}\ \mathrm{e}^{-\beta\mathcal{H}_N\left(r^N,p^N\right)}}{\Delta_N(P,T)} \qquad (1.22)$$

1.3.6: Grant Canonical (μVT) Ensemble

In grand canonical system, matter can be exchanged among the systems in the ensemble. In this ensemble all the systems are characterized by fixed values of V, T and chemical potential, μ. The constancy of T and μ is ensured by supposing that the systems in ensemble are in equilibrium with a reservoir with which they can exchange both heat and matter. The phase space in this ensemble is the union phase-spaces corresponding to all values of the variable N and the ensemble probability density gives the probability both that the system contains N particles and that the coordinate and momenta of the particle are respectively $\vec{r}^N$ and $\vec{p}^N$. At equilibrium the probability density is

$$f_0(\vec{r}^N,\vec{p}^N,N) = \frac{1}{N!}\frac{h^{-3N}\exp(N\beta\mu)\exp[-\beta\mathcal{H}_N(\vec{r}^N,\vec{p}^N)]}{\Xi(\mu,V,T)}$$

Where the grand canonical partition function Ξ is given by

$$\Xi = \sum_{N=0}^{\infty} \frac{h^{-3N}}{N!} \exp(N\beta\mu) \iint exp[-\beta\mathcal{H}_N(\vec{r}^N,\vec{p}^N)]\, d\vec{r}^N, d\vec{p}^N \qquad (1.23)$$

1.4: Equilibrium particle Densities and Distribution functions

Phase-space probability density $f_0^{(N)}(\vec{r}^N,\vec{p}^N,t)$ although describes the system in detail, we may not need this detailed description always. If we are interested only in the behaviour of a sub set of particles of size n, say, then the unwanted information can be eliminated by integrating $f^{(N)}$ over the coordinates and momenta of the remaining (N-n) particles. We therefore define a reduced probability density function $f^{(N)}(\vec{r}^N,\vec{p}^N,t)$ for *n<N by*

$$f^{(N)}(\vec{r}^N,\vec{p}^N,t) = \frac{N!}{(N-n)!} \iint f^{(N)}(\vec{r}^N,\vec{p}^N,t)\, dr^{(N-n)} dp^{(N-n)} \qquad (1.24)$$

Where we use the notation $\vec{r}^N \equiv \{\vec{r}_1,\vec{r}_2,\vec{r}_3,\dots\dots..,\vec{r}_n\}$and $\vec{r}^{N-n} \equiv \{\vec{r}_{n+1},\vec{r}_{n+2},\dots\dots..,\vec{r}_N\}$. The meaning of $f^{(N)}(\vec{r}^N,\vec{p}^N)d\vec{r}^N, d\vec{p}^N$ is $\frac{N!}{(N-n)!}$ times the probability of finding any subset of n particles in the reduced phase-space element $d\vec{r}^N, d\vec{p}^N$ at time t, irrespective of the coordinates and momenta of the remaining particles. The factor *N!/(N-n)!* is the number of ways of choosing *n* particles from *N.*

For a system at equilibrium, integration of a reduced phase-space distribution function over the reaming momenta yields an equilibrium particle density $\rho^{(n)}(\vec{r}^N)$, where $\rho^{(n)}(\vec{r}^N)d\vec{r}^N$ is *N!/(N-n*)! times the probability of finding n particle of the system with coordinate in the element$d\vec{r}^N$ of coordinate space, irrespective of the positions of the remaining particles and irrespective of all momenta. The particle density and the equilibrium particle distribution function provide a complete but compact description of the structure of a fluid. Knowledge of particle distributions of any system are sufficient to calculate equation of state and other thermodynamic properties of the system.

In a Canonical ensemble (NVT), the *n*-particle density is defined as

$$\rho_N^{(n)}(\vec{r}^N) = \frac{N!}{(N-n)!}\frac{\iint exp\left[-\beta\mathcal{H}_N(\vec{r}^N,\vec{p}^N)\right]d\vec{r}^N, d\vec{p}^N}{Q_N(V,T)} \tag{1.25}$$

$$= \frac{N!}{(N-n)!}\frac{\int exp[-\beta U_N(\vec{r}^N)]d\vec{r}^{(N-n)}}{Z_N(V,T)}$$

And is normalised such that

$$\int \rho_N^{(n)}(\vec{r}^N)d\vec{r}^N = \frac{N!}{(N-n)!}.$$

For a homogeneous system, where $\rho_N^{(1)}(\vec{r})$ is independent of $\vec{r}$, we can write

$$\int \rho_N^{(1)}(\vec{r}) = \frac{N}{V} = \rho$$

In the special case of ideal gas, $U_N(\vec{r}^N) = 0$ and thus $Z_N(V,T) = V^N$. Thus the n-particle density of the ideal gas

$$\rho_N^{(n)}(\vec{r}^N) = \frac{N!}{(N-n)!}\frac{\int d\vec{r}_{n+1}, d\vec{r}_{n+2}, \ldots\ldots\ldots, d\vec{r}_N}{V^N} \tag{1.26}$$

$$= \frac{N!}{(N-n)!}\frac{V^{N-n}}{V^N}$$

$$= \frac{N!}{(N-n)!\,N^n}\rho^n$$

Similarly, the two particle density of an ideal gas is given by

$$\rho_N^{(2)}(\vec{r}_1,\vec{r}_2) = \rho^2\frac{N!}{N^2(N-2)!} = \rho^2\frac{N(N-1)}{N^2} = \rho^2(1-\frac{1}{N}).$$

The n-particle distribution function $g_N^{(n)}(\vec{r}_n)$ is defined in terms of the corresponding particle density by

$$g_N^{(n)}(\vec{r}^n) = \frac{\rho_N^{(n)}(\vec{r}_1,\ldots,\vec{r}_n)}{\prod_{i=1}^{n}\rho_N^{(1)}(\mathrm{r_i})}.$$

For a homogeneous system

$$g_N^{(n)}(\vec{r}^n) = \frac{\rho_N^{(n)}(\vec{\mathrm{r}}^{\mathrm{n}})}{\rho^n}$$

or

$$\rho^n g_N^{(n)}(\vec{r}^n) = \rho_N^{(n)}(\vec{\mathrm{r}}^{\mathrm{n}}) \qquad (1.27)$$

The *n*-particle distribution function measure the extent to which the structure of the fluid deviates from complte randomness. If a system is isotropic as well as homogeneous, the pair distribution function $g_N^{(2)}(\vec{r}_1,\vec{r}_2)$ is a function of only separation, $r_{12} = |\overrightarrow{r_1} - \overrightarrow{r_2}|$; it is thus usually called the ‘radical distribution’ function and written simply as *g(r).* The function*g(r)* is very useful quantity to understand the structure and thermodynamics of the liquid system.

The particle density can also be written in terms of δfunction of position.

$$\langle\delta(r-r_1\,)\rangle=\frac{1}{Z_N}\int\delta(r-r_1)\exp[-\beta V_N(r_1,r_2,\ldots\ldots,r_n)]dr^N \qquad (1.28)$$

$$=\frac{1}{Z_N}\int\ldots.\int exp[-\beta V_N(r_1,r_2,\ldots\ldots,r_N)]\,dr_2\;\ldots\ldots dr_N \qquad (1.29)$$

Comparing with equation (1.21), it shows that

$$\rho_N^{(1)}(r)=\langle\textstyle\sum_{i=1}^{N}\delta(r-r_i)\rangle \qquad (1.30)$$

This represents the ensemble average of microscopic particle density $\rho(r)$.In a similar way, the average of a product of two δ −functions is given by

$$\langle\delta(r-r_1)\delta(r^{'}-r_2)\rangle=\frac{1}{Z_N}\int\delta(r-r_1)\delta(r^{'}-r_2)\exp[-\beta V_N(r_1,r_2,\ldots\ldots,r_n)]dr^N, \qquad (1.31)$$

whichimplies that

$$\rho_N^{(2)}(r,r^{'})=\langle\textstyle\sum_{i=1}^{N}\sum_{j=}^{N}\delta(r-r_1)\delta(r^{'}-r_2)\rangle. \qquad (1.32)$$

In a straight forward way, it can be shown that

$$\langle\frac{1}{N}\textstyle\sum_{i=1}^{N}\sum_{j=}^{N}\delta(r-r_j\;+r_i)\rangle=\frac{1}{N}\int\rho_N^{(2)}\,(r^{'}+r,r^{'})dr^{'} \qquad (1.33)$$

If the system is both homogeneous and isotropic then,

$$\langle\frac{1}{N}\textstyle\sum_{i=1}^{N}\sum_{j=}^{N}\delta(r-r_j\;+r_i)\rangle=\frac{\rho^2}{N}\int g_N^{(2)}\,(r,r^{'})\mathrm{dr}^{'}=\rho g(r) \qquad (1.34)$$

The above equation is the simple formulation of g(r) in terms of the position of the particles. This structural quantity is experimentally measurable (radiation scattering experiment) and often used to deduce various physical properties of fluids. The definition of *g(r)* implies that on average the number of particles lying within the range r to $(r + dr)$ from a reference particle is $4\pi r^2 \rho g(r) dr$ and the peaks in $g(r)$ represent “shells” of neighbors around the reference particle. Integration of $4\pi r^2 \rho g(r)$ up to the position of the first minimum in the g(r) therefore provides an estimate of the number of first nearest-neighbours, commonly known as “coordination number”.

The static structure factor S(k) is a quantity which is directly measurable from scattering experiments and this quantity can be expressed as the correlation of the Fourier components of the density viz.

$$S(K) = \langle \frac{1}{N} \rho_K \rho_{-K} \rangle \tag{1.35}$$

ρ_K is the Fourier component of microscopic density given by

$$\rho_K = \int \rho(r) \exp(-iK.r)\, dr = \sum_{i=1}^{N} \exp(-iK.r_i) \tag{1.36}$$

The second equality appears due to use of equation (1.30) and subsequent integration involving δ function.

Use of equation (1.36) into equation (1.35) yields

$$S(K) = \langle \frac{1}{N} \sum_{i=1}^{N} \sum_{j=1}^{N} \exp(-iK.r_i) \exp(-iK.r_i) \rangle \tag{1.37}$$

$$= 1 + \langle \frac{1}{N} \sum_{i=1}^{N} \sum_{j \neq i}^{N} \exp(-iK.(r_i - r_j)) \rangle$$

$$= 1 + \frac{1}{N} \iint \exp[-iK.(r - r')]\, \rho_N^{(2)}(r - r') dr dr'$$

$$= 1 + \rho \int g(r) \exp(-iK.r)\, dr \tag{1.38}$$

Now, assuming that the system is translationally invariant, we get

$$\rho g(r) = (2\pi)^{-3} \int [S(K) - 1] \exp(iK.r)\, dK \tag{1.39}$$

Simplification of this gives

$$S(K) = 1 + 4\pi\rho \int_0^{\infty} r^2 \frac{\sin(Kr)}{Kr} g(r) dr \tag{1.40}$$

1.5: Time Correlation Functions and Transport Coefficients

Similar to structural properties, statistical mechanics also provides relation between the time correlation function and dynamical properties.[1]Generally, the time correlation between two different quantities A and B is described as

$$C_{AB}^{norm} =< \delta A \delta B >/\sigma(A)\sigma(B) \qquad (1.41)$$

The absolute values of C_{AB} is normalized in such a way that its values lies in between 0 to 1. Values near 1 indicate high degree of correlation. This relation can be used to calculate time dependency of a function if the desired property is being evaluated at two different time steps. The time integral of time correlation function is often related with microscopic transport properties. The non-normalized form of this time correlation function is

$$C_{AB}(t) = \langle \delta A(t) \delta B(0) \rangle_{ens} = \langle \delta A\big(\Gamma(t)\big) \delta B(\Gamma(0)) \rangle_{ens} \qquad (1.42)$$

$$C_{AB}^{norm}(t) = C_{AB}(t)/\ \sigma(A)\sigma(B) \qquad (1.43)$$

For identical phase space function, the time correlation is known as auto correlation function ([C_{AA}(t)].

$$C_{AA}^{norm}(t) = C_{AA}(t)/\sigma^2(A) = C_{AA}(t)/\sigma^2(A) \qquad (1.44)$$

This quantity is very important since this can provide a clear picture of the dynamics of the fluids. The integral (from 0 to ∞) of this quantity is called correlation time (t_A) which is often used to calculate microscopic transport properties. The flourier transform of t_A is generally correlated to experimental spectra.

Transport coefficients are defined in terms of the response of a system to a perturbation. In case of diffusion coefficient, it is related in between particle flux and concentration gradient. Any transport coefficient is in general infinite time integral of an equilibrium time correlation function of the form

$$\gamma = \int_0^\infty dt \ < \dot{A}(t)\dot{A}(0)> \qquad (1.45)$$

Hereby, γ is the transport coefficient and $\dot{A}$ is the time derivative of A, the variable term present in perturbation of the Hamiltonian. The above relation is known as Green-Kubo relation. Similarly, one can integrate the right hand side of the above relation to obtain another relation, known as Einstein relation which relates transport coefficient $\gamma$with the quantity A such that

$$2t\gamma = \ \langle (A(t) - A(0))^2 \rangle. \qquad (1.46)$$

For example, the diffusion coefficient (D) of 3D fluid can be expressed by using these equations.

$$D = \frac{1}{3}\int_0^\infty dt\, \langle v_i(t).v_i(0)\rangle \qquad (1.47)$$

Where ϑ_i(t) is the centre of mass velocity of a single molecule. The corresponding Einstein relation is

$$2tD = \frac{1}{3}\langle |r_i(t) - r_i(0)|^2\rangle \qquad (1.48)$$

$r_i(t)$is the position of molecule. The Einstein relation is applicable in case of very long times.

1.6:Nature and Scope of the Present Work

In the present thesis,we present molecular dynamics simulation results of our investigations on structure and dynamics of water in bulk, and at molecular and nanoscopic interfaces.The present thesis consists of six chapters and a brief discussion of each of these chapters is given below.

In **Chapter 1**, the present thesis starts with a very general introduction about importance and applicability of water and aqueous solutions, microscopic local structure and dynamics of bulk water and how the structure and dynamics get modified at interfaces. As a theoretical tool we have used molecular dynamics simulation throughout these studies. Therefore, a brief introduction about the molecular dynamics simulation methodology has been presented in this chapter. As a result of molecular dynamics simulation, we obtain time evolution of the phase-space in terms of trajectories (sets of positions and momenta of all the particles) of the system. From these microscopic variables, various structural, thermodynamic and dynamic properties of the system can be obtained through the application of classical statistical mechanics. Therefore, we present here a brief theoretical description of statistical mechanical *n*-body distribution functions which are used for gauging local structure of a fluid and the time correlation function, which is used for calculating various dynamical quantities. Finally, in the last part of the Chapter 1, the nature and scope of the present thesis is discussed.

Water is known to be an anomalous liquid. There are around 73 different anomalies involving structural, thermodynamic and dynamic properties of water.[12,68] Out of all these anomalies, density anomaly (temperature of maximum density at 277K) is the most talked-about anomaly of bulk water.[13, 69,70] A large body of work has been devoted to understand the correlation, if any, between the local structural motif and the density anomaly.[71] However, contradictory predictions and observations about this correlation have made this field ever challenging.[72-96] In **Chapter 2** of this thesis, we have therefore explored different structural aspects of liquid water at ambient pressure to understand the origin of its density anomaly. In order to explore structural and dynamic properties of water by using the classical force-field based molecular dynamics simulation, an accurate model of water is necessary. In the course of this work it is found that computed results on various structural parameters and properties as a function of temperature as obtained from different available atomistic models of water are considerably different. This model dependence of the results clearly obstructs further progress in this direction and necessitates investigation of a single parameter through which all these results from different models can be correlated. In this work, we have established a new yardstick (average number of hydrogen bonds), which is able to correlate apparently disparate results from all these water models. Further, by introducing a new definition of 1st solvation shell of a water molecule in the bulk water, the competitive effects of thermal expansion and contraction due to angular distortion have been shown to lead to the density anomaly of water along the 1 atm isobar. The present work clearly demonstrates that density anomaly of water at ambient pressure can be explained without invoking the concept of structural and density inhomogeneity of water. Apart from structural and density anomalies, water is known to possess a number of dynamic anomalies as well. As the structural and thermodynamic properties of bulk water are shown to be model dependent, the dynamical properties also show considerable dependence on the details of the water model used in the MD simulation. Therefore, here the objective is to check whether average number of hydrogen bond, which is able to correlate disparate structural properties obtained from different models into a single context, can also correlate disparate results obtained from different water models on the dynamics of bulk water. Although disparate results on temperature dependence of structural and thermodynamic properties obtained from different models are found to be correlated in terms of average number of hydrogen bonds, similar correlation among the results on dynamical properties of water arising from different water models in terms of average number of hydrogen bonds does not exist.

Isotopically substituted water i.e. deuterium oxide (D_2O), commonly known as heavy water is an important material in view of its relevance in nuclear, chemical, medical and pharmaceutical industries.[97-108] Molecular dynamics simulation is an enviable theoretical tool to calculate various properties of heavy water at ambient as well as extreme conditions of temperatures and pressures. However, the bottleneck in this direction stems from the absence of a suitable atomistic model of heavy water. A three-site SPC/HW heavy water model, to the best of our knowledge, is the only model available for heavy water. Although this model is shown to reproduce properties of heavy water at ambient condition quite accurately, its applicability has never been tested beyond the ambient condition.[97] In **Chapter 3**, we have therefore investigated the applicability of this model at different temperatures in the range of 223K to 360K at ambient pressure by calculating various thermophysical properties and comparing them with the available experimental or literature values. What emanates from this study is that, the SPC/HW model although reproduces experimental data for heavy water at room temperature appreciably well, it largely fails at lower range of temperatures. A comparative study of different thermophysical and structural properties of D_2O (SPC/Hw) and H_2O (SPC/E) has also been presented. Finally, the effect of various potential parameters such as molar mass and partial charges on atoms on the results has been estimated and the findings can act as a guide for further development of a new model for heavy water.

So far we have dealt with structure, dynamics and properties of bulk water and heavy water. Interesting modifications of structural, dynamic and thermodynamic properties of water can be observed when water meets interfaces.[19,29,30,109-119] The interface may arise due to solvation of different solute molecules in water or due to physical contact of water with a large extended solid surface. In the former case a molecular interface is generated and it is interesting to know whether structural integrity of water will be retained in presence of such molecular interfaces. In this connection, structural information of two molecular interfaces namely that of urea-water and guanidinium chloride (GdmCl)-water are extremely important as these two interfaces are relevant to protein denaturation.[120-133] The **Chapter 4** of this thesis deals with the structural and dynamical aspects of these interfaces and its relevance in elucidating role of water in the underlying mechanism of protein denaturation. This chapter is divided into two parts. In **Part A**, we have investigated the effect of increasing concentration of urea on various structural and dynamical properties of water in the solution.[23] By calculating various order parameters that gauge the structural integrity of water, it has been demonstrated that tetrahedral and hydrogen bonding structure of urea remain unaffected at least up to the concentration of 9M urea. Exploration of the dynamical features of the aqueous urea solution reveals that with increasing concentration of urea, translational diffusivity decreases considerably, whereas the rotational dynamics remains almost unaltered with the increasing urea concentration.

The **Part B** of this chapter has dealt with another molecular interface created due to solvation of guanidinium (Gdm) chloride, another very useful chemical denaturant of protein, in water. Mainly the effect of increasing concentration of guanidinium chloride (GdmCl) on the structural and dynamical properties of water has been thoroughly investigated here. The two major issues, one dealing with the staked ion-pair formation of the Gdm moieties and the other on the influence of guanidinium ion on the tetrahedral and hydrogen bonding structures of water in the aqueous solution of GdmCl, have been investigated. What transpires from this study is that the water structure is not significantly perturbed by the presence of GdmCl. The finding from this study supports the so-called direct mechanism of protein denaturation according to which Gdm moieties of the denaturant directly attacks the similar (arginine) moieties of the protein in parallel-staking orientation. In order to confirm it we have further extended our study[24] by incorporating one polypeptide into the aqueous solution of Gdmcl and confirmed the existence of such staking between the Gdm ion and the arginine moiety of the peptide. We are also able to establish that such parallel staking orientations (of the arginine moieties) can be observed in case of temperature denaturation of an arginine based peptides. Apart from these, various dynamical properties at different concentrations of the GdmCl have also been calculated.

Manifestation of various properties of water at a nanoscopic or larger interface formed by water and a large surface is dramatically different from the same at the molecular level interface. It has a huge significance in terms of bio-macromolecular stability and protein folding if the interface is made up of nanoscopic or larger hydrophobic objects and water. In fact, for a nanoscopic or larger hydrophobic solute in water, a new interaction, the so called hydrophobic interaction originates and it is thought that the hydrophobic interaction is responsible for self-assembly and aggregation/folding of many bio-macromolecules. [109-119]However, measuring hydrophobicity of such a nanoscopic interface using the conventional method of measuring contact angle is rather difficult and therefore defining new order parameters to estimate hydrophobicity at the nanoscale is essential. The **Chapter 5** of this thesis deals with the characterization of hydrophobicity at the nanoscale. For this, we have considered a nanoscopic paraffin like plates in water and hydrophobicity has been tuned by altering the attractive part of the plate-water dispersion interaction. We have calculated different structural parameters and follow their changes as a function of degree of hydrophobicity. In this work, we are able to identify a few order parameters, each one of which can be a promising descriptor to gauge the hydrophobicity at the nanoscale.

In all these investigations as described in **Chapters 2-5**, we were involved in the modelling at the atomistic lengthscale. In many cases, where we deal with extended solid-water interfaces such as nanomaterial-water interfaces, modelling at the atomistic lengthscale may be computationally expensive and therefore use of a coarse-grained (CG) description might be beneficial. In this context, a spherically symmetrical two-lengthscale potential[134-137] has been found to reproduce almost all the anomalies of liquid water. In **Chapter 6** of this thesis we have used this coarse-grained description to study the hydration and dewetting behaviour of one of the very important nanomaterial C_{60}. Using molecular dynamics simulation, it is demonstrated how solvation characteristic changes with the changes in the degree of attractiveness in the interaction between the atoms of the C_{60} and CG water.

Finally, in **Chapter 7**, a brief summary of the work described so far has been presented. This chapter also describes how the present work can be extended in near future. It will also describe how the knowledge emanated from the present studies can be used in understanding structure and dynamics of fluids at non-aqueous solute-solvent interfaces.

Chapter 2

Structural and Dynamical Correlations in Water and its Density Anomaly

2.1: Introduction

Water, one of the most ubiquitous and abundant materials on earth, has central importance in most of the chemical and biological processes.[12]Liquid water is not only used as an universal solvent, it is considered to be the matrix of life as well. The small molecular size, high dielectric constant, strong electrostatic interactions, high diffusivity and ability to manifest hydrophobic interaction among hydrophobic groups present in it make it different from all other liquids and can be held responsible[14,16,17] for its remarkable ability to dissolve or stabilize varieties of solutes including proteins, nucleic acids, lipids etc. In chemical and biological processes, solvents play a very important role in deciding a solute's structural stability and its chemical and biophysical activities. Actually, life evolves in water medium and proteins manifest its fascinating activities in aqueous medium only. The solvation process is basically controlled by the interaction of the solvent molecules with the solutes. Because of its extended hydrogen-bonded network structure, water is different from many simple liquids.

Water is an intriguing liquid not only because it has a completely different open tetrahedral local structure as compared to a closed packed local structure of a simple liquid, but also due to its number of anomalous properties.[138-143]It is believed that a relationship exists between the local structure and the anomalous properties of water. A large number of studies[71-77] has been devoted to understand this relationship by using atomistic models of water. Different groups have used different models of water and have come up with seemingly disparate results. Three-site models, because of their simplicity and less computational demand, are extensively used in bio-molecular simulation. Four- and five-site models being more detailed yield better results as compared to the three-site models, but at the cost of computational economy associated with the three-site models. However their accuracy in reproducing properties of water is not directly linked to the microscopic details of the molecular description in the model. As for example, results obtained from four-site models such as TIP4P/2005[52,79] and TIP4P-Ew[80]are better than those obtained from a more involved five-site TIP5P[53] model. Although local structural order as predicted by radial distribution function or structure factor *S(Q)*, which can be obtained experimentally, has direct connection[67] to many of the properties of water, analyses of these structural correlations do not provide any direct clue to understand the anomalies of water. This problem is further compounded by apparently disparate results for structural, thermodynamic and density anomalies obtained from these models.[83] Therefore, one of the major hurdles in this direction is the non-existence of a common framework to compare these apparently disparate results obtained from different water models. Efforts in this direction have been made and it has been observed[83] that many of the water properties are temperature-shifted for different models. In order to understand local structure and anomalies of water better, a direct relation between the structure forming capabilities of all these models and the density anomaly of water has to be established. To achieve this aim, in the present work we compare various local orders and anomalies of water as obtained from different water models by identifying a key structural parameter that governs properties of water and therefore reconciles disparate findings obtained from different models.

As has already been mentioned, water has a number of anomalies and the best known of all these anomalies is the density anomaly, in which average bulk density of water shows a maximum at around 4°C at ambient pressure. Despite many efforts,[52,53,67,71-96] a simple and comprehensive explanation for the anomalies of water is still lacking. Even in recent past it was intensely argued on the nature of local structural motif of liquid water. A long standing view emerged[96] from x-ray and neutron scattering experiments, thermodynamics data, and molecular simulations has interpreted liquid water in terms of a locally tetrahedral liquid structure, where a water molecule is H-bonded on an average to four nearest neighbors. This traditional view was recently challenged by Wernet et al.[144], who showed using x-ray Raman and absorption spectroscopy along with theoretical calculation that the structure of first coordination shell in liquid water is not tetrahedral. Instead, they claimed that room temperature liquid water consists of a large fraction (98%) of broken H bonds and on an average each water molecule is associated with only two strong H bonds. However, this view has been strongly contended by many groups.[145-148]By using state-of-the-art experimental techniques, atomistic and ab-initio molecular dynamics simulations, these groups have reestablished[90,145-149]the traditional picture that water is a tetrahedral hydrogen bonded network with some broken bonds.

Many people have tried to find out a universal relationship between the density and structure of water, primarily because the relation is fundamental to the understanding of water's anomalous properties and also due to the existence of varieties of structures in ice. The most important of the several hypotheses[84-85]proposed in recent literatures is the liquid-liquid critical point view, according to which in the supercooled region water has a metastable critical point associated with a first order phase transition between a high-density liquid (HDL) and a low-density liquid (LDL) phases. By extending this hypothesis into the ambient region, water's anomalous properties can be interpreted as interplay between the structurally different HDL and LDL phases of water. In fact, in a recent experimental investigation, Huang et al.,[88]based on their analysis of $S(Q)$ data at low Q region, have proposed that extended clusters of HDL and LDL are present even at ambient conditions. This inference has been drawn on the basis of observed enhancement of $S(Q)$ in the low Q region and has been interpreted in terms of density fluctuations of two structurally distinct clusters of different densities. However, this view has been strongly debated by many groups.[76,89-91]Matsumoto[76] has found that two opposing linear correlations, normal thermal expansion against temperature and contraction due to angular distortion, are responsible for the density anomaly of water without invoking structural heterogeneity. Clark et al.[89]and Soper et al.[90] have shown that the enhancement of *S(Q)* at small angle (i.e. small *Q*) is a consequence of normal density fluctuations of the stochastic processes present in a single component fluid. Their simulation of TIP4P-Ew water has shown no bimodality in the density histogram in the length scales ranging from 0.6 to 6 nm and thus emphasizes the fact that enhancement of *S(Q)* at low-*Q* is not due to coexistence of two different local structural motifs in liquid water at the ambient condition. It has been demonstrated further by Sedlmeieret al.[91] that there are only small spatial correlations between local density and structural fluctuations, indicating no direct connection between density-density correlation and spatial correlation of structure in liquid water. Poole and coworkers[92] and Tse and coworkers[93] although have found mixture-like behavior and density fluctuation in supercooled water, no density inhomogeneity has been observed[93] in water at ambient conditions. In a very recent simulation study, Limmer et al.[150] have explored free energy landscape of water for a range of temperatures and pressures including state points where amorphous behaviour is unstable with respect to the crystal. They could not find more than a single liquid basin in the entire range of temperatures and pressures and thereby exclude the possibility of the proposed liquid-liquid critical points. However, in support of the findings of Huang et al.[88], very recently Patey and coworkers[94]have shown that if water can be considered as a mixture of two species having different local angular arrangements as measured by the tetrahedral order parameter, considerable concentration fluctuations can occur even at ambient condition and this concentration fluctuation correlates density fluctuation, providing support and explanation of the notion of structural polyamorphism in water.

However, this analysis[94] is based solely on considering water as a mixture of two different kinds of molecular arrangements distinguished entirely by the tetrahedral order parameter, $q_{i,}$ a quantity used to estimate extent of tetrahedrality in a water molecule *i*.The median value of the q_i has been used as a demarcation between two structurally different local motifs, one with more and another with less orientationally ordered structures. Therefore, the underlying assumption is that all the water molecules having q_i values less than the median have the same fixed local structure, which is structurally distinct from the structural motif of a water molecule with q_i value above the median. However, local structure and hence the tetrahedral order parameter q_i of a molecule is changing at every instant of time and moreover, the median of the q_i values changes with temperature. Therefore, ensemble average of these instantaneously changing orientational arrangements may not lead to a description of water as a mixture of two different structurally distinct entities. Moreover, unless we know explicitly about the origin of a particular q_i value i.e. what local structural arrangement corresponds to what q_i value, it is a very difficult to conceive water as a mixture of two structural arrangements even temporally. It is well known[90] that at a low enough temperature, distribution of q values is unimodal with a single peak at around $q=0.83$, suggesting almost tetrahedral arrangements of the four neighbors of a central molecule. As we increase the temperature, a new peak appears at an intermediate q value of around 0.5. No clear explanation of this low-q peak is available in the literature. A deeper insight[95]into the origin of the low-q peak in the distribution of tetrahedral order parameters and its relation with water's local structure is therefore essential to understand the relation of this local order (as represented by the q value) with local structural motifs of water.

In the present investigation, we therefore intend to focus our attention in correlating local hydrogen bonding structure with different structural orders and density anomaly of water. In the process we analyze the origin of low-q peak in the distribution of tetrahedral order parameters i.e. the correspondence of the low-q peak to the local structural motif. Present study based on computer simulations of various models of water suggests that water can be viewed as a dynamical mixture of distinctly different solvation shells of differently (two-, three-, four-, five-) hydrogen-bonded molecules. By taking into consideration the void space between first and second shells of water, the density anomaly can then be nicely interpreted in terms of the change in composition of this mixture with the change in temperature without incorporating the idea of large length scale structural polyamorphism.

Apart from a number of structural and thermodynamic anomalies, water is known to possess a number of dynamical anomalies as well.[151-155] In the backdrop of preceding investigation on correlation between structural orders and thermodynamic anomalies, it is tempting to investigate whether any such correlation exists between these orders and its dynamical anomalies as well. As already mentioned in case of structural and thermodynamic anomalies, the first step towards establishing such a correlation is to find out a suitable structural order parameter, which can concur disparate dynamical properties obtained as a result of using different models of water. The main objective of this part of the work is to verify whether average number of hydrogen bonds, which is shown to correlate disparate structural and thermodynamic properties obtained from different water models, can also reconcile disparate dynamical properties resulting from different water models.

2.2: Models and methods:

In the present investigation, we have used six different rigid body atomistic models of water having fixed bond lengths and bond angles. These are TIP3P,[48,49]SPC,[50]SPC/E,[51]TIP4P, TIP5P[52] and TIP4P/2005[53]. In each of these models only oxygen atom is considered to be a Lennard-Jones (LJ) interaction site and the partial charges are distributed on atomic sites as well as virtual sites in some of the cases.

For all the simulations, we have used 512 water molecules placed in a cubic box. The simulations were performed in NPT ensemble with molecular dynamics extended system approach of Nose and Anderson.[64]Periodic boundary conditions and minimum image convention were used in all three directions. For all three site models, the bonds and the angle of a water molecule were constrained by fixing two bonds and HH distance using RATLE algorithm and the Ewald method was adopted for treating electrostatic interactions. Equations of motion were integrated using velocity Verlet algorithm with a time step of 2 fs. For four and five site models, we have used GROMACS[156] simulation program with PME method for electrostatics. All the simulations were carried out at a target pressure of 1 atm at a number of target temperatures, range of which for each model is shown in Table 2.1. For simulations at temperature 285K and below, first 10 ns was discarded for equilibration and trajectories for next 10 ns have been stored for analyses whereas for state points with temperature 285K and above first 3 ns was discarded for achieving equilibrium and next 5 ns runs have been stored for analyses.

Table 2.1: Temperature range and TMD of all the water models

Model	**SPC/E**	**SPC**	**TIP3P**	**TIP4P**	**TIP4P/2005**	**TIP5P**
Temperature range in K	223-373	200-373	150-373	223-360	246-370	260-348
TMD (K)	240	221	200	260.5	285	285
<n_{HB}> at TMD	3.76	3.75	3.74	3.68	3.69	3.38
q_4	0.715	0.716	0.692	0.694	0.691	0.689
Q_6	0.271	0.270	0.268	0.270	0.269	0.271

Local orders: Ice has an almost perfect three-dimensional hydrogen-bonded network with tetrahedral arrangements. For a perfectly tetrahedral ice like structure, there are four nearest neighbours around a central water molecule in the 1st shell and another twelve neighbours in the 2nd shell. Unlike ice, in bulk water there are broken hydrogen bonds due to randomness introduced by thermal energy and therefore perfect tetrahedral local order is not maintained. In order to measure the magnitude of oriental order in liquid water, two different orientational order parameters[71,75] for 1st and 2nd shells have been used here.

Tetrahedral order parameter and tetrahedral angle: Tetrahedral order parameter, q_i used to define extent of tetrahedrality of the local water structure involving four molecules in the 1st shell of a central water molecule *i* is defined as

$$q_i = 1 - \frac{3}{8}\sum_{j=1}^{3}\sum_{k=j+1}^{4}\left[\cos\theta_{jik} + \frac{1}{3}\right]^2 \qquad (2.1)$$

Where $\theta_{jik}$is known as tetrahedral angle formed by neighbours *j* and *k* with the central molecule *i*. The average value of the tetrahedral order parameter averaged over all the molecules N is then defined as

$$q_4 = \frac{1}{N}\left\langle \sum_{i=1}^{N} q_i \right\rangle. \qquad (2.2)$$

It quantifies the tetrahedral order of the system by measuring the deviation from ideal tetrahedral structure. In the above equation, angular brackets $\langle\ \rangle$ represent ensemble average. The equation is being formulated in such a way that the value of q_4 varies in the range of 0 to 1. When the central water molecule is located at the centre of a perfect tetrahedron with four nearest neighbours occupying the four vertices, values of $\cos\theta$ should be -1/3 and in that case

q_4 is equal to 1 [see equation. (2.1)]. For a perfectly random orientation, six angles formed by the combinations of any two of the four neighbours with the central molecule, are independent of each other. In this case, the value of the constant term in equation (2.1) can beobtained[71] from angular averaging of each of the terms in the summation viz. $\frac{\int_0^{\pi}\left[\cos\theta+\frac{1}{3}\right]^2 \sin\theta d\theta}{\int_0^{\pi}\sin\theta d\theta}=4/9$. In order to get a q_i value of zero for the random uncorrelated orientations, the normalization constant of 3/8 before the summation in the equation (2.1) arises from the contributions of six angles as 1/(6×4/9) as used by Errington and Debenedetti.[71] In the present investigation, apart from using four neighbours, we would like to calculate the tetrahedral order parameter for a central molecule with 2 and 3 (H-bonded) neighbours as well. Thereby the numbers of combined angles associated with a central molecule having 3 and 2 neighbours are three and one respectively. Accordingly, we have used modified normalization constants of ¾ [i.e. 1/(3×4/9)] for a central molecules with three neighbours and 9/4 [i.e. 1/ (1×4/9)] for a central molecule with two neighbours so that the tetrahedral order varies between 1 (perfectly tetrahedral) and 0 (uncorrelated random configuration).

Orientational order parameter for the second shell: Although the first shell of a water molecule in ice is almost tetrahedral, second shell of the hexagonal ice crystal forms an hcp lattice. In order to characterize the angular orientation of the second shell molecules around a central water molecule, therefore another order parameter Q_{6i} is generally used. It measures the angular preference of the twelve second-shell neighbours with respect to a central molecule towards fcc, bcc or hcp structures. In order to compute this quantity, 12 hypothetical bonds connecting each of the 12 second-shell neighbours and the central molecule are assigned and for each bond its azimuthal and polar angles (θ,ϕ) are computed.

Then the average of the spherical harmonics $\overline{Y}_{lm}(\theta,\phi)$ over all the 12 bonds of the central molecule *i* is calculated and from the average spherical harmonics the function

$$Q_{li} = \left[\frac{4\pi}{2l+1} \sum_{m=-l}^{m=l} \left| \overline{Y_{lm}} \right|^2 \right]^{1/2} \qquad (2.3)$$

is then calculated.[75] For *l=6* the average value of the orientational order parameter Q_6 for N molecules is calculated from the equation

$$Q_6 = \frac{1}{N} \sum_{i=1}^{N} Q_{6i} \ . \qquad (2.4)$$

Value of $Q_6$is large for most crystals; for example, it is 0.574 for *fcc,* 0.511 for *bcc*, and 0.485 for *hcp* structures and for uncorrelated systems, Q_6=0.289.

Hydrogen bond: Along with above mentioned orientational order parameters, number of hydrogen bond, n_{HB}, a water molecule forms with its neighbours, is considered as an alternative order parameter to measure extent of local arrangement of water molecules. The geometrical definition of the hydrogen bond is being adopted throughout this study. It takes into account both inter molecular separation, which is missing in case of orientation order parameters and associated angles involving oxygen as well as hydrogen atoms of two hydrogen-bonded water molecules. Thus, in our view, it carries a detailed description of the first shell than coordination number or q_i of a central molecule. According to the geometric criteria, two water molecules are considered to be H-bonded only if the inter-oxygen distance is less than 3.5 Å and simultaneously the hydrogen-oxygen (H-bonded) distance is less than 2.45 Å along with the H-O····O angle being less than 30°.Although the minima of the oxygen-oxygen radial distribution function (RDF) varies with temperature from around 3.2 to 3.75 in the temperature range studied here, we have chosen oxygen–oxygen distance to be 3.5

Å in all the cases as the change in OO distance has negligible effect on the average number of hydrogen bonds.

2.3: Results and Discussion:

2.3.1: Correlation of Structural Orders, Density anomaly and Hydrogen Bonding Network of Water

Two order parameters frequently used in analysing local structure of water are tetrahedral order parameter q_4 and orientational order parameter Q_6.The tetrahedral order parameter q_4,which measures the extent of tetrahedrality in the local structural environment involving one central water molecule and its four nearest neighbors, is calculated from the angles made by a central water molecule with any two of the four nearest neighbours. The orientational order parameter Q_6,on the other hand, measures angular arrangements of the 2nd shell neighbouring molecules with respect to a central water molecule. These two order parameters along with radial distribution functions provide angular and spatial arrangements of water in its local structure. In order to investigate temperature dependence of local structural order in water, we have calculated tetrahedral order parameter q_4 and orientational order parameter Q_6 as defined by equations (2.2) and (2.4) respectively for six different water models namely SPC, SPC/E. TIP3P, TIP4P, TIP4P/2005 and TIP5P at different temperatures. The temperature dependence of these two order parameters along P=1 atm. isobar for different water models is shown in Figure2.1(a) and (b) respectively. All the models follow the same general trend that the order parameters monotonically decrease with the elevation of temperature. But, the values of the order parameters obtained from different water models at a particular temperature are significantly different. It is important to note that different water

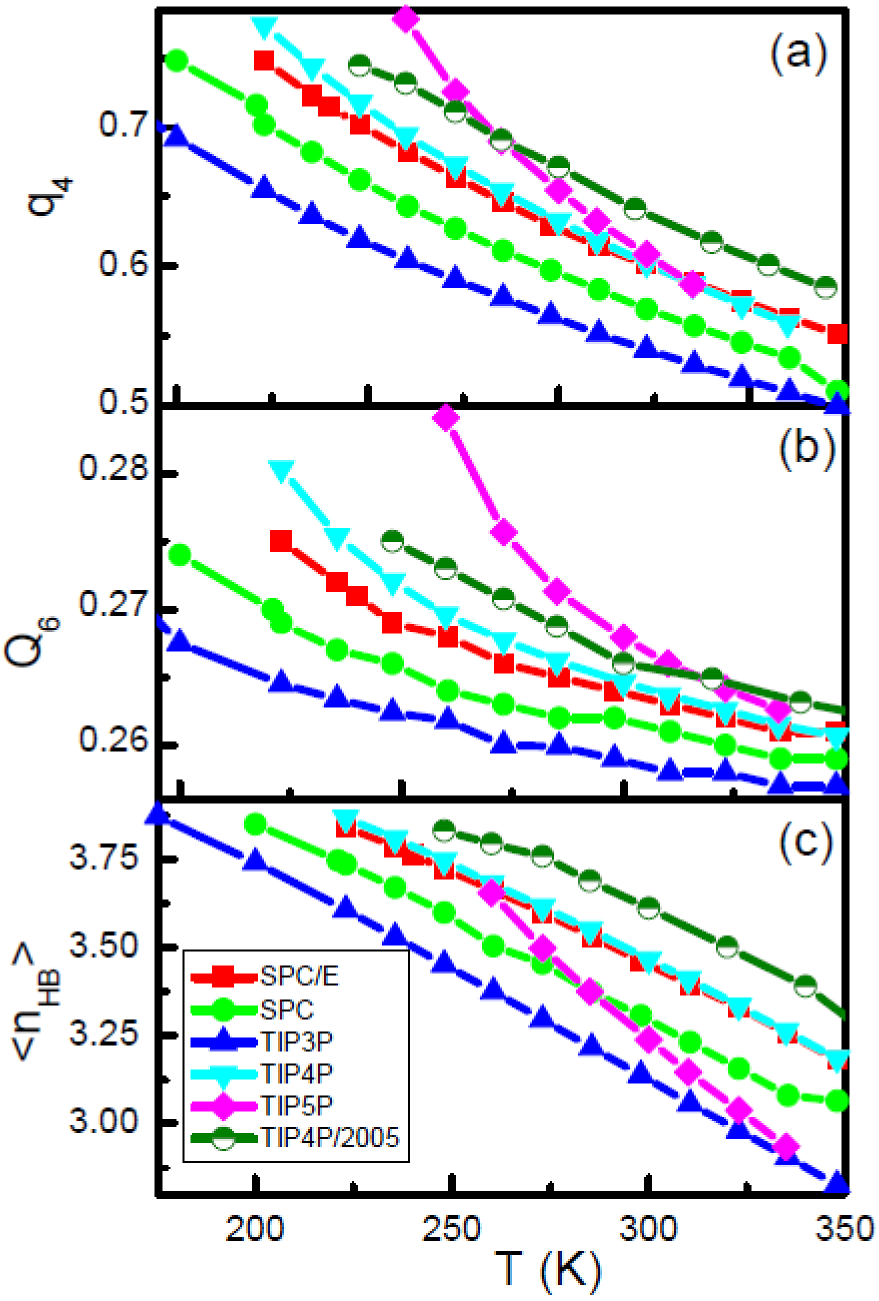

Figure2.1.Average values of (a) the tetrahedral order parameter, q4, (b)the orientational order parameter, Q6, for the second shell water molecules, and (c) the number of hydrogen bonds as a function of temperature for different models of water.

models differ from each other in molecular geometry and inter-molecular potential parameters resulting in significantly different hydrogen bonding network structure. This is illustrated in the plots of Figure2.1(c), which demonstrates the temperature dependency of the average number of H-bonds, $<n_{HB}>$for different water models. At a particular temperature, different models yield different $<n_{HB}>$. We know from previous study in literature that hydrogen bond is an integral part of water structure. Therefore, it can be expected that non-equivalence of average numbers of hydrogen bonds obtained from different models could be the reason for the disparate structural orders shown in Figure2.1(a) and (b). We therefore intend to verify whether $<n_{HB}>$ can be considered as a key parameter to reconcile apparently disparate temperature trends of the properties of water obtained from different water models.

Since both q_4 and Q_6 are related to mutual angular arrangements of 1st and 2nd shell neighbouring water molecules respectively, hence there is a probability of existence of a correlation between these orientational order parameter and $<n_{HB}>$, which is also dependent on the mutual orientation and distance between two molecules. Indeed when these two order parameters are represented as a function of $<n_{HB}>$, except TIP5P water model, all other models yield strikingly similar results (see Figure 2.2(a) and (b) for q_4 and Q_6 respectively). It signifies existence of a relationship between the orientation order parameter and H-bonding network structure of water over a wide range of temperatures. Existence of such a correlation is not so surprising in case of q_4, because it is calculated by considering four nearest neighbours, majority of which are hydrogen-bonded to the central molecule. However, the nice correlation observed between Q_6 and $<n_{HB}>$ [see Figure 2.2(b)] is a bit surprising as Q_6 is calculated based on the angular arrangements of the water molecules in the second shell with respect to a central molecule because it is highly improbable that a 2nd shell neighbour is directly connected to centre molecule through hydrogen bonding. The striking correlation between $Q_6$and $<n_{HB}>$ may be attributed to extended hydrogen bonding, This is probably because a molecule in the 2nd shell is connected to that in the 1st shell neighbour through hydrogen bonding, for which a specific relative angular arrangement between the two water molecules from these two shells are required and thus, orientation of the 2nd shell molecules is indirectly influenced by the orientation of the 1st shell water molecules, based on which q_4 has been calculated.

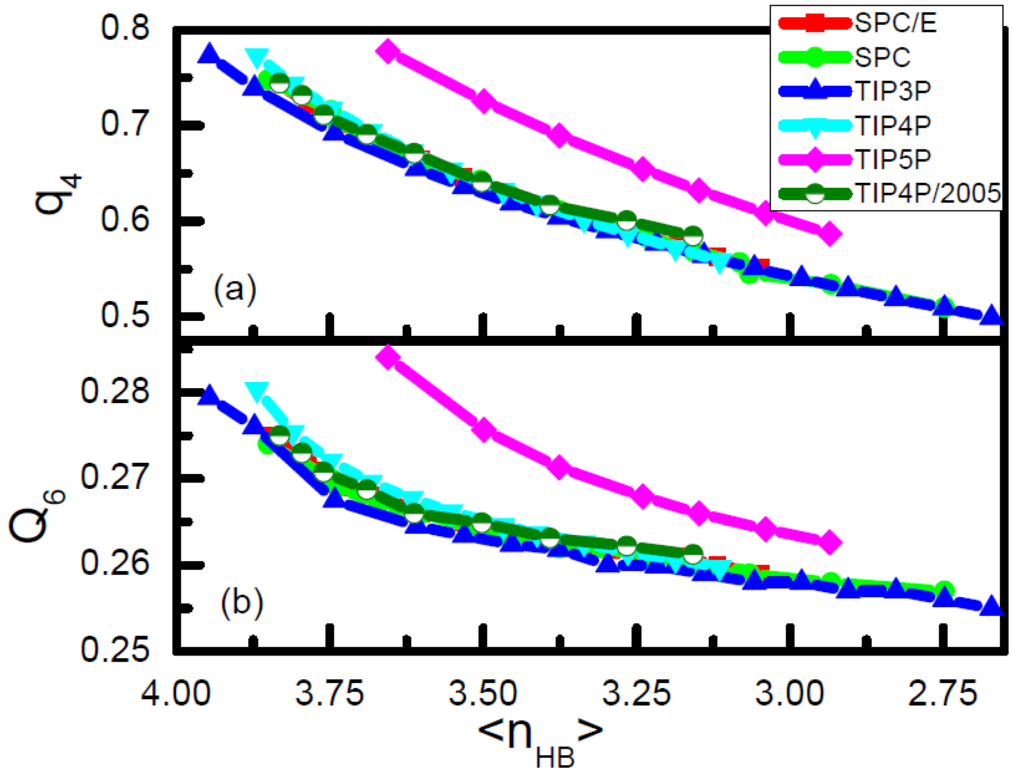

Figure 2.2. Average values of (a) the tetrahedral order parameter, q_4, and (b) the orientational order parameter, Q_6, as a function of the average number of hydrogen bonds, $\langle n_{HB} \rangle$, for different models of water.

Unlike q_4, Q_6 or $<n_{HB}>$, each of which decreases steadily with the increase of temperature, average density of water as a function of temperature passes through a maximum. When bulk average density of water is plotted as a function of temperature, it is found (see Figure 2.3(a)) that results evaluated from different water models are significantly different. In particular, locations of temperature of maximum density (TMD) (see Table 2.1) obtained from different water models are widely varied. However, when the densities from these different models are plotted as a function of $<n_{HB}>$ in Figure 2.3(b), we found data from all the models except TIP5P to be almost coinciding, forming a master curve (although plot of TIP3P model is slightly up-shifted, location of the TMD coincides with other models). The concurrent density peaks signify that the state corresponding to the TMD possesses a unique value of $<n_{HB}>$ irrespective of the models used. The values listed in Table 2.1 in fact reveal that TMD of any water model is associated with a fixed number of hydrogen bonds, $<n_{HB}> \approx 3.7$ and more interestingly, water has a specific orientational preference as indicated by almost the same values of q_4 and Q_6 at their respective TMDs irrespective of the water.

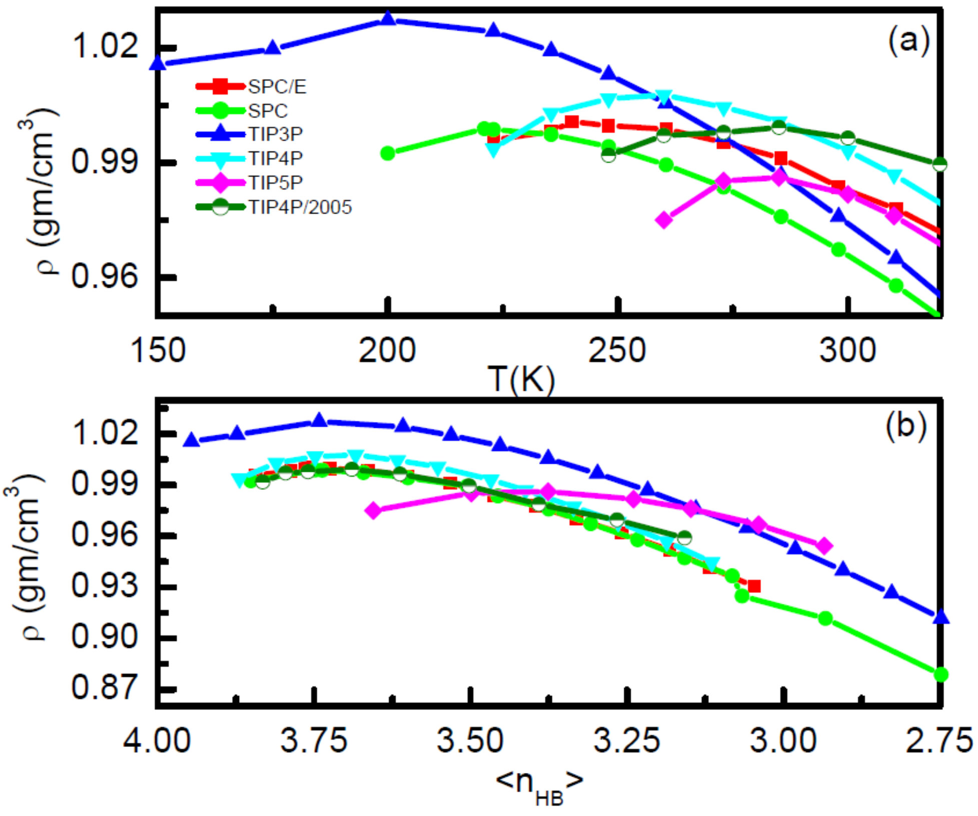

Figure2.3. Average density of water for different water models as a function of (a) temperature and (b) average number of hydrogen bonds.

models used. The TIP5P water model deviates considerably from the master curve formed by all other models. The problem related to TIP5P water model is well known in the literature[83,157] and it is probably because the increased preference for TIP5P water molecules to act both as tetrahedral hydrogen bond donors and acceptors.[158] It is also interesting to observe that the slope of the $<n_{HB}>$ vs. T plot for TIP5P model (see magenta line in Figure 2.1(c)) is quite different from that of any other model

In case of simple liquid, the RDF is generally considered to be one of the most vital structural order parameter, which can represent short ranged radial order and hence the local structural motif of a spherically symmetric liquid. As we have already discussed, water is a tetrahedral liquid and that is why, two more order parameters namely, tetrahedral and 2nd shell orientational order parameters are required to gauge the local structural arrangements of water completely. In the context of unifying the results obtained from different water models, it is therefore, necessary to check whether average number of hydrogen bonds, $<n_{HB}>$ can reconcile disparate RDFs obtained from different water models. To investigate this, we have calculated RDFs of different water models at different temperatures. It is found that at a given temperature, RDFs obtained from different water models are not the same. This has been illustrated in Figure 2.4. At 298K, the RDFs obtained from different water models are quite dissimilar. This difference is very prominent in the region of 2nd solvation shell peak and in the trough region between the 1st and 2nd solvation shell peaks. In order to check whether average number of H-bonds $<n_{HB}>$can reconcile different RDFs obtained from different models, we resort to compare these RDFs with respect to $<n_{HB}>$.As we already know that all the water models at their respective TMD yield the same $<n_{HB}>$, we have therefore compared the RDFs obtained from different water models at the TMD. This has been illustrated in Figure2.5. It is now clearly seen that the RDFs of all the six water models considered here almost coincide with each other and thus <n_{HB}>can be considered as a common order parameter which introduces independency in the choice of models.

In order to check the correlation of <n_{HB}> with the distribution of tetrahedral order parameter, P(q_4), we have shown the calculated results in Figure 2.6(a). We have chosen a low-temperature region (which is below the TMD) and a high temperature region (which is above the TMD) for each model and the temperature for each model is chosen in such a way that value of <n_{HB}>remains almost the same for whatever water model we use. In the low temperature region, expected trend of unimodal distribution with a peak at a high q_4 value has been observed and different models yield identical distributions if values of <n_{HB}> are the same (see that lines of blue, navy, cyan and violet are almost overlapping). In the high temperature region a much broader bimodal distribution has been observed and distributions

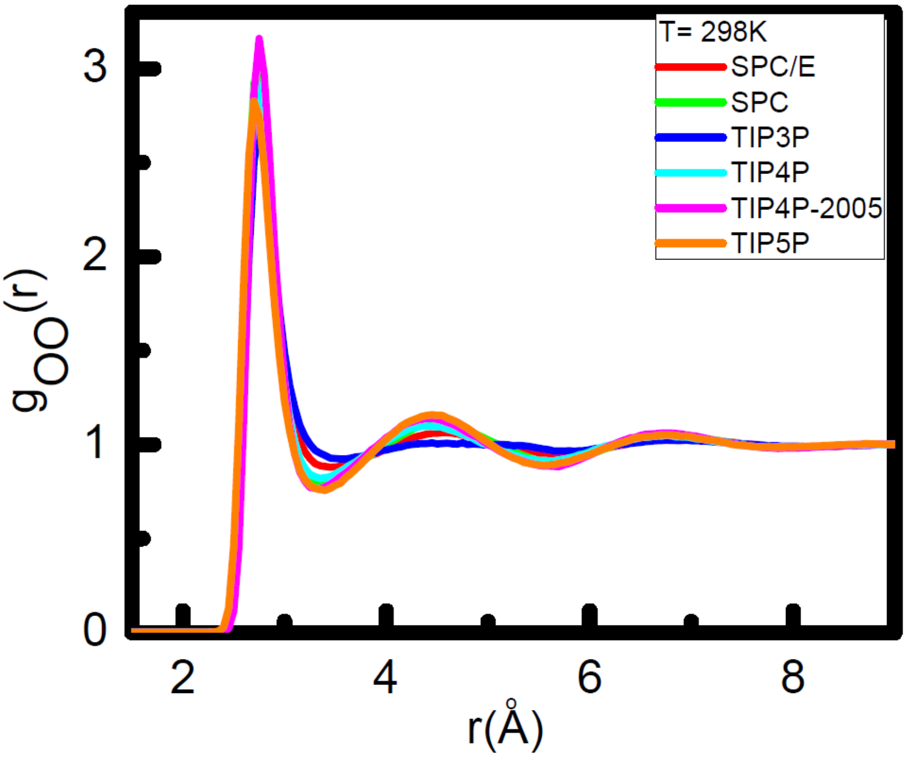

Figure 2.4. Radial distribution functions ofwater molecules around a central water molecule at 298K for each model.

obtained from different water models yield again almost coinciding distribution if the average number of hydrogen bonds is the same (see all the curves with red, orange, pink and red colors). Thus, it illustrates the uniqueness of tetrahedral angular distribution obtained from different water models if viewed as a function of $<n_{HB}>$. Similar results have been obtained in previous investigations.[83,88] Besides distribution of q_4, that of Q_6 i.e. $P(Q_6)$ also follows the same general trend (not shown here). Another important quantity related to water structure is the structure factor s(k). In order to further check the validity of $<n_{HB}>$ as a key parameter to correlate results from different models, we present in Figure 2.6 (b) and (c) s(k) obtained from different water models. Like the $P(q_4)$ vs. $q_4$plot, here too we have shown results for a low temperature region (Figure 2.6(b)) and a high temperature region (Figure 2.6.(c)). The s(k) values from different water models are exactly overlapping with each other if the values of $<n_{HB}>$ are almost the same in both the temperature regions.

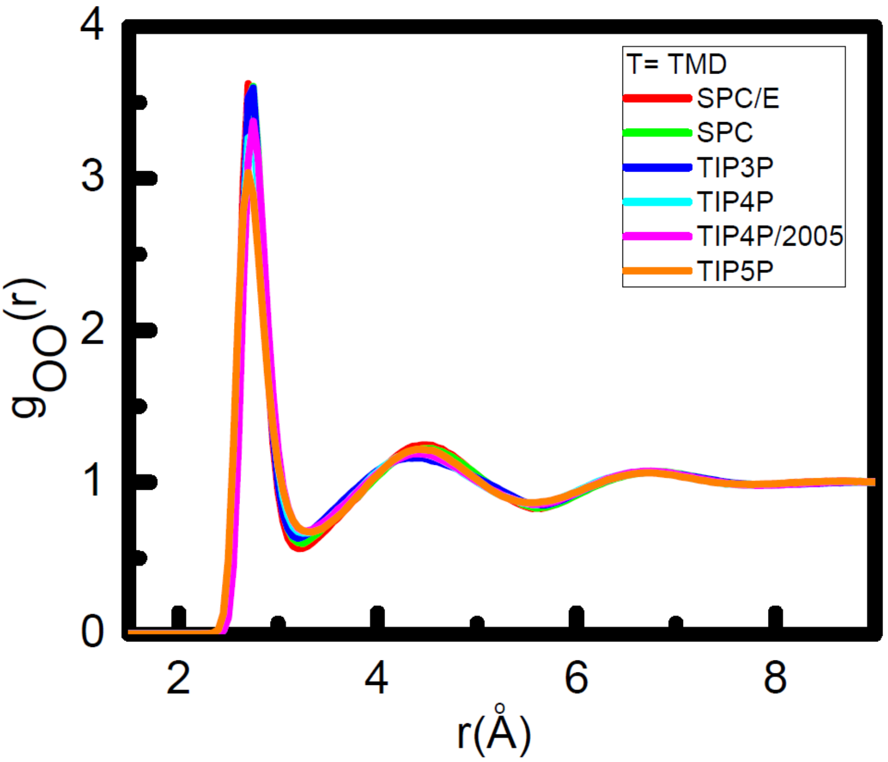

Figure 2.5. Radial distribution functions of water molecules around a central water molecule at T=TMD for each water model.

All these observations confirm the existence of a correlation between hydrogen bonding network of water and orientational order parameters as well as average density. This correlation makes one interested to analyse local hydrogen bonding structure of water in a greater detail. Since we have shown the uniqueness of various structural orders and densities obtained from different models as a function of average number of hydrogen bonds, $<n_{HB}>$, now we can choose any one model for further detailed investigation and we have chosen well-studied SPC/E model for that. Unlike in crystalline state, where almost all the molecules are four hydrogen-bonded, in liquid water a molecule can form *n* number of hydrogen bonds where *n* varies from *1 to 6*. Therefore, average number of hydrogen bonds, $<n_{\mathrm{HB}}>$ at a particular temperature, has contributions from all *n*-hydrogen-bonded molecules with *n=1-6.* In Figure 2.7(a), we have shown percentage of *n*-hydrogen-bonded molecules as a function of temperature. It is seen that four hydrogen-bonded molecules dominate at lower temperature region. Elevation of temperature leads to increase of two- and three-hydrogen-bonded molecules but decrease of four hydrogen-bonded molecules. There is very little change in the percentage of the five hydrogen-bonded molecules in the entire temperature range. Henceforth, we use $C_{\mathrm{HB=n}}$ to designate a central molecule, which forms *n*-hydrogen bonds with the neighbouring molecules. For example, $C_{\mathrm{HB=2}}$ represents a water molecule having only two hydrogen bonds with the neighbouring molecules and so on. It has been found that the percentage of $C_{\mathrm{HB=n}}$ with *n=1* as well as *6* (or more) is very less and can be ignored for further analyses. So, we shall confine our attention to the cases of $C_{\mathrm{HB=n}}$ with *n=2-5*. To form a hydrogen bond, certain geometrical criteria involving distance and angle need to be fulfilled. But in case of orientational order parameters (q_4 or Q_6) we select a fixed number of nearest neighbours viz. 1st to 4thnearest neighbours in case of q_4 and 5th to 16th molecules (distance wise) for Q_6 calculations around a central molecule, irrespective of the relative distance and orientation of each of these neighbouring molecules with respect to the central molecule. It might be possible that a molecule, which is considered for q_4 calculation,

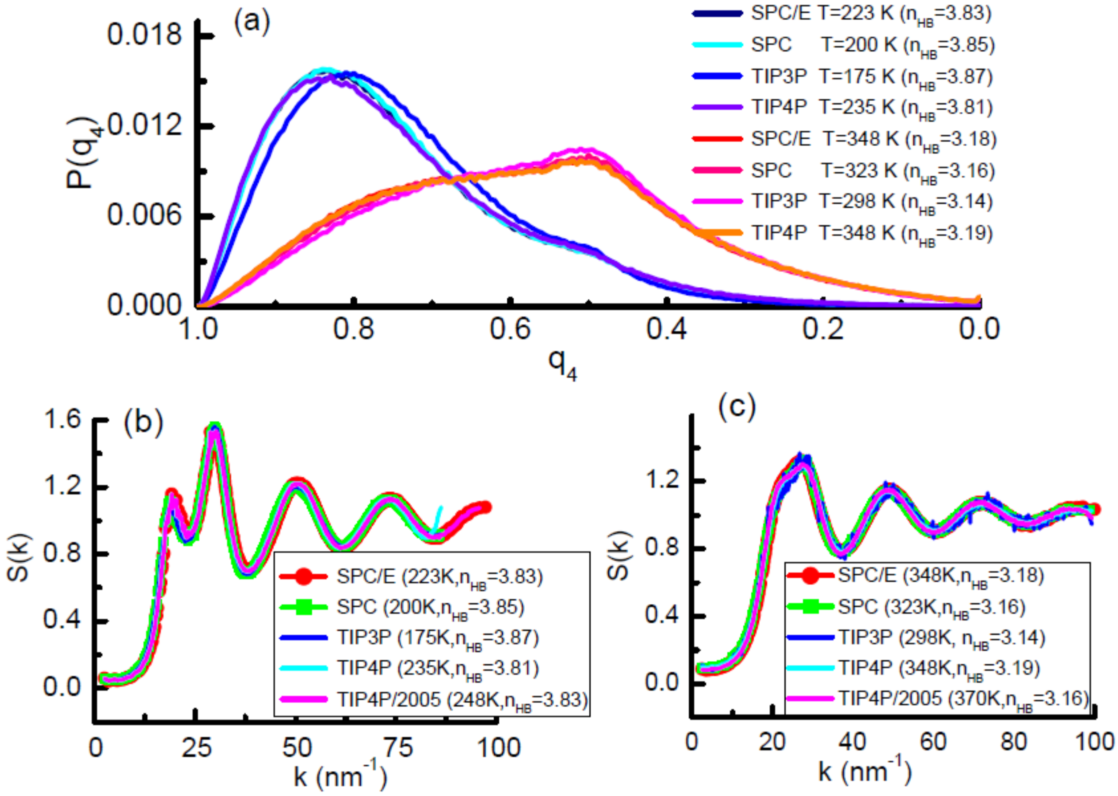

Figure 2.6. (a) Probability distribution $P(q_4)$ of the tetrahedral order parameter, q_4, for different water models. Distributions at lower temperatures for systems with almost the same ⟨nHB⟩ in the range 3.81−3.87 (shown by lines with blue, violet, navy, and cyan colors) as obtained from different water models are almost overlapping. Similarly, those at higher temperatures for systems with almost the same $\langle n_{HB} \rangle$ in the range 3.14−3.19 (shown by lines with red, pink, magenta, and orange colors) also have similar distributions irrespective of the water model used. Static structure factors obtained from different water models (b) in the low temperature region and (c) high temperature region with almost the same number of average hydrogen bonds in each case.

does not take part in the hydrogen bonding due to its not satisfying any of the hydrogen-bonding (HB) criteria and vice versa. Thus, we need to check if a central molecule forms *n* hydrogen bonds i.e. $C_{HB=n}$, whether all these *n* molecules are also the first *n* nearest neighbours. For that we have calculated a factor, P_{CNHB} defined as P_{CNHB} = *[Number of water molecules attached to central molecule via HB]/ [Number of above hydrogen-bonded molecules that fall within n nearest neighbour molecules from the central molecule]*. This

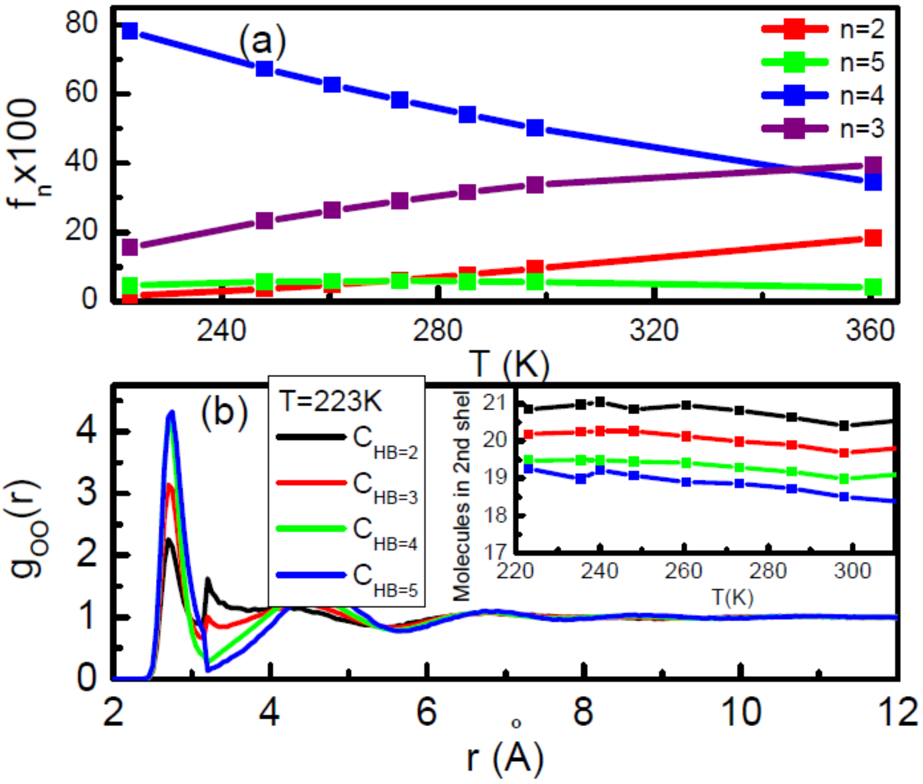

Figure2.7.(a) Percentage of water molecules having n hydrogen bonds as a function of temperature and (b) radial distribution functions of water molecules around a central water molecule having n hydrogen bonds, i.e., $C_{HB=n}$ with n = 2−5 at T = 223 K. In the inset, the number of water molecules in the second solvation shell as obtained from the integration of the radial distribution function has been shown as a function of temperature.

factor is calculated to be close molecule. It might be possible that a molecule, which is considered for q_4 calculation, does not take part in the hydrogen bonding due to its not satisfying any of the hydrogen-bonding (HB) criteria and vice versa. Thus, we need to check if a central molecule forms *n* hydrogen bonds i.e. $C_{HB=n}$, whether all these *n* molecules are also the first *n* nearest neighbours. For that we have calculated a factor, P_{CNHB} defined as P_{CNHB} *= [Number of water molecules attached to central molecule via HB]/ [Number of above hydrogen-bonded molecules that fall within n nearest neighbour molecules from the central molecule]*. This factor is calculated to be close to unity for all $C_{HB=n}$ throughout the temperature range. Hence, we can consider that in case of $C_{HB=n}$, these *n* hydrogen-bonded molecules are also the first *n* nearest neighbours with respect to the central molecule.

In order to investigate the effect of hydrogen bonding on the relative radial arrangement of water molecules, we have calculated oxygen-oxygen radial distribution functions (RDF) with the restriction that the central molecule is *n* hydrogen-bonded (for $n=2$-5). It is important to note that there is no restriction in choosing neighbouring molecules around the central molecule. These RDFs are shown in Figure 2.7(b) and it is found that features of the RDF are very much influenced by the number of hydrogen bonds the central molecule is attached with. First of all, irrespective of the value of *n*, g(r) plots show well defined shell structure. Moreover, integration of *g(r)* up to a distance corresponding to the 1^{st}minimum of *g(r)* yields nearly *n* number of molecules for $C_{HB=n}$ confirming that $C_{HB=n}$ has *n* nearest neighbours, all of which are H-bonded to the central molecule and thus they form the 1^{st} shell for this central molecule. Now in order to check further whether we can really define the 1^{st} shell by considering only these *n* H-bonded neighbours of a central molecule, we have calculated average distances of the n^{th} and $(n+1)^{th}$ molecules when the central molecule is *n* hydrogen-bonded i.e. for $C_{HB=n}$. In Figure 2.8(a), we have shown the distance r_n or r_{n+1}relative to the same at T=223K to check whether it has expanded or shrunk at a temperature T relative to its value at T=223 K. It is interesting to observe that average distance of the *n*th molecule is gradually increasing, while that of *(n+1)*th molecule is decreasing with increasing temperature, irrespective of the value of *n.* In other words, the *n*th molecule (with respect to its position at T=223K) moves outward from the central molecule and *(n+1)th* molecule moves inwards towards the central molecule as the temperature increases. This is even true for $C_{HB=5}$, and cannot be explained on the basis of conventional definition of the first shell with four neighbouring molecules. By conventional definition, for $C_{HB=5}$, both 5th and 6th molecules should be in the second shell and therefore their distances from the central molecule should have identical temperature dependence. But we found that 5th and 6th molecules behave in opposing fashion in this case as the temperature is raised. In summary, we have found that for a central molecule $C_{HB=n}$, *n*th water molecule always expands whereas *(n+1)*th molecule contracts with respect to the central molecule. So, whether the distance of any nearest neighbour molecule from the central one would increase or decrease with the increase of temperature, is dependent on the value of *n* for a $C_{HB=n}$(i.e. number of hydrogen-bonded neighbours the central molecule possesses). For example, if the central molecule has 2 hydrogen bonds, then the distance of the 2nd (*n*th) molecule from the central one will increase and that of the 3rd (*(n+1)*th) molecule will decrease. This general picture is clearly observed in Figure 2.8(a). Thus, we can define 1st shell of a molecule on the basis of number of hydrogen-bonded neighbours the central molecule has. As we have already observed (See Figure 2.7(a)) that water consists of various $C_{HB=n}$ molecules, therefore, water can be viewed as a broken H-bonded network with different *n*-hydrogen-bonded (*n=1-6*)molecules with their distinct solvation shells. The radial position of *n*th and the *(n+1)*th molecules can then be regarded as outer boundary of the 1st shell and inner boundary of the 2nd shell, respectively of a central molecule $C_{HB=n}$.

Besides translational correlation, we have also investigated the effect of H-bonded and non-H-bonded neighbours on orientational order of the nearest neighbour molecules around a central molecule. In this case also we have classified molecules into different groups according to the number of hydrogen-bonded neighbours it has. For calculating tetrahedral

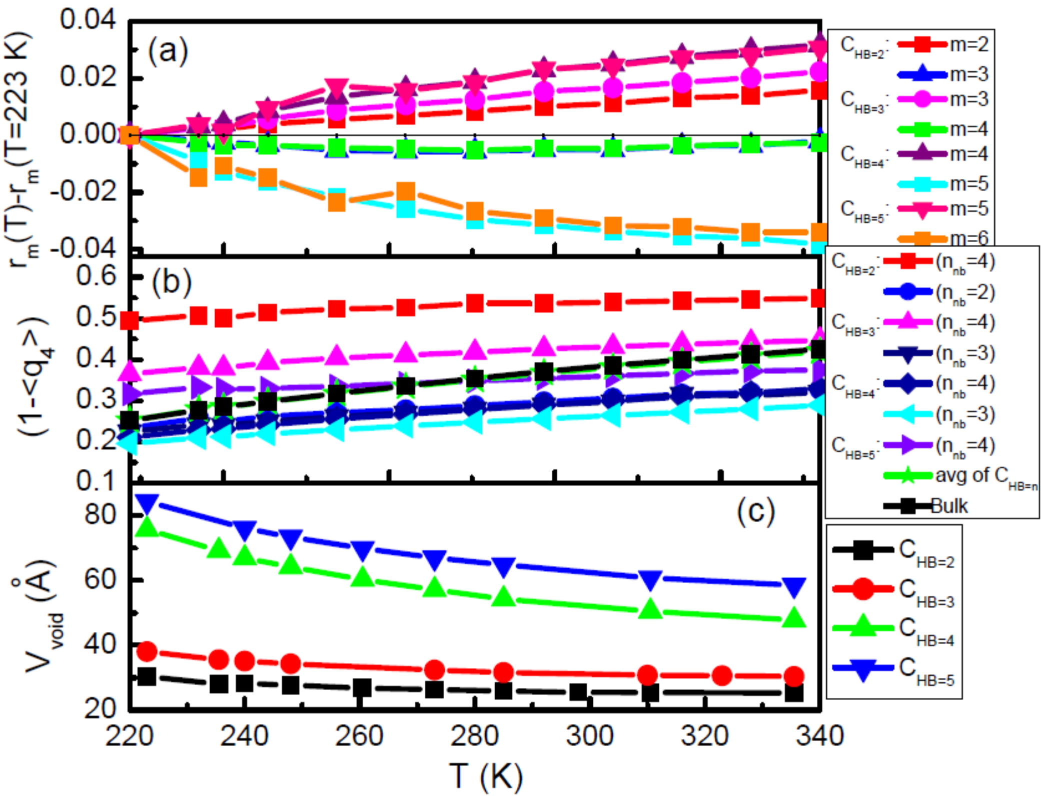

Figure 2.8. (a) Average distance r_n of the nth nearest neighbor at a temperature T relative to its distance at T = 223 K from the central molecule C_{HB}=n. The thin black horizontal line in the middle is a demarcation line between those with expansion and contraction. (b) Deviation of the tetrahedral order parameter q_4 from an ideal tetrahedral value of 1 as calculated for a central molecule $C_{HB=n}$ by considering the usual definition of four nearest neighbors as well as n nearest neighbors as a function of temperature. (c) Volume of the void space between the first and second solvation shell of a central water molecule $C_{HB=n}$, the solvation shell of which is defined by considering n water molecules (not four) as a function of temperature.

order parameter, q_4,of a central molecule with $C_{HB=n}$, we have considered two definitions. In one case usual definition with *4* neighbouring molecules has been considered, and in the other case, a modified definition by considering only *n* nearest neighbours (those H-bonded) to the central molecule $C_{HB=n}$ has been considered (see Method section). The modified equation has been used in case of $C_{HB=2}$ and $C_{HB=3}$ but for $C_{HB=5}$ we have used conventional definition with only 4 neighbours. In Figure . 2.8(b), we have shown deviation (1-$\langle q_4 \rangle$) of the $q_4$values from the perfectly tetrahedral value of 1 as calculated for different groups of molecules as a function of temperature. It is interesting to observe that in general, the deviation is larger in case of $C_{HB=n}$, for *n* not equal to 4. For example, if the number of neighbouring molecules (n_{nb}) considered is greater than *n* (no. of hydrogen-bonded neighbours), then the deviation is larger as compared to the cases when we take $n_{nb}=n$ in calculating q_4. It is observed that the deviation from tetrahedral value of 1 is more for the red line with square (for which we have considered $n_{nb}>n$) than that for the blue line with circles (for which we have considered $n_{nb}=n$) for the central molecule $C_{HB=2}$and also the magenta line with up-triangle ($n_{nb}>n$) has more deviation than the orange line with down triangle ($n_{nb}=n$) for the central molecule $C_{HB=3}$. Therefore it turns out that if we consider conventional solvation shell with four neighbouring molecules, it is the non-hydrogen-bonded (to the central molecule) neighbour that causes the deviation in tetrahedral order and induces asymmetry in local water structure. It is shown earlier by using conventional definition of $q_4$that $C_{HB=2}$ and $C_{HB=3}$ molecules are associated with the low-q_4 peak in the distribution of tetrahedral order parameter.[28] But the origin of this deviation is not clearly understood. When we compare q_4 values calculated by using only *n* neighbouring molecules of $C_{HB=n}$, with $n=2$-*4* (i.e. for the cases $C_{HB=2}$, n_{nb}=2, $C_{HB=3}$, n_{nb}=3, $C_{HB=4}$, n_{nb}=4) we have found the deviation (see lines with blue circles, orange down triangles and dark blue diamonds) to be less and quite close to each other. If we consider even first three neighbours for $C_{HB=4}$, or first 2 neighbours of $C_{HB=3}$ the tetrahedral order parameter does not change very much. It clearly shows that all hydrogen-bonded neighbours are preferentially occupying tetrahedral angular positions around a central molecule throughout the temperature range, irrespective of *n* of the central molecule. Only in case $C_{HB=5}$, although all the four neighbouring molecules (considered for q_4 calculation) are H-bonded, the deviation is slightly more than all other $C_{HB=n}$ calculated with $n_{nb} \leq n$. In this case since the central molecule is H-bonded with 5 neighbouring molecules, due to geometrical restriction all five molecules cannot be perfectly tetrahedrally coordinated and therefore, any two neighbours with the central molecule makes an angle different from the tetrahedral angle. In general, non-hydrogen-bonded molecules possess lower symmetry and occupy sites other than tetrahedral. The present result thus reveals that the steady decrease of q_4 values or increase of the deviation (using usual definition of four nearest neighbours) with temperature should not be attributed to distortion of tetrahedral symmetry of all the neighbouring molecules, instead it is a result of increasing proportion of non-hydrogen-bonded molecules (having non-tetrahedrally coordinated to the central molecule) in the 1st shell at higher temperatures. As the percentage of molecules with $C_{HB=2}$& $C_{HB=3}$ increases with temperature, non-hydrogen-bonded molecules also increases leading to more distortion in tetrahedral arrangements. It was shown[76]earlier that distortion in tetrahedral structure is one of the factors responsible for anomalous density trend of water. But how these distortions occur with respect to the local structure of water was not clear. Present observation is very significant to understand the molecular arrangement of the 1st shell, where first shell is defined by nearest 4 molecules. It is now clear that among the 4 molecules in the conventional first shell, some molecules that are H-bonded to the central molecule show entirely different structural properties (mostly occupying tetrahedral positions) from those not H-bonded to the central molecules (inducing distortion to the tetrahedral arrangements). In this Figure we have also shown the deviation values (black square) of bulk water as calculated from usual definition involving 4 neighbouring molecules and those calculated by considering new definition of solvation shell considering only *n*-hydrogen-bonded neighbours weighted by the respective proportions of $C_{HB=n}$. It is interesting to observe that these two results are in excellent agreement. Thus, the results presented in Figure 2.8(b) further confirm that the structure of a solvation shell of a molecule depends on the H-bonding characteristic of the central molecule and reinforce the view that water can be considered as a normal H-bonded liquid with broken hydrogen bonds having different proportions of *n*-hydrogen-bonded water molecules with distinct newly defined solvation shells.

It is shown in an earlier study[76] that density anomaly is a result of two linear correlations: the homogeneous expansion of oxygen-oxygen distance and contraction due to angular distortion against temperature. These two opposing correlations can now be easily understood by analyzing the results of Figures. 2.7 and 2.8. In Figure 2.8(a) we have found that for a central molecule $C_{HB=n}$, the distance of the n^{th} neighbour increases, but that of the $(n+1)^{th}$ neighbour, which is not hydrogen-bonded to the central molecule (and therefore causes more angular distortion), contracts (cf. Figure 2.8(b)) with respect to the central molecule as the temperature increases. Thus, the present results not only corroborate the findings of earlier work[76], but also pinpoint the exact mechanism by which expansion and contraction occurs. It can be further illustrated from Figure 2.7(b), in which it is shown that for $C_{HB=n}$ with $n=4$ and 5, the first two peaks are well separated with a deep shallow between the two, but for $C_{HB=n}$ with $n= 2$ and 3, where there are non-hydrogen-bonded neighbours(for which angular distortion is more), first two peaks are very close to each other. In order to corroborate this picture, in Figure 2.8(c) we have shown the void volume associated with the solvation shell of a central molecule $C_{HB=n}$, where the void volume is defined as the space available between two concentric spheres of radii r_{n+1} and r_n around the central molecule

$C_{HB=n}$. It is interesting to observe that at all temperatures, void volume between the (newly defined) 1st and the 2nd shells for the central molecule $C_{HB=n}$ with $n=4$ or 5 is much more than that for $n=2$ or 3. It is also evident (see Figure 2.8(c)) that void volume decreases with increasing temperature in all the cases and the rate of decrease is n dependent. How this change in void volume with temperature contributes to the density anomaly of water has been discussed later.

The distribution of q_4 at a lower temperature is unimodal with a single peak (at a q_4 value close to 1) corresponding to almost tetrahedral configuration and as the temperature is increased, another peak develops at a lower q_4 value of around 0.5 (see inset of Figure 2.9(b)). It is intriguing to observe that this new peak appears at a particular q_4 value only. As we know that elevation of temperature in general increases randomness, which can flatten the distribution, but it should not prefer any preferred angular arrangement. Therefore, the development of a new peak corresponding to a particular angular orientation (represented by

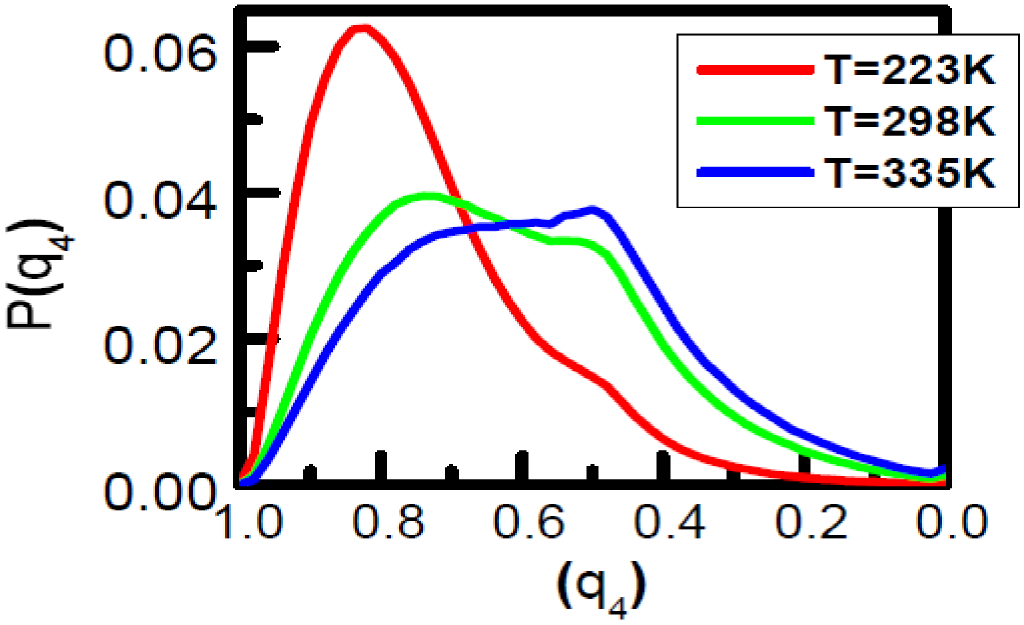

Figure 2.9. Distributions of tetrahedral order parameter, $P(q_4)$ vs temperature.

a value of q_4=0.5) at a higher temperature is quite puzzling. The usual calculation of q_4 takes into account angular arrangements of nearest four molecules from the central one. The angle θ_{jik} extended by two neighbours (*j* and *k* water oxygen atoms) at the central water oxygen (*i* water oxygen site) is the angle with which the tetrahedral order parameter is defined and hence it is known as tetrahedral. angle. The plots of distributions of these tetrahedral angles at different temperatures are shown in Figure 2.10. It is evident from this Figure that at low temperature tetrahedral arrangement is favoured as indicated by a large peak at around $\cos\theta$=-0.333 corresponding to the tetrahedral angle of around109°. With the elevation of temperature, height of this tetrahedral peak decreases giving rise to a new non-tetrahedral peak at around $\cos\theta$=0.6. This picture is consistent with the decrease in peak height of the P(q_4) distribution at around q_4=0.8 and subsequent development of a new peak at around

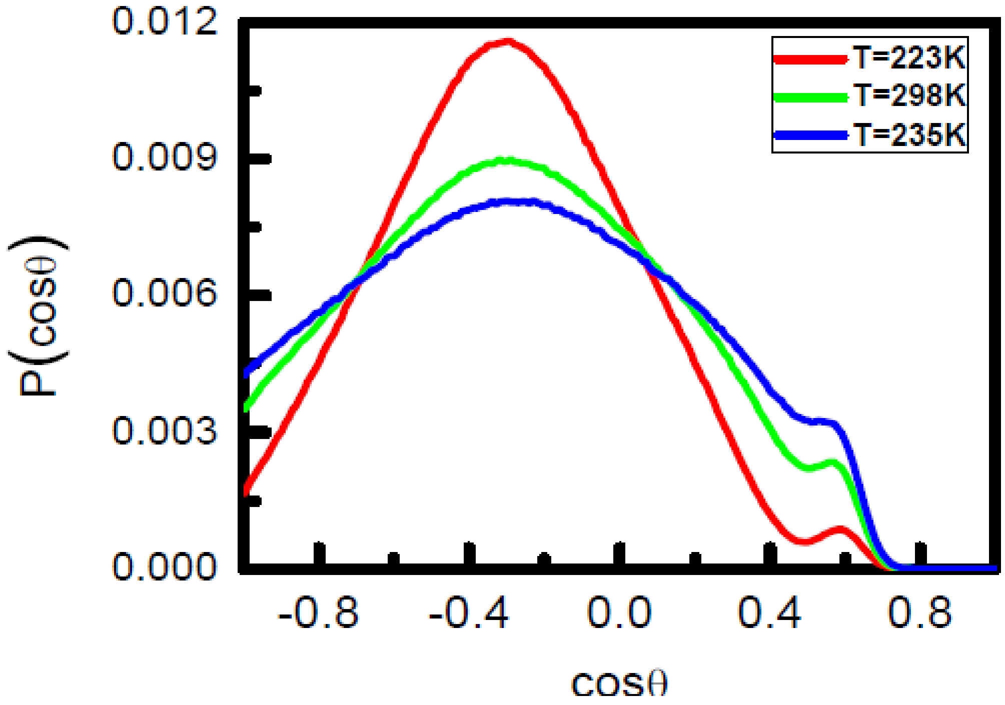

Figure 2.10. Distributions P(cosθ) of the cosine of angle θ made by first four neighbors as a function of temperature.

q_4=0.5 as the temperature decreases. We have already shown (cf. Figure 2.8(b)) that the neighbours that are not hydrogen-bonded to the central water molecule induce more deviation from the tetrahedral arrangement than those H-bonded to the central molecule. In order to understand the origin of the new peak (Figure 2.9, 2.10) in the distribution P(q_4) as well as P(cosθ) distributions at a higher temperature, we have further analysed angular arrangements of the neighbouring molecules around a central molecule $C_{HB=n}$ (i.e. the central molecule having *n* H-bonded neighbours). We have classified angle θ_{jik} into three groups: *(1)* both *j* and *k* are hydrogen-bonded to the central molecule *i*, *(2)j* and *k*, both are non-hydrogen-bonded to the central molecule *i* and (3) only one of *j* and *k* is hydrogen-bonded with the central molecule *i*. We have used distribution of $cos\theta$ instead of q_4 (in order to get rid of the square of $cos\theta$term in q_4 equation) to get a clearer picture of the angular arrangement. When we consider category *(1)* stated above, we found a unimodal distribution of $cos\theta$ (see Figure 2.11(a)), with only one peak corresponding to an almost tetrahedral angle. Also, it has been found that the peak position of the distribution does not change much with temperature. This observation is in accordance with the outcome of Figure 2.8(b), which shows a very small change in the q_4 values with the increase in temperature, provided only hydrogen-bonded molecules have been taken into account for the q_4 calculation. The category *(2)* above is possible when the central molecule is hydrogen-bonded to only two of its neighbours i.e. $C_{HB=2}$ [so that in the conventional solvation shell of 4 neighbours, the central molecule has two non-hydrogen-bonded neighbours]. Existence (see Figure 2.11(b)) of only one sharp peak at around $cos\theta$ = 0.6 corresponding to the q_4 value of around 0.5 (i.e. $\theta=53\text{-}60°$) has been observed. In the third category, the angle we consider is extended at the central molecule by one neighbor, which is hydrogen-bonded and the other one, which is not H-bonded to the central molecule. In this case (see Figure 2.11(c)), it is further surprising to find that apart from the sharp peak at around $cos\theta$ =0.6, a new broad peak appears at around $cos\theta$=

0 in the distribution. The development of this new angular arrangement (corresponding to *cosθ* =0.0) makes the analysis further complicated.

If we consider a usual definition of 1st shell then we have one central molecule surrounded by four neighbours. Here we have calculated total number of hydrogen bonds formed among these five molecules (one central molecule and its four nearest neighbours). In this calculation, H-bonding of the 1st shell neighbours with the molecules from the second shell has not been considered. We have found four hydrogen bonds inside the conventional 1st shell for $C_{HB=n}$ irrespective of the value of *n*. It is also observed that in case of $C_{HB=4}$, the

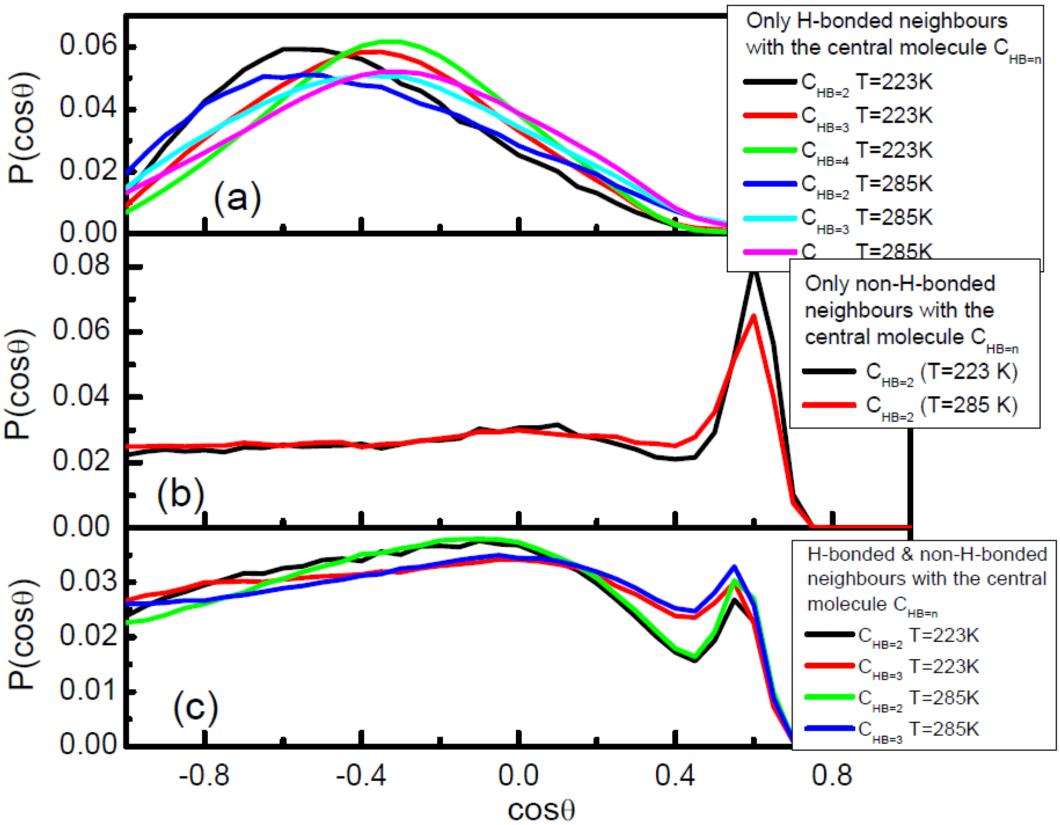

Figure 2.11. Distributions P(cosθ) of the cosine of angle θ made by (a) two hydrogen-bonded, (b) two non-hydrogen-bonded, and (c) one hydrogen-bonded and the other non-hydrogen-bonded nearest neighbors to the central molecule C_{HB}=n.

central molecule is involved in all the four hydrogen bonds with no inter-neighbour hydrogen bond between any two of the neighbouring molecules. For $C_{HB=3}$ and $C_{HB=2}$, there are respectively three and two hydrogen bonds involving the central molecule and the neighbours. Therefore, remaining hydrogen bond/s (one for $C_{HB=3}$ and two for $C_{HB=2}$) is/are resulting from the inter-neighbour hydrogen bonding involving two neighbouring molecules only (i.e. no involvement of the central molecule). We have further investigated how this hydrogen bond, which is not associated with the central molecule, is formed. In case of $C_{HB=3}$, we have found that this hydrogen bond is actually between the 4th neighbour, which is non-hydrogen-bonded to the central molecule and any one of the rest three neighbours that is already hydrogen-bonded to the central molecule. Whether the fourth non-hydrogen-bonded (to the central molecule) neighbour has any preference for selecting (for hydrogen bond formation) one among the three neighbours (those hydrogen-bonded to the central molecule) has also been investigated. The probability of forming a hydrogen bond by the 4th non-hydrogen-bonded (to the central molecule) neighbour with any of the three other neighbours (that are centrally hydrogen-bonded) has been found to be ~0.33. Therefore, all three centrally hydrogen-bonded neighbours are equally probable to form this H-bond with the 4th molecule, which is not hydrogen-bonded with the central one. This observation that all the three hydrogen-bonded neighbours are equally susceptible to form H-bond with the 4th centrally non-hydrogen-bonded neighbour supports our hypothesis that 1st salvation shell can be defined according to the number of hydrogen bonds the central molecule is having. In case of $C_{HB=2}$, out of total four H-bonds in the 1st shell, two involves the central molecule and the remaining two hydrogen bonds are among the neighbours (no involvement of the central molecule). In this case, two non-hydrogen-bonded (to the central molecule) neighbours always form a H-bond between them (probability is 1) and another hydrogen bond is formed between a centrally H-bonded neighbour and any one of the two (equally probable) centrally non-hydrogen-bonded neighbours (calculated probability is around 0.5).

As has been discussed earlier, in case of $C_{HB=3}$, three molecules have occupied three tetrahedral positions. It is expected that the 4th neighbour, the non-hydrogen-bonded one,

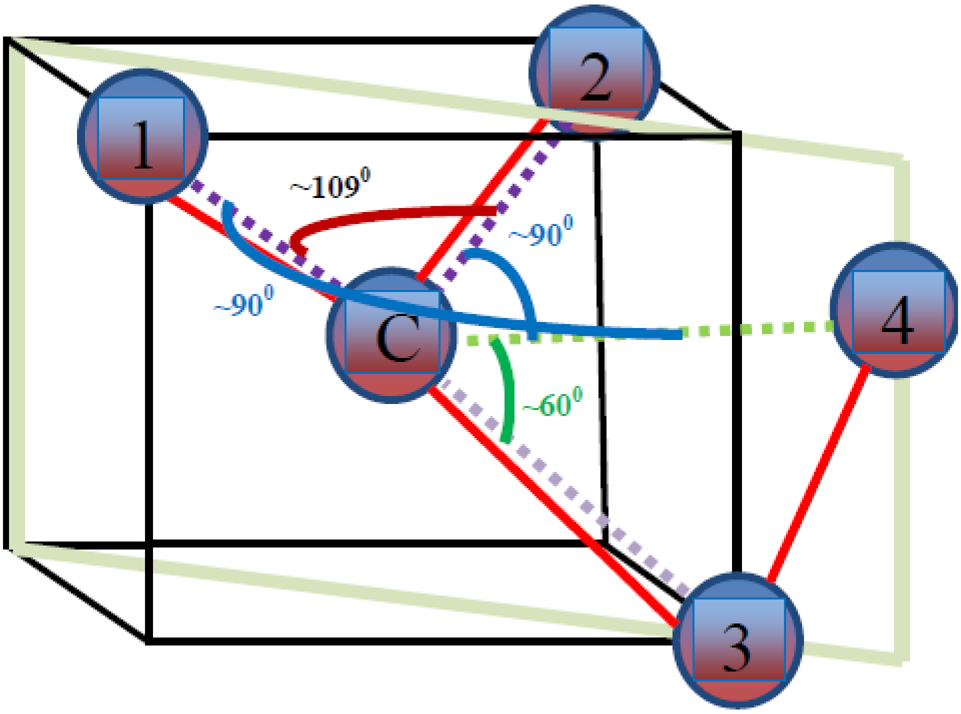

Figure 2.12. A schematic representation (not to scale) of a central molecule C, which is hydrogen-bonded to three water molecules in the conventional first shell. The hydrogen bonds have been shown by red lines, whereas dashed lines are to guide the eye for measuring angles among the neighbors with the central molecule. The fourth molecule is approaching the central molecule along the diagonal plane (shown by the light green parallelogram) in such a way that it makes 90° angles with two (residing on the other diagonal plane of the cube and designated as 1 and 2 in the picture) of the three hydrogen-bonded (to the central one) neighbors. It also makes a small angle of around 60° with the third H-bonded neighbor (designated as 3) and forms a hydrogen bond with the third neighbor. Energetic cost due to steric hindrance for the formation of such a small angle instead of a tetrahedral angle is probably compensated by the gain in energy due to H-bond formation between the neighbors 3 and 4.

would approach from the side where there is vacant tetrahedral site. But in that case the angle formed by this neighbour with the central one and any other neighbour in the first solvation shell would have been close to tetrahedral angle of around 109°. But we found (see Figure 2.11(c)) two peaks, one at $cos\theta$ =0.6 corresponding to a small angle of around 50-60° and another at around $cos\theta$ =0.0 corresponding to an angle of around 90°. Therefore, this 4th molecule approaches the central molecule from the opposite side of the vacant tetrahedral site in such a way that it forms a right angle with the two neighbours and forms a hydrogen bond with the remaining one. This situation has been shown schematically in Figure 2.12. The 4th molecule comes along the diagonal plane containing 3rd neighbour and the central molecule from the side of the third neighbour with which it forms a hydrogen bond (the red line representing hydrogen bond between the two neighbours designated by 3 and 4 in Figure 2.12) and thus makes a smaller angle ($\cos\theta \approx 0.6$) with the central molecule and the third neighbouring molecule. In the process, it forms two other angles corresponding to about $\cos\theta \approx 0.0$ (right angle), with 1st and 2nd neighbouring water molecules (that reside on the other diagonal plane of the cube) involving the central molecule (see Figure 2.12). Angles related to $C_{HB=2}$ shown in Figure 2.11(c) can also be explained in the same manner. In summary, the appearance of the main peak in the q_4 distribution at around q_4=1 originates (see inset of Figure 2.11(b)) from those neighbours that form H-bonds directly with the central molecule. Whereas, the 2nd peak of P(q_4) at a higher temperature can be attributed to the formation of inter-neighbour hydrogen bonds. This situation arises only in cases of $C_{HB=2}$ and $C_{HB=3}$. As the fraction of molecules having $C_{HB=2}$ and $C_{HB=3}$ and therefore population of the non-hydrogen-bonded (to the central molecule) neighbours increases with temperature, the intensity of the 2nd peak (at q_4=0.5) increases accordingly.

Then we have looked into the anomalous density trend of water in the light of this new definition of the 1st shell based on $C_{HB=n}$. We have already seen that with the increase in temperature, the distance of the n^{th} molecule from the central molecule $C_{HB=n}$ (i.e. the radius of the newly defined 1st shell) increases whereas the inner boundary of the second shell (as defined by the distance of the $(n+1)^{th}$ molecule from the central molecule $C_{HB=n}$) approaches towards the centre. Thus, the void space between the 1st and the 2nd shells reduces with temperature. It is important to note[15] that the region up to the 2nd minimum of the radial distribution function $g_{OO}(r)$ contains all the information related to density or volume. We have divided this region into three parts, *(i)* the 1st shell as defined by the newly defined solvation shell according to the number of H-bonds associated with the central molecule, *(ii)* the void space i.e. the space between the outer boundary of the first shell (of radius r_n) and the inner boundary of the 2nd shell (distance from the central molecule is r_{n+1}) and *(iii)* the 2nd shell. As usual we have assumed that both the shells are spherical in nature. For the calculation of orientational order parameters (q_4 and Q_6), conventionally, positions of the 4th and the 16th molecules are considered to be the outer boundaries of the 1st and the 2nd shells respectively. As we have defined the 1st shell in a different way (by taking *n* neighbours around a central molecule $C_{HB=n}$), the outer boundary of the 2nd shell also needs to be redefined. For that, we have computed number of molecules in the 2nd shell by integrating (see insert of Figure 2.7(b)) the RDF for all $C_{HB=n}$, where lower and upper limits of integration have been chosen accordingly from the troughs of the respective RDF. It is found that irrespective of the nature of the central molecule (i.e. value of *n* in $C_{HB=n}$), number of molecules in the second shell varies between 19.5 and 20.5. We have also calculated average distance of the 16th molecule for each central molecule $C_{HB=n}$, and we have found $<r_{16}>$to be around *4.8* Å, which is close to the upper integration limit chosen in the above mentioned integration. Then we have calculated volume or density by considering k^{th} molecule as the boundary of 2nd shell, where *k* varies from 16 to 20 and we have found that there is almost no significant change in volume/density trend for these different *k* values. Therefore, we have considered the position of 16th molecule as the outer boundary of 2nd second shell for our

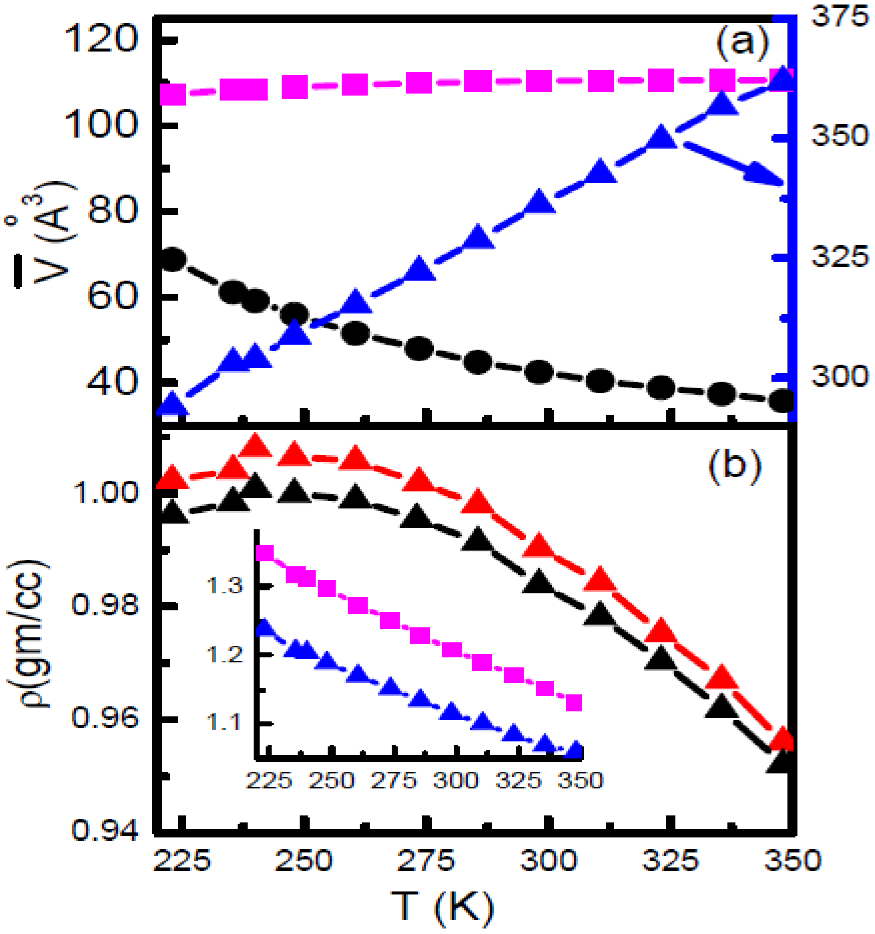

Figure 2.13 (a) Volumes of the first shell (magenta squares), the second shell (blue triangles), and the void space between the two shells (black circles) of SPC/E water as a function of temperature. The blue curve follows the scale on the right axis, whereas the magenta and black curves follow that on the left axis. (b) Density ρ in g/cc of SPC/E water as a function of temperature. The red line with triangles represents the density of water in the second shell including the void space between the two shells. The black line with triangles represents the average bulk density of water. Inset: The magenta line with squares represents the density of the first shell, whereas the blue line with triangles represents the density of only the second shell (without the void space).

volume/density calculation. The volume of the 2nd shell has been calculated by subtracting the volume of a smaller sphere of radius r_{n+1} from that of a larger sphere of radius r_{16} where r_{n+1} and r_{16} represent the positions of the $(n+1)^{th}$ and the 16th neighbours respectively of a central molecule $C_{HB=n}$. Similarly the volume of the void space between the 1st and the 2nd shells has been calculated by subtracting the volume of a smaller sphere of radius r_n from that of a larger sphere of radius r_{n+1}. In Figure 2.13(a) we have shown the average volume of the 1st and the 2nd shells and the void volume between the two shells separately. Since in our definition of the 1st shell, number of neighbours are not fixed (dependent on the number of H-bonds of the central molecule), the volume of the 1st shell is calculated as $\overline{V} = \sum_{n=1}^{5} V_n f_n$, where $V_n = \frac{4\pi}{3} r_n^3$ and f_n is the fraction of molecules having n hydrogen bonds. As shown in Figure 2.13(a), volume of the 1st as well as the 2nd shell increases with increase in temperature. This expansion of the 1st shell has already been shown in Figure 2.8(a), where average distance of the n^{th} neighbour of a central molecule $C_{HB=n}$ having n hydrogen bonds increases with increasing temperature. And it is true for any n. The change in volume of the 1st shell with temperature is not much, i.e. the 1st shell is quite incompressible. It is important to note that unlike these two shells, the volume of the void space between the two shells decreases (see Figure 2.13(a), black curve) with temperature. We have also calculated the density of these different regions corresponding to 1st shell and 2nd shell. During density calculation, we have to remember that the numbers of molecules in the 1st and 2nd shells vary according to the value of n of the central molecule $C_{HB=n}$. We have also calculated the density of the 2nd shell by incorporating the void space into the 2nd shell (i.e. starting from n^{th} to 16th molecules). The following equation has been used for the calculation of densities in different regions:

$$\rho = \frac{\sum_{n=1}^{5} N_n f_n}{\overline{V}},$$

where, ρ is the average density and N_n and f_n are number of molecules inside the given volume $\overline{V}$ and fraction of molecules with n hydrogen bonds respectively. For example, for the 1st shell, $N_n=n+1$ (n hydrogen-bonded neighbours and the central molecule) and for the 2nd shell $N_n=16-n$. As shown in Figure 2.13(b), the densities of 1st and 2nd shells monotonically decrease with increasing temperature and thus cannot explain the density maximum of water. Elevation of temperature leads to increase in oxygen-oxygen distance and volume. That is why we observe decrease of densities of the 1st and 2nd shells. However, when we consider density of the 2nd shell by incorporating the void space between the 1st and the 2nd shells, it increases first and then decreases with increasing temperature. Thus it can describe the non-monotonic density trends with respect to temperature. The location of the TMD (T_{TMD}=240 K for SPC/E model) and the overall trend of the temperature dependence of the average bulk density have been reproduced correctly. So, the second shell including the void space is the responsible region for density anomaly. Importance of the second shell in explaining anomalous density trend has been noted earlier.[15]A molecular theory of liquid water also highlights[52] the importance of longer-than-near-neighbor ranged interactions. It clearly states that a detailed treatment of local order alone corresponding only to the tetrahedral local structure without invoking the effect of longer ranged interaction cannot describe the thermodynamic properties of network forming liquid like water. We have already shown that the structure of 1st shell is very much governed by $C_{HB=n}$. With the increase in temperature, thermal expansion is always there, but it is the void volume that determines the anomalous expansion of water and this void volume decreases as the percentage of $C_{HB=4}$ gradually decreases and that of $C_{HB=2}$ or $C_{HB=3}$ increases. It is because, the void volume associated with $C_{HB=2}$ as well as $C_{HB=3}$ is much less as compared to the same associated with $C_{HB=4}$ and $C_{HB=5}$.

And as angular distortion associated with $C_{HB=2}$ or $C_{HB=3}$ is more, overall distortion also increases with the increase in temperature.[76]So in essence, water can be viewed as a normal dynamic mixture of different solvation shells defined according to the number of hydrogen-bonded neighbours of the central molecule. Temperature dependence of the behaviour of all these solvation shells is distinctly different. Hydrogen bonding status of the central molecule governs not only the property of the 1st shell, but that of the 2nd shell and the void space also. The anomalous density change of water with temperature can then be attributed to the change in the proportions of these different solvation shells (i.e. hydrogen bond distribution) by properly taking into account the density change in the region of the second shell and the void space between the 1st and the 2nd shells.

2.3.2: Correlation of Hydrogen Bonding Network and Dynamics of Water

As mentioned in the Chapter 1, molecular dynamics technique, apart from providing structural and thermodynamic quantities, can provide information about translational and rotation dynamics of water as well. Investigation in this direction clearly demonstrates that similar to structural and thermodynamic anomalies, water also exhibit dynamical anomalies.[158-170]Contrary to the general perception, in a region of pressure or density, increase in pressure/density leads to increase in translation diffusion coefficient and at a certain pressure or density the diffusivity reaches to a maximum value (D_{max}),[171-175] and beyond this pressure (or density), a normal trend of decreasing diffusivity with increasing pressure (or density) is observed. There is also a region in the T-P plane, where pressure of water is negative, diffusivity (D_{min}) at lower temperatures passes through a minimum as a function of increasing pressure or density.[171,174]The rotational dynamics of bulk water also shows differentanomalousbehaviour.[171] The anomalies related to mobility of water are not well understood even after so many decades. P. G. Debenedetti and co-workers showed that almost all the anomalies exhibited by bulk water lie in a common region of the phase diagram.[71]In order to understand the effect of structure on dynamics (if any), a lot of work has been carried out. Recent works suggest that tetrahedral local structure along with the associated defects are responsible for both structural and dynamical anomalies of bulk water.[174,175] Stanley and co-workers showed that the average number of hydrogen bonds and its distribution play an important role in dynamical anomalies too.[169]It is seen in Chapter 2 that hydrogen bonds and its distributions play an important role in structural and

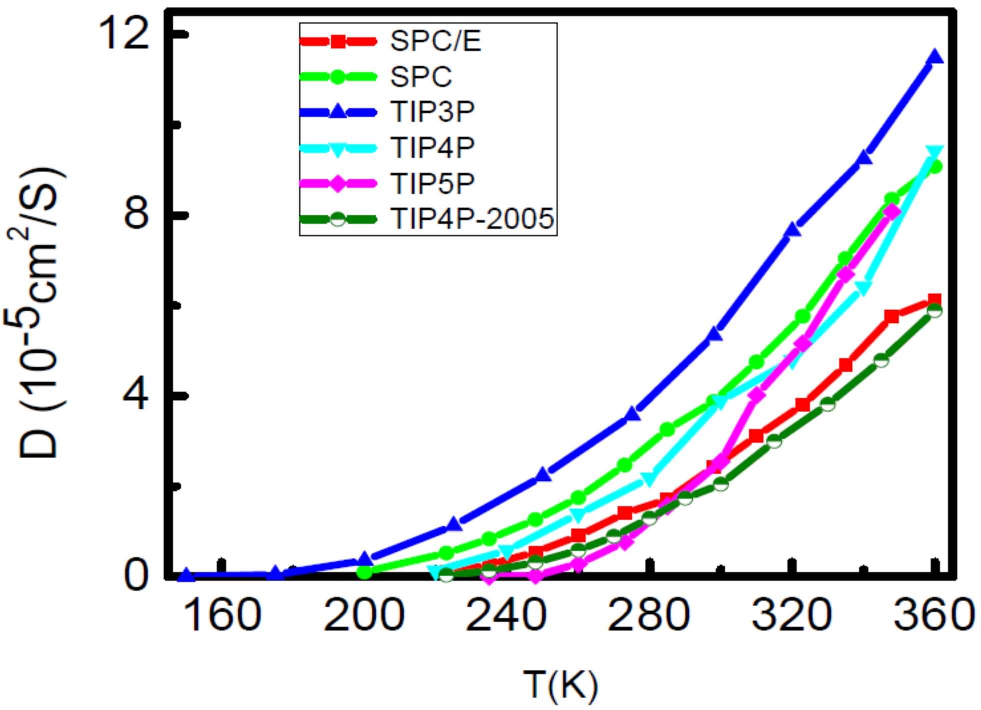

Figure 2.14 Diffusion of bulk water calculated from MSD at different temperature.

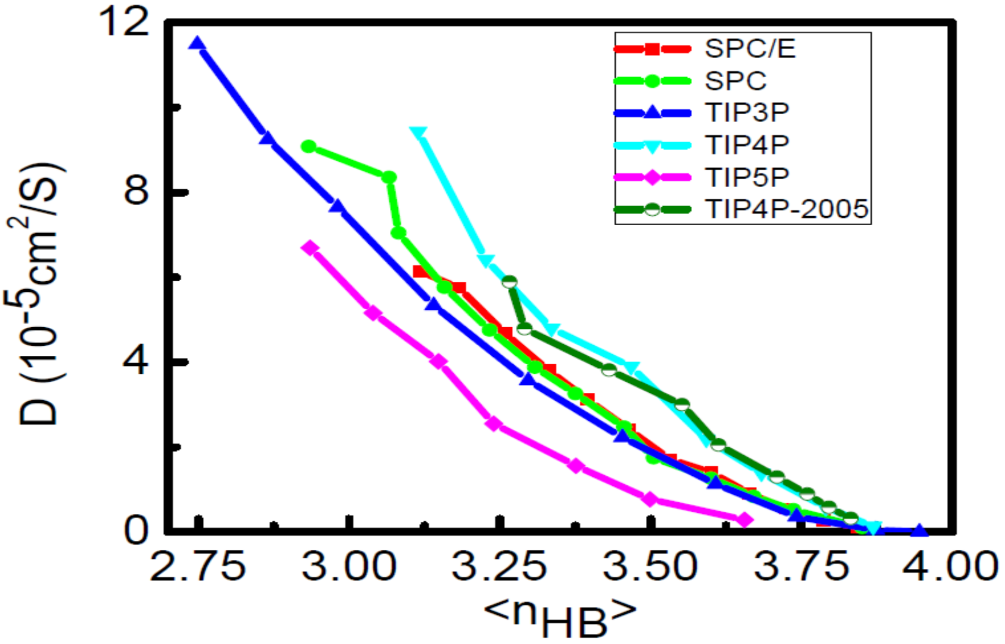

Figure 2.15 Diffusion of bulk water calculated from MSD comparing by average number of hydrogen bond.

thermodynamic properties of water. In particular, it is shown that if the average number of hydrogen bonds, <n_{HB}> is considered as an order parameter, disparate structural and thermodynamic results obtained from different water models can be reconciled. This new finding encourages us to explore the role of <n_{HB}>for correlating dynamical properties obtained from different water models too. Thus, we have computed several dynamical properties of bulk water as a function of temperature to investigate whether any such correlation exists. The calculated translational diffusion coefficients of water as obtained from the slope of the mean square displacement using Einstein relation over a wide range of temperatures at ambient pressure (see Figure 2.14) are quite different for different water models. In the low temperature region, as expected, diffusivity values are negligibly small due to arrest of the thermal motion. Among these models, TIP3P and SPC water models overestimate translational diffusion coefficients as compared to corresponding experimental values, but diffusivity exhibited by TIP4P-2005 and SPC/E models are quite comparable to the experimental values. However, when we observe these diffusivity values as a function of average number of hydrogen bonds (see Figure 2.15), we do not find any apparent correlation among the results obtained from different water models. Unlike structural order parameters, translation diffusivity values are not well correlated with the average number of hydrogen bonds, $<n_{HB}>$. At a very high value of $<n_{HB}>$ (in the low temperature region) diffusivity values obtained from different models (except TIP5P) are not very different. It can be understood easily that in this region of temperatures (at ambient pressure) thermal motions are slow due to low temperature.

In order to investigate the correlation of rotational diffusivity with the average number of hydrogen bonds, $<n_{HB}>$, we have also calculated different rotational correlation functions of water over a wide range of temperatures using different water models. We have calculated orientational dynamics of water molecules in terms of time correlations function $\Gamma_l^{\alpha}(t)$ of the orientational vector u_α defined as

$$\Gamma_l^{\alpha}(t) = \langle P_l\big(u_\alpha(t).u_\alpha(0)\big)\rangle \qquad (2.5)$$

where P_l is the Legendre polynomial of order l. It defines the time evolution and hence the orientational dynamics of the molecular vector u_α. The angular brackets in the above equation represent the average over time origins as well as the number of molecules. In the present work, two unit vectors *(i)* dipole moment vector $u_\alpha = \mu$ *(ii)* OH bond vector ($u_\alpha = OH$) have been considered. We have considered first ($l = 1$) and second order ($l = 2$) Legendre polynomial. In the previous section it is shown that at TMD, different water models yield same number of average number of hydrogen bond$<n_{HB}>$.Therefore, in order to investigate whether $<n_{HB}>$ can be a unifying structural parameter for different models, we have compared time correlation functions as obtained from different water models at their respective TMD. The first (Γ_1^μ) and second order (Γ_2^μ) time correlation functions of the dipole moment (μ) vector of water are shown in Figure 2.16, 2.17 respectively. and OH bond vector (*OH*) have been It illustrates that the decay of the correlations obtained from the TIP4P, TIP5P and TIP4P/2005 are quite similar and this is understandable because the TMD of these three models are very close to each other. This is even true for the case of SPC and SPC/E water models. The results thus strongly point out the fact that unlike spatial properties, rotational dynamics of water is not influenced by the average number of hydrogen bonds; instead temperature plays a decisive role on the rotational relaxations.

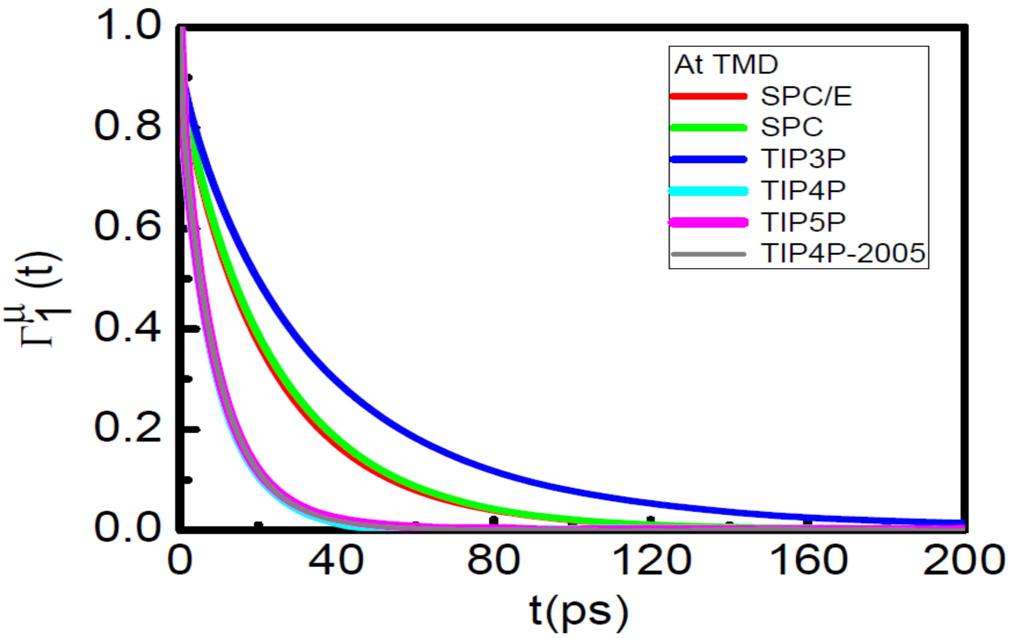

Figure 2.16 Time correlation function of dipole moment vector(μ)of water molecule comparing at TMD for Legendre polynomial(l=1).

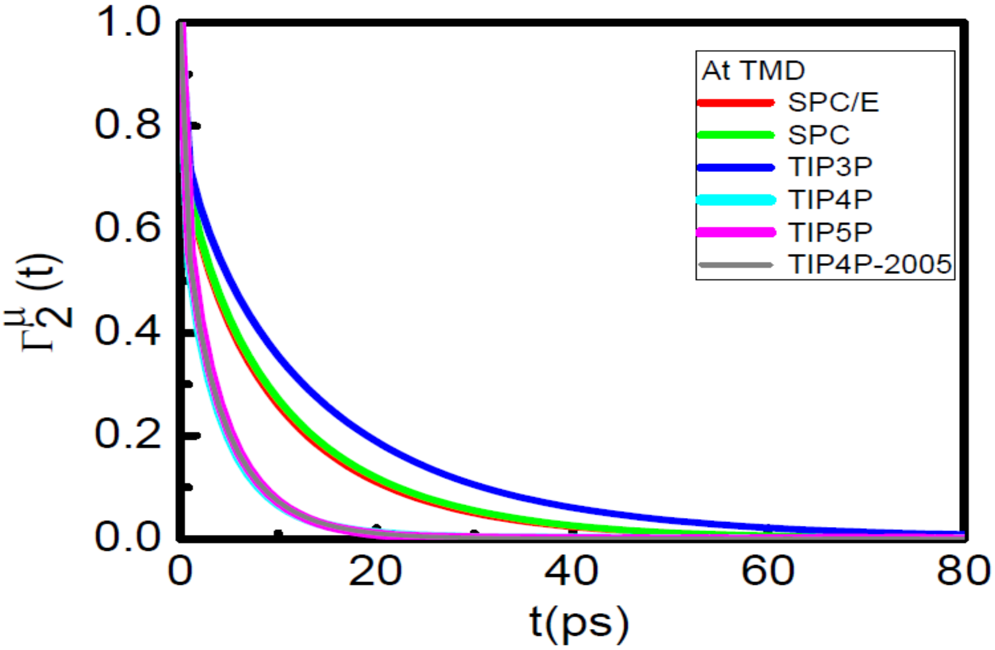

Figure 2.17 Time correlation function of dipole moment vector(μ) of water molecule comparing at TMD for Legendre polynomial(l=2).

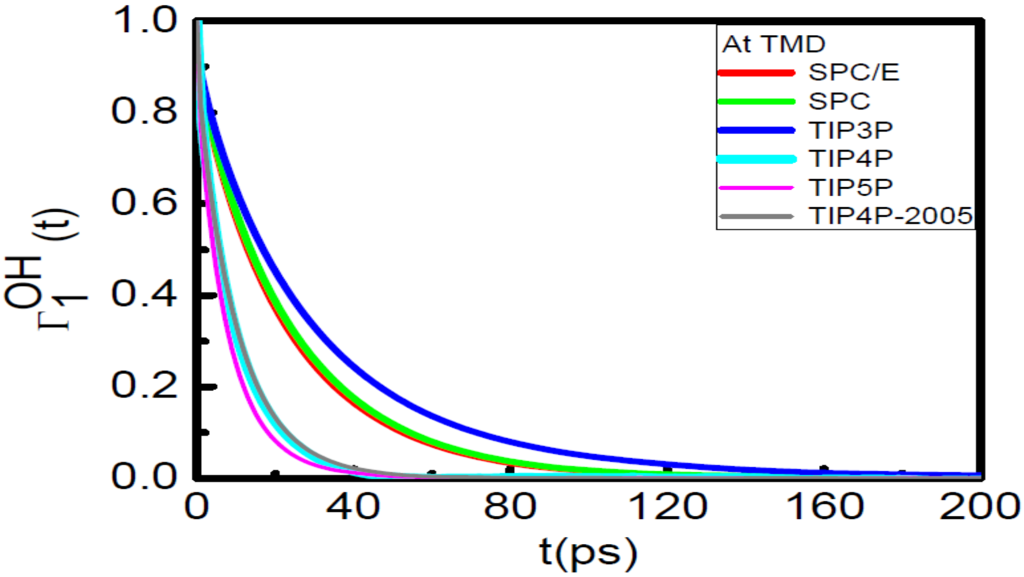

Figure 2.18Time correlation function of OH bond vector(OH)of water molecule comparing at TMD for Legendre polynomial(l=1).

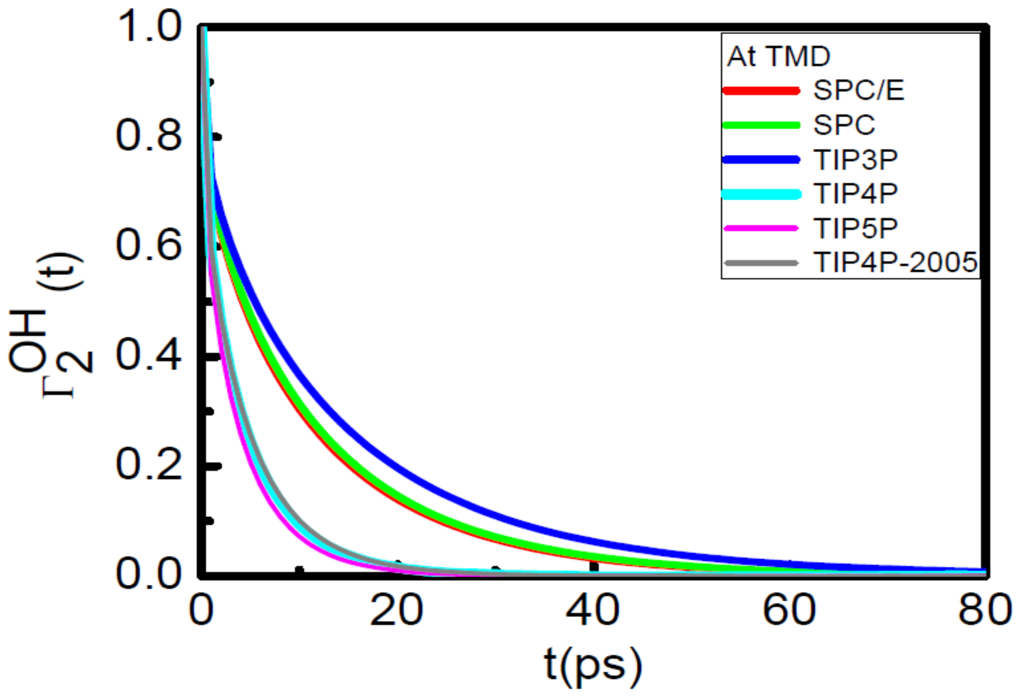

Figure 2.19 Time correlation function of OH bond vector (OH) of water molecule comparing at TMD for Legendre polynomial (l=2).

2.4: Summary and Conclusions

We show that hydrogen bonding network structure dictates structural orders and anomalies of water. In particular, the average number of hydrogen bonds correlates well not only with tetrahedral and second shell's orientational orders, but with structure factor and the density anomaly of water as well. Thus, disparate results on temperature dependence of various structural orders and TMD as obtained from different water models have been concurred by correlating these results in terms of average number of hydrogen bonds. Our result is consistent with the recent observation[83] that all water models follow the same structural pattern by a temperature shift. This is understandable because shift in temperature changes the average number of hydrogen bonds. Further, we wanted to check whether the same structural parameter, the average number of HB, can also reconcile disparate results on dynamics as obtained from different water models. Contrary to the observations made on the effect of average number of hydrogen bonds on different structural parameters and thermodynamic properties, translational and rotational (i.e. dynamical) properties of water as obtained from different water models cannot be reconciled into a single context by this very structural parameter, the average number of hydrogen bonds. Our results demonstrate that the dynamical properties of water are sensitive to temperature rather than the average number of hydrogen bonds. An in-depth analysis of the H-bond network of the water molecules reveals that the solvation shell of a water molecule can be defined not by the average number of four neighbours, but by the number of hydrogen-bonded neighbours of the central molecule. It has been observed that for a central molecule $C_{HB=n}$, the distance of the n^{th} molecule from the central molecule always increases and that of the $(n+1)^{th}$ molecule always decreases with the increase in temperature. This result is consistent with the findings of Matsumoto,[76] who observed that density anomaly is a result of interplay of the monotonic oxygen-oxygen distance extension and angular distortion of the tetrahedral network upon change of temperature. However, origin of the angular distortion in the tetrahedral network was not clear. In this investigation, we put forward a lucid explanation of the relation of tetrahedral distortion and volume contraction against temperature. First, we have shown that the distortion arises from those water molecules that are not directly hydrogen-bonded to the central molecule. All the hydrogen-bonded (to the central molecule) neighbours occupy tetrahedral positions around the central molecule even at higher temperatures and therefore have minimal angular distortion. It is the non-hydrogen-bonded (to the central molecule) neighbour, which induces distortion in the tetrahedral arrangement. We have also identified the origin of the appearance of the second peak in the distribution of tetrahedral order parameters at higher temperatures. This second peak appears due to asymmetrical approach of a non-hydrogen-bonded neighbour towards the central molecule in such a way (see Figure

2.12) that it forms a hydrogen bond with another neighbour, which is already hydrogen-bonded to the central molecule. Because of this hydrogen bond formation between the non-hydrogen-bonded neighbour with the other neighbour, which is already hydrogen bonded to the central molecule of the type $C_{HB=2}$ or $C_{HB=3}$, angle extended by these two neighbours to the central molecule is much smaller (see the peaks at $cos\theta$ =0.6 and 0.0 in Figures. 2.10 and 2.11) than the usual tetrahedral angle of around 109° (see 2.12). Our result is consistent with the recent work of Netz and coworkers,[91] who have shown that the additional peaks at low q_4 values arise from the two- and three-hydrogen-bonded molecules. However, it is important to note that not all the four neighbours of a 2- or 3-hydrogen-bonded water molecule (designated as $C_{HB=2}$ or $C_{HB=3}$ here) are orientationally distorted. In fact, we have found that all the neighbours that are hydrogen-bonded to the central molecule (irrespective of the hydrogen bonding status of the central molecule) are (almost) tetrahedrally coordinated to the central molecule, and it is the non-hydrogen-bonded neighbour (one in case of $C_{HB=3}$ and two in case of $C_{HB=2}$) that distorts the tetrahedral angular arrangement. The present result therefore contradicts recent finding[94] in which water has been viewed as a mixture of two components based on the median of the q_4 values. Finally, we have correlated this tetrahedral distortion with volume contraction in the following way. The volume of the void space (space between the 1st and the 2nd shell) associated with the central molecule having 4 tetrahedral neighbours is much more than the same associated with a central molecule having one or more non-tetrahedral neighbours (those causes more angular distortion) and the decrease of void volume against temperature in the former case is more as compared to that in the later case (see Figure2.8). We have finally found that the volume of the void space between the 1st and the 2nd shell of a central molecule along with that of the 2nd shell collectively determines anomalous density trend of water. Experimental result[85] on water structure also predicts that density change in water is associated with the structural change in the second coordination shell. If we consider water as a dynamic mixture of various solvation shells of *n*-hydrogen-bonded (with *n=2-5*) water molecules, the volume of the second shell along with the void space between the 1st and the 2nd shells of this mixture follows the correct non-monotonic density change with temperature and therefore explains density anomaly of water (see Figure 2.13). It is important to emphasise that this mixture is not made up of any spatially correlated extended clusters of molecules, as posited by Huang et al.[88] to interpret their small angle structure factor data and also not consisting of orientationally correlated clusters[94] of water molecules having a range of q_4 values. Rather, as the present investigation suggests, water can be viewed as a temporal mixture of differently hydrogen-bonded water molecules, with the composition of this mixture being instantaneously changing due to thermal motion. Density anomaly of water is a consequence of neither spatial nor orientational polyamorphism, but a result of natural fluctuations[89,90]of hydrogen-bonded network arising due to usual stochastic processes in a single component fluid. The present result is consistent with the experimental finding of Smith et al.[146] that shows that distribution of hydrogen bonding geometries and energies in liquid water are continuous and that of Head-Gordon et al.[149] that describes water as a tetrahedral hydrogen-bonded network. In summary, our finding is in contradiction to the assumption of density heterogeneity made in Refs. 88 and 94 and in line with the view that liquid water is a random network of hydrogen bonds, with fleetingly broken bonds, that is perpetually undergoing topological reorganization as inferred in Refs. 76, 89, 91, 96, 147 and 149.

Isotopically substituted water i.e. deuterium oxide (D_2O), commonly known as heavy water is an important material in view of its relevance in nuclear, chemical, medical and pharmaceutical industries. Molecular dynamics simulation is a viable theoretical tool to calculate various properties of heavy water at ambient as well as extreme conditions of temperatures and pressures.[97,98] However, the bottleneck in this direction stems from the absence of a suitable atomistic model of heavy water. A three-site SPC/HW heavy water model, to the best of our knowledge, is the only model[97] available for heavy water. Although this model is shown to reproduce properties of heavy water at ambient condition quite accurately, its applicability has never been tested beyond the ambient condition. In the next Chapter, we have therefore investigated the applicability of this model at different temperatures in the range of 223K to 360K at ambient pressure by calculating various thermophysical properties and comparing them with the available experimental or literature values.

Chapter 3

Structure, Thermophysical Properties and Dynamics: A Comparative Study of Water and Heavy Water

3.1: Introduction

Although the chemical properties of water and heavy water are quite similar, a considerable number of differences in their thermo physical properties exist due to the substitution of hydrogen in water by deuterium forming heavy water (D_2O)[97,98]. Because of heavy nuclear structure and isotope effect, deuterium and heavy water have found wide applications in various areas such as nuclear technology, spectroscopy[99] and medicine. The relevant uses of D_2O as moderator for high energy neutrons in a nuclear reactor, fusion material for fusion technology, as solvents in neutron scattering[100,101] and NMR-spectroscopy, in synthesis of various drugs[102] are to mention a few. Further, it is extensively used as a tracer (no significant change in the chemical environment of deuterium due to identical electronic structure with hydrogen atom) for many biological and geological systems.[103] The high heat capacity, heat of vaporization, dielectric constant and elevation of density with decreasing temperature enable water and heavy water to play a key role in most of the biological processes[103]. High self-diffusion coefficient[104] and dielectric constant,[105] its network forming ability[73] by forming hydrogen bonds with neighbouring water molecules are some of the salient features that make water and heavy water a universal solvent.

A large number of simulation studies of bulk water[107,176,205] have been reported in the literature. Information extracted from these studies helps us to understand many complex phenomena involving water and predict various bulk properties of water even at various state points that are inaccessible to experiments. Bulk properties of water are the result of the manifestation of many-body interactions among water molecules in the condensed phase and are functions of the inherent inhomogeneous local order[67,87,177] of water as described by the oxygen-oxygen, oxygen-hydrogen and hydrogen-hydrogen radial distribution functions. Due to polar nature of water with hydrogen as a constituent atom in it, hydrogen bond[178] distribution and energy are responsible for manifestation of many anomalous properties of water. As chemical nature of hydrogen and deuterium is similar, all these aspects of water should not be very different from those of heavy water. However, there are differences in many physical and chemical properties of the two substances. This can be attributed to lower zero point energy of heavy water as compared to water and as a result, the deuterium bonds are energetically stronger than hydrogen bonds with internal arrangements[73] considerably ordered[179-183] at a given temperature.

Because of the central importance of water in chemistry, biology and physics, extensive studies have been devoted to model water at the atomistic scale.[51,80,181-196] As a result, a large number of models have been developed over the years. However there are only a few models available for heavy water. Although a few attempts have been made to understand the isotope effect on protein hydration[184] using molecular dynamics simulation, where interaction of heavy water has been oversimplified by considering it[185,186] to be the same as that of a simple point charge/extended (SPC/E)[51] model of water with mass of the deuterium atom considered to be twice as that of the proton. Some path integral quantum simulations [6, 183-196] of heavy water based on usual water potentials such as ST2, SPC, and TIP4 have also been reported. Although this method is quite accurate due to incorporation of the quantum effect, which is important for small atom like hydrogen or deuterium, it is computationally very demanding. Therefore, simulations of complex systems with a large number of molecules are difficult. Recently, a three-site model (SPC/HW) of heavy water based on SPC/E[51] model of water has been developed[1] and used in MD simulation to extract structural and thermodynamic data at ambient condition. It has been shown that this model is quite accurate as far as reproduction of heavy water properties[38] at standard temperature and pressure is concerned.

However suitability of a model potential needs to be tested in terms of transferability across various state points. In the present investigation, therefore, we intend to test the suitability of the newly developed[1] SPC/HW model across state points ranging from cold to hot liquid phases below the boiling point along *P=1* atmosphere isobar. For this purpose, we have performed a series of MD simulations of bulk heavy water and calculated various structural, thermodynamic and dynamical properties of heavy water in the temperature range of *T=223* to *373* K along *P=1 atm* isobar. Results obtained from the present study have been compared with those from experiments wherever possible.

3.2:Models and methods:

As in case of SPC/E model,[51] in this model[1] also a heavy water molecule is characterized by three interaction sites corresponding to the central oxygen and two deuterium atoms with fixed O-D distance of *0.1* nm and angle DOD *109.47°*. The charges on oxygen and deuterium are equal to *-0.870e* and *+0.435e* respectively. The site corresponding to the oxygen atom interacts with the same from other molecules through the usual Lennard-Jones (LJ) interaction and no LJ interaction has been considered for deuterium site. For all charged sites Columbic interaction has been considered. Size and energy parameters for the LJ potential were taken as $\sigma=3.17$ Å and $\varepsilon=0.65$ kJ/mol. The mass of the deuterium and oxygen were taken to be *2.01355* and *16.000* respectively. The cut-offs for LJ interaction and for the real part of the Ewald sum were taken as *0.9* nm. A cubic box of *512* D_2O molecules was considered. The simulations were performed in isothermal-isobaric (NPT) ensemble with molecular dynamics extended system approach of Nose and Anderson[10] Periodic boundary conditions were applied in all three directions and Ewald method[10] was applied to compute electrostatic interactions. The bonds and the angle of the water molecule were constrained by using RATLE algorithm[10,198]. Equations of motion were integrated using velocity Verlet algorithm[10] with 2 fs time step. All the simulations were carried out at a target pressure of 1 atm and at different target temperatures ranging from 223 K to 373 K. For the state points with temperature higher than 285 K, systems were equilibrated for 3 ns and next 3 ns were used for analyzing data. In cases of lower temperatures (273 K and below), we found that longer simulation runs are necessary to achieve equilibration. So for all these states, we have considered equilibration for 10 ns and next 10 ns have been used for data collection and analyses.

3.3: Results and Discussion:

3.3.1: Structure and Thermophysical Properties

We have presented here various structural and thermo-physical properties of heavy water in the temperature range of T=223 K to T=373 K. For comparison, we have also calculated various properties of water from the simulations of SPC/E water.

Radial distribution functions: Radial distribution function is one of the most standard and widely used tools in experiments, theory and simulations to gauge structural order in a many-particle condense phase. Fourier transform of this quantity is related to the scattering intensity. In Figure 3.1, we have shown how oxygen-oxygen radial distribution function g_{OO}(r) of heavy water varies with temperature. This function describes the radial arrangement or distribution of oxygen atoms[67] around a central oxygen atom of heavy water. At a very low temperature T=223 K, the peaks of the $g_{OO}(r)$ plot are quite high and sharp. The trough between the first and the second peak is very low, indicating almost solid[199] like structure. As the temperature is increased, heights of the first and second peaks decrease and height of the trough between the two increases. In order to quantify it, we have shown in Figure 3.2, the values of $g_{OO}(r)$ at the first peak, $g_{max}(r_{max})$ and at the trough between the first and the second peaks $g_{min}(r_{min})$. It is seen that peak height at T=223 is around 4.4 and decreases steadily with

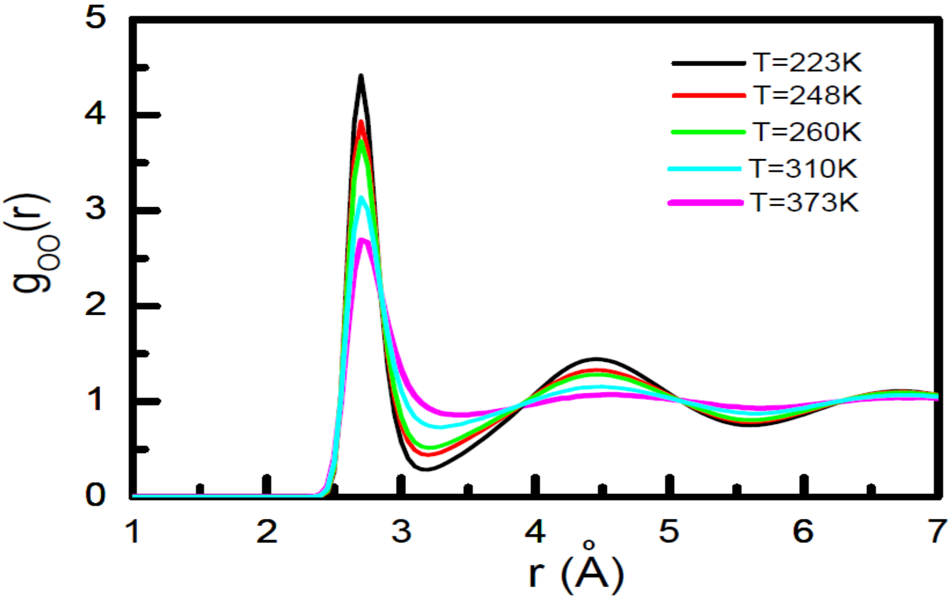

Figure 3.1.Oxygen−oxygen radial distribution functions $g_{OO}(r)$ for heavy water at 1 atm pressure and at different temperatures as indicated in the plot.

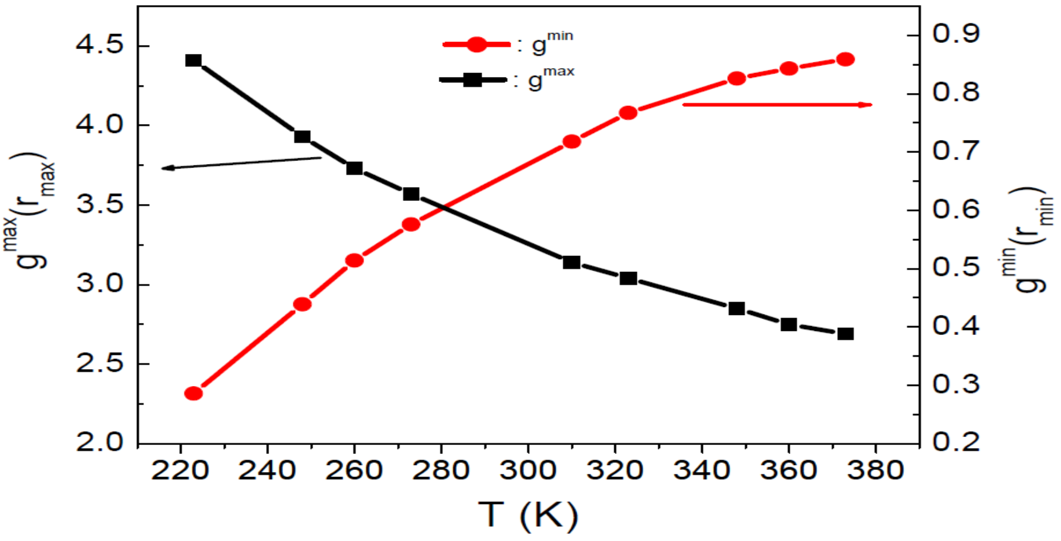

Figure 3.2.Values of the oxygen−oxygen radial distribution function, $g_{max}(r_{max})$, at the first peak (black line with scale on the left axis as indicated by a black arrow) and those $g_{min}(r_{min})$ at the trough between the first and the second peaks (red line with the scale on the right axis as indicated by a red arrow) as a function of temperature.

temperature and at T=373 K it is around 2.7. On the other hand, trough between the first and the second peak increases from 0.28 at T=223 K to 0.86 at T=373 K. The positions of the peaks and troughs remain almost unchanged throughout all the temperatures. Increasing height of the troughs and decreasing height of the first peak in the $g_{OO}(r)$ curves with temperature, in general, indicate that the system is going from ordered to less ordered state

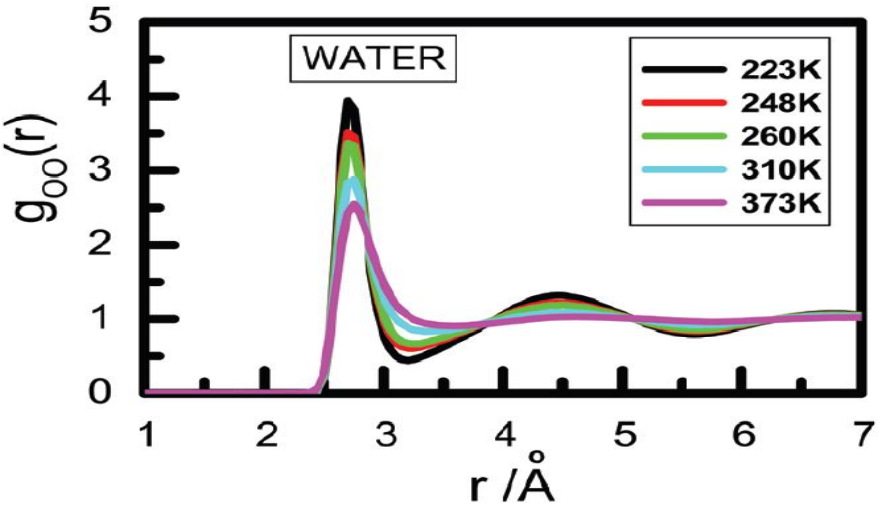

Figure 3.3.Oxygen−oxygen radial distribution functions $g_{OO}(r)$ for SPC/E water at 1 atm pressure and at different temperatures as indicated in the plot.

with the increase in temperature. For comparison, we have also shown $g_{OO}(r)$ and $g_{max}(r_{max})$, $g_{min}(r_{min})$ values of SPC/E water in Figure 3.3 and 3.4 respectively. Similar trend for both the plots as a function of temperature has been observed. Detailed comparison shows that SPC-HW heavy water is more ordered as compared to SPC/E water.

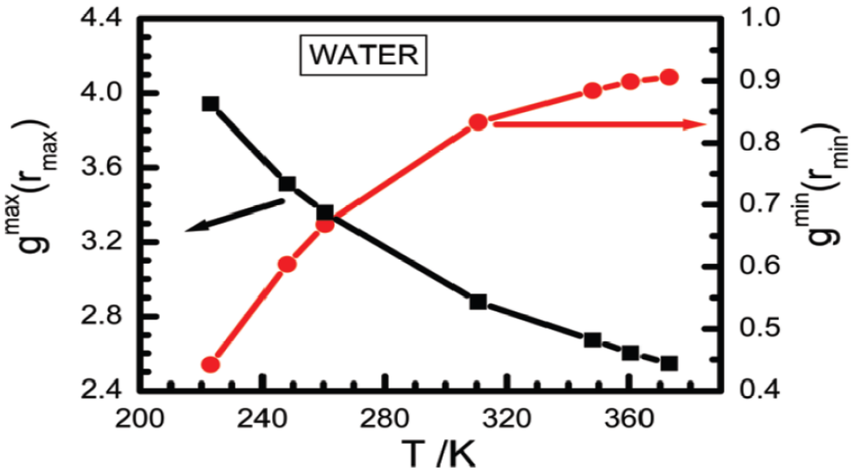

Figure 3.4. Values of the oxygen−oxygen radial distribution function, $g_{max}(r_{max})$, at the first peak (black line with scale on the left axis as indicated by a black arrow) and those $g_{min}(r_{min})$ at the trough between the first and the second peaks (red line with the scale on the right axis as indicated by a red arrow) as a function of temperature.

Density: We have also calculated the average density of heavy water as a function of temperature and values are listed in Table 3.1. The density in *gm/cc* has been calculated from block-averaged volume <*V*>by, $\rho(gm/cm^3) = (N/<V>(nm^3))(M_w/6.022E2)$, where Nis the number of D_2O molecules in the simulation box and M_w is the gram molecular weight of heavy water. As the temperature is increased from T=223K, volume decreases and therefore density increases up to T=260 K and then volume increases and density decreases as we increase the temperature from 260K to T=335.5 K. Therefore, the density maximum in the present case appears at around T=260 K. The present model, thus, underestimates temperature of maximum density (TMD) when compared with the same from the experiment.[188,200] However, all three-site rigid models[176,162] of water also have the problem of underestimating the TMD and present model of heavy water is not an exception. In case of

Table 3.1: Temperature dependence of the average volume and density of heavy water.

SPC/HW Heavy Water			SPC/E Water		
Temperature (*K*)	Volume (nm^3)	Density (*gm/cc*)	Temperature (*K*)	Volume (nm^3)	Density (*gm/cc*)
223	15.45501	1.10151	223	15.37232	0.99622
230	15.41717	1.10422	235.5	15.33810	0.99844
235.5	15.39182	1.10603	248	15.31528	0.99992
242	15.34760	1.10921	260.5	15.32998	0.99896
248	15.33058	1.11044	273	15.38145	0.99562
255	15.30577	1.11224	285.5	15.44591	0.99146
260.5	15.29925	1.11272	298	15.58400	0.98268
265	15.30162	1.11254	310.5	15.65491	0.97822
273	15.31857	1.11131	323	15.78154	0.97038
280	15.31306	1.11171	335.5	15.91985	0.96195
285.5	15.32707	1.11070	348	16.08434	0.95211
290	15.34241	1.10958	360.5	16.25885	0.94189
298	15.37585	1.10718			
305	15.40761	1.10489			
310.5	15.43470	1.10295			
315	15.46938	1.10048			
323	15.52023	1.09687			
330	15.58175	1.09254			
335.5	15.63487	1.08883			

water, this problem has been circumvented by using four- and five-sites rigid models. Recently it has been shown[188] that incorporation of quantum effect using path integral MD

(PIMD)[189] simulation has improved the results. In the same table 3.1 we have also shown the density of water as represented by SPC/E model for comparison. In this case we found that density/volume increases/decreases as we increase the temperature from 223 K to 248 K and then decreases/increases with the increase of temperature. Thus in this case TMD is at around 248 K, which is underestimated by around 29 degree when compared with the experimental TMD value.[176]

Average number of hydrogen bonds ($<n_{HB}>$): Water and heavy water are network forming liquids. In the crystalline state, a water or heavy water molecule is hydrogen bonded with almost four nearest neighbours and in the liquid state too considerable hydrogen bonding persists. We follow here the geometric definition[201] of hydrogen bond (HB). The average number of HB per heavy water molecule, $<n_{HB}>$ is shown in Figure 3.5 as a function of temperature T for SPC/HW model. The number of hydrogen bonds per heavy water molecule, $<n_{HB}>$ is monotonically decreasing with increase in temperature. At T=223 K, because of the low temperature, average number of HB per molecule is around 3.9, very close to the perfect tetrahedral coordination ($<n_{HB}>=4$). As the temperature is raised, because of the thermal motion, average number of HB decreases and finally at T=373 K, it reaches a value of 3.3. At room temperature T=298 K, average number of HB is around 3.6. For comparison, in the same Figure we have shown $<n_{HB}>$ as a function of temperature for SPC/E water (red lines). It is found that number of hydrogen bond for water is less than that of heavy water at any given temperature. Thus SPC/HW heavy water is better hydrogen bonded than SPC/E water.

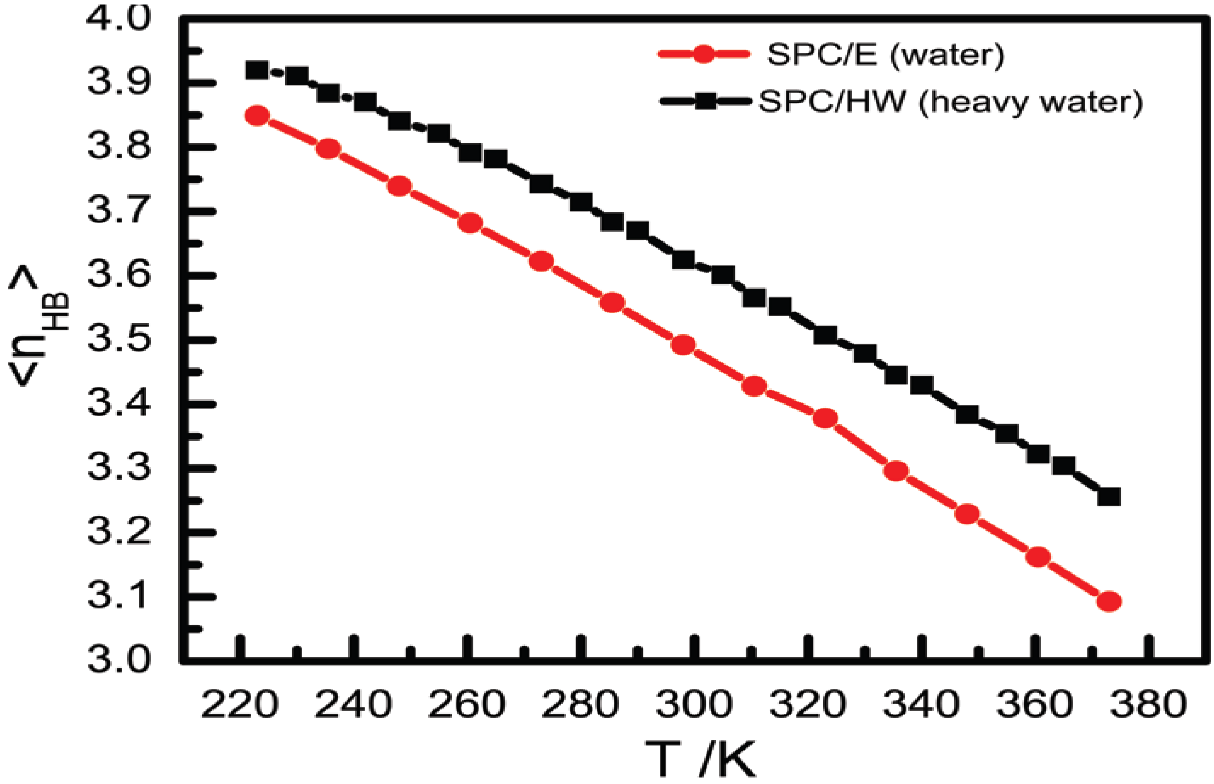

Figure3.5. Values of average number of hydrogen bonds, ⟨n_{HB}⟩, as calculated from the simulation trajectory for heavy water (black line with symbols) and SPC/E water (red line and symbol) as a function of temperature along P = 1 atm isobar.

Average potential energy and heat of vaporization (ΔH_{vap}): Average potential energy of heavy water as obtained from the SPC/HW model has been calculated by taking block average of the instantaneous potential energy data and finally it is corrected for self-polarization by subtracting the self-energy of 6.286 kJ/mol for the SPC/E-HW model[2]. The corrected par particle potential energy <E>/N as a function of temperature is displayed in the inset of Figure 3.6. There is almost a linear increase of the potential energy with temperature. From these potential energy values we can calculate heat of vaporization according to the approximate formula:

$$\Delta H_{vap} = -\frac{<E>}{N} + RT \qquad (3.1)$$

where N is the number of water molecules, R is the universal gas constant and T is the temperature in Kelvin. In the above equation $\langle \cdots \rangle$ represents ensemble average. In deriving the above formula, potential energy of the gas phase, E_{gas} is taken as zero and *PV* term of the liquid phase is considered to be too small as compared to the same of the gas phase and thus neglected. The *PV* term for the gas phase has been evaluated by assuming ideal gas behavior of the water vapor. No correction[80] has been incorporated for taking into account the quantum and other effects during the calculation. The computed heat of vaporization of bulk heavy water as a function of temperature has been shown along with other reported[97,202-205] results in Figure 3.6.a A linearly deceasing trend of the ΔH_{vap} with temperature has been observed, and this trend is similar to that observed in the experimental and other theoretical findings at moderate to high temperatures. [202-205] The simulated value is quite close to the experimental value[97] at T=298 K, but at higher values of temperature, deviation of the same from the experimental data increases. This discrepancy may arise from the approximations involved in the above equation and/or for neglecting the quantum effect. Recent studies[181,191,202] have shown that incorporation of quantum effect improves the result for heat capacity. The calculated heat of vaporization data have been finally fitted to an empirical equation of the form $$\Delta H_{vap} = 68.603 - 0.08723T + 0.005T^2 \qquad (3.2)$$

and therefore can be used to obtain the ΔH_{vap} at any desired temperature. For comparison, we have also calculated ΔH_{vap} for SPC/E water at different temperatures and shown in Figure 3.6. b. In case of water, the rate of change of heat of vaporization with temperature is more as compared to SPC/HW heavy water. Comparison with experimental data shows SPC/E model overestimates experimental data at lower temperatures, whereas underestimates the same at higher temperatures.

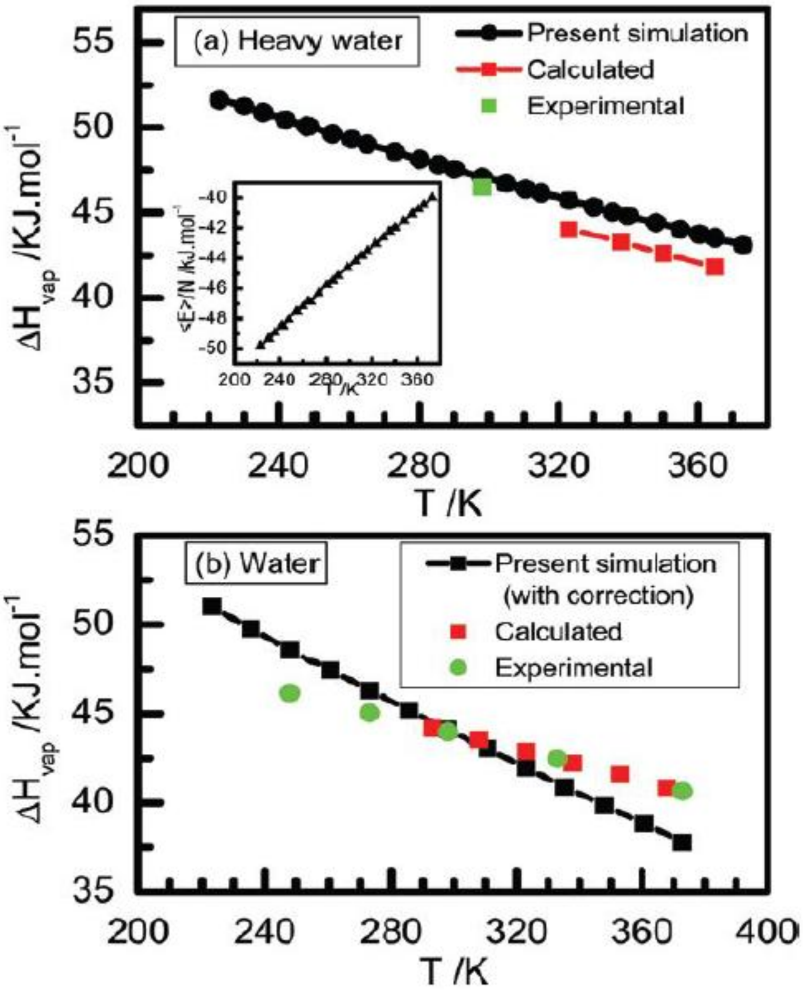

Figure 3.6.Computed heat of vaporization, ΔH_{vap}, along with the available experimental results for (a) heavy water and (b) SPC/E water at different temperatures along the P = 1 atm isobar. The inset in panel a shows the potential energy per particle for the same.

Constant pressure heat capacity (C_p): The constant temperature heat capacity C_p has been calculated here from the finite difference derivative of the enthalpy, H with respect to

$$C_p = \frac{H(T+\Delta T) - H(T-\Delta T)}{2\Delta T} \qquad (3.3)$$

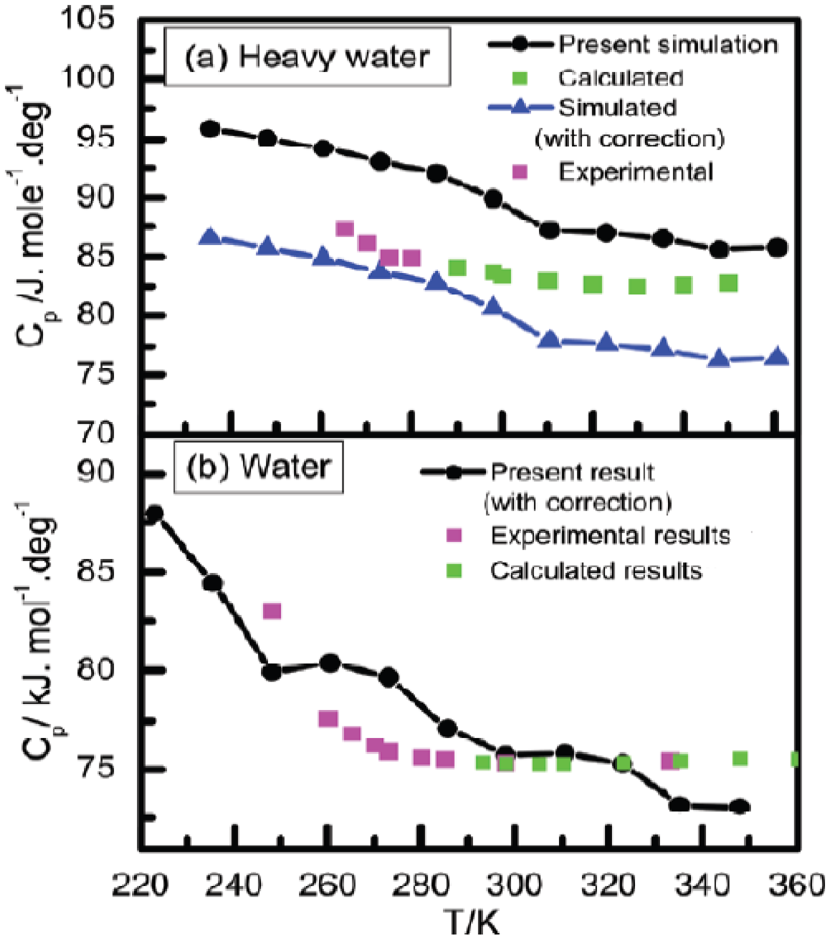

Figure 3.7.Isobaric heat capacity Cp of (a) heavy water and (b) SPC/E water at different temperatures along the P = 1 atm isobar.

temperature T using the formula The constant pressure heat capacity is an important quantity as it is related to the existence and stabilities of various phases of water. In Figure 3.7.a, we have shown the results for heavy water as obtained from the present simulation along with other experimental and calculated results. It has been observed experimentally[202-207] that the

C_p decreases with temperature. Similar trend (see Figure 3.7. a) has been observed in the present simulation results also, although the individual value differs from the experimental ones by almost a constant magnitude, particularly at higher temperatures. Present simulation results overestimates experimental values. A correction term can be added to this for compensating the intramolecular vibrational modes and this has been estimated[51] at T=300K to be around –9.3 J mol^{-1}K^{-1}. In absence of this correction term at other temperatures, we have added the same constant term at all temperatures. The corrected results underestimate experimental values. Again neglect of the quantum nature of the deuterium atom may be the reason for this difference and in fact it has been shown recently that path integral simulation, which takes into account quantum effect, improves the result for the heat capacity of water immensely.[203,206] The simulation results for c_p of SPC/E water as a function of temperature have also been shown in Figure 3.7.b along with other results. Although overall agreement with the experimental result is good, experimental minimum in the heat capacity has not been well reproduced.

Isothermal Compressibility (*κ_T*): The isothermal compressibility κ_T is defined[176,23,209] as

$$\kappa_T = -\frac{1}{V}\left(\frac{\partial V}{\partial P}\right)_T = \frac{\langle V^2\rangle - \langle V\rangle^2}{k_B T\langle V\rangle}, \qquad (3.4)$$

where V, T and P are volume, temperature and pressure of the system respectively. In Figure 3.8(a) we have shown κ_T for heavy water as calculated from the simulation trajectory over the whole temperature range. There are oscillations in the calculated data and the oscillation is more in the low temperature region. In order to compare the result with the available experimental data, in Figure 3.8(b) we have plotted experimental data[210] along with calculated data as a function of scaled temperature *T/TMD*, where *TMD* is the temperature of maximum density. In the present case TMD is around 260K where as the experimental TMD

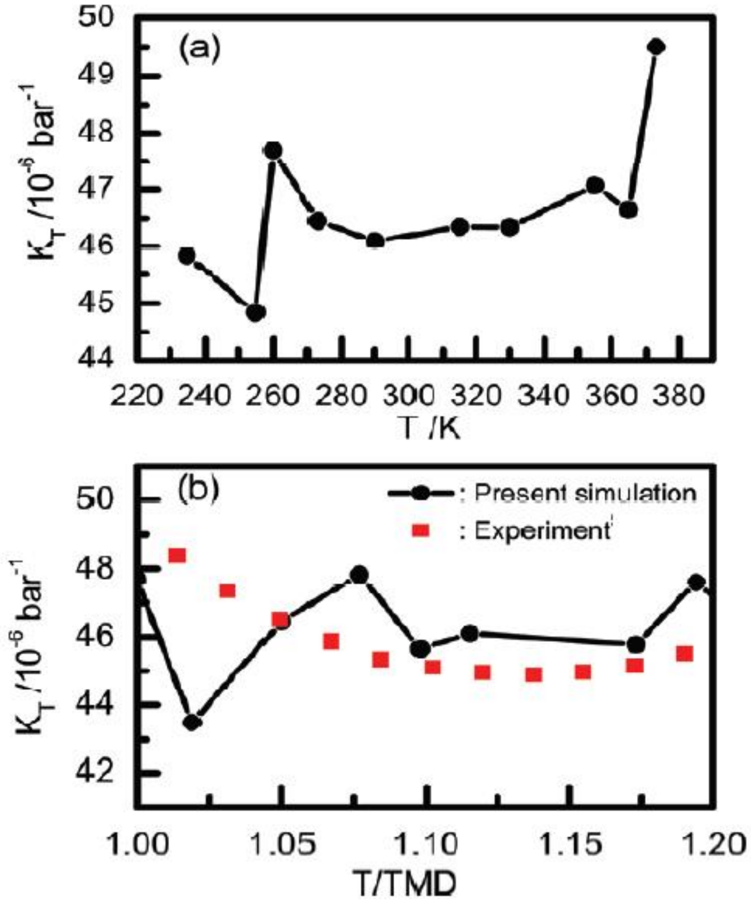

Figure 3.8.Isothermal compressibility κ_T of heavy water along P = 1 atm isobar as a function of (a) absolute temperature, T, and (b) T/TMD, where TMD is the temperature of maximum density for this model.

of heavy water is around 284 K.[188]Although individual values are in overall agreement with those from the experiment, because of the inherent oscillation in the calculated data, it is difficult to predict whether a minimum exists in the calculated isothermal compressibility vs. temperature plot.

Static dielectric constant (ε_0): The static dielectric constant $\varepsilon_0$was calculated[211,212] from the total dipole moment M (=$\Sigma\mu_i$, where μ_i is the molecular dipole moment of the i^{th} molecule) based on the equation

$$\varepsilon_0 = 1 + \frac{4\pi}{3\langle V\rangle k_B T}\left[\left\langle M^2\right\rangle - \left\langle M\right\rangle^2\right], \qquad (3.5)$$

Where k_B is the Boltzmann constant and $\langle V\rangle$ is the average volume of the simulated system. In Figure 3.9.(a), we have shown the present simulation results for the static dielectric constants of heavy water as a function of temperature. The static dielectric constant ε_0 increases with the decrease in temperature. In the low temperature region there is considerable oscillation of the values of ε_0 as a function of temperature. It is well established[13] that calculation of dielectric constant from simulation is quite difficult as the convergence of the calculation is very slow. This problem increases further in the low temperature region. In the present calculation ε_0 is calculated by averaging over 5 ns time scale for temperature above 273 K and for the lower temperatures the averaging is performed over 10 ns. In the same Figure, we have included the results from the experiments (red points) and it is found that the present results are in reasonably good agreement with those from experiment.[107] There is at least 50% decrease in the dielectric constant of water when temperature is reduced from T=223 K to T=373 K. At T=298 K the calculated dielectric constant is 67.7 as compared to 78 obtained from experiment. We have also calculated these quantities for SPC/E water model at different temperatures and the dielectric constant ε_0, G_k

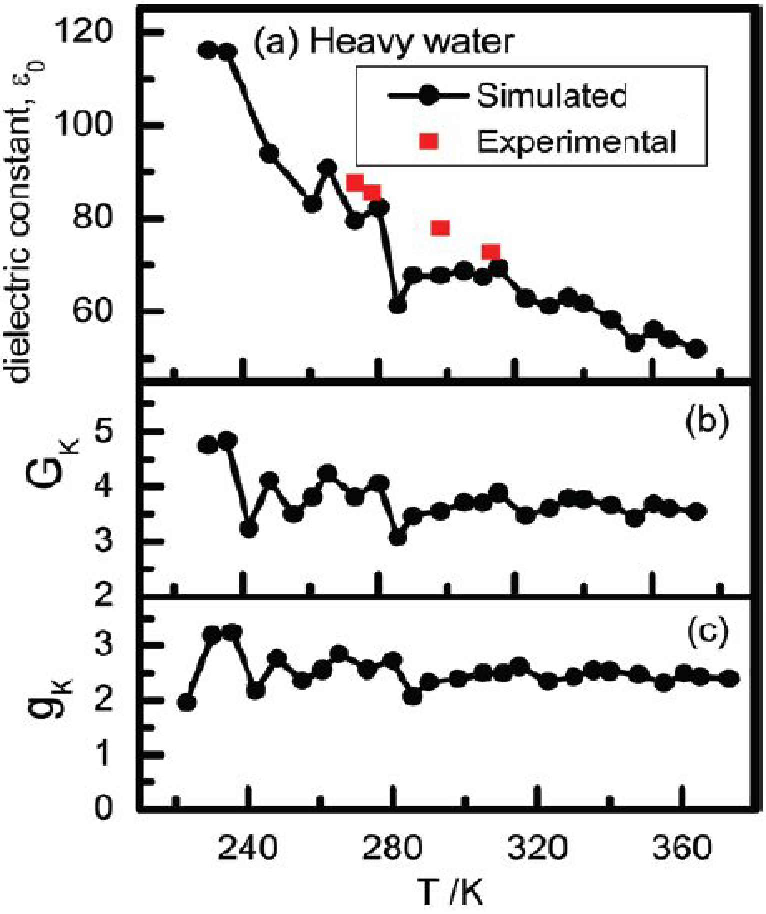

Figure 3.9.Plots of (a) static dielectric constant ε_0, (b) finite system Kirkwood factor G_k, and (c) infinite system Kirkwood factor g_k as calculated from the simulation trajectory using a dipole fluctuation formula for heavy water at different temperatures along P = 1 atm.

and g_k are shown in Figure 3.10. Like heavy water, in this case also considerable fluctuation has been observed in the calculated quantities. It is important to mention that dielectric constant is calculated from the fluctuation of the total dipole moment and this quantity converges very slowly.[107] At room temperature, around 4-5 ns of simulation time is necessary for averaging and the problem of convergence is even more at lower temperatures and at around 235 K, a simulation time of 7-8 ns is required for averaging.

Finite and infinite system Kirkwood factors $G_k$and g_k: The finite system Kirkwood factor G_k is calculated from the formula[107]

$$G_k = \frac{\langle M^2 \rangle - \langle M \rangle^2}{N \langle \mu^2 \rangle}, \qquad (3.6)$$

and the infinite system Kirkwood factor g_k is related to G_k through the relation

$$g_k = \frac{2\varepsilon_0 + 1}{3\varepsilon_0} G_k . \qquad (3.7)$$

These two quantities for heavy water are shown in Figure 3.9(b) and (c). There is not much variation of these properties with temperature except that at a very low temperature below T=240 K there is a sudden increase of the values. At room temperature the calculated values G_k and g_k are *3.56* and *2.39* respectively. However because of the large fluctuation associated with the values at lower temperature range, no comments can be made on this increase in the values below T=240 K. For SPC/E water G_k and g_k are shown respectively in Figure 3.10(b) and (c). These two quantities, like water, do not vary much with temperature except at a very low temperature.

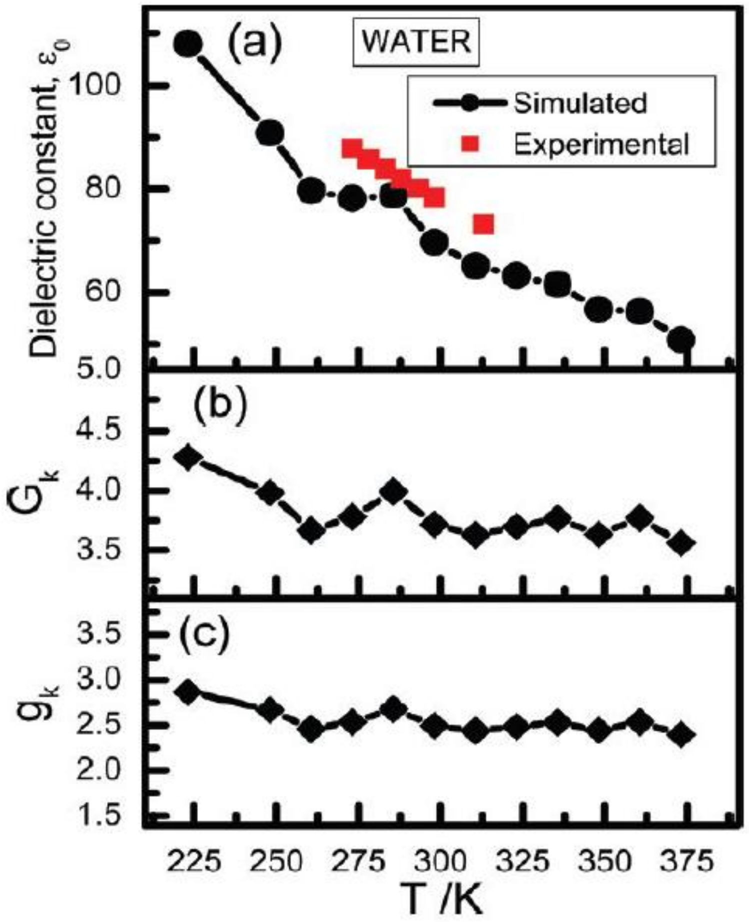

Figure 3.10.Plots of (a) static dielectric constant ε_0, (b) finite system Kirkwood factor G_k, and (c) infinite system Kirkwood factor g_k as calculated from the simulation trajectory using dipole fluctuation formula for SPC/E water at different temperatures along P = 1 atm.

Thermal expansion coefficient α_P: The thermal expansion coefficient has been calculated by using a finite difference expression

$$\alpha_P = \frac{1}{V}\left(\frac{\partial V}{\partial T}\right)_P = \frac{1}{V(T)}\left(\frac{V(T+\Delta T)-V(T-\Delta T)}{2\Delta T}\right)_P, \qquad (3.8)$$

where, V(T) is the volume of the system at temperature T and ΔT is taken as 12.5 K. The calculated values are plotted as a function of temperature and shown in Figure 3.11(a) for

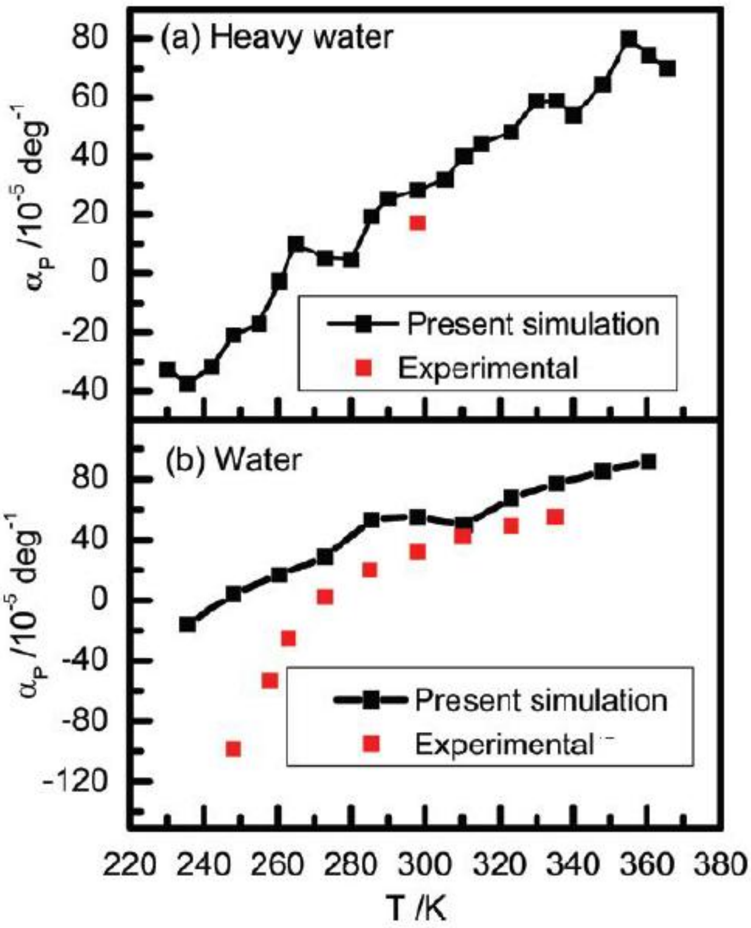

Figure 3.11. Plot of thermal expansion coefficient α_P as calculated from the simulation trajectory for (a) heavy water and (b) SPC/E water at different temperatures along P = 1 atm using a finite difference formula.

heavy water and in Figure 3.11(b) for SPC/E water. The thermal expansion coefficient values are monotonically increasing with increasing temperature and the values changes sign from negative to positive at around T=260 K, where we observed the density maximum. The variation of this quantity with temperature is almost linear with local oscillations in the values. No experimental data is available on the temperature dependence of the α_P values of heavy water. However, the calculated value is very close to the experimental value at 298 K. For water experimental data for α_P are available and comparison with the results from simulation of SPC/E model shows that at lower temperature there are large deviations from the experimental values.[176]

3.3.2: Dynamics

Molecular dynamics simulations have been used to investigate translational and rotational dynamics of bulk heavy water for a wide range of temperatures using the SPC/HW model. Translation diffusivity (D) at different temperatures has been evaluated by using Einstein relation involving mean square displacements and time (Eq.(1.50)).In Figure 3.12, we have shown the diffusion coefficients for heavy water (red lines with filled squares) as obtained from the present molecular dynamics simulations. As expected (see Figure 3.12), the diffusion coefficient values gradually increase with temperature. In the same plot, diffusion coefficients derived from the present simulation study for heavy water have been compared with the corresponding experimental results (green triangles). The results show that SPC/HW model underestimates diffusion coefficient values obtained from experimental investigations. Finally, these diffusivity values for heavy water have also been compared with those(see blue curve with filled circles) obtained from simulations of water using SPC/E water model. As expected, it is seen that water has higher diffusivity than heavy water at all temperatures.

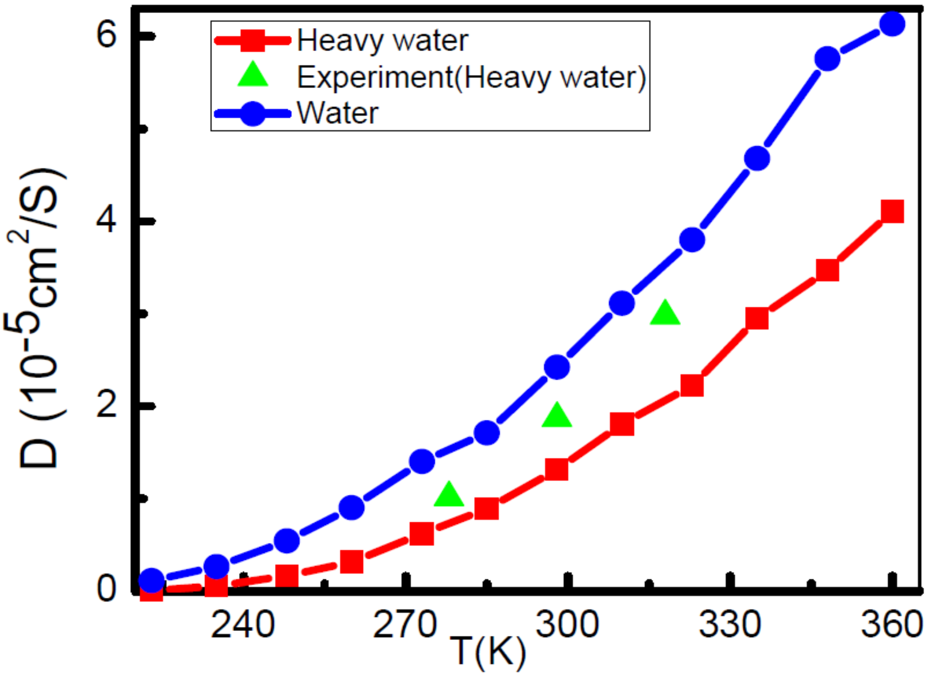

Figure 3.12 Diffusion of bulk water calculated from MSD at different temperature.

As heavy water is a network forming liquid due to extended hydrogen bonded network formation among its constituent molecules, rotational or orientational dynamics of the heavy water molecule plays an important role in the stability and dynamics of hydrogen bond networks. Here we use molecular dynamics simulations to calculate different orientational time correlation functions (TCF) to gauge the rotational mobility of these heavy water. Our main intention is to investigate the temperature dependence of the rotational dynamics of heavy water by calculating orientational time correlation functions of different molecular vectors of the heavy water. We calculate time correlations function $\Gamma_l^{\alpha}(t)$ of the molecular orientational vector u_{α} defined as

$$\Gamma_l^{\alpha}(t) = \langle P_l\big(u_{\alpha}(t).u_{\alpha}(0)\big)\rangle \qquad (3.9)$$

Where P_l is the Legendre polynomial of order l. It defines the time evolution and hence the orientational dynamics of the molecular vectoru_{α}. The angular brackets in the above equation represent average over time origins as well as the number of molecules. In the present work, two unit vectors namely (i) dipole moment vector ($u_\alpha = \mu$) (ii)OD bond vector ($u_\alpha = OD$)

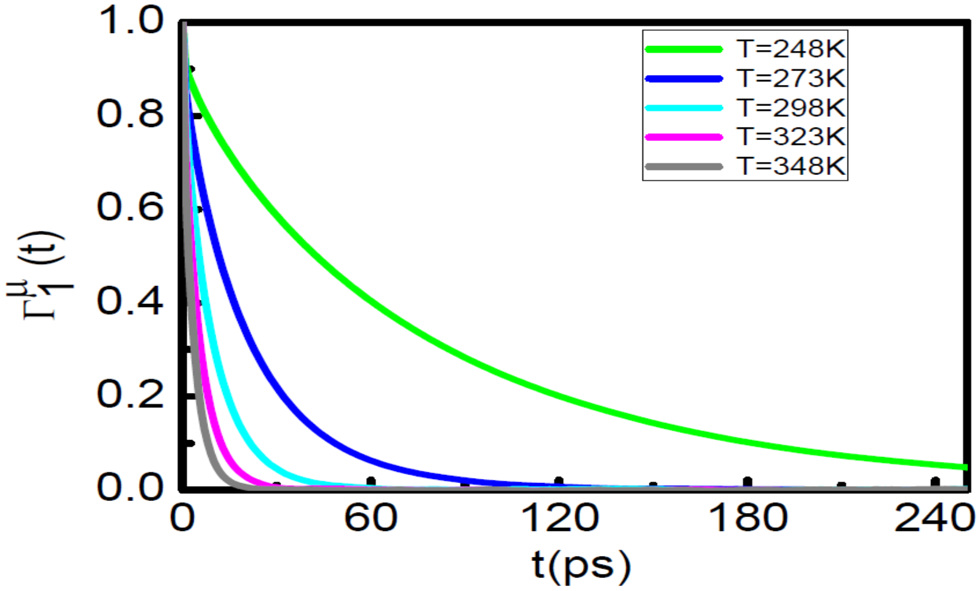

Figure 3.13.Time correlation function of the dipole moment vector (μ) of SPC/HW heavy water at different temperatures for Legendre polynomial of order $l = 1$.

have been chosen to investigate the effects of temperature on rotational dynamics of heavy water. We have considered Legendre polynomial of order 1 and 2 (l=1,2) for this exploration. The time correlation functions corresponding to the dipole moment vector (μ) of the heavy water have been shown in Figure 3.13 and Figure 3.14 for l=1 and l=2 respectively. The same has been illustrated in Figure 3.15 and Figure 3.16 for OD bond vector. All the Figures demonstrate the fact that with the rise in temperature, rotational motion becomes faster and hence the rotational time constants decreases with temperature. The effect of temperature on both the unit vectors selected here (μ, *OD*) are quite similar for first order Legendre polynomial. In case of TCF involving 2nd order Legendre polynomial, surprisingly, the observation is not similar. The decay of the TCF of the dipole moment vector is quite rapid in

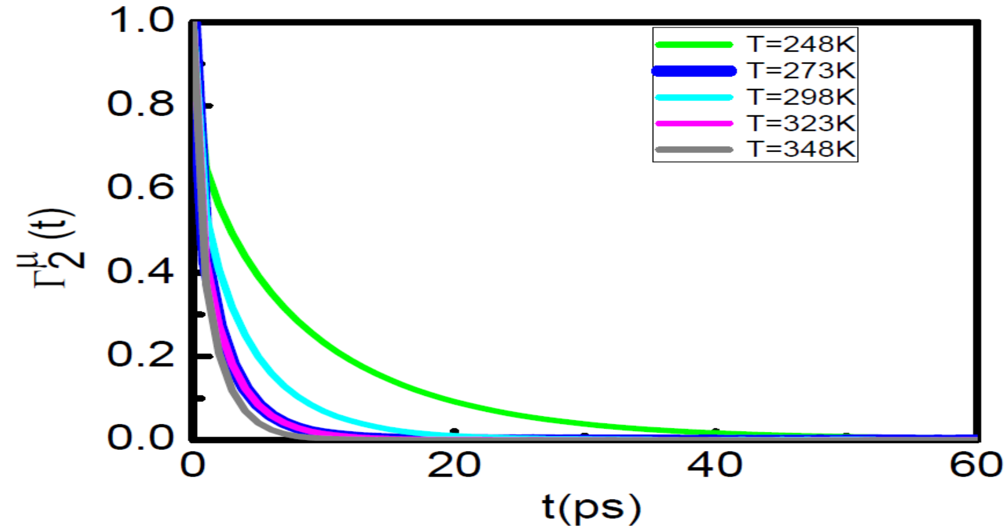

Figure 3.14 Time correlation function of dipole moment vector (μ) of SPC/HW heavy water at different temperatures for the second order Legendre polynomial $l = 2$.

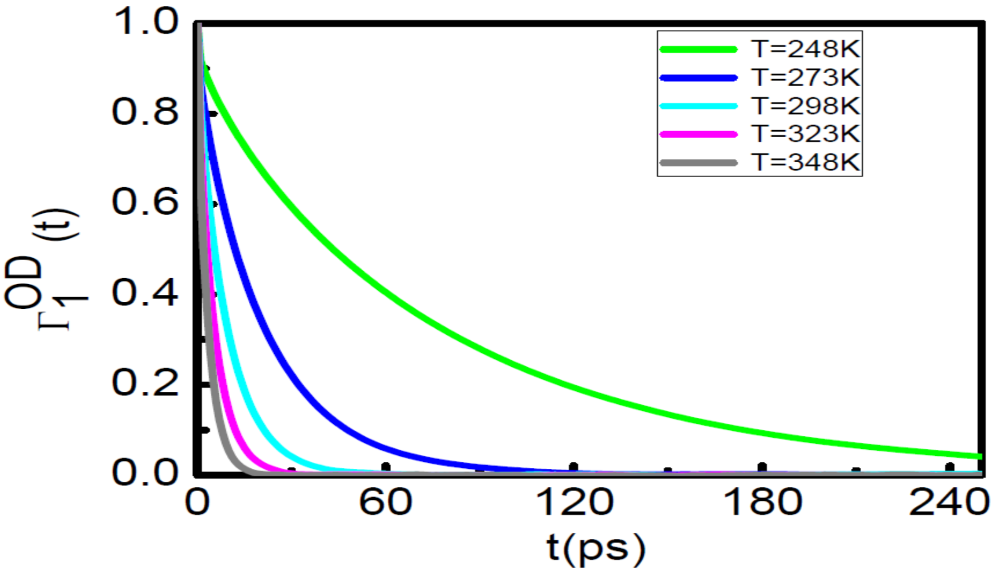

Figure 3.15 Time correlation function of the OD bond vector of SPC/HW heavy water at different temperatures for Legendre polynomial of order $l = 1$.

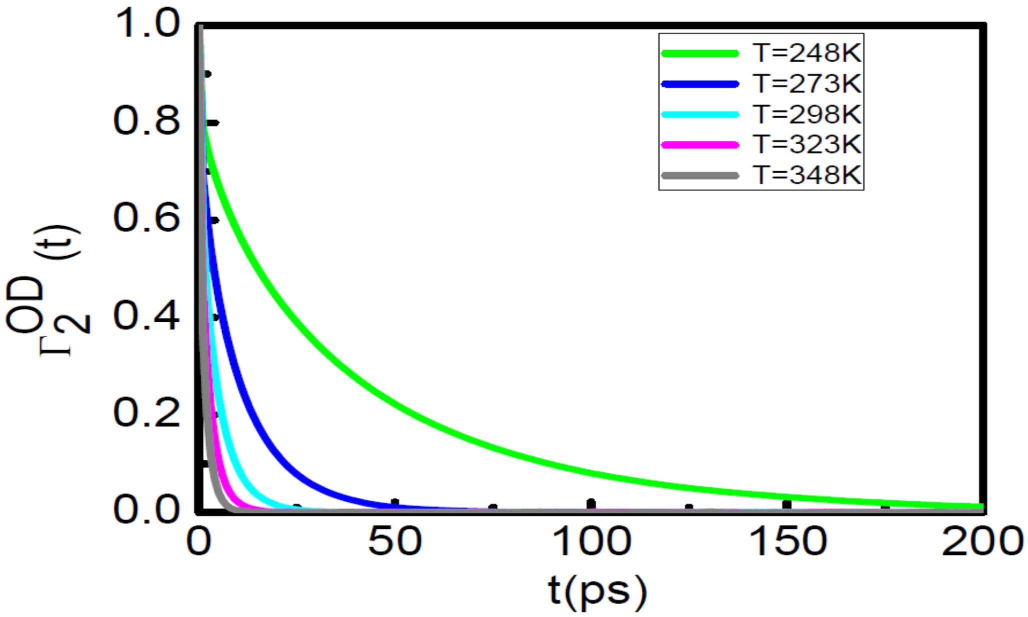

Figure 3.16 Time correlation function of OD bond vector of SPC/HW molecule comparing at different temperature for Legendre polynomial of order $l = 2$.

comparison to the same for OH bond vector. This phenomenon is quite surprising and it needs further investigation.

3.3.3: Effect of potential parameters on the results

It has been observed so far that various quantities calculated for SPC/HW and SPC/E models although show similar trends, individual values are quite different. It is important to remember that these two models are geometrically exactly the same and they differ from each other in mass and in the only force field parameter, the partial charges on the atoms. Therefore, in order to assess the effect of these two parameters on the calculated results, we have performed two additional sets of simulations. In one case, 3 different simulation systems have been considered, all of which have same potential parameters (including partial charges on the atoms) except that the mass of the hydrogen atoms are different. We have considered hydrogen masses 1, 2 and 3 representative of hydrogen, deuterium and tritium respectively. In another set we have considered various simulation systems, in each of which, heavy water mass has been used, but charges on the atoms have been different in different systems. Except charges, all other potential parameters are the same in all these simulated systems. In Figure 3.17, we have shown the effect of mass as well as charge on the calculated density by plotting scaled density $\rho\sigma^3$(where σ is the size parameter of the oxygen atom as given in the dynamical properties has also been investigated. We have calculated and shown in Figure 3.19,

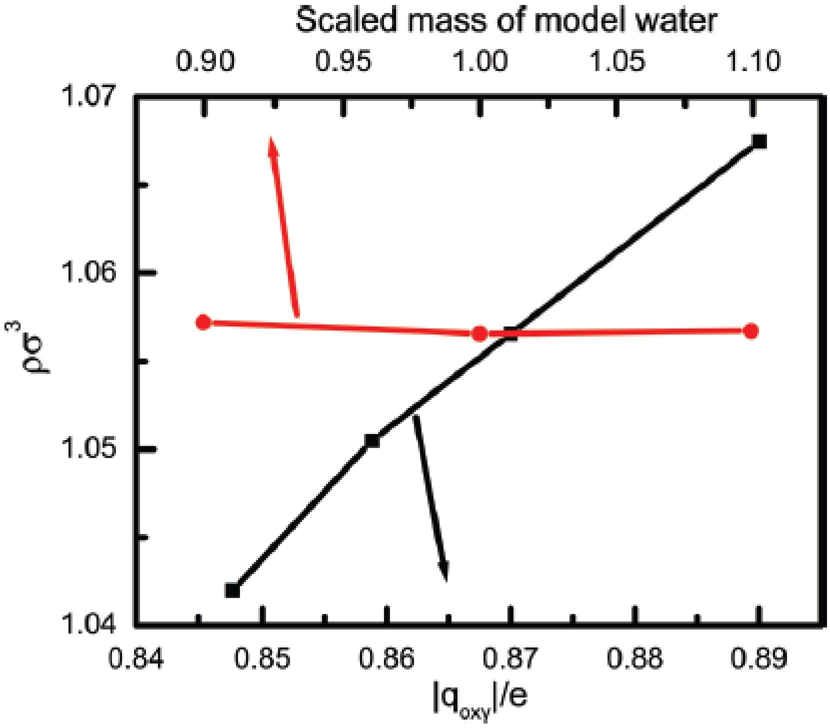

Figure 3.17. Scaled density $\rho\sigma^3$ (where ρ is the number density and σ is the LJ size parameter) as a function of partial charge on the oxygen atom (black line with the bottom axis as indicated by a black arrow) and as a function of mass (red line and top axis for mass as indicated by a red arrow) of model water scaled by the heavy water mass.

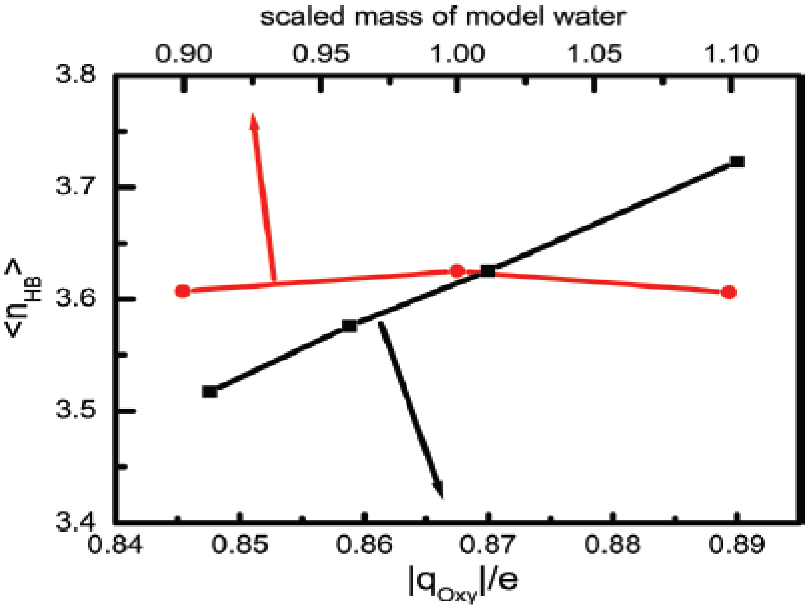

Figure 3.18.Average number of hydrogen bonds, ⟨n$_{HB}$⟩, per water molecule as a function of partial charge on the oxygen atom (bottom axis as indicated by a black arrow) and as a function of mass (top axis as indicated by a red arrow) of model water scaled by the heavy water mass.

force field) as a function of mass of water scaled by that of heavy water (as shown by the top axis) and also as a function of absolute value of charge on the oxygen atom, |q_{oxy}| (as shown by the bottom axis). In this case the value of the mass is fixed to that of a heavy water. It is clear from this plot that there is no significant effect of mass on the scaled density, but there is considerable effect of partial charges of the atoms on the density. In Figure 3.18, we have shown the average number of hydrogen bonds per water molecule <n_{HB}> as a function of mass as well as charge on the oxygen atom and we found similar trend as that observed in Figure 3.17. Effect of mass on the calculated quantity is not significant, whereas charge has significant effect on the same. The effect of mass and partial charges on the atoms on various the mean squared displacements of these modified water models having different masses. As the slope of the MSD is related to the diffusivity, the diffusivity of the oxygen (of water/heavy water) also modifies (although slightly) with the change in the mass (see the first

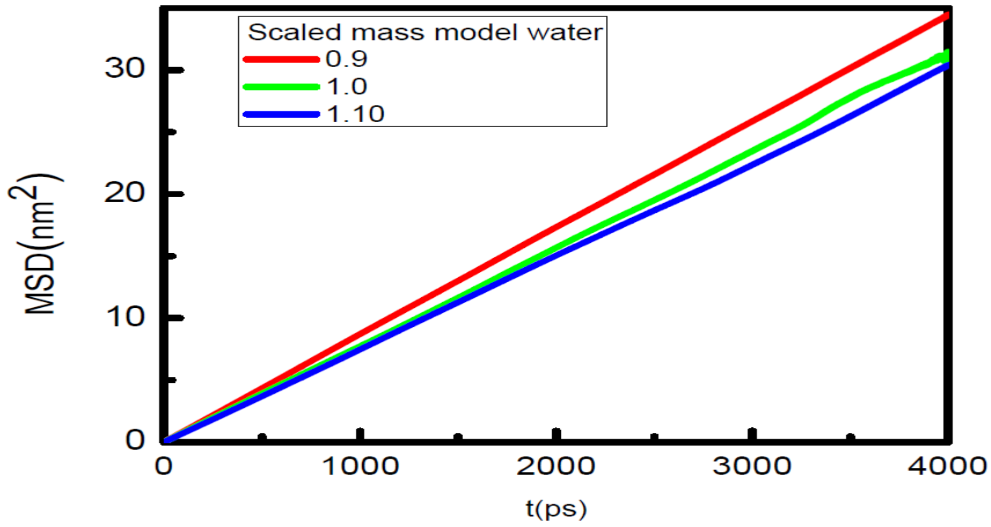

Figure 3.19. Mean square displacement (MSD) of water molecule as a function of mass model water scaled by the heavy water mass.

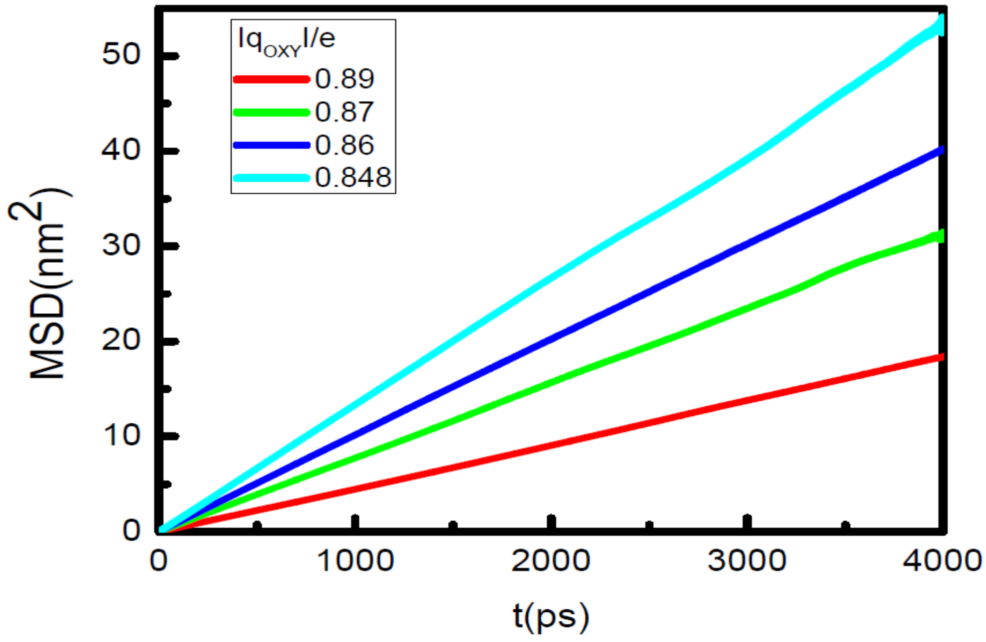

Figure 3.20 Mean square displacement (MSD) of heavy water molecule as a function of partial charge on oxygen of heavy water molecule.

two columns of the Table 3.2. This is quite expected as particle with heavier mass will move slower. It is important to notice that like density and <n_{HB}>, in case of diffusivity also, the Mean square displacement (MSD) of heavy water molecule as a function of partial charge on oxygen of heavy water molecule. effect of charge is more pronounced. This is evident from the plots of the MSDs for different partial charges (see Figure 3.20) and from the last two columns of the Table 3.2. Thus, the present study Clearly demonstrates that the partial charge on the atoms of water/heavy water is a sensitive parameters and one can thus tune this parameter to obtain an improved model of heavy water.

Table 3.2: Effect of mass and partial charge on bulk diffusion of water/heavy water model.

Effect of mass		**Effect of partial charge**	
Scaled mass	**Diffusion($10^{-5}cm^2/sec$)**	**$\lvert q_{OXY}\rvert$/e**	**Diffusion($10^{-5}cm^2/sec$)**
		0.89	0.7629
0.9	1.4188	0.87	1.3165
1.0	1.3165	0.86	1.6679
1.1	1.2767	0.848	2.1773

3.3.4: Summary and Conclusions

We have used extensive molecular dynamics simulations of heavy water in the temperature range of 223K to 373 K at 1 atm pressure to calculate various structural and thermo physical properties of heavy water as obtained from the newly developed SPC/HW model. For comparison, we have also calculated and presented here various properties of water as obtained from simulations of SPC/E model. The present 3-site rigid model of heavy water, like all the 3-site rigid models of water, underestimates the temperature of maximum density. Present study predicts it at $T=260$ K instead of experientially observed value[188] at $T=284$ K. The model gives more or less good results throughout the whole temperature range spanning cold and hot liquid below the boiling point. The variation of dielectric constant, ε_0 as a function of temperature is not smooth, with many local oscillations. It is probably due to the well-known convergence problem[107] associated with the calculation of ε_0 from simulation trajectory. Other quantities such as heat of vaporization, constant pressure heat capacity and coefficient of thermal expansion varies with temperature smoothly. Like all 3-site water models, the present model of heavy water also yields satisfactorily good results for various properties, but exact agreement with the experimental results as far as liquid anomalies are concerned is not so good. We have also calculated the dynamical properties of heavy water at a wide range of temperatures. Both translational diffusion coefficients and rotational time constants have been obtained from the MD simulations and the effect of temperatures is shown to be as usual.

Present simulation results on structural, thermodynamic and dynamic properties of heavy water indicate that the SPC/HW model of heavy water requires further modifications. The SPC/HW model is a variant of SPC/E model and it differs from the SPC/E model only due to different partial charges on atoms and due to change of mass. We have therefore investigated the effects of these two parameters on various calculated properties and demonstrated that the effect of charge is significant, whereas that of mass is not so prominent. It is interesting to know how various structural parameters of heavy water such as order parameters for tetrahedrality, H-bond distribution, orientational parameter for the second solvation shell molecules etc. vary with temperature and their possible relation with various thermodynamic anomalies of water and heavy water. Investigation in this direction is in progress.

So far we have dealt with structure, dynamics and properties of bulk water and heavy water. Interesting modifications of structural, dynamic and thermodynamic properties of water can be observed when water meets interfaces.[30,109, 133, 213,214,215,216] The interface may arise due to solvation of different solute molecules in water or due to physical contact of water with a large extended solid surface. In the former case a molecular interface is generated and it is interesting to know whether structural integrity of water will be retained in presence of such molecular interfaces. In this connection, structural information of two molecular interfaces namely that of urea-water and guanidinium chloride (GdmCl)-water are extremely important as these two interfaces are relevant to protein denaturation.

Chapter 4

Water at Molecular Lengthscale Interfaces

Depending on the nature and size of the solute, properties of bulk water changes when a solute is dissolved in it. According to the size of the solute, the lengthscale of the interface and hence properties of the solution change.[19] The interface may be created due to solvation of different small solutes in water or due to solvation of larger molecules like protein as well as physical contact of water with a large extended solid surface. In the former case a molecular interface is generated and it is interesting to know whether structural integrity of water will be retained in presence of such molecular interfaces. Proteins and other biological molecules exist in their aqueous solution in folded state. It is well known that urea and guanidinium chloride (GdmCl), due to their uncanny ability to unfold proteins, are universally used as chemical denaturants forproteins.[109,133,] The mechanism of such denaturation process is still debated.[109,122,123,125,127,132,133,217-222] The exact mechanism by which these small molecules(urea and guanidinium ion) bring changes in microscopic environment and facilitate denaturation process is still unknown despite a large number of studies, both experimental and theoretical, have been devoted in this direction.

In fact, there are two schools of thought as far as the mechanism of the denaturation is concerned.[132,223-253] One is the “direct mechanism”, according to which the small denaturant molecule binds directly to the protein at the surface and inside the protein moiety and thereby opens up the protein structure.[223-248] is Another probable mechanism is the so called “indirect mechanism”, which describes the denaturation process as an indirect effect. In this case, the denaturant first breaks the tetrahedral network structure of water and thus helps water to enter and invade the protein interior. [132,249-253] It is still not clear, by what mechanism, indirect or direct, these two denaturants urea and GdmCl denature protein and whether both of them follow the same mechanism. In some cases, it may also so happen that both the pathways are operational. Although, both urea and guanidinium ion are structurally quite similar, these two species have quite different chemicalnature. Urea is a non-polar molecule whereas GdmCl is an ionic species. Due to its ionic character, guanidinium ion (Gdm^+) can interact with the charge groups of the protein through Coulombic interaction. One interesting aspect of the aqueous solution of GdmCl is the counter-intuitive same charge ion-pair formation. It will be interesting to investigate the implication of this same charge ion-pair formation on the water structure as well as on the process of protein denaturation. In this connection, detailed knowledge of two molecular interfaces namely that of urea-water and GdmCl-water are extremely important. This chapter is divided into two parts. In **Chapter 4-A**, we analyze structural and dynamical details of aqueous solution of urea at different concentrations in the light of its effect on water structure and dynamics and its implication in protein unfolding mechanism . In **Chapter 4-B**, the details of the effect of GdmCl on the water structure and dynamics, the propensity of the ionic guanidinium moiety (Gdm^+) to form stacked ion-pair in its concentrated aqueous solution and its implication and relation to both arginine-arginine assembly in case of protein folding and arginine-Gdm+ direct interaction in case of the protein denaturation process are thoroughly discussed.

Chapter 4

PART-A

Structure and Dynamics of Aqueous Urea Solution: Is Urea a Structure Breaker?

4.A.1: Introduction

Aqueous urea solution has received a lot of attention[10,29,57,61,62,65,67,71,75,109,122,123,125,127,132,133,217-278] over the last few decades and is still continuing to be a subject of intense research. There are several reasons behind it. First, aqueous urea solution at high concentration is widely used to denature proteins[109,122] and therefore has general biological relevance.[123] Apart from that, urea-water aqueous solution has many interesting properties such as enhancement of solubility of long chain hydrocarbons,[125,217] prevention of micelle formations[218,219] etc. Finally, urea-water systems can be considered as an important test case to understand aqueous solvation of a neutral solute with both hydrophobic and hydrophilic (those providing hydrogen bonding sites) groups.[133,220-222] Although it is well known that a fine balance between water-water, water-urea and urea-urea interactions regulates the behaviour of aqueous solution of urea, fundamental understanding of the correlation between structural aspects of this solution and the above mentioned properties is still lacking.

In this context, the most important issue that the scientists around the world are trying to understand is: how urea denatures a protein? Two important pathways have been proposed to explain the denaturation process. At present, the most wide-spread view[223-247] is that urea directly attacks the polar backbone as well as nonpolar residues of a protein helping water to penetrate into the core. In another very popular hypothesis suggested by Frank and Franks[248] in the 1960s, it is posited that urea breaks the tetrahedral network structure of water and thus acts as a structure-breaker or chaotrope and indirectly helps in denaturing proteins in water. Since then, many experimental and theoretical studies have been devoted to understand how structure of water changes in presence of urea and have produced disparate results yielding three distinctly different views. In some works, it is claimed that urea disrupts water structure and thus urea is termed as a structure-breaker or chaotrope. Many others have termed urea as structure-maker or kosmotrope as they find urea to enhance water structure.

Both of these two views point to the peculiar behaviour of urea in changing structure of water and suggest “indirect effect”[132,249-253]of urea on protein denaturation. Apart from these two extreme views, another group of findings suggests that there is no or only negligible changes in the structure of water due to addition of urea. This view suggests urea’s action through direct effect; in which urea followed by water penetrates the native protein molecule to denature it.[254-259]In addition to these views, many researchers also suggest both direct and indirect effects of urea in the denaturation process.

In order to understand the effect of urea on the water structure, it is essential to know about the detailed structure of pure water (in absence of urea). Water is an intriguing liquid due to its many anomalous properties and tetrahedral network structure. However, linking these anomalous properties of water to its structure has been a difficult task. One famous idea about water structure and its relation with different anomalies is that the water is a mixture of two different structural moieties, one of low density tetrahedral liquid phase and the other of high density liquid phase.[87,95]In recent years, it has been intensely debated[88,89,260]on the existence of high-density and low-density structural motifs at ambient water. Water structure is predominantly tetrahedral due to formation of a three-dimensional hydrogen-bonded network, although molecules with fleetingly broken hydrogen bonds contribute significantly to the non-tetrahedral signature depicted by the distribution of tetrahedral order parameters. There is a long-standing debate on the extent and nature of perturbation in the tetrahedral structure of water due to addition of urea. The cause of this debate is probably due to lack of proper applicability of a suitable framework for quantitatively describing structure of water in presence of urea.

Many experimental studies such as NMR, neutron scattering, dielectric relaxation and thermodynamic measurements have yielded contrasting results on the influence of urea onwater structure. Raman band analysis of Walrafen[261]and NMR analysis of Sacco et al.[262]have indicated urea to be a structure-breaker. From the ultrasonic attenuation measurements[127]on aqueous solution of urea and a polymer, it has been observed that between 2-4 M urea concentrations, there is a significant reduction in relaxation time and it has been attributed to cooperative breakdown of water structure around the polymer. From the recent FTIR spectroscopic study[245]on aqueous solution of trimethylamine oxide (TMAO), urea, and guanidine hydrochloride (GdnHCl), it has been observed that presence of these solutes decreases the strength of the hydrogen bond between water and the infrared probe. It is concluded from this study that although urea and GdnHCl can perturb the hydrogen-bonding property of water, their protein-denaturing ability does not arise from a simple indirect mechanism. Using vibrational sum frequency spectroscopy, Cremer and coworkers[263]have probed interfacial urea molecules residing at the interface between bovine serum albumin and water and concluded that the urea breaks water structure. Combining neutron scattering and molecular dynamics simulation, Soper et al.[264]haveshown that the first solvation shell of water does not change with the increasing concentration of urea. However, the orientational distribution as calculated in this work has indicated substantial distortion of the tetrahedral structure in the aqueous urea solution.

Similarly, there are many studies that report urea as a non-interfering solute as far as structure of water is concerned. In this case, urea's ability to denature protein is explained on the basis of direct preferential interaction of urea with polar and non-polar groups of the protein. Many such experimental and simulation studies[223,229,255] with almost similar conclusions have been reported. Recent dielectric spectroscopy study[62]has claimed that urea and water are readily interchangeable in the H-bonding network of water, and therefore urea does not act as a strong structure-breaker of water. Tera-Hertz absorption spectroscopy study[256]of aqueous solution of urea has found no evidence of structure breaking effect of urea and suggested direct rather than indirect effect of urea on protein denaturation. Using polarization-resolved mid-infrared pump-probe spectroscopy, Bakker and coworkers[247]haveconcluded that urea does not change the strength of the hydrogen-bond interactions between water molecules. They have also found that a small fraction of the water molecules strongly immobilized by urea can form two hydrogen bonds with the two sites of the same urea molecule. Very recently, using vibrational spectroscopy and molecular dynamics simulation, Skinner and coworkers[266] have observed that all absorption spectra are insensitive to urea concentration suggesting that urea only weakly perturbs the water structure. The work of Tsai et al.[267]illustrates that urea molecules distribute uniformly in water networking without disturbing it. This view has been supported by various researchers by analyzing RDF of water-water and/or urea-water at varying concentration, temperatures and pressures.[132,229,230,268-270]By comparing RDFs of water in the urea-water system at various urea concentrations, Wallqvist et al.[225]have showed that urea molecules preferentially get adsorbed into polar residues of the protein and there is no structural distortion of water in presence of urea. In a very recent, state-of-the-art simulation study based on combined parallel tempering and metadynamics simulation, Parrinello and coworkers[236]have investigated the effect of urea on the β-Hairpin conformational ensemble and protein denaturation mechanism and have inferred that a preferential direct interaction exists between urea molecules and protein backbone. Pettitt and coworkers,[254]on the basis of calculated activity coefficients of urea, hydrogen bond lifetime and average number of hydrogen bonds have shown that urea solution is near ideal and thus water structure is not perturbed. Based on proximity criterion, which provides[271] detailed local structure around sub-structures such as atoms, functional groups etc., Kuharsky et al.[272]haveanalyzed infinitely dilute solution of urea and found no significant structural and energetic perturbation in water due to the presence of urea.

Many studies have mentioned that both direct and indirect effects are responsible for denaturing effect of urea. Recent NMR study of Almarza et al.[273]has found that the initial step of urea denaturation is guided by direct interaction. However, they have suggested the breaking of hydrophobic collapse due to indirect effect as the final steps for protein denaturation. Similarly, the work of Nilsson and coworkers[250]hasalso suggested both direct and indirect effects of urea on protein denaturation. Bennion et al.[132]haveused MD simulation to show the involvement of both direct and indirect mechanisms in the denaturation process.

In a recent development, Stumpeet al.[274]haveshown both average number of hydrogen bonds per water molecule and water-water radial distribution functions to be independent of urea concentration and inferred that water molecule in the hydrogen bond network of water is easily substituted by urea molecule through water-urea hydrogen bond formation. This work also reveals that water-water hydrogen bond is stronger than water-urea hydrogen bond, and this may be the driving force behind self-aggregation of urea in its concentrated solution. Although they are unable to detect any structural change in the water network due to addition of urea, from the comparison of hydrogen bond energy of water-water and water-urea pairs, they have described urea as a structure-maker or “kosmotrope”. From the analyses of Kirkwood-Buff integrals, Chitraet al.[275]have described urea as a slight structure-maker.In an earlier work, Vanziet al.[133]haveevaluated the hydration heat capacity of urea and from that concluded that the solute appears to enhance the water structure. In a recent publication, Yamzaki et al.[276] also have discovered that water is more structured in urea-water solution as compared to the same in the bulk.

Most of the computational studies are based on the analyses of radial distribution functions (RDFs).[67] Although the RDF is a central statistical mechanical quantity, which signifies two-particle reduced distribution function describing structure of a homogeneous isotropic liquid, [67]it cannot quantify angular distortion if any in the hydrogen-bonded, tetrahedral structure of water. The relative angular arrangement of water molecules around a central water molecule is of prime importance to understand any orientational distortion in the hydrogen-bonded network. In fact, there are some studies in which it is shown that various angular distributions of water in concentrated aqueous urea solution is quite different from the same in pure water. Since water is a tetrahedral liquid, any measurable distortion in this tetrahedral arrangement due to addition of urea will signify breakdown of water structure. Various order parameters in liquid water have been developed and extensively used to quantify tetrahedral order in pure water as a function of temperature and other thermodynamic parameters. Exactly on this line, Idrisssi et al.[277] have analyzed distortion if any in the tetrahedral local structure of water in presence of urea. They have calculated various order parameters using nearest neighbor approach. Their results have indicated considerable distortion in the local structure of water and thus they have described urea as a structure-breaker.

However, in calculating various radial and orientational parameters, they considered only water molecules (not urea) as neighbors of a reference water molecule. Considering the fact that a large number of studies[132,225,229,230,247,254,256,265-270] have shown that urea mixes well with the water and that it is able to substitute[274] for water in the hydrogen-bonded network very well from geometric and steric consideration, it is reasonable to expect that in the solvation shell of a water molecule, some of its nearest water neighbors will be replaced by urea molecules. Thus, while considering the tetrahedral arrangement of the four nearest neighbors around a reference, central water molecule, some of the vertices of the tetrahedron may be occupied by urea sites preserving the tetrahedral structure. In this article, by properly taking into account the nearest-neighbor sites irrespective of whether it is from urea or water, it is shown that the local tetrahedral structure of water is not broken by urea even at as high a concentration as 9 molar (M). The analysis of orientational structure has been done by carefully analysing average tetrahedral order parameter, distributions of tetrahedral order parameters, hydrogen-bonding angles and angles (triplet angle) extended at a central water molecule by two of its nearest neighbors. Radial arrangements of neighboring water molecules have also been analyzed by calculating average, fluctuation and distribution of radial distances of n^{th} nearest neighbor. It is also important to check how the dynamics is influenced by the increasing concentration of the urea. Molecular dynamics simulation provides a very useful root to explore translational as well as orientational dynamics of the water molecules in the solution. Here we have calculated translational diffusivity of water from the slope of the calculated mean square displacements vs. time plots. The rotational or orientational dynamics of the water molecules in the system has also been explored by calculating time correlation function of the dipole moment vector of the water molecule.

4.A.2:Models and Methods

In the present investigation, we have used TIP4P/2005[52]rigid body atomistic model of water having fixed bond lengths and bond angles. This model is a new variant of the TIP4P model and is able to reproduce most of the anomalies of water. For urea, we have used a flexible model with bond, angle and dihedral terms in the intra-molecular potential in addition to usual non-bonded Lennard-Jones and Coulomb interactions. The details of the urea model are given in Ref. 277. In order to check robustness of the results obtained with respect to urea models, we have performed additional simulations with KBFF[270] and AMBER[279] models of urea. The calculated values of order parameter q_4 (see Eq. (2)) as a function of urea concentration, as obtained from different models, show the same general trend and in accordance with the conclusions of this work. Aqueous urea solutions of different concentrations are prepared by considering a pre-equilibrated water box of appropriate size and then substituting some of the water molecules by urea to achieve a specific concentration. Specific details of the numbers of urea (N_U) and water (N_W) molecules with the volume of the boxes and molarity of the resulting solutions are given in Table 4.a.I. Although we have studied a wide concentration range from 0 to 9 M of aqueous urea solutions, concentration range of 6-8 M is important for protein denaturation studies.

All the simulations were performed in NPT ensemble[10]using molecular dynamics extended system approach[65]of Parrinello and Rahman to fix pressure and Berendsen algorithm[62] to fix temperature. Periodic boundary conditions and minimum image conventions were used in all three directions. For water, the bonds and the angle of a water molecule were constrained by LINCS algorithm[61]andparticle-mesh Ewald(PME) method[57,278]was adopted for treating electrostatic interactions. Equations of motions were integrated using Leap-frog algorithm[10]with a time step of 0.5fs. All the simulations were carried out at a target pressure of 1 atm and a target temperature of 300 K using GROMACS[156]simulation package. All the analyses were performed using our home-grown software. For all simulations, trajectories for the first 10 ns were discarded for equilibration and the same for the next 4 ns have been stored for analyses.

Local orders: In case of a perfectly tetrahedral structure, there are four nearest neighbors in the 1st solvation shell and another twelve neighbors in the 2nd solvation shell around the central water molecule. Radial distribution functions depict radial arrangements of neighbouring water around a reference, central water molecule, but cannot provide any information about the angular preferences of the neighbouring molecules. So, In order to measure the extent of oriental orders of the water molecules in the 1st and 2nd shells of a reference water molecule, two different orientational order parameters[71,75] have been used here.

Tetrahedral order parameter and Triplet angle: In this approach, a tetrahedral order parameter q_i is associated with each of the water molecules in the system. The parameter q_i measures the degree of tetrahedrality of the 1st solvation shell by using four nearest neighbors:

$$q_i = 1 - \frac{3}{8}\sum_{j=1}^{3}\sum_{k=j+1}^{4}\left[\cos\theta_{jik} + \frac{1}{3}\right]^2 , \qquad (4.a.1)$$

where 'i' is the central molecule and $\theta_{jik}$is angle formed by neighborsand k at the reference, central water molecule i. The value of this quantity is 1 for a perfect tetrahedral structure and the normalization factor of 3/8 before the summation ensures the value of q_i to be zero for a perfectly disordered system. Since there are four neighbors, there are 6 angle terms in the summation and each term contributing 4/9 due to angular averaging. In order to get a q_i value of zero for the random uncorrelated orientations, therefore the normalization constant of 3/8 arises from the contributions of six angles as 1/(6 × 4/9) as used by Errington and Debenedetti.[71]n the present investigation, apart from using four neighbors, we have considered central molecules with two and three neighbors as well (see Result and Discussion). For calculating the tetrahedral order parameter in those cases we have used proper normalization. Details of how these normalization constants have been calculated are given in chapter-2.The average valueq_4, the tetrahedral order parameter, is calculated by averaging over all the N molecules and over the ensemble using the following equation

$$q_4 = \frac{1}{N}\left\langle \sum_{i=1}^{N} q_i \right\rangle . \qquad (4.a.2)$$

The angle $\cos\theta_{jik}$ (see Eq. (1))which is also known as triplet angle is itself a very sensitive order parameter to gauge the local tetrahedral orientation of any two nearest neighbors of a central molecule and hence we have used the distribution of this triplet angle also in our present analysis.

Table 4.a. 1: Different Systems Simulated in This Work

N_u	N_w	X_u Urea Mole fraction	Volume (nm^{-3})	Molarity (M)
0	512	0.0	15.37	0
20	812	0.024	25.81	1.29
60	872	0.064	30.507	3.27
120	993	0.114	38.60	5.16
120	873	0.121	34.95	5.70
120	783	0.133	32.26	6.18
120	699	0.147	29.76	6.70
180	631	0.2219	32.14	9.30

Hydrogen bonds: Since water is a hydrogen-bonded, network forming liquid, average number ($<n_{HB}>$) of hydrogen bonds (HB) and its distribution are two useful quantities to measure any structural changes in water. To identify a HB, we have used a standard geometric criterion, according to which two water molecules are considered to be H-bonded only if (i) the inter-oxygen distance is less than 3.5 Å, (ii) the hydrogen-oxygen (H-bonded) distance is less than 2.45 Å and (iii) the H-O····O angle is less than 30°. Water-urea hydrogen bonds are also calculated using the same criteria. In this case NH_2 and carbonyl oxygen atom sites of urea are considered for hydrogen bonding.

4.A.3:Results and Discussion

4.A.3.1: Structure

In this study we are concerned about the local structure of water. The local structure of water is generally described by both radial and orientational arrangements of molecular sites around a central molecule. One such analysis is performed by calculating intermolecular distance distribution, often expressed as radial distribution function (RDF). In case of homogeneous spherically symmetric systems, RDF is a very useful quantity to study liquid structure. But in case of a liquid like water, where directional bonding leads to tetrahedral network structure, angular distribution of neighbors around a central molecule is also of prime importance. Assuming water structure to be nearly tetrahedral, tetrahedral order parameter (see Eqs.(1) and (2)) provides a good measure of angular arrangements of the nearest neighbors around a central molecule. Any deviation of this order parameter in presence of urea from its pure water value indicates angular distortion in the water structure. However, in such calculations of radial and orientational distributions, it is very important to choose nearest neighbors properly. Unlike pure water, in which all the neighbors of a central water molecule are water only, in a binary mixture of urea and water, first four neighbors (distance wise) can be either water or urea molecules. In this analysis, we first examine how tetrahedral order parameter and its distribution, calculated on the basis of all the four nearest *water* neighbors (neglecting urea as a neighbour),change as a function of urea concentration. In Figure4.a.1(a), we have shown average value of the q_4^w, calculated on the basis of four nearest *water* neighbors only, as a function of urea concentration. The superscript *w* indicates that the value of q_4 is calculated by considering all the four neighbors as water (without

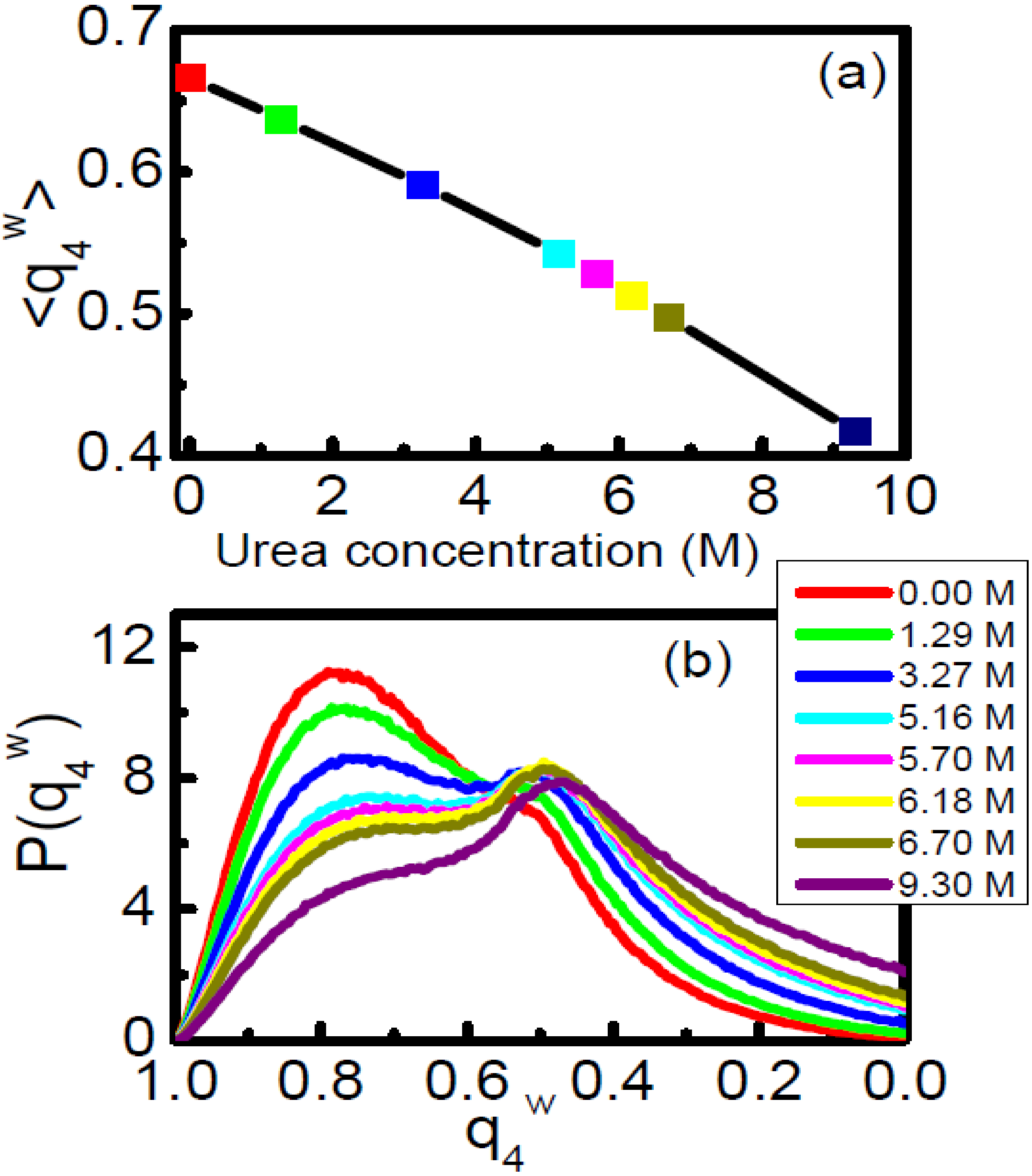

Figure 4.a.1. (a) Average tetrahedral order parameter $\langle q_4^w \rangle$ considering all four water neighbors (no urea molecule is considered as a neighbor) of a reference water molecule as a function of molar concentration of urea and (b) distributions $P(q_4^w)$ of tetrahedral order parameters. Different colors correspond to different urea concentration as shown in the legend.

considering urea). A steady decrease of the average value $<q_4^w>$is observed as the concentration of urea increases from 0 M to around 9 M, indicating a clear disruption of the tetrahedral structure of water. The distributions ($P(q_4^w)$) of the tetrahedral order parameter, q_4^w, also show (see Figure4.a.1(b)) marked variation as the concentration of urea is increased. The distribution $P(q_4^w)$ for pure water (red line) has one major peak at a q_4 value of around 0.8 corresponding to the tetrahedral structure of water (for a perfectly tetrahedral arrangement q_4 should be 1) and another small peak at around 0.5. There was no clear explanation about the origin of this non-tetrahedral peak at around q_4=0.5. In chapter -2,this non-tetrahedral peak has been shown to be originated from those neighboring molecules that are not hydrogen bonded to the central, reference water molecule. As the concentration of urea is increased, the tetrahedral peak in the distribution decreases and the non-tetrahedral peak increases. Similar trend is observed by Idrissi et al.[277] who concluded that this change is due to breaking of tetrahedral structure of water by urea.

Water has a hydrogen bonded network structure. Thus, the distribution of the hydrogen-bonded angle,θ_{HB}, formed between the line joining the oxygen atom of the central molecule and the oxygen atom of one of its neighbors and the O-H bond of that neighbor, provides geometric picture of orientational preference of the hydrogen bond network. Comparison of the distributions of pure water with the same for binary water-urea solutions of different concentrations may give us idea about orientational distortion, if any, in the hydrogen bond network of water. In Figure4.a 2(a), we have shown the distribution, $P(\theta_{HB})$ of the *first* water neighbour for pure water as well as for urea-water solutions with different concentrations. We find no significant changes in peak positions and intensities as the concentration of urea is increased. In case of *second* water neighbour also (see Figure4.a.2(b)), no significant changes in the distribution as a function of urea concentration is observed. However, if we consider the third (see Figure4.a.2(c)) and the fourth (see Figure

4.a.2(d)) water neighbors, significant changes in the distributions as a function of urea concentration have been observed. Similar observation has been made by Idrissi et al. (Ref 277) and they have concluded it to be due to breaking of hydrogen bonded network structure of water in presence of urea.

It is suggested and shown by Idrissi et al.[277] that the effects of urea concentration on average value and its fluctuation of the distance, r_n of the n^{th} water neighbour from reference, central water molecule are significant. Here too, with the TIP4P-2005 model of water and by considering only water as neighbors, we find a change in average value,$\langle r_n^w \rangle$for $n \geq 3$(see

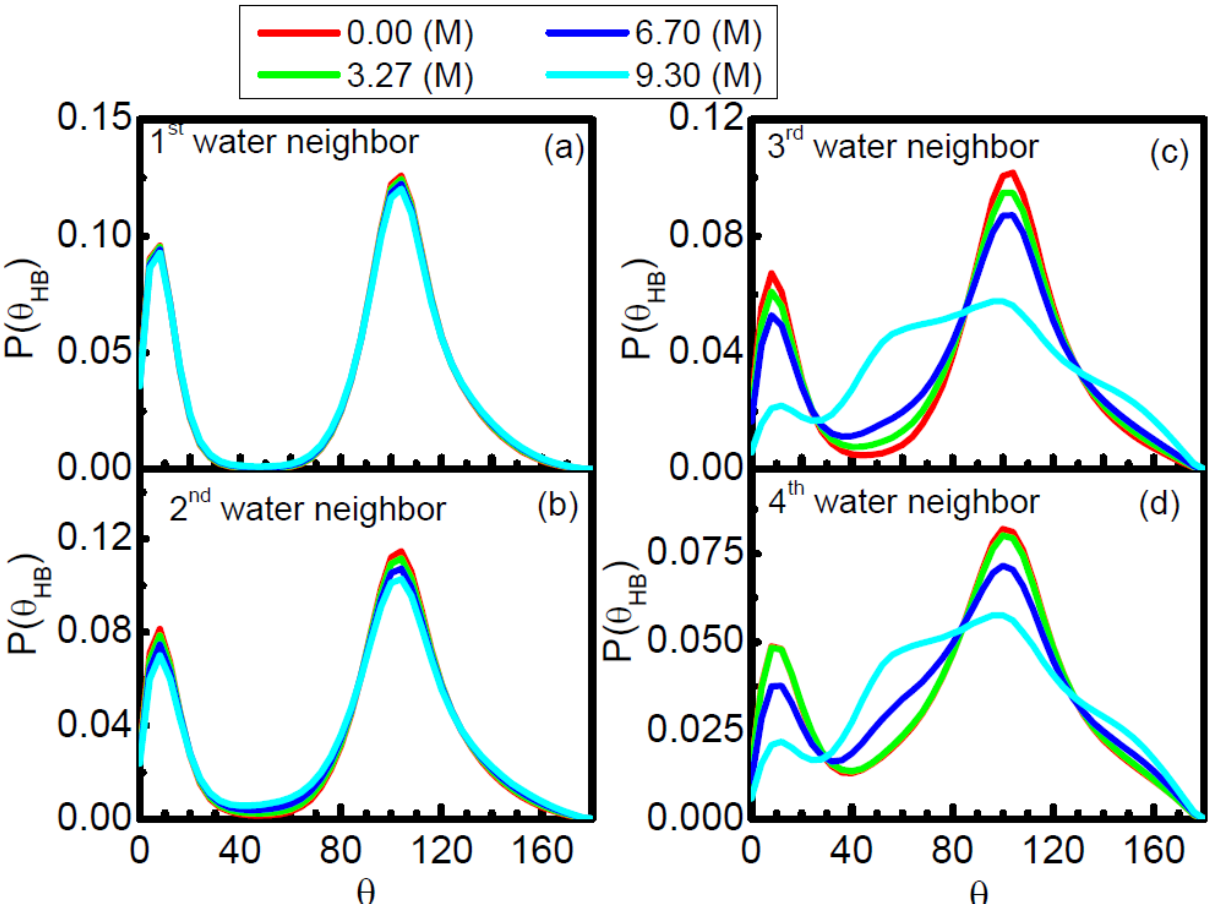

Figure 4.a.2. Distributions $P(\theta_{HB})$ of the hydrogen bonding angle formed by a reference water molecule and one of its neighbors. The hydrogen bonding angle θ_{HB} is the angle formed by the line joining the two oxygen atoms and the OH bond vector. In panels a−d distributions for four nearest water neighbors are shown. In this case urea is not considered as a neighbor.

Figure4.a.3(a)) as a function of urea concentration. Corresponding fluctuations are shown in Figure4.a.3(b) and a more pronounced change in this quantity as a function of urea concentration is observed. Thus, the present result also seems to reinforce the idea that water

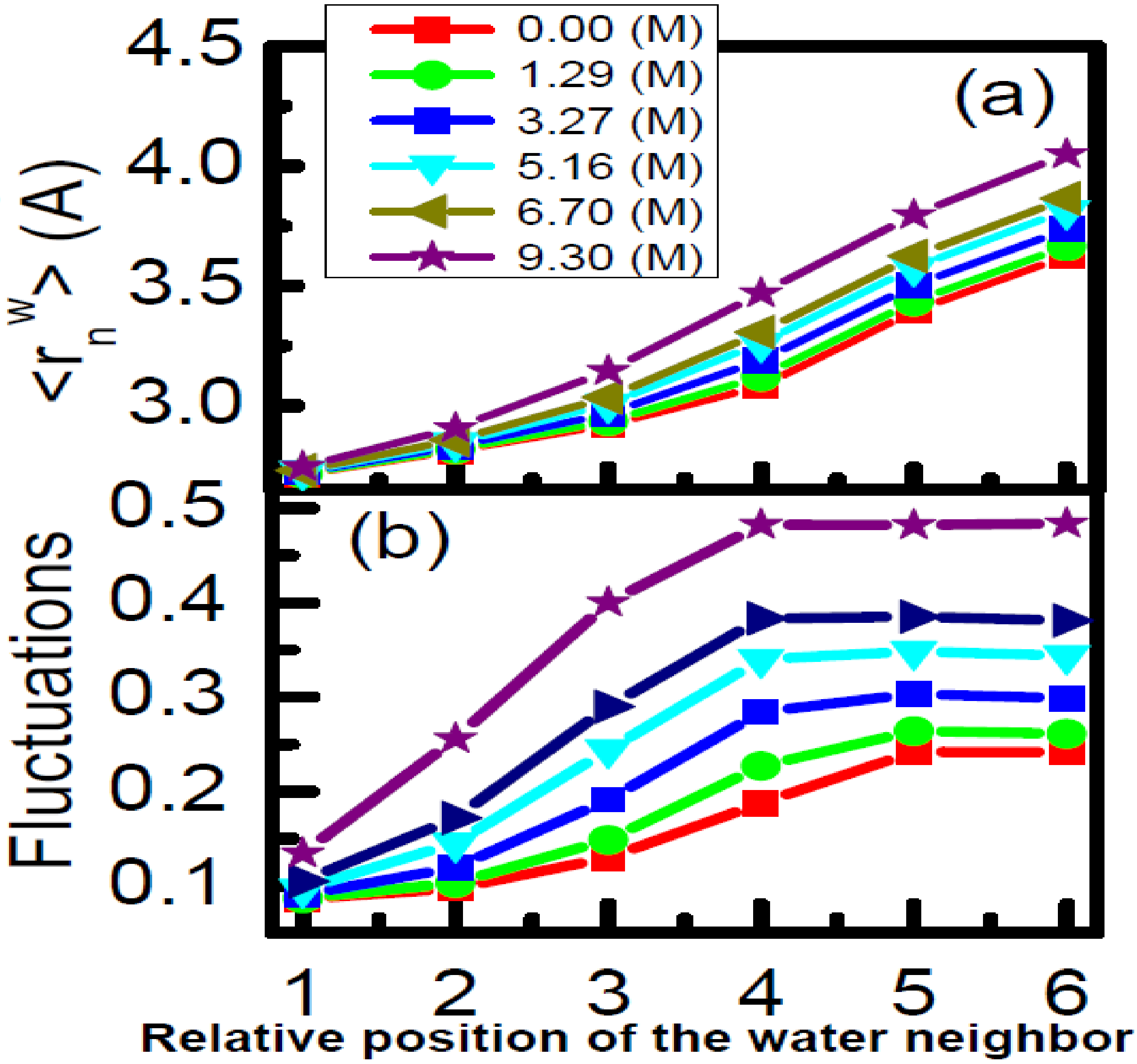

Figure 4.a.3. (a) Average oxygen−oxygen distance of the n^{th} *water neighbor from a reference water molecule for first six water neighbors;(b) fluctuations in the above-mentioned quantities.*

structure is broken in presence of urea. It is important to emphasize at this point that in all the above cases, we have considered only *water* neighbors i.e. while choosing nearest neighbors we have selected (distance-wise) first four water molecules without considering urea as a neighbour. As shown in many earlier works[71]that urea readily replaces water in the hydrogen bonding network of water and therefore it may so happen that the water molecules, which were 3rd or 4th nearest neighbors of a central water molecule in bulk water, are now replaced by one or more (sites of) urea molecules in concentrated urea solution. In other word, these 3rd or 4th nearest water neighbors may not always reside within the so called first solvation shell (which we considered to be of radius 3.15 Å) because of their replacement by (site/s of)

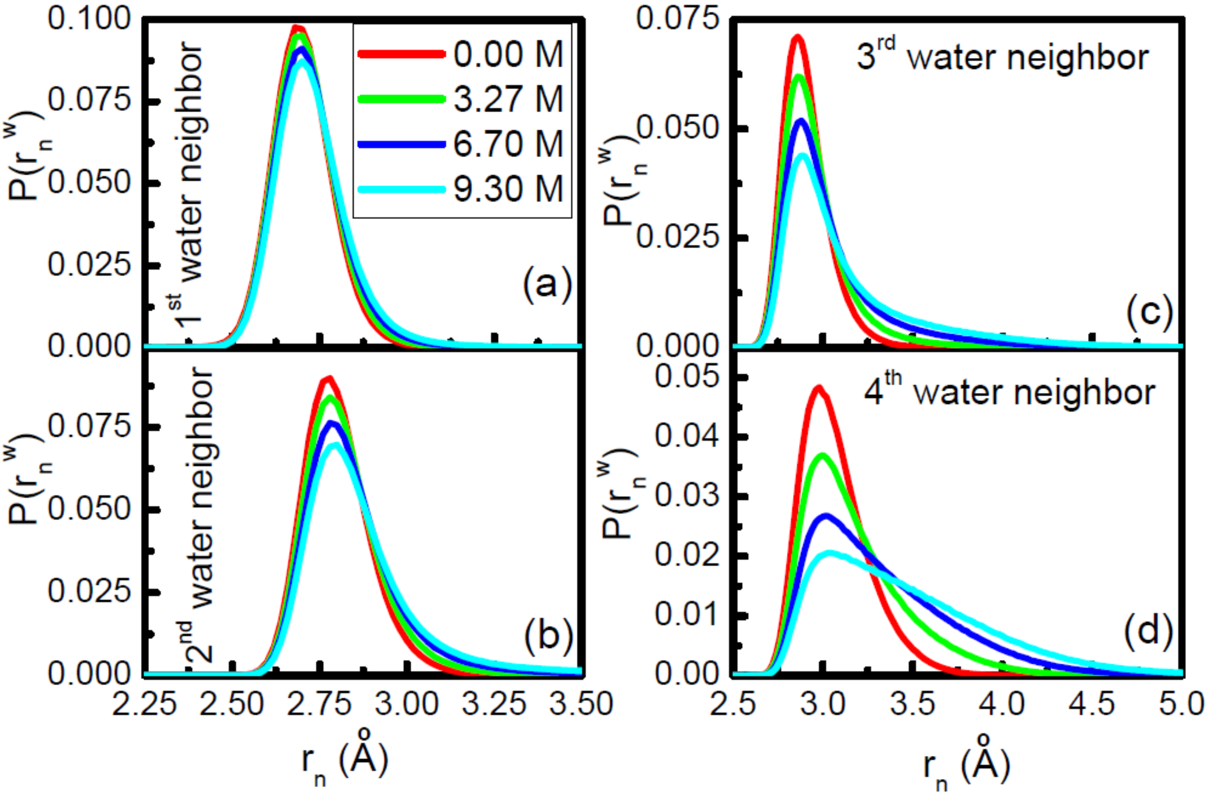

Figure 4.a.4: Distributions $P(r_n)$ of the distance r_n of the nth water neighbor from a reference water molecule for n = 1−4 are shown in panels a−d.

urea molecules. In order to get an idea about how these *water* neighbors are radially distributed around a central water molecule, we have shown in Figure4.a.4, the distribution of the distances (r_n) of the n^{th}($n=1$-4) *water* neighbour from the central water molecule. It is clearly visible (see Figure4.a.4(d)) that in a concentrated urea solution, the distributions of the 3rd and 4thnearest *water* molecules extend well beyond 3.15 Å. Therefore, there is a significant chance that these *water* neighbours are now replace done or more sites of the urea molecules in the concentrated aqueous urea solution. In order to get that insight, we have calculated the probability, $P(n, U)$ that the n^{th} neighbour (distance wise from a central water molecule) is urea as follows:

$$P(n, U) = \frac{N_U^n}{N_T^n}, \qquad (4.a.3)$$

where, N_U^n is the number of occurrences that (site/s of) Urea (U) occupies the n^{th} nearest neighbour position and N_T^n is total occurrences that Urea and Water occupies the n^{th} nearest neighbour position. Therefore, the probability $P(n, W)$ that the n^{th} neighbour (distance wise from a central water molecule) is water is given by $(1 - P(n, U))$. In Figure4.a.5, we have shown both the probabilities (urea as well as water). It is seen that the probability of 3rd or 4thneighbouring position of a reference water molecule being occupied by a urea molecule is increasing (see lines with triangles) steadily with increasing urea concentration. Consequently, the probability that the n^{th} position is occupied by water is decreasing as shown by lines with circles. For example, the probability of fourth neighbour being a urea molecule at the urea concentration C_U=*9.00* M is about 37%. Therefore, if we consider all the four neighbors around a central water molecule as *water*, there is a 37% chance that the fourth nearest neighbour is urea and not water; and therefore if we consider 4th nearest *water* molecule as one of the neighbors in the first solvation shell to calculate radial and orientational order parameters, there is a high probability that these order parameters will show significant deviations from their respective bulk water value, as these water molecules are now in the second solvation shell. While calculating any order parameter based on nearest neighbors, it is, therefore, desirable to consider both urea and water sites while choosing the first four (distance wise nearest) neighbors around a central water molecule.

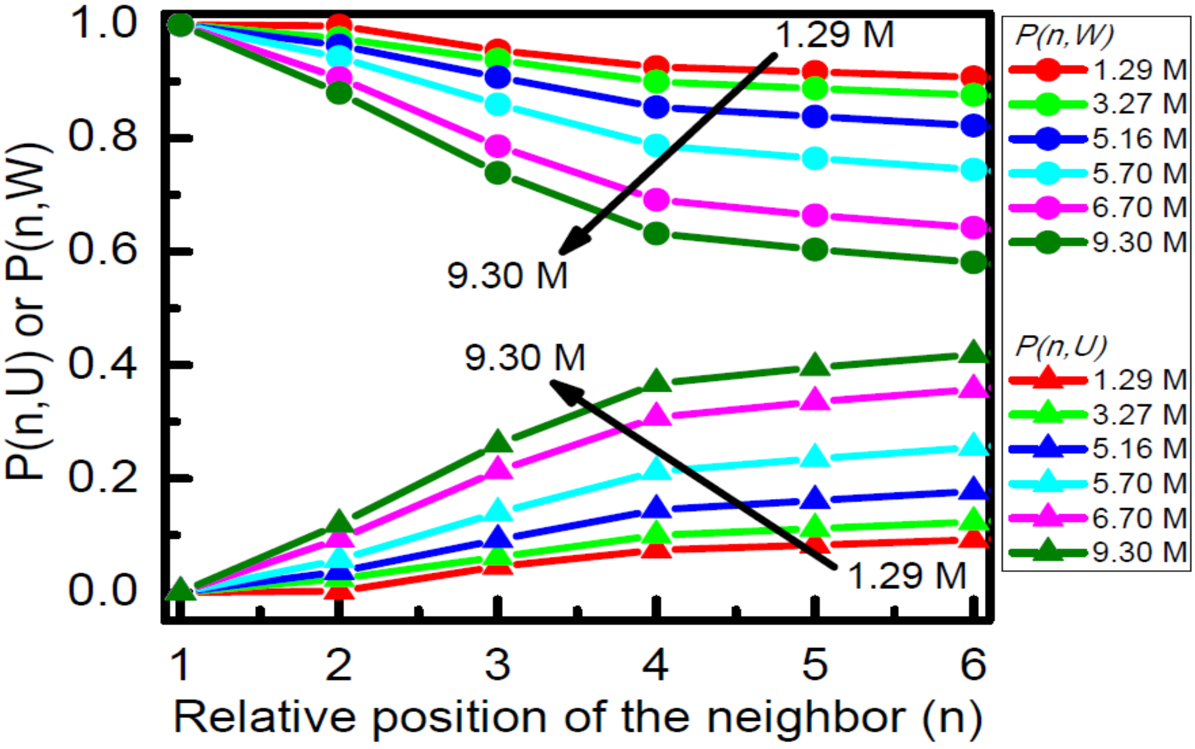

Figure 4.a.5. Probability P(n,U/W) that the nth neighbor of a reference water molecule is a urea/water site as a function of urea concentration. P(n,W) data are shown by lines with filled circles and P(n,U) data are shown by lines with filled triangles.

Now, let us recalculate our previously calculated quantities (as shown in Figures.4.a.1-4) by considering *n* nearest neighbors irrespective of whether the neighbors are urea or water.In Figure4.a.6, we have shown the distributions of positions of the n^{th}neighbour for *n=1-6*. In this calculation, apart from water, we considered urea also as a neighbour if it is (distance-wise) within the first four neighbors of a reference water molecule. It is now clear from the plots in Figure4.a.6 that irrespective of the urea concentration, the distributions $P(r_n)$ are almost the same for $n=1-4$ (compare this Figure with Figure4.a.4).

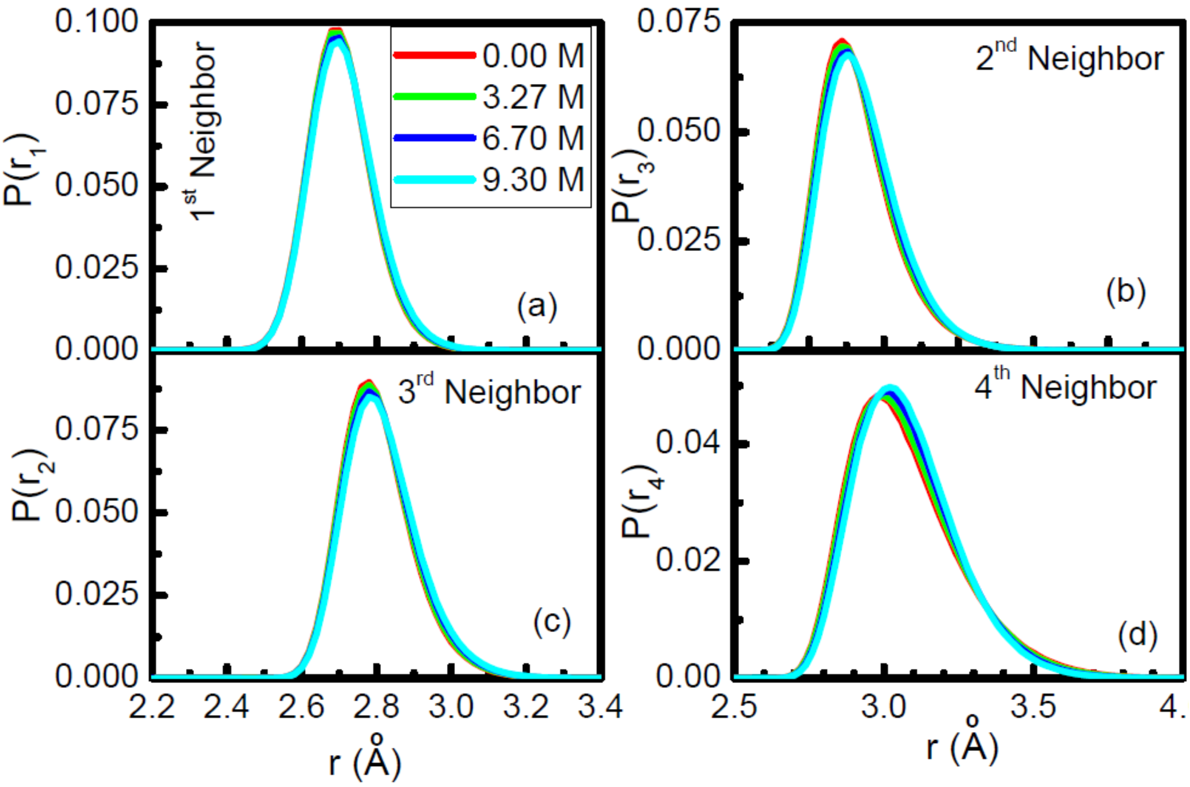

Figure 4.a.6. Same as in Figure4.a.4 except that now in choosing the first n neighbors, sites of urea and water both are considered.

To calculate average distance $<r_n>$of the n^h neighbour and its fluctuation for $n=1-6$, now we have considered first n nearest sites (of a reference water molecule) irrespective of whether it is from urea or water. The calculated quantities are shown in Figure4.a.7. In this calculation, we have considered sites from both urea and water as neighbors. It is interesting to observe (see Figure4.a.7(a)) that the average distance $<r_n>$ of the n^{th} neighbouring site does not change at all up to $n=4$ with the increase in urea concentration (compare these plots with

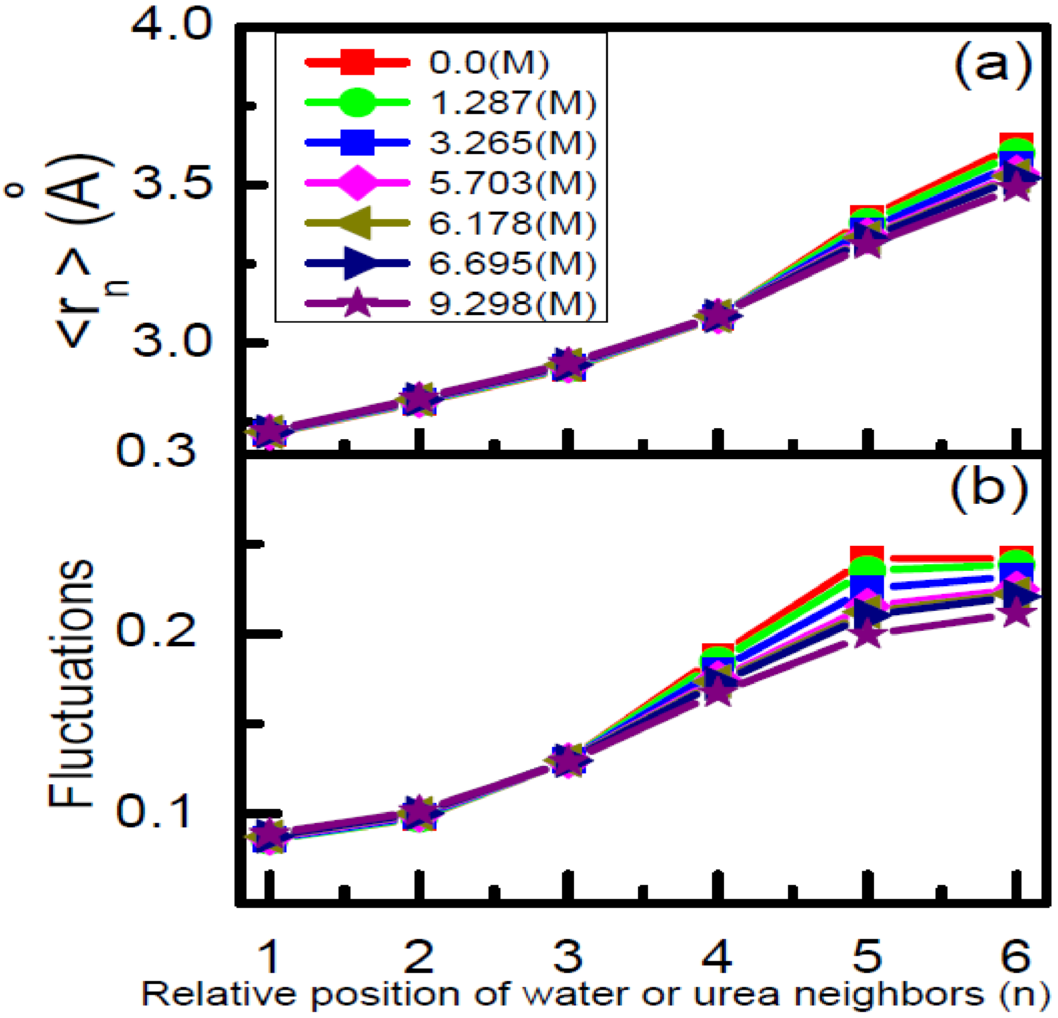

Figure 4.a.7. Same as in Figure4.a 3 except that now sites of urea and water both are considered in choosing the neighbors of a reference water molecule.

the same in Figure 4.a.3(a)). If we calculate the fluctuations of these distances in the same way as above, then it is seen (see Figure4.a.7(b)) that with the increase in urea concentration, fluctuations also do not change appreciably up to 4th nearest neighbour (compare this result with the same in Figure4.a.3(b)). These results thus illustrate that one or more urea sites nicely substitute water molecules in the solvation shell of water in such a way that the radial arrangements of the remaining water neighbors in the first solvation shell remain the same as that in pure water. It is well known that hydrogen bond formation is a driving force behind the tetrahedral network structure of water and it is expected that if tetrahedral network is distorted or broken, then it will affect the hydrogen bonding geometry also. Thus, it will be useful to check the distribution of hydrogen bonding angle, θ_{HB} as a function of urea concentration. In this calculation also, while selecting the first *n* neighbors of a reference water molecule, we have considered both urea and water as a neighbour. After designating

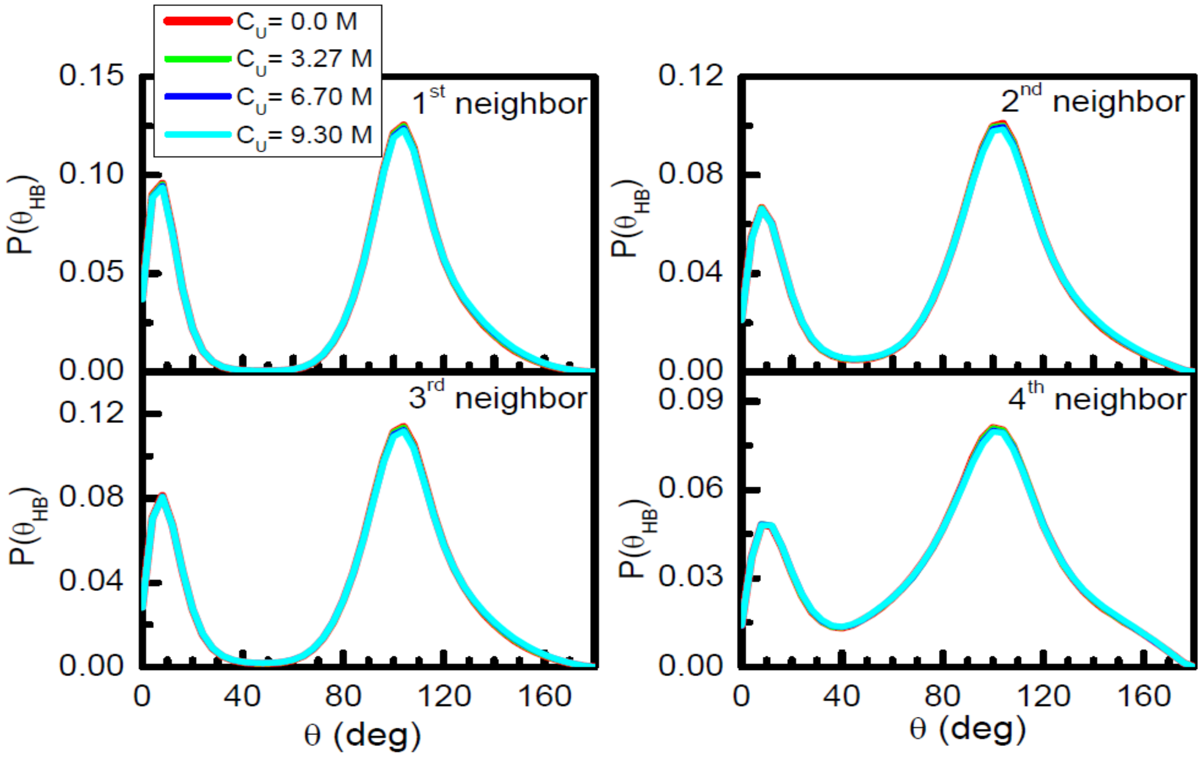

Figure 4.a.8. Same as in Figure 2 except that now we choose four nearest neighbors irrespective of whether it is urea or water and then calculate the required hydrogen bonding angle between the reference water molecule and that water neighbor, which is within the first four(distance-wise) neighbors.

The first four neighbors (whether it is water or urea sites), we calculate the angle θ_{HB} by considering only n^{th}(where $n \leq 4$) neighboring water molecules(not urea). Now,*P(*θ_{HB}*)* distributions calculated in this way are shown in Figure4.a.8. As the Figure suggests, no

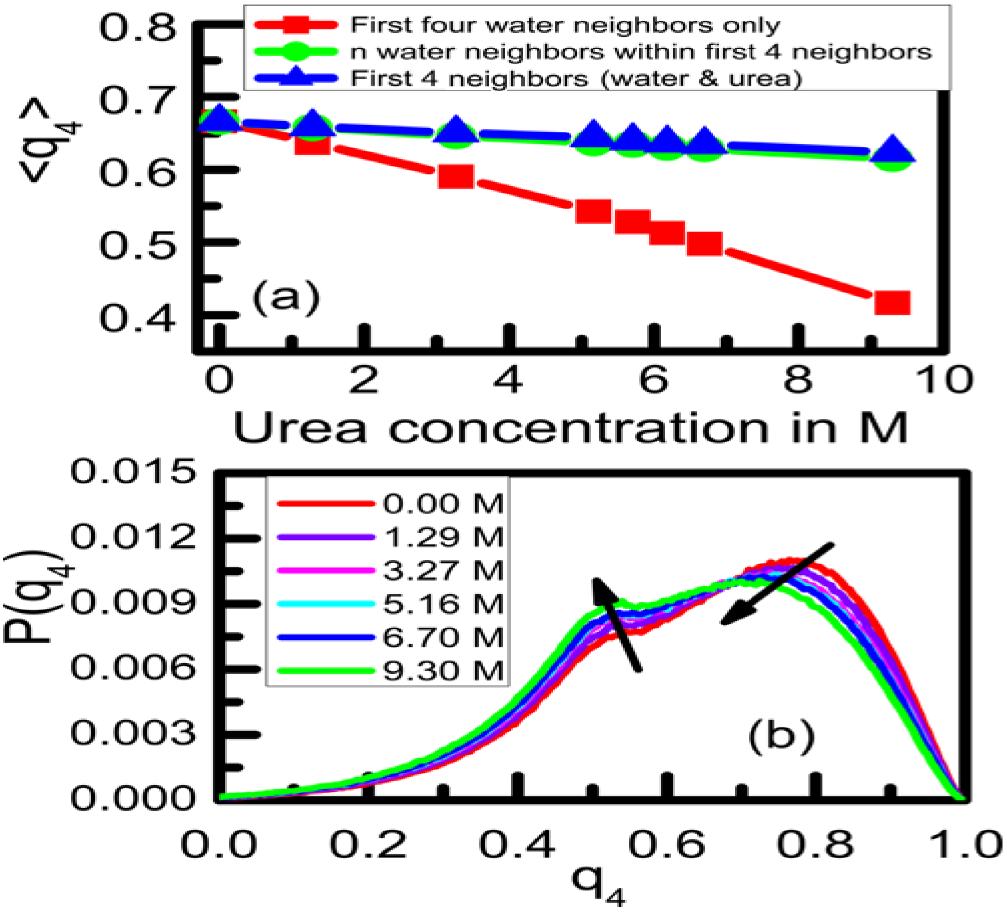

Figure 4.a.9. (a) Average tetrahedral order parameter ⟨q_4⟩ as a function of molar concentration of urea. Red line with squares represents results obtained when we choose the first four water molecules as the four nearest neighbors. Now, first we select four nearest neighbors irrespective of whether it is urea or water and then calculate q_4 by considering only those water molecules that are within the first four(distance-wise) chosen neighbors. Green line with circles represents results obtained by considering n ($n \leq 4$)) water neighbors that are within the first four nearest neighbors. We have used proper normalization for the cases where the number of nearest neighbors is less than four (see Models and Methods section). The calculated result by considering both urea and water if they are within the first four neighbors is shown by the blue line with triangles. (b)Distributions $P(q_4)$ of tetrahedral order parameter q_4 corresponding to the green line in Figure 9a. Different colors correspond to different urea concentration as shown in the legend.

distortion in the $P(\theta_{HB})$ distribution for any of the first four neighbors is observed as the concentration of urea is increased up to 9.3 M. The basic difference between this result and the same shown in Figure4.a.2 originates from the fact that now we are considering a urea site also to be a neighbouring site; thus discarding those water molecules that are not really within the first four nearest neighbors of a given water molecule (but they are within the first four *water* neighbors). In other words, the distortion shown in Figure 4.a.2 in case of 3rd or 4thneighbour at high urea concentration is originating from the water molecules residing outside the first solvation shell.

It is now worth examining how the average value ($<q_4>$) of tetrahedral orders parameter, q_4 and its distribution change with the change in urea concentration. We have shown in Figure 4.a. 9(a), the average values of the tetrahedral order parameter, $<q_4>$calculated in three different ways: *(i)*by considering all four nearest neighbors as “water” (without considering urea as a neighbour) as shown by red line with symbols *(ii)* by considering first four nearest neighbours, where these neighbors can be both urea and water (blue line with symbol) and *(iii)*by taking only n (with $n \leq 4$) "water”molecules (not urea) that are within the first (distance-wise) four neighbors. In this case, if $n < 4$, we have used proper normalization (see Models and Method Section) for q_4 calculation. It is interesting to observe that if q_4 is calculated by the 2ndmethod (i.e. by considering both urea and water while selecting first four neighbors and also considering all these four neighbors in the angle calculation), the average value of q_4 does not change (blue line with symbols) much with the increase in urea concentration. When we consider all the four neighbors as water (1st method), there is a drastic decrease in the average q_4 values as a function of concentration of urea, C_U. This deviation is because of the fact that now the probability that the 3rd or 4th water molecule is outside the first solvation shell (or beyond first four neighbors) has increased with increasing urea concentration (see Figure 4.a.5) and thus when we consider that all the four neighbors are water, basically we are including the outside (the solvation shell) water molecule, which contributes to the deviation. It is interesting to check whether the water molecules residing within the first solvation shell (where the first solvation shell is assumed to be formed by four nearest neighbours irrespective of whether these molecules/sites are from urea or water), restore the tetrahedral arrangement even in highly concentrated urea solution. For that, we have calculated average q_4 by considering only those water molecules residing within the first solvation shell (3rd method described above) and in this case also, we do not observe (see green line with symbols in Figure4.a.9(a)) considerable change in average values with increasing concentration. This line is almost coincident with the blue line as calculated by considering four nearest water or urea neighbors. This confirms that the water neighbors within the first solvation shell are tetrahedrally arranged, and only those who are beyond the first four neighbors, contribute to the deviation shown in Figure4.a.1(a).

In order to get further insight, we have shown in Figure4.a.9(b) the distributions (P(q_4)) of q_4, calculated in the following way: First designate first four neighbors of a water molecule considering both water and urea as neighbors and then calculate the distribution P(q_4) by considering only n (with $n \leq 4$) water neighbors that are within the first 4 neighbors (this situation corresponds to green line in Figure 4.a.9(a)). The distributions at different urea concentrations are almost coincident (compare with Figure4.a.1(b)) showing that urea does not appreciably break the water structure. However, a critical observation of the distributions reveals that there is a slight decrease in the tetrahedral peak appearing at high q_4 and a slight increase in the non-tetrahedral peak at low $q_4$values. Not only that, the decrease of the tetrahedral peak is also associated with a slight shift towards low q_4 value. A pertinent question then arises: is this minute change in the P(q_4) distribution with increasing urea concentration a result of breakdown of the tetrahedral water structure?

To understand this, it is important to know the origin of the appearance of the non-tetrahedrall q_4 peak, which appears even in P(q_4) of bulk water. The angle involved in the q_4 calculation is formed by two neighbouring water molecules extended at the central, reference water molecule. In the chapter-2, we have shown that the high q_4 tetrahedral peak originates if both the neighbors are hydrogen-bonded to the central molecule and the low q_4(non-tetrahedral) peak originates if both the neighbors are not hydrogen-bonded to the central molecule and also if one of them is hydrogen-bonded but the other is not hydrogen-bonded (to the central water molecule). So, in order to get correct angular distribution, one requires knowledge about the hydrogen bonding pattern of water.

In Figure 4.a.10(a),we have shown the average number of hydrogen bonds, $<n_{HB}>$, as a function of urea concentrations (C_U) for three different cases. The green line shows the $<n_{HB}>$ formed by a central water molecule with another water molecule and it decreases with increasing C_U. The blue line depicts the change in $<n_{HB}>$ formed by a central water molecule with a urea neighbour as a function of urea concentration and clearly it is seen that $<n_{HB}>$ is increasing as a function of C_U. It is interesting to observe that when we calculate $<n_{HB}>$ formed by a central water molecule with both water and urea molecules, we find almost no change in $<n_{HB}>$ as a function of C_U. Thus, it clearly illustrates that some of the water-water hydrogen bonds of bulk water are nicely substituted by the water-urea hydrogen bonds in concentrated aqueous urea solution. Similar observation was made by Stumpe at al.[274]In order to get further insight, we have also calculated percentages of *n*-hydrogen-bonded water molecules of two different types namely, (i) water-water and (ii) water-urea hydrogen bonds. In Figure4.a.10(b) we have shown HB distribution of bulk water, in which only water-water hydrogen bonds are presents. In Figure4.a.10(c)-(f) we have shown both water-water (upper panel) and water-urea (lower panel) HB distributions for aqueous urea solutions of different urea concentrations. As

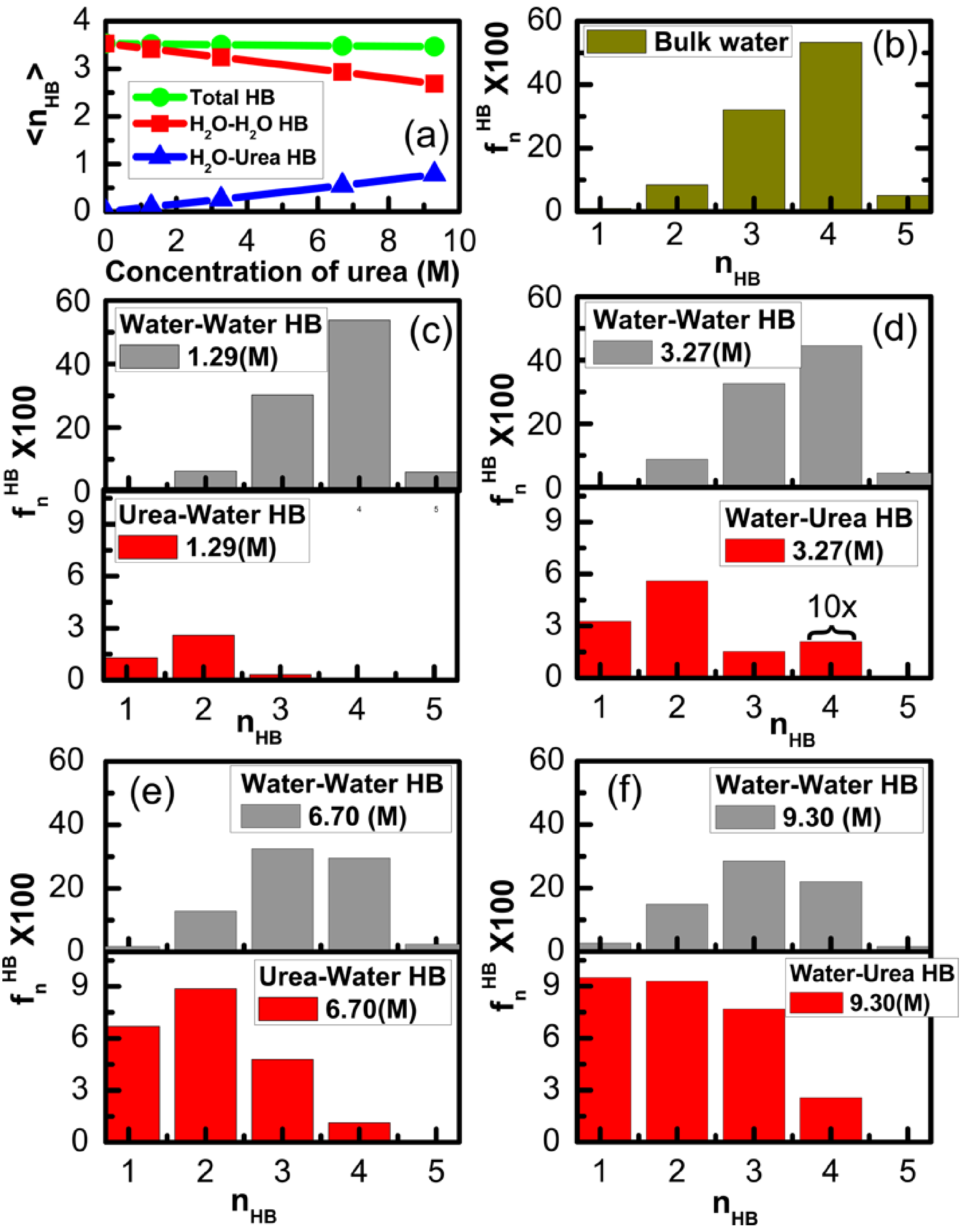

Figure 4.a.10. (a) Average number of hydrogen bonds ⟨n_{HB}⟩ as a function of concentration of urea. (b) Distribution of hydrogen bonds in bulk water. Plots c−f represent distributions of water−water (upper panel in each Figure) and water−urea (lower panel in each Figure) hydrogen bonds at different urea concentrations.

the concentration of urea is increasing (see upper panels of Figure4.a.10(c)-(f)), we find that there is a steady and substantial decrease in the percentage of *four* hydrogen-bonded (n_{HB}=4) water molecules. Same is the case for *five* hydrogen-bonded (n_{HB}=5) water molecules. On the other hand, number of *two* hydrogen-bonded water molecules (n_{HB}=2) increases steadily with the increasing urea concentration. It is interesting to observe that the percentage of *three* hydrogen-bonded (n_{HB}=3) water molecules remain almost the same as C_U is increased. It may be due to the fact that when one of the four hydrogen-bonds (in case of n_{HB}=4) of a water molecule breaks due to addition of urea, water molecules with n_{HB}=3 is generated, but this increase in number of n_{HB}=3 water molecules is offset by the decrease in number of n_{HB}=3 water molecules resulting from the conversion of *three* hydrogen bonded (n_{HB}=3) to *two* hydrogen-bonded (HB=2) water molecules due to presence of urea. Now, looking at the water-urea hydrogen bond distributions (see lower panels of Figure4.a.10(c)-(f)), we find that at the lowest urea concentration studied here, there is only *one*-hydrogen-bonded water (forming HB with urea) and at higher urea concentrations, populations of *two*- and *three*-hydrogen-bonded (with urea) water molecules increases. In general, as the urea concentration is increased, proportion of water-urea hydrogen-bonded molecules increases. This is consistent with the above observation regarding water-water hydrogen bonds. Thus, it shows how water-water hydrogen bonds are nicely replaced by water-urea hydrogen bonds as the concentration of urea increases.

Now, the change in the P(q_4) distribution due to addition of urea can be better understood if we analyze the distribution P($cos\theta$) of the cosine of the angles formed by two of the first four neighbors at the reference, central water molecule. First, we choose four nearest neighbors considering both urea and water sites as neighbors. For calculating angle formed by two neighbors extended at the central molecule, we restrict ourselves only to water neighbors (not urea neighbors). The P(*cosθ*) distributions at different urea concentrations as a function of *cosθ* as shown in Figure4.a.11(a) show a large broad peak near $\cos\theta = -\frac{1}{3}$,

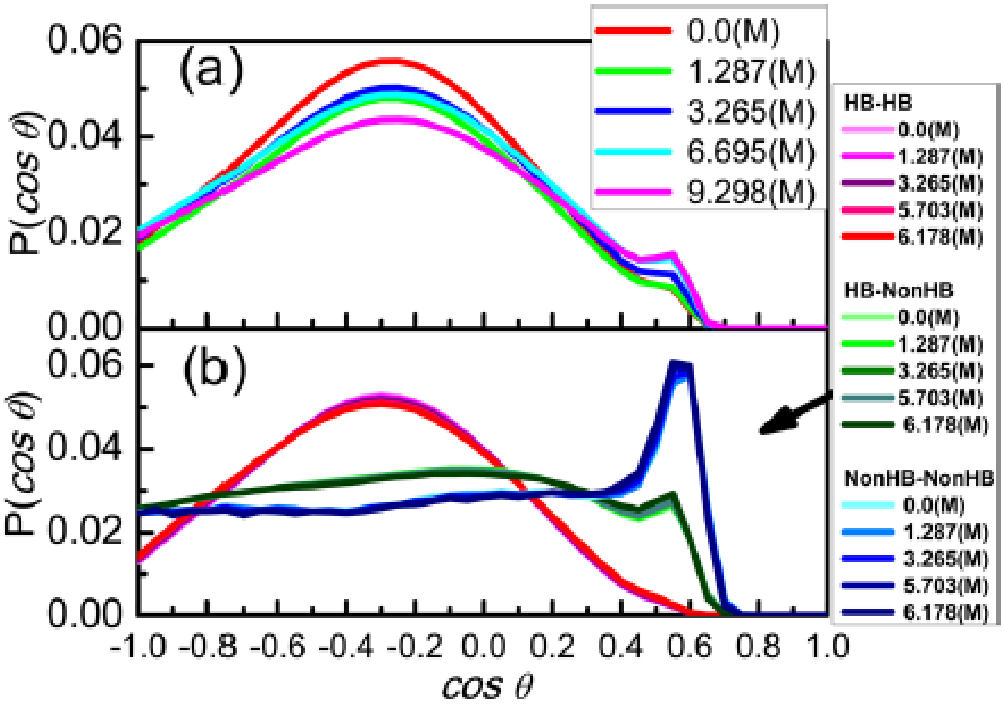

Figure 4.a.11. (a) Distribution P(cosθ) of cosine of the triplet angle cosθ (for definition see Models and Methods section) at different urea concentrations (see the legend for different concentrations). (b)Distributions P(cosθ) of the cosine of angle θ made by (i) two hydrogen-bonded (family of red curves), (ii) two non-hydrogen bonded(family of blue curves), and (iii) one hydrogen-bonded and the other non-hydrogen-bonded (family of green curves) nearest neighbors at the central molecule.

corresponding to the tetrahedral peak and a small kink at around $\cos\theta = 0.5$ corresponding to non-tetrahedral peak of the q_4 distribution. As the concentration of urea increases, the intensity of the tetrahedral peak decreases and that of the non-tetrahedral peak increases. If we now classify the two neighbors that form the angle in terms of whether they are hydrogen-bonded to the central, reference molecule, three different combinations are possible: (1) both the neighbors are hydrogen bonded to the central molecule (let us call it HB-HB) (2) one neighbor is hydrogen-bonded to the central molecule and the other is not (HB-nonHB) and (3) both the water neighbors are *not* hydrogen-bonded (nonHB-nonHB) to the central molecule. If we look at the P($cos\theta$) of these three combinations (see Figure4.a.11(b)), we find that the tetrahedral peak near $\cos\theta = -\frac{1}{3}$originates from HB-HB combination (see the group of reddish colored cruves); whereas the non-tetrahedral peak at around $\cos\theta = 0.5$ arises due to the angles formed at the central molecule by HB-nonHB or nonHB-nonHB combinations of neighbors (see groups of bluish and greenish graphs). It is interesting to observe that the intensities of these normalized distributions do not change with urea concentration. But as we have seen in Figure4.a.10, the relative proportion of these H-bonded neighbors changes as a function of urea concentration, the HB-HB, HB-nonHBand the nonHB-nonHB combinations also change leading to an intensity change in the P($cos\theta$) distribution shown in Figure4.a.11(a). Thus in essence, the slight change in the distribution P(q_4) as a function of urea concentration is a result of change in the proportions on n-hydrogen bonded molecules, not due to breaking of local tetrahedral structure of water.

4.A.3.2: Dynamics

In order to understand the effect of urea concentration on the translational dynamics of water and urea, MSDs of water and urea in the aqueous solution of urea at different concentrations have been calculated. The mean square displacements for urea (top panel) and oxygenof water (bottom panel) are shown in Figure 4.a.12. The translational diffusion coefficient of the water molecules is related to the slope of the MSD in the long time limit. Thus, from Figure 4.a.12 it is evident that presence of urea modifies translational diffusivities of both water (see Figure 4.a.12(top panel)) and urea (see Figure4.a.12(bottom panel). As the concentration increases slope of MSD decreases, indicating a decrease in diffusivity with the increasing concentrations.

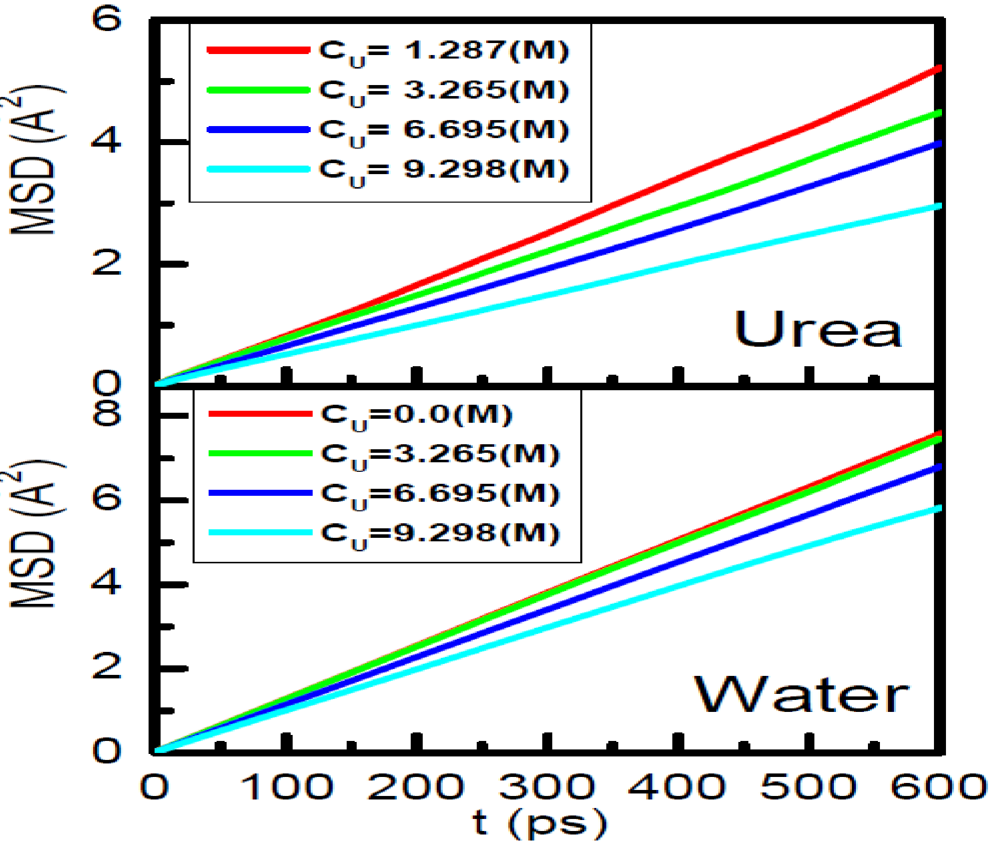

Figure 4.a.12. Mean squared displacements (MSDs) of (a) urea and (b) water molecules as a function of time at different urea concentrations (see the legends for different concentrations).

Similar trend has been observed in many earlier studies.[254,280] Orientational dynamics in terms of dipole moment vector of the tip4p/2005 water molecules at different urea concentration has also been studied. (see Chapter-2 and Chapter-3 for detailed description). We have calculated TCF of the dipole moment vector of the water molecule at different urea concentration. Time correlation functions corresponding to 1st order and 2ndorder Legendre Polynomials, Γ_1^{μ} and Γ_2^{μ} respectively have been calculated and shown in Figures. 4.a.13 and 4.a.14respectively.It is interesting to note that in case of rotational or orientational relaxation of the dipole moment vector of water, the effect of increasing urea concentration is negligibly small. This observation is consistent with that obtained from the experimental study of Rezus et al.[247]

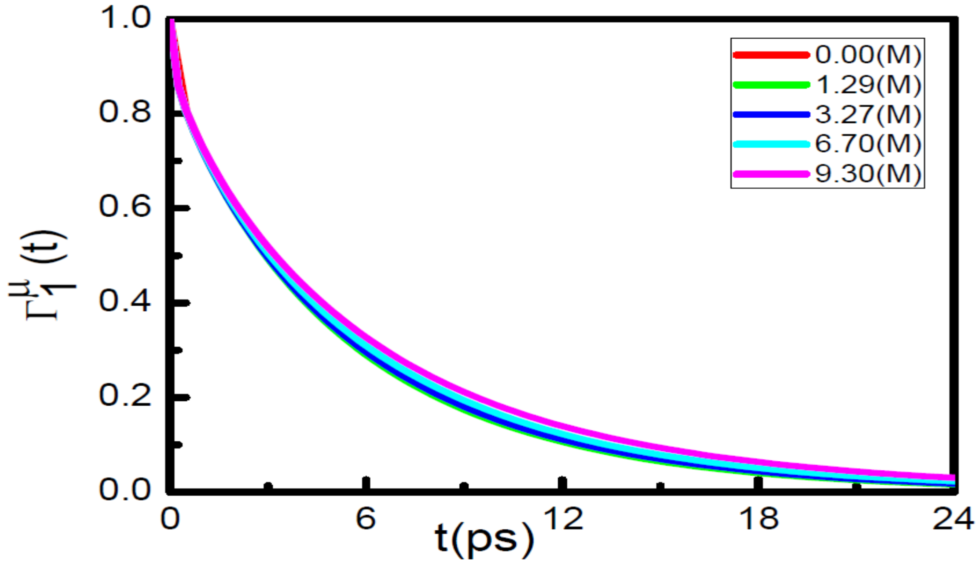

Figure 4.a.13.Time correlation function of dipole moment vector (μ) of tip4p/2005 water molecule comparing at different urea concentration for Legendre polynomial (l=1).

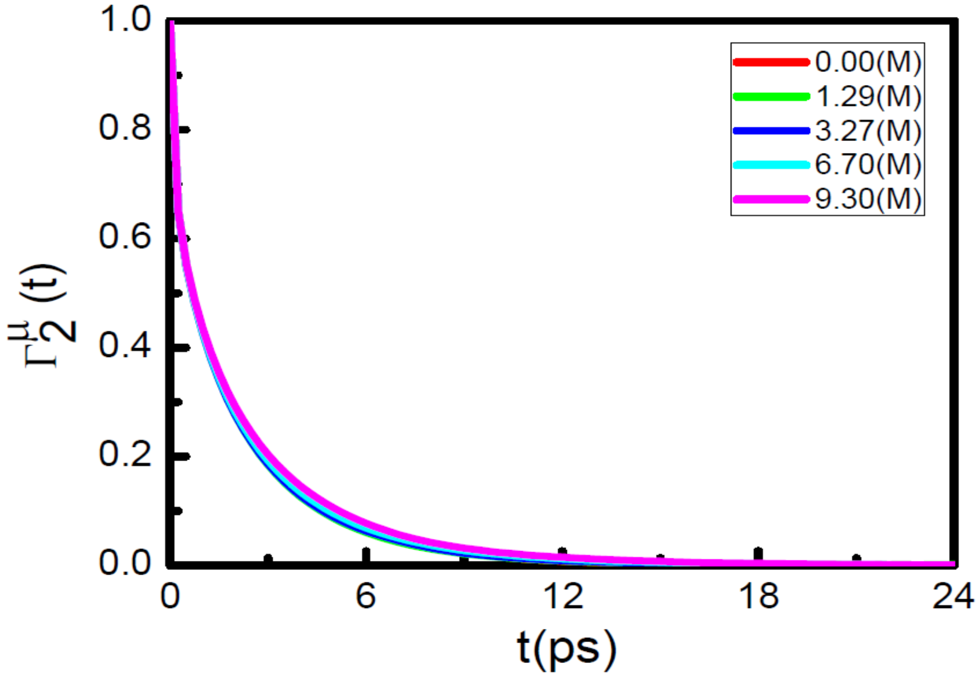

Figure 4.a.14.Time correlation function of dipole moment vector (μ) of tip4p/2005water molecule comparing at different urea concentration for Legendre polynomial (l=2).

4.A.4: Summary and Conclusions

Aiming at elucidating the effect of urea on the local structure and dynamics of water, we have performed molecular dynamics simulations of aqueous urea solutions of different concentrations ranging from 1.29 M to 9.30 M. As already mentioned, previous investigations have contradictory conclusions about the effect of urea on water structure. Recent investigation of Stumpe et al.[274] have inferred through their analysis of various local structural parameters that urea does not break the tetrahedral structure of water. However, their analysis of energetic quantities suggests structure making ability of urea. On the contrary, the results presented by Idrissi et al.[277]using various orientational and radial order parameters to quantify local structural arrangements of water show that the tetrahedral structure of water is broken in presence of urea at high concentrations. The order parameters calculated in this work are based on the nearest neighbour approach,in which angular or radial arrangement of the first four neighbors with respect to the central reference water molecule is measured. Thus, this approach heavily relies on the correct choice of the four nearest neighbors. In bulk water, all the four nearest neighbors of a reference water molecule are always water, whereas in a concentrated aqueous urea solution, a nearest neighbour position can be occupied either by water or by (site of) a urea molecules (see Figure4.a.5). In a concentrated aqueous urea solution probability of one or more water neighbors being replaced by (site/s of) one or more urea molecules is more. In the present investigation, we have shown that if we choose four neighbors as the first four *water* molecules [without considering urea as a neighbour], average tetrahedral order parameter and its distribution (see Figure4.a.1) change significantly from the bulk water results; indicating breakdown of tetrahedral water structure. Results with the same conclusions can be drawn from the measurements of average and fluctuations of distances of all the four neighbouring water molecules (see Figures.4.a.3-4). It is interesting to observe the distributions of hydrogen bonding angle formed by one of the four nearest water neighbors with the reference (central) water molecule. The distribution of this angle does not change from its bulk water value for the 1st or 2nd*water*neighbour, whereas the same for the 3rdor 4th*water*neighbour changes significantly with increasing urea concentration. It may prompt us to conclude that tetrahedral structure of water is broken. However, in a concentrated urea solution there are around 26% and 37% probabilities that the third and fourth nearest neighbouring positions respectively can be occupied by urea and not by water (see Figure4.a.5). Therefore, it is very important to consider urea molecules (apart from water molecules) as a neighbour of a reference water molecule. If we do not consider the fact that urea can also be a neighbour and take all the four neighbors as water, then the 3rd or 4th water neighbour may not be actually the 3rd or 4th nearest neighbour. These water molecules in concentrated aqueous urea solution are in the second solvation shell. The deviation in the calculated quantities from their bulk water values in concentrated aqueous urea solution is thus resulting from these outside (the first solvation shell) water molecules. When we consider both urea and water molecules in choosing nearest neighbors and calculate all the order parameters representing different orientational and radial orders, we find almost negligible changes in these order parameters as a function of urea concentration. These results thus suggest that usual tetrahedral structure of water is maintained; only some of the water molecules are substituted by (site/s of) urea molecules. A careful observation of distributions of tetrahedral order parameters (see Figure4.a.9 and 11) indicates that there is a small change in the distribution as a function of urea concentration and therefore it is required to scrutinize it further. At this point it is important to remember that liquid water at finite temperature is not perfectly tetrahedral and it is a broken hydrogen-bonded network consisting of water molecules with one, two, three, four, five and more number of hydrogen bonds. Proportion of these different types of hydrogen-bonded water molecules changes with various external parameters such as temperature, pressure etc. Recently, it was shown in chapter-2 that if proportions of these different types of hydrogen-bonded water molecules change (due to change in temperature in that case), tetrahedral peak in the distribution of q_4 diminishes and non-tetrahedral peak increases. In the present investigation also, we find that there is a considerable change in the proportions of *n*-hydrogen-bonded molecules with the increase in urea concentration and we have shown that the slight change in P(q_4) is due to this change in hydrogen bonding pattern of water in presence of urea. The present investigation thus asserts that radial, tetrahedral and other orientational structures of water remain largely unaffected by the presence of urea even at high concentrations. Present result thus supports the conclusion made by Grubmullar and coworkers[71] and others[132,225,229,230,247,254,256,265-270]that water structure is not changed significantly due to urea and oppose the idea that urea acts as structure-breaker as demonstrated by Idrissi et al.[277] and others.[127,132,247-253,261-263]Present results ascertain that water structure is not broken with the addition of urea. However, interpretation of protein denaturation by urea requires further analyses on thermodynamic link between solvent structure in terms of solute-solvent and solvent-solvent radial distribution functions and protein stability[231,281]and this can be easily studied through Kirkwood-Buff approach.[282,283]Denaturant urea can have considerable effect on the manifestation of hydrophobicity at the nanoscale.[29]Further investigation in this direction is in progress. We have also found that translational diffusivities of water and urea change considerably but orientational dynamics remains almost unchanged on addition of urea. Modification of water dynamics[247,284]may have a definite role in the protein denaturation process. In fact, there are contradicting views[247,266] in this matter, and therefore, further investigations are required to resolve the issue. Another important area of very recent research deals with the role of urea on nucleic acid conformations and stability.[285-286]Further studies are required in this direction.

Chapter 4

PART-B

Effect of Concentration on Like-Charge Pairing of Guanidinium Ions, Proteins and on the Structure and Dynamics of Water

4.B.1: Introduction

Guanidinium chloride (Gdmcl) and urea at high concentrations (≥ 5M) are popular denaturants[109,121-132]of proteins and nucleic acids. Out of these two denaturants, guanidinium (Gdm) ion of Gdmcl is a positively charged ionic species and therefore, it is expected that it will act in a different manner than urea. The Gdm moiety structurally resembles a part of the moiety in the arginine (ARG)side chain of the protein. Presence of clustering of arginine residues in many proteins indicates that arginine-arginine interaction at protein interfaces stabilizes protein-protein interaction[287-293]and the Gdm-Gdm interaction inside the core is one of the driving forces for protein folding and stability. However, Gdm moiety being positively charged, stacking of two such moieties is counterintuitive. In fact, like-charge ion-ion interactions in condensed phases are prevalent and its different manifestations are intriguing and important in view of its relevance in chemical, biological and physical sciences. It is well known from Coulomb’s law that like-charge ions repel each other. However, in condensed phase, because of the presence of many other species, the like-charge ion-pair formation is possible. In this context, formation of ion-pair between two guanidinium (Gdm^+) ions in the aqueous solution of guanidinium chloride (Gdmcl)[294-299]is of special interest due to several reasons. First, Gdmcl acts as an effective denaturant for proteins and nucleic acids and therefore it is essential to know the mechanism of its action and its relation with the ion-pair formation. Apart from that, structural similarity of guanidinium ion with the arginine side-chain of a protein may explain the existence of conglomeration[287-293]of multiple arginine residues in many proteins. Moreover, guanidinium-water system is a simple and important test case to understand the origin of like-charge attraction in condensed phase.

Despite many theoretical and experimental studies[12,133,225,232-255,264-275,300-308] over the years, the molecular mechanism by which guanidinium ion acts as denaturants for proteins and nucleic acids in aqueous solutions remains unresolved. Many early studies[241,242] have indicated alteration in hydrophobic interaction[29,30]as a cause for the denaturation. Many groups[12,223,235,249,248,264,304-308] pointed out that the denaturation byGdmcl is effected by preferential solvation of nonpolar groups of the macromolecules. However, there is divided opinion on whether direct or indirect mechanism that dictates the denaturation process. The indirect mechanism[133,225,234,239,241,242,250,255,265, 275,300-304] posits that the denaturant first breaks the tetrahedral and hydrogen bonded network of water and thereby helps water indirectly to invade into protein or nucleic acid interior. On the other hand, direct mechanism[223,232, 235,249,277,305-308] predicts that Gdm$^+$ ion first attacks polar as well as nonpolar residues of the protein and causes the macromolecule structure to open up.

With regard to direct mechanism, it is important to know how two arginine groups in protein behave. As already mentioned the presence of conglomeration of arginine groups in many proteins has direct relevance to protein folding and stability of protein-protein interaction. Based on this arginine-arginine pair formation propensity, many arginine based synthetic drug molecules have been synthesized. Gdm$^+$ ion can interact with protein moiety through direct Coulomb interaction or through van der Waals interaction. However, conglomeration of arginine or ion-pairing of Gdm$^+$ ions in its aqueous solution is counterintuitive as two same charge ions come close to each other and signifies the role of van der Waals or dispersion interaction. It is now almost certain that Gdm$^+$ ions at high concentrations form like-charge ion-pairs in solution.

The early study of Mason et al.[309]using neutron diffraction experiments, had shown that the guanidinium ion in its aqueous solution is one of the most weakly hydrated cation and they posited that due to this weak hydration, denaturation takes place via direct preferential mechanism. However, subsequent neutron scattering and molecular dynamics (MD) simulation study of Brady and coworkers[310]have shown that Gdm$^+$ ion has a well-defined hydration shell. A bimodal hydration structure of Gdm$^+$ ion with the N-H groups making well-ordered hydrogen bonds (HB) whereas the planar face being relatively deficient in interaction with water has been predicted. The most important outcome of this study is the identification of like-charge ion pairing of Gdm^+ ions which are stacked parallel to each other. They justified that this parallel stacking ability enable Gdm^+ ion to interact favourably with hydrophobic, aromatic side chains of the protein.

Recent computational study by Vazdar et al.[297]using ab-initio MD simulation has also identified like-charge ion pairing. Amphiphilic character and van der Waals interaction between the Gdm^+ ions have been postulated to be responsible for such contact ion pair formation defying like charge repulsion. Jungwirth and coworkers[299] using MD simulation and capillary electrophoresis experiment have demonstrated that guanidinium cations form like-charge pairing with the positively charged side chains of arginine-containing peptides in aqueous solutions but found no such effect for sodium cations and/or lysine polypeptide. Orientational dependence of the affinity of the Gdm^+ ions at the water-vapor interface has also been investigated and it was found that the population of guanidinium ions oriented parallel to the interface is greater in the surface region than in bulk. For other orientations, the trend is opposite.[300]In fact like-charge ion-pair formation in aqueous solution of Gdmcl was predicted[294,296] by calculating potential of mean force (PMF) between two Gdm^+ ions in water. Although contact pair minimum has been observed, but stability of the contact pair state is shown[250]to be dependent on the details of the models. Most of these studies have used either infinitely dilute solution or a solution with finite concentration of the Gdm^+ ion.

Although many recent studies on protein denaturation by Gdmcl have argued in favour of direct mechanism, it is also worthwhile to know whether Gdm^+ ion breaks tetrahedral and hydrogen bonding network of water. Guanidinium ion is known to be an effective denaturant for proteins and nucleic acids when present at high concentration in its aqueous solution. Therefore, effect of Gdmcl concentration on the formation of Gdm^+ ion-pair and on tetrahedral and hydrogen bonding structure of water is essential. In fact, a recent molecular dynamics simulation study[307]of aqueous solution of guanidinium chloride at different concentrations has addressed this issue. They have found like-charge ion pairing at moderate Gdmcl concentration but contrary to general intuition that increase in Gdmcl concentration will increase the ion-pair formation; they predicted decrease in the population of contact pair state and subsequent increase in solvent separated state. However, this conclusion is based on the comparison of first and second peaks of the Gdm-GdmRDF (g_{CC}(r)) at different concentrations. At this point, it is important to mention that simple comparison of the peak heights of Gdm-Gdm RDFs of solutions with unequal concentrations is erroneous as the individual RDF is normalized by the respective bulk concentration. Mandal et al.[307] have also shown that both tetrahedral and hydrogen bonding structure of water are broken with the increasing concentration of Gdmcl. In calculating these quantities, they considered only water (not any sites of Gdm^+ and chloride ion) as neighbors. However, in a concentrated solution of Gdm^+ ion, which has many potential hydrogen bonding sites, it is expected that some of the first solvation shell “water neighbors” will be replaced by (site/s of) Gdm^+ ion and/or chloride ion. In fact, we have shown in chapter-2 and chapter-4.a that in case of aqueous urea solution that in a sufficiently concentrated urea solution, the probability of the fourth neighbor (distance wise) being a urea molecule is about 37% in a 9 M urea solution. It is shown that normal calculation of tetrahedral order parameter by considering four nearest “water neighbors” around a water molecule leads to erroneous result as the probability of the fourth “water neighbor” being outside the solvation shell increases at high concentrations. Thus, proper choice of nearest neighbor is essential in such cases. It is therefore important to revisit the MD results on guanidinium chloride aqueous solution and check whether really like-charge ion-pair formation decreases with increase in Gdmcl concentration and whether Gdmcl really breaks the water structure.

In this work, we have therefore performed molecular dynamics simulations of aqueous solution of Gdmcl at varying concentrations to verify the effect of increasing concentration of guanidinium chloride on the like-charge ion-pair formation as well as on the local structure of water. In order to investigate the direct interaction mechanism aspect of chemical denaturation of a protein by Gdmcl, we have also simulated an arginine (ARG) rich peptide in an aqueous solution of 6 M Gdmcl. In this case it is important to know whether Gdm+ ion of the Gdmcl salt attacks the Gdm moiety of the ARG side chain and if so, whether they form a parallel stacking orientation. It is also important to know which part of the ARG side chain of the protein/peptide is directly attacked by Gdm^+ ion of Gdmcl. In what follows, In Sec. 2, models used and methods of simulation adopted will be discussed. In Sec. 3A, the results on dependence of Gdmcl concentration on like-charge ion-pair formation is discussed. In Sec. 3B, effect of increasing concentration of Gdmcl on the radial, hydrogen bonding and tetrahedral structure of water will be discussed. In Sec. 3C, the results on dynamic properties of different species in solution at various Gdmcl concentrations have been presented. In Sec. 3D, we have discussed the results obtained from a simulation of an arginine-rich peptide in 6M aqueous Gdmcl solution. Finally, a concluding remark summarizing main outcome of this work will be presented in Sec. 4.

4.B.2: Models and methods

The force field used for guanidinium ion is fully flexible with bond, angle and dihedral terms in the intra-molecular potential along with usual non-bonded Lennard-Jones and Coulomb interactions. Namely CHARMM22 force field[307,310]has been used for guanidinium ion. For water, we have used TIP4P/2005[52]rigid body atomistic model with fixed bond lengths and bond angle. This new variant of the TIP4P model is superior to original TIP4P model in terms of reproducing most of the anomalies of water. However, in order to reproduce the results obtained by Mandal et al.,[307] we have used TIP3P water model also. Some of the results with TIP3P water model are shown in this chapter. Different concentrations of aqueous solutions of GdmCl are prepared by randomly placing requisite number of Gdmcl molecules in a pre-equilibrated water box of appropriate size. Specific details of the numbers of Gdmcl (N_{Gdmcl}), water (N_W) molecules and Gdmcl mole fraction (X_{Gdmcl}) with the volume of the boxes and molarity of the resulting solutions are given in Table 4.b.I.

In order to prepare the peptide-water-Gdmcl system, an arginine-rich 26 residue peptide (PDB ID: 2MIA)[311]was immersed into a pre-equilibrated solution of 6 (M)Gdmcl. All the overlapping water molecules were removed. The final starting configuration thus has one peptide molecule immersed in a cubic simulation box (with box size around 6.7 nm) containing6000 water and 1100guanidinium chloride molecules. A snapshot of the simulation system is shown in Figure 4.b.1A. Out of the 26 residues of the peptide, 11 residues of 2MIA peptide are ARG residues. This side chain of the ARG is shown in Figure 4.b.1B.

All the simulations were performed using GROMACS[156]simulation package. After initial energy minimization all the simulations were run in NPT ensemble[10]with periodic boundary conditions using molecular dynamics extended system approach[10]of Parrinello and Rahman[65] to fix pressure and Berendsen algorithm[62] to fix temperature. For water, we constrain the bonds and the angle of a water molecule by LINCS algorithm[61]andelectrostatic interactions were calculated using particle-mesh Ewald(PME) method.[57,278] Equations of motions were integrated using Leap-frog algorith[10]with a time step of 0.5fs. All the simulations were carried out at a target pressure of 1 atm and a target temperature of 300 K. For equilibration of the Gdmcl solution, we have discarded first 20 ns trajectories and trajectories for the next10 ns have been stored for analyses. In order to check the effect of finite box size and finite length of simulation trajectory, we have also performed a simulation of ~6 M Gdmcl solution with a larger box. In this case, we have 500 guanidinium chloride molecules and 2350 water molecules with a box size of 5.021 nm. In case of smaller system sizes (systems 1G, 2G, 3G, 4G-1 (see Table 4.b.I)),we have discarded first 20 ns trajectories for equilibration and trajectories for the next 10 ns have been stored for analyses. For the larger Gdmcl-water system (system 4G-2) we have discarded first 60 ns trajectory for equilibration and next 5 ns have been used for further analyses. For the protein solution, we have discarded initial 50 ns trajectory for equilibration and the next 10 ns trajectory has been stored for analyses. Most of the post analyses of the simulation trajectory have been performed using our home-grown software. Only various RDFs involving protein residues are obtained from GROMACS analyses programs.

Table 4.b.1: Different Systems simulated in this work

System	N_{Gdmcl}^{*}	N_{w}^{*}	X_{Gdmcl}^{*}	Volume(nm^3)	Molarity (M)
1G	0	512	0.0	15.365	0.0
2G	42	870	0.04605	30.469	2.289
3G	84	768	0.09859	32.157	4.338
4G-1	125	587	0.1755	31.704	6.548
4G-2	500	2350	0.1754	126.582	6.558

*N_{Gdmcl}, N_W are number of Gdmcl and water molecules respectively, X_{Gdmcl} is the Gdmcl molefraction.

Local orders: We know that in case of a perfectly tetrahedral structure, there are four nearest neighbors in the 1st solvation shell of a central molecule. Oxygen-oxygen radial distribution function of water describes radial arrangements of neighboring water around a reference, central water molecule, but cannot provide any information about the angular preferences of the neighbouring molecules. In order to get information about angular preferences of the neighbors around a central water molecule, an order parameter known as tetrahedral order parameter is used. In order to assess structural (hydrogen bonding) integrity in presence of solutes or salts, average number of hydrogen bonds and the distribution of hydrogen bonding angle will be useful used.

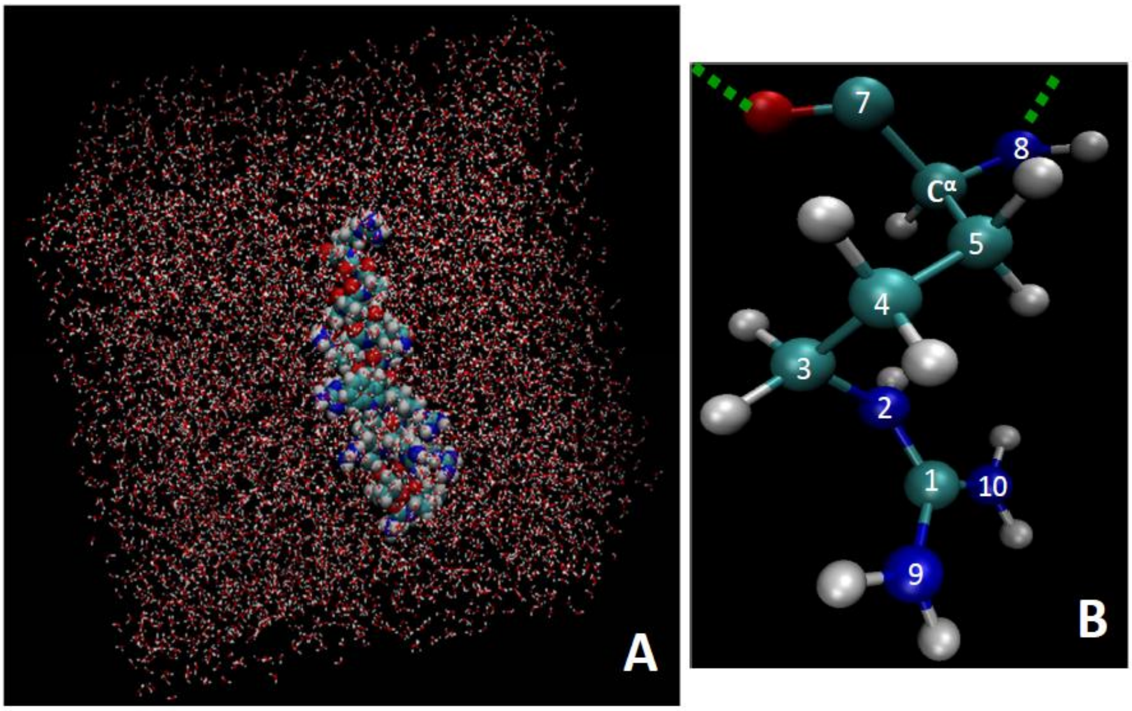

Figure4.b. 1. (A) Snapshot of a typical configuration of peptide−water system. (B) The arginine residue, shown as a ball-and-stick model. Blue atoms are nitrogen, red atoms are oxygen, green atoms are carbon, and gray atoms are hydrogen. Dashed lines show the extension of the main chain.

Tetrahedral order parameter: In this approach, a tetrahedral order parameter q_i is defined for each water molecule in the system by considering its four nearest neighbors. The parameter q_i is defined by[71]

$$q_i = 1 - \frac{3}{8}\sum_{j=1}^{3}\sum_{k=j+1}^{4}\left[\cos\theta_{jik} + \frac{1}{3}\right]^2 , \qquad (4.b.1)$$

where '*i*' is the central molecule and θ_{jik} is angle formed by neighbours *j* and *k* at the reference, central water molecule *i*. For a perfect tetrahedral angle, $\cos\theta_{jik}$= -1/3 and thus q_i=1 and for a perfectly random arrangement, angular integration of the term within square bracket in Eq. (4.b.1) yields 4/9. Since there are four neighbors and therefore 6 angles in the summation, this contribution come out to be 8/3. Therefore the pre-factor 3/8 before summation makes the second term 1 and hence q_i equal to zero for a random arrangement.[70]The above equation is valid for a central molecule with four nearest neighbors. In the present investigation, we have used the above equation for water molecules with two and three neighbors by modifying the constant term before the summation. Details of how these normalization constants have been calculated are shown in chapter-2.The average valueq_4, the tetrahedral order parameter, is calculated by averaging over all the N molecules and over the ensemble using the following equation

$$q_4 = \frac{1}{N}\left\langle \sum_{i=1}^{N} q_i \right\rangle. \qquad (4.b.2)$$

Hydrogen bond: Water is a network forming hydrogen-bonded liquid. Two important order parameters namely average number ($<n_{HB}>$) of hydrogen bonds (HB) and its distribution are used to gauge any change in hydrogen bonding structure of water. The standard geometric criterion, according to which two water molecules are considered to be H-bonded only if (i) the inter-oxygen distance is less than 3.5 Å, (ii) the hydrogen-oxygen (H-bonded) distance is less than 2.45 Å and (iii) the H-O····O angle (often known as HB angle and denoted by θ_{HB})is less than 30° has been used to identify a hydrogen bond between two water molecules. Distribution of the HB angles θ_{HB} formed by any of the nearest neighbors of a central molecule.

4.b.3:Results and Discussion:

4.B.3.1: Structure

4.B.3.1.a: Ion-pair Formation and its Concentration Dependence

Let us first discuss about like-charge ion-pair formation of the guanidinium ions. The effect of Gdm^+ ion concentration on the extent of like-charge ion-pair formation can be estimated from the change in Gdm-Gdm radial distribution function (RDF) with concentration. In Figure 4.b.2, we have therefore shown the RDF among carbon atoms of the

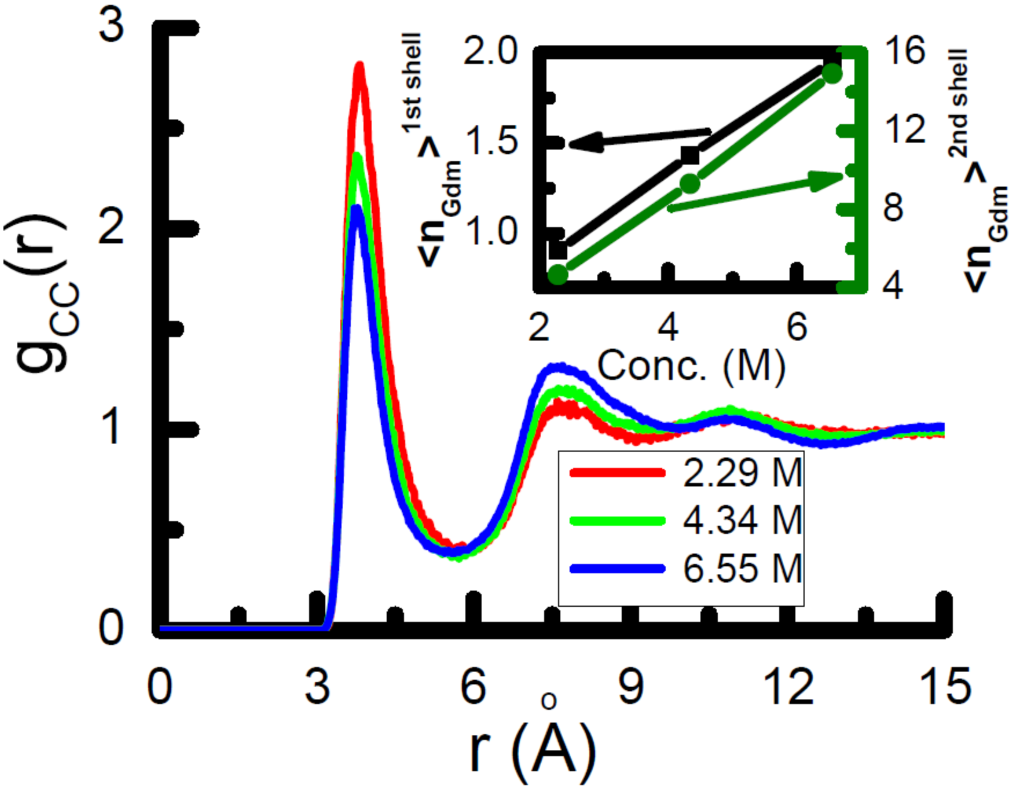

Figure4.b.2.a Radial distribution functions of the carbon atom of the guanidinium moiety around the same for three different concentrations. Distance r is measured as intermolecular distance between the carbon atoms of two Gdm moieties. In the inset, numbers of Gdm^+ ions in the first (shown by black line and left-hand-side axis) and second (shown by green line and right-hand-side axis) solvation shells have been shown.

Gdm$^+$ ions, g_{CC}(r) at different concentrations of the Gdmcl. The large first peak at 3.7-3.8 Å between two carbon atoms not only signifies aggregation, but stacking (parallel orientation) of the like-charge Gdm$^+$ ions. Had it been in-plane side-by-side pairing, carbon-carbon distance would have been more. In order to check whether there is any water molecule present between two Gdm$^+$ ions, we have plotted RDF, $g_{C\text{-}Ow}$ between carbon atom of the Gdm$^+$ and oxygen atom of water (see lower panel of Figure 4.b.3). The first peak at around 3.7 Å between carbon atom of Gdm$^+$ and oxygen atom of water confirms that there is no water molecule between two Gdm+ ions at their closest separation. If we look at the RDF of chloride ion around the carbon of Gdm$^+$ ion as shown in Figure 4.b.3 upper panel, it is clear that the first peak appears at around 4 Å. Therefore, chloride ion also does not come between

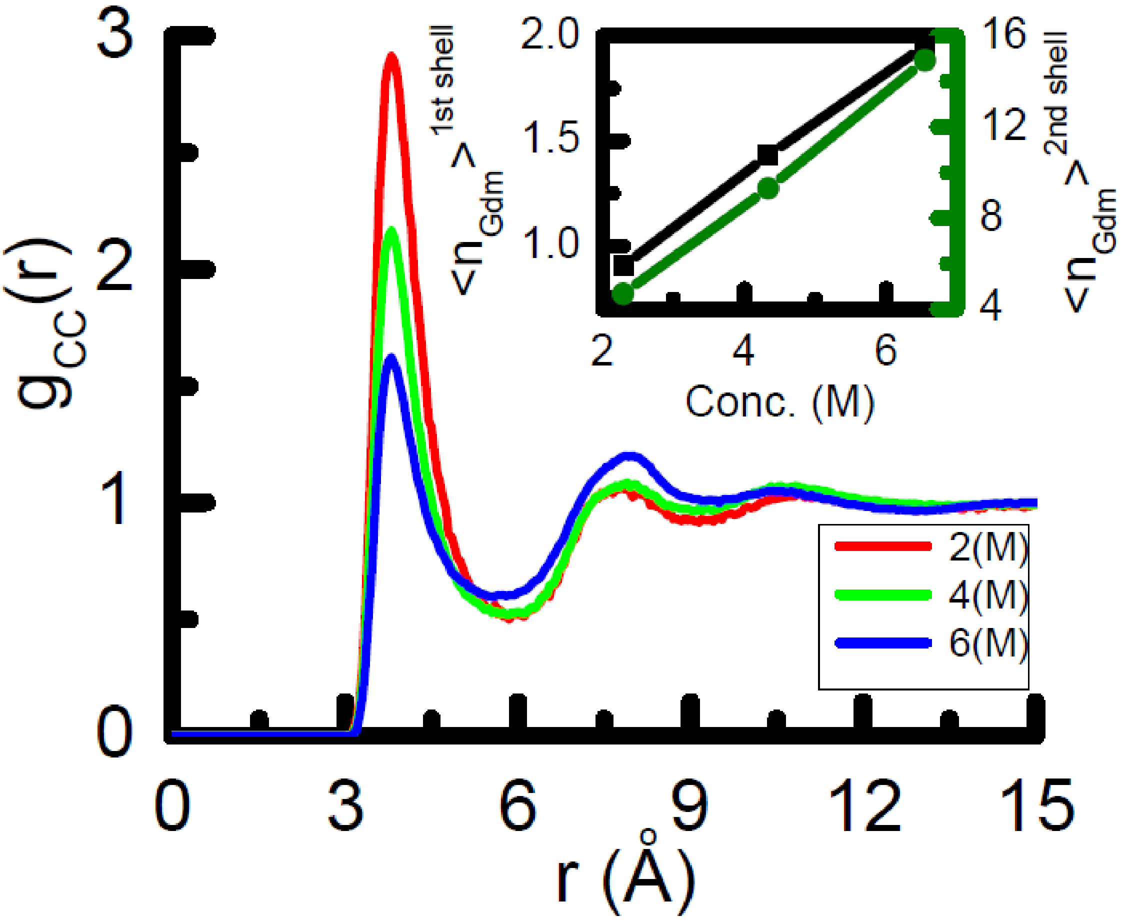

Figure4.b.2.b Same as in Figure 4.b.2.a for Tip3p water model.

two stacked Gdm$^+$ ions. The second peak of g_{CC}(r) in Figure 4.b.2.a is at around 7.7 Å and represents the solvent separated state. Similar observations have been made earlier.[307] Recently Vazder et al.[295,297] using ab-initio MD simulation have also found existence of counterintuitive like-charge gdm$^+$-gdm$^+$ ion pair formation. The stability of such "electrostatics-defying" ion-pairs in a stacked conformation has been attributed to the

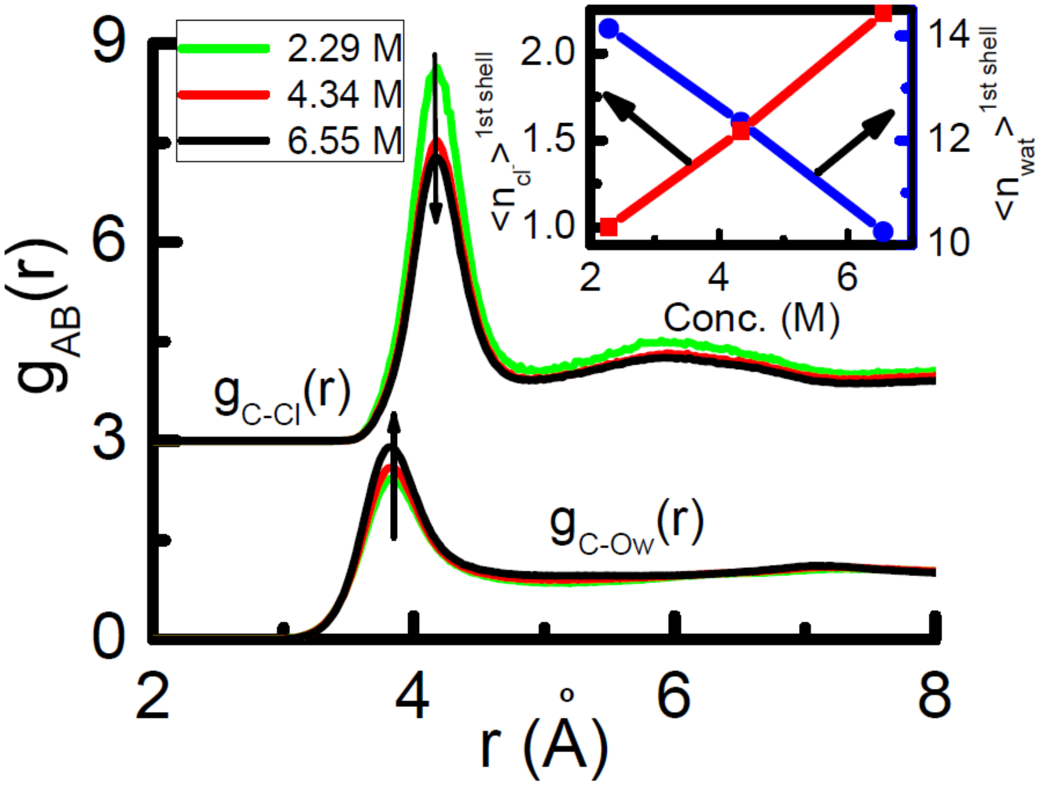

Figure 4.b.3.Radial distribution functions of O_w of water (lower panel) and chloride ion (upper panel) around the carbon atom of guanidinium moiety. The RDF of the chloride ion, g_{C-Cl}(r) is shifted upward by 3 units for clarity. In the inset, numbers of chloride ions (shown by red line and left-hand axis) and water molecules (shown by blue line and righth and axis) in the first solvation shell of the Gdm$^+$ ion are shown.

amphiphilic nature of the guanidinium ions. Due to planarity, aromaticity, and nonuniform charge distribution, the faces of the Gdm$^+$ cation are hydrophobic and weakly hydrated, whereas the guanidinium ion forms hydrogen bonds with water molecules in itsmolecular plane.[295,297]

The most surprising observation is the way RDF changes with increasing Gdmcl concentration. With increasing concentration of Gdmcl, height of the first peak of the $g_{CC}(r)$ decreases and that of second (solvent separated state) peak increases. It is very tempting to conclude from these changes in RDF that Gdm^+- Gdm^+ contact pair formation decreases and solvent separated pair formation increases with increasing Gdmcl concentration. Mandal et al.[307] have observed similar variation in RDF and inferred that extent of contact ion pair state is decreasing with increasing Gdmcl concentration and that of solvent separated state is increasing. However, it is very important to note at this point that RDFs at different concentrations are normalized by respective bulk concentration and therefore comparing the peak heights of RDFs for estimating number of molecules in the solvation shells at two different concentrations is misleading. Although height of the first peak of a RDF is a measure of density of contact pair state relative to bulk concentration, it does not tells us about absolute number of nearest neighbors. In this situation, it is better to integrate the RDF up to appropriate distances corresponding to first and second solvation shells to get the number of Gdm^+ ions in contact pair and solvent separated states respectively. Whether really formation of contact pair state is decreasing with increasing Gdmcl concentration, we have integrated the $g_{CC}(r)$ upto the first minimum of RDF. In the inset of Figure 4.b.2.a, we have shown the numbers of Gdm^+ moieties in the first and the second solvation shells as a function of Gdmcl concentration. It is interesting to observe that numbers of Gdm^+ ions in both contact pair state (black line, left hand axis) and solvent separated state (green line, right hand axis) increase with increasing concentration. It is important to emphasize that contrary to the observation based on peak heights of the RDFs, actual number of ions present in the 1st and 2nd shells follow monotonic increase with Gdmcl concentration. However, maximum number molecules a solvation shell of a particular species can accommodate is restricted by molecular geometry and packing. Therefore, number of solvation shell molecules may not be linearly increased by further increase of Gdmcl concentration. Thus, the result presented so far demonstrates that the formation of like-charge ion-pairsas well as solvent separated ion-pairs does not really decrease with Gdmcl concentration. Both are increasing with increasing Gdmcl concentrations. As far as water and chloride ions are concerned (see Figure 4.b.3) the integrated value of the number of water molecules in the first solvation shell of Gdm^+ ion decreases and that of chloride ions increases (see the inset of Figure 4.b.3). Thus, as the concentration of Gdmcl increases, number of water molecules decreases and that of chloride ions increases in the first solvation shell of a Gdm^+ ion. The formation of ion-pair and its increase with increase in Gdmcl concentration has a special significance in denaturation mechanism. The higher propensity of the Gdm^+ moiety to undergo like-charge ion-pair formation at high concentration implies that these Gdm^+ ions will form similar like-charge ion-pairs with the arginine and other similar aromatic moieties of the protein residues and thereby replace water molecules from the protein surface and denature it. Our observation here is based on the improved TIP4P/2005 water model. However, all the trends in the results are the same if we use TIP3P water model as used earlier.[307]All the results using TIP3P model of water are also given in this chapter for better comparison (see fig. *Figure4.b.2.b)*. As already mentioned, in order to check the reliability of the results presented here with respect to system size and finite time dependence, we have further simulated the highest concentration Gdmcl solution by considering a larger system size and for a longer time (see system 4G-2 in the Table 4.b.I).The calculated radial distribution functions between two Gdm^+ carbon atoms, the carbon atom of the Gdm^+ and chloride ion, the carbon atom of Gdm^+ and oxygen of water and between oxygen-oxygen (of water) are shown in Figure 4.b.4. Results from smaller system size and shorter simulation trajectories are compared with those obtained from larger box size and longer simulation time and in all the cases excellent agreements have been observed indicating the results presented here based on smaller system size and shorter trajectories are trustworthy.

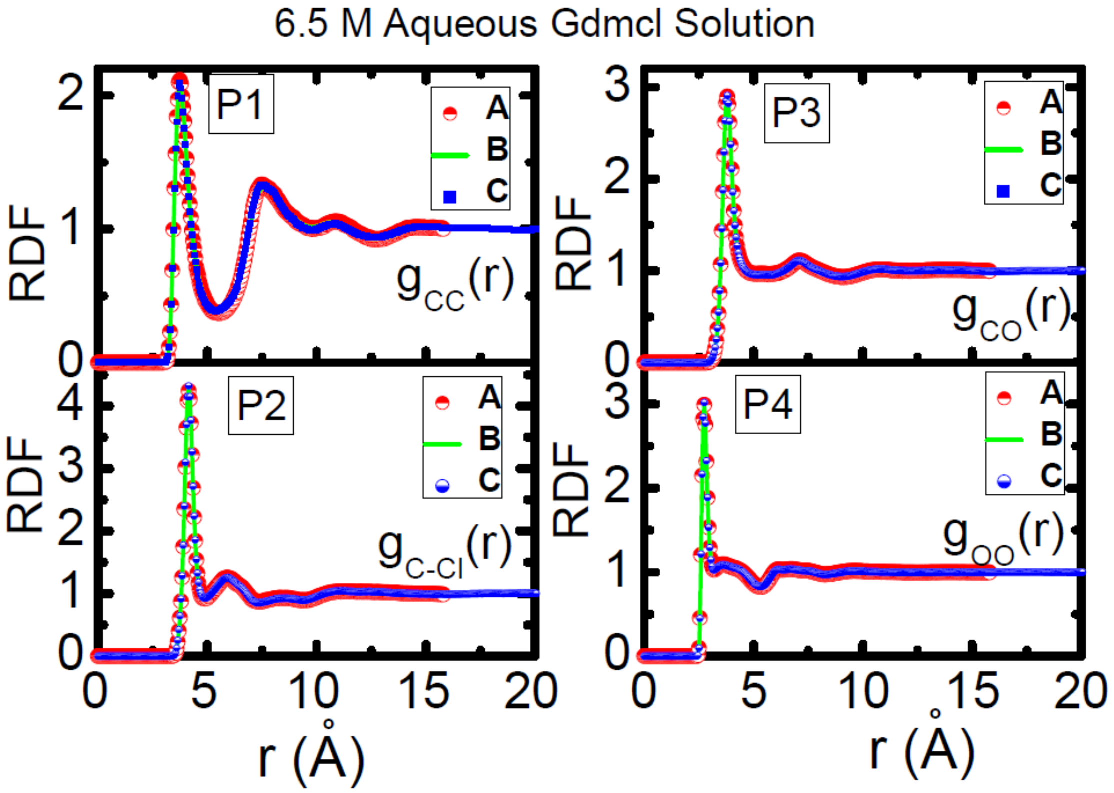

Figure 4.b.4 Effect of total time steps and box size used for simulation on RDF function.

Stacking of Guanidinium Ion Moieties:

Implication of the stacking of Gdm moieties at a reasonably high Gdmcl concentration in its aqueous solution is twofold. Close stacking of guanidinium moieties indicates that this denaturant attacks the protein residues of similar nature and gets stacked into the protein interior and interfaces and thus denatures the protein by direct interaction mechanism. In order to get an idea about relative orientation of the two Guanidinium ions in solution in its contact pair state, we have calculated the distribution of the angle ϕ between two molecular planes of two Gdm moieties. The schematic representation of the two molecular planes inclined at an angle $\phi$is shown in Figure4.b.5. The distributionsP(ϕ) of the angles ϕ made by the Gdm^+ moieties present in the contact pair state for three different concentrations of Gdmcl have been shown in Figure4.b.5. Two peaks near 0°and 180° in the distribution signify almost parallel stacking orientation between two Gdm^+ moieties. As the concentration of Gdmcl is increasing, there is a slight reduction in the peak heights (as in case of g(r) of Figure 4.b.2.a and 4.b.2.b). This slight decrease is due to variation in bulk concentrations.

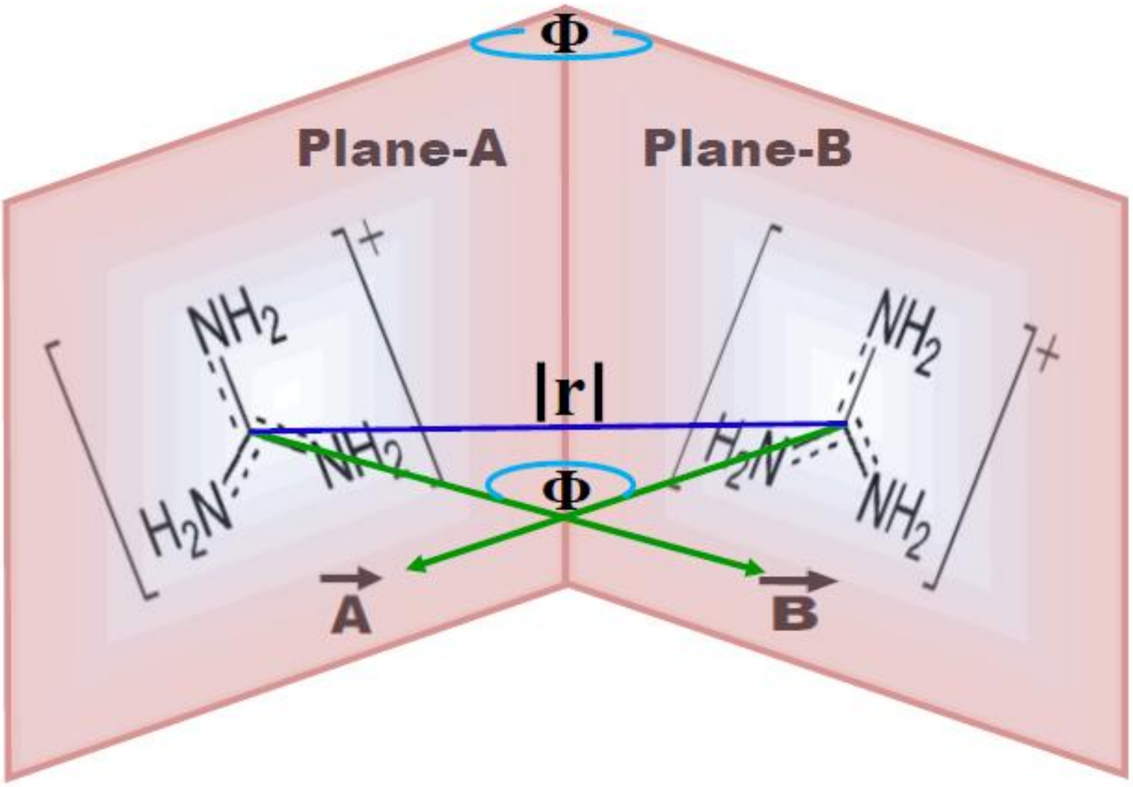

Figure 4.b.5 Schematic representation of two molecular planes of guanidinium ions inclined at an angle ϕ.

On the other hand, arginine residue of a protein resembles guanidinium moiety. Despite the highly repulsive nature of closely spaced like-charged groups, close stacking of arginine residues in a protein structure as been often observed.[287-289]Thus, Gdm^+-Gdm^+ stacking may have direct relation with protein folding and stability. Since denaturation of protein occurs at a high temperature, it is therefore expected that parallel stacking orientation between two arginine moieties will be disrupted at a high temperature. In order to check the effect of temperature on the parallel stacking orientation between two Gdm^+ ions, we have simulated aqueous solution of Gdmcl at different temperatures and calculated the distribution of the angle ϕ and these are shown in Figure 4.b.7. As expected, we found that at higher temperatures, preferred parallel orientation of the Gdm^+ moieties gets disrupted and orientation becomes almost homogeneous. Thus it indirectly supports the fact that during high-temperature denaturation close parallel stacking of arginine moieties gets disrupted with no preferential orientation.

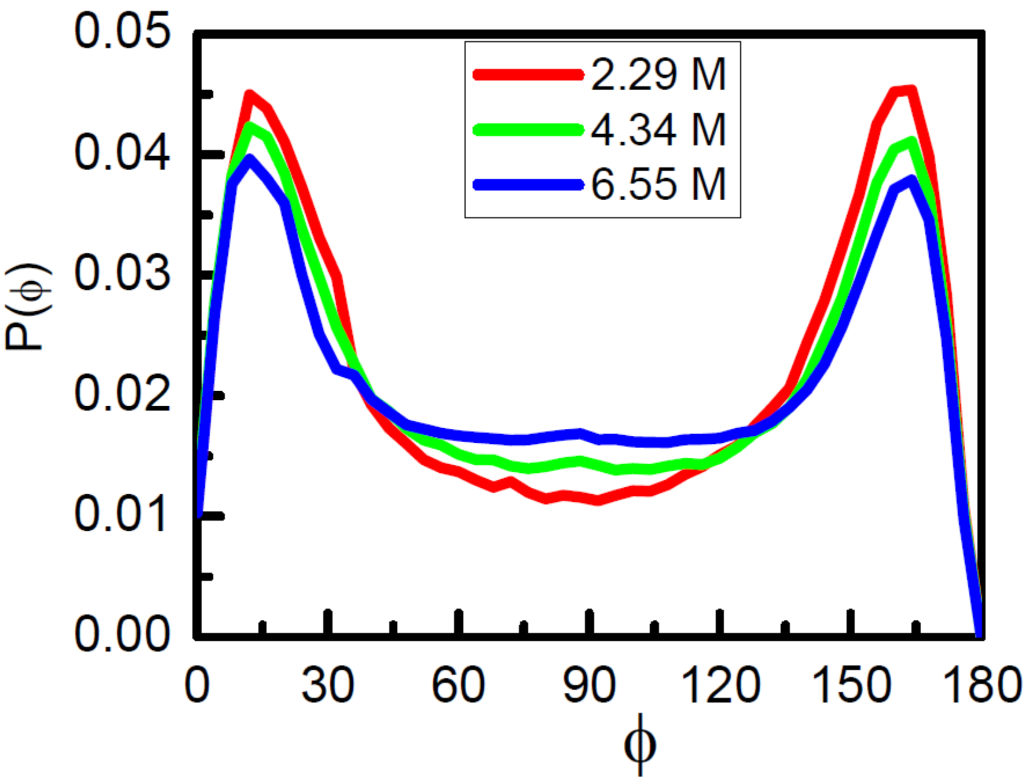

Figure 4.b.6. Distributions P(ϕ) of the angles ϕ made by the perpendiculars drawn from two guanidinium molecular planes at three different GdmCl concentrations.

It is well known that purely hydrophobic solutes aggregate in water and for nanoscopic or larger hydrophobic solutes, the spontaneous contact pair formation is dewetting induced.[29,30]The analysis of potential of mean force of nanoscopic hydrophobic solutes has demonstrated[55] huge stabilising (negative) solvent induced contribution to the PMF at a distance corresponding to the contact pair formation. In the present case, the potential of mean forces ($w(r)$) between guanidinium moieties at different concentrations have been calculated from the g(r) between two Gdm moieties as

$$w(r) = -k_{\boldsymbol{B}}T \ln g_{CC}\,(r) \qquad (4.b.3)$$

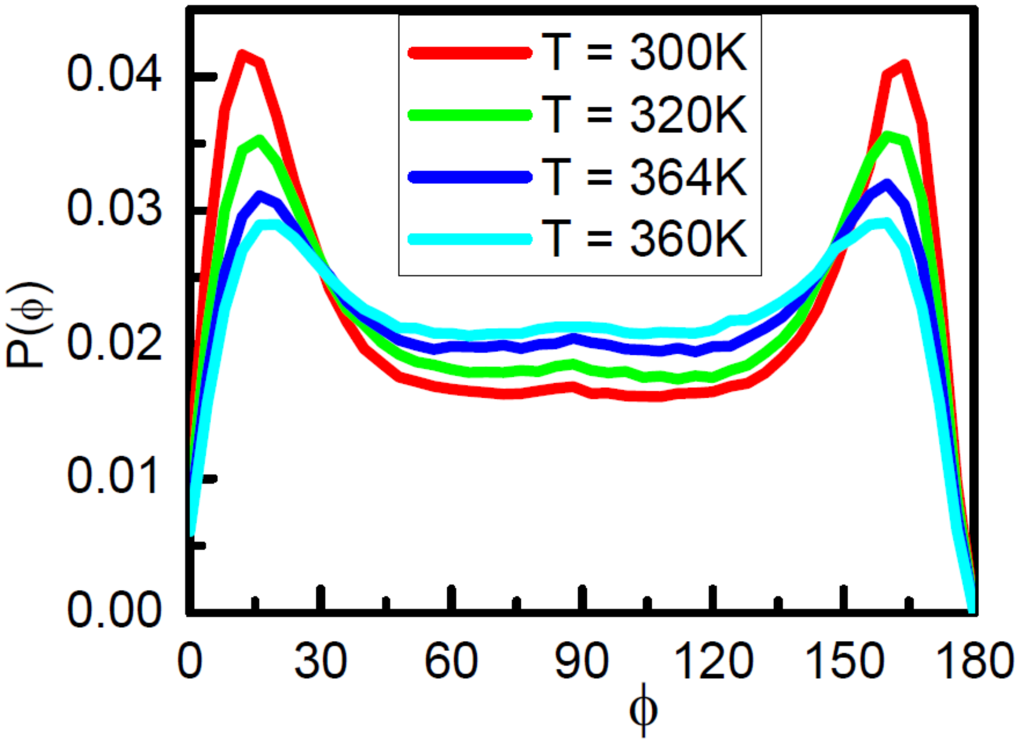

Figure 4.b.7. Distributions P(ϕ) of the angles ϕ made by the perpendiculars drawn from two guanidinium molecular planes at four different temperatures.

where, k_B and $T$are Boltzmann constant and temperature in Kelvin respectively. The difference between total PMF and direct interaction $U_{solu}(r)$ between the solutes gives rise to solvent contribution $w_{solv}(r)$ to the total $w(r)$, viz.,

$$w(r) = U_{solu}(r) + w_{solv}(r). \qquad (4.b.4)$$

In order to get direct solute-solute interaction component, we have performed vacuum (without any water molecule) simulation of Gdmcl at different concentrations. The carbon-carbon (of Gdm moieties) RDF calculated from the vacuum simulation is then converted according to Eq. (4.b.3) to get $U_{solu}(r)$. Finally, solvent induced contribution to PMF has

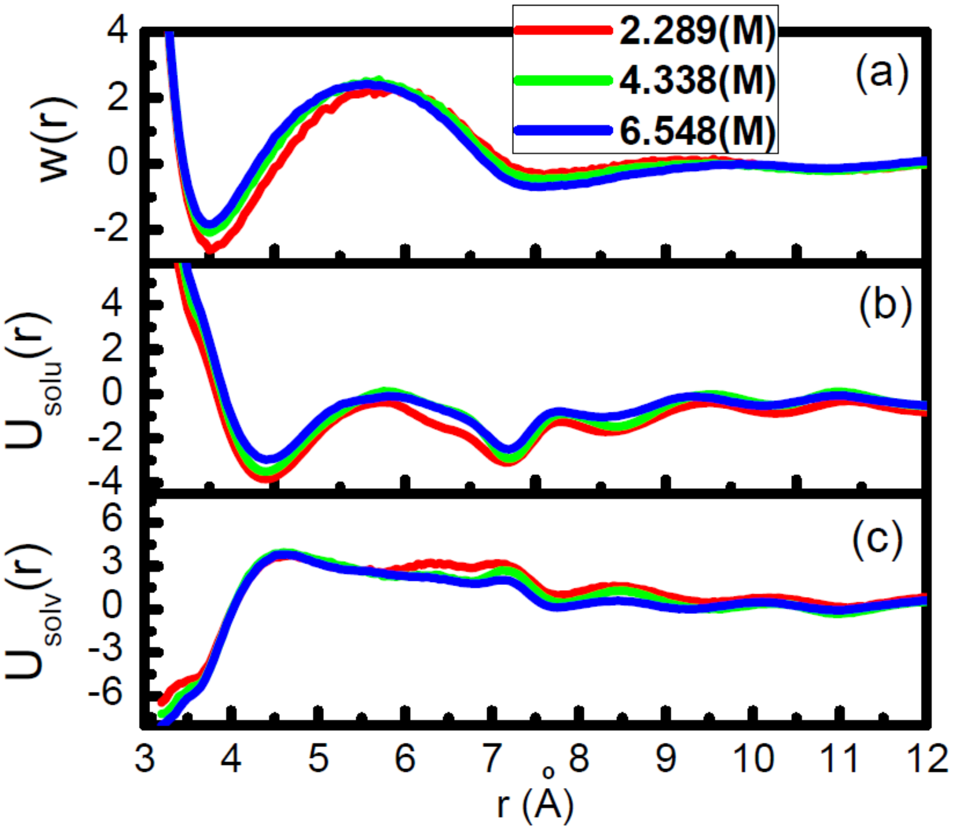

Figure 4.b.8. (a) Potential of mean force values (w(r)) among the guanidinium moieties at three different concentrations of GdmCl salts. (b) Direct solute−solute interaction $U_{solu}(r)$ as obtained from vacuum simulations of GdmCl at different concentrations. (c) Solvent-induced contribution, $w_{solv}(r)$, to the PMF at different GdmCl concentrations.

been obtained by subtracting $U_{solu}(r)$from$w(r)$ according to Eq. (4). These quantities are shown in Figure 4.b.8. It is interesting to observe that the first minimum of $U_{solu}(r)$ appears (see Figure4.b.8.(b)) at a larger distance than that of $w(r)$. Since in vacuum simulation there are no water molecules, two positively charged Gdm$^+$ moieties cannot come very close to each other. It therefore appears that the close stacking of Gdm$^+$ ions in the aqueous solution (see Figure 4.b.2.a or 4.b.7(a)) is stabilized by the presence of the water molecules. The contribution of the solvent to this stabilization is demonstrated by solvent contribution ($w_{solv}(r)$) to the PMF. From the plots of $w_{solv}(r)$ as shown in Figure4.b.8(c) it is evident that the solvent induced contribution is stabilizing (negative)the contact pair state. However not so much dependence of the concentrations of the Gdmcl was observed in the $w_{solv}(r)$.

It is important to note that Mandal et al.[307] misinterpreted the decrease in the peak height of the first peak of $g_{CC}(r)$ with Gdmcl concentration as decrease in the ion-pair formation. As denaturation occurs at sufficiently high Gdmcl concentration, therefore they ruled out the direct interaction mechanism. They subsequently demonstrated that indirect mechanism by breaking the water structure is responsible for guanidinium chloride's action as protein denaturant. In order to look into this aspect, in the following section we have presented results on the effect of Gdmcl concentration on water structure.

4.B.3.1.b: Effect of GdmCl Concentration on Water Structure

Although indirect evidences suggest that Guanidinium ion denatures protein by direct preferential interaction, existence of the indirect mechanism, which posits breakdown of water structure as a reason for chemical denaturation, cannot be ruled out unless effect of guanidinium chloride on the water structure is examined. Therefore, here we present the effect of increasing Gdmcl concentration on the local structure of water. Water is a three-dimensional hydrogen bonded network of tetrahedral structures. In order to assess the effect of Gdmcl concentration on water structure we have therefore looked into details of radial, tetrahedral and hydrogen bonding structures of water.

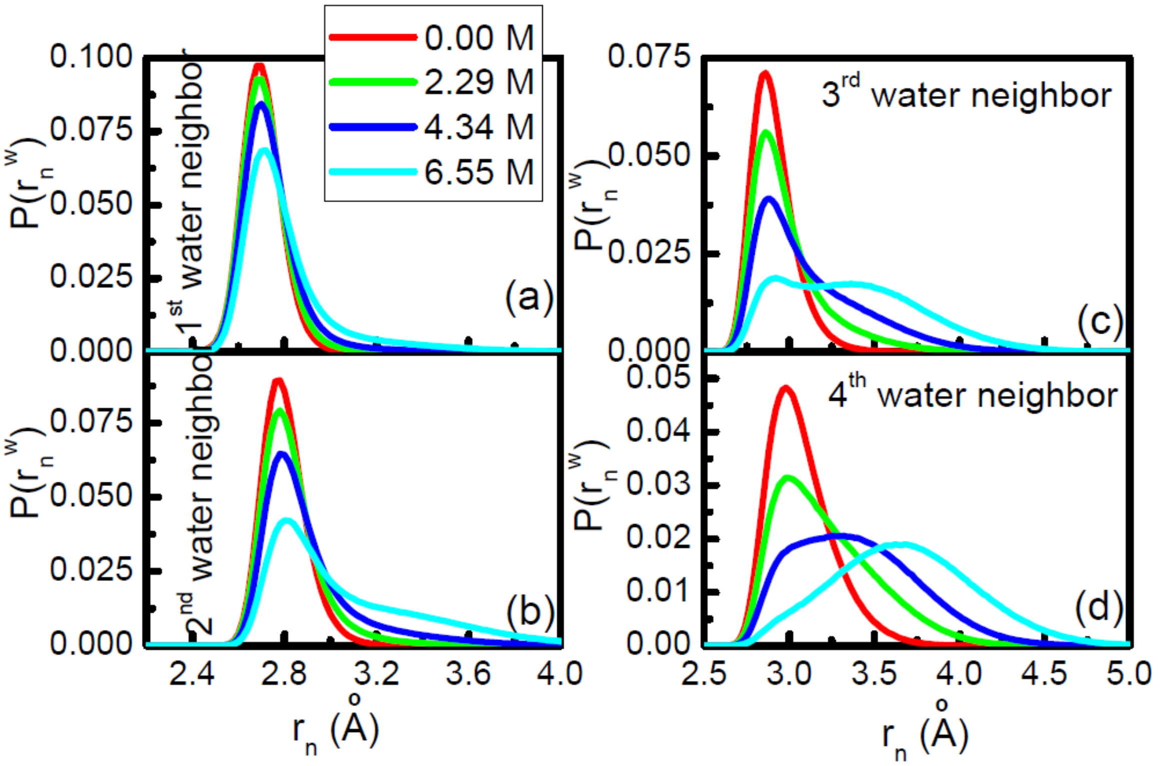

Figure 4.b.9.Distributions $P(r_n^w)$ of the distances r_n of the nth water neighbor from a reference water molecule for n=1-4 are shown in four different panels (a)-(d).

Radial Structure: One usual way of looking at the radial structure of a fluid is by looking into the radial distribution function (RDF). Although RDF gives average radial structure, detailed information about the radial structure can be obtained by following nearest neighbor Approach (see chapter-4a).In order to check whether structure of water changes with increasing concentration of Gdmcl, we have, therefore, calculated distribution of radial distances of the nearest neighbors. In case of bulk water, we know that there are on an average four water neighbors around a central water molecule. We have shown the distributions of first four “water neighbors” $P(r_n^W)$ with n=1-4 in Figure 8(a)-(d). It is seen that the distributions for the first and the second neighbors do not change considerably, whereas the same for third and fourth neighbors changes considerably with increasing Gdmcl concentration. This type of distortions in the radial distributions of neighbors is generally

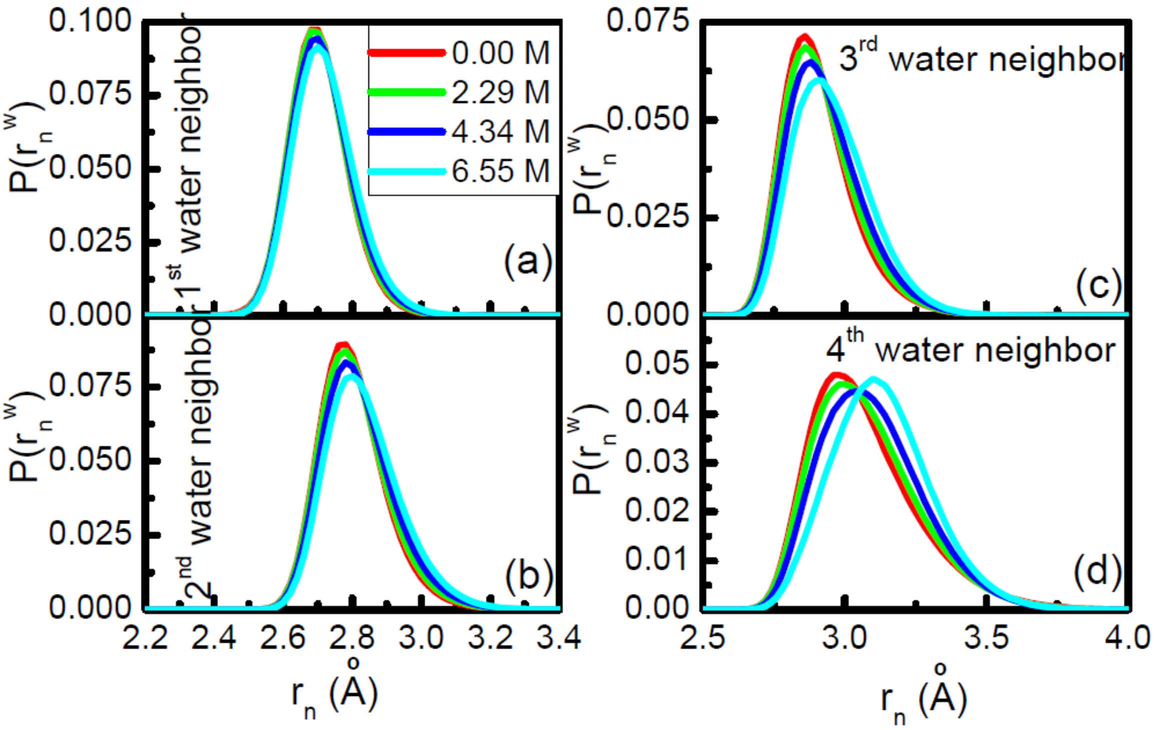

Figure 4.b.10.Same as in Figure 4.b.9 except that now in choosing neighbors, sites of Gdm$^+$, Cl$^-$ and water all species are considered.

attributed to the distortion in water structure. However, if we look at these distributions carefully, at higher concentrations and for third and fourth neighbors, distributions move outwards considerably beyond the average radius (around 3.5 Å) of the first solvation. Therefore, it is evident that at high Gdmcl concentrations a significant fraction of 3rd and 4th"water neighbors" goes out of the first solvation shell and probably other entities like Gdm$^+$ and Cl$^-$ ions enter into the first solvation shell of water [see inset of Fig 4.b.1 and

4.b.2.a As Gdmcl concentration increases numbers of Gdm^+ (Figure 4.b.2a inset) and Cl^- (Figure 4.b.3 inset) increase]. In the above case we have considered only water molecules in choosing first four neighbors. However, as we have found that in a concentrated Gdmcl solution, probability of occupying the 3rd and 4th neighboring positions of a central water molecule by another water molecule decreases, it is important to choose correct nearest neighbors considering all the other species also to be probable neighbors. Thus, the distortion observed in case of 3rd and 4th"water neighbors" at higher Gdmcl concentrations may be arising due the water molecules that are outside the first solvation shell (generally considered to be around 3.5 Å) of water. In order to correctly choose nearest neighbors, we have first chosen four neighbors distance wise considering all the species (O_W, Gdm^+,Cl^-) in the solution as probable neighbors and the same distributions of radial distances are now calculated by considering only those water molecules that are within the first four neighbors. These distributions are shown in Figure 4.10.(a)-(d). As expected, now we do not find any considerable distortion in any of these distributions. Therefore, although more and more water molecules are going out of the solvation shell, radial structure of those present within the first solvation shell are not disrupted with increasing concentration of the Gdmcl. In an earlier study we have demonstrated the same for concentrated urea solutions in chapter-4a.

Tetrahedral Structure: In a perfect tetrahedral network (as in ice) a central water molecule is surrounded by its four nearest neighbors sitting at the vertices of a tetrahedron forming the first solvation shell. One usual way of measuring tetrahedrallity of tetrahedrality coordinate fluid is to calculate average tetrahedral order parameter (cf. Eq. (2)) and corresponding distribution. Similar quantities have been used earlier in chapter 4a to gauge the tetrahedrality of urea-water solution. We have calculated average tetrahedral order parameter, $<q_4>$ in two different ways: by considering (i) distance-wise first four "water neighbors" (without considering other species in solution as probable neighbors) and (ii) n (≤ 4) water molecules which are within the (distance-wise) first four neighbors (considering Gdm$^+$, Cl$^-$ also to be probable neighbors of the central water molecule). As it is shown in Figure 4.b.11.a 4.b.11.b, when we consider only four "water neighbors" without considering the possibility of other species(Gdm$^+$, Cl$^-$) being the neighbors, average tetrahedral order parameter decreases significantly with increasing Gdmcl concentration (see red line in Figure 4.b.11.a and

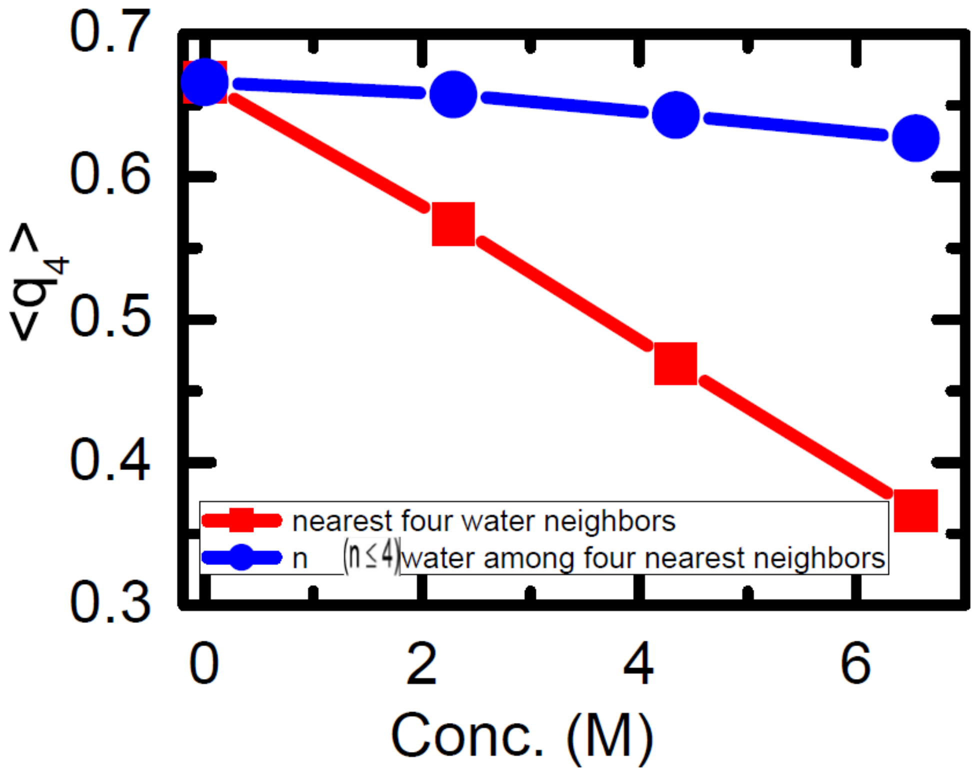

***Figure 4.b.11.a** Average tetrahedral order parameter <q_4>calculated by considering all the four water neighbors (no other species in solution is considered as a neighbor) of a reference water molecule as a function of molar concentration of Gdmcl (red line with diamond symbol) and the same calculated by considering all the species (Gdm$^+$, Cl$^-$ of Gdmcl and O_w of water)in solution as probable neighbours and choosing only those n (≤4) water molecules that are within the first four neighbors (Blue line with circles).*

4.b.11.b). This is understandable because as we have seen in Figure 4.b.9 that in this case, many of the 3rd and 4th "water neighbors" actually reside outside the first solvation shell. Therefore, if we consider these second shell water molecules in our $<q_4>$ calculation, since they are not in the vertices (in a concentrated solution some of the vertices are occupied by other species) of the tetrahedron, $<q_4>$ value will decrease. However, while choosing neighbors if we consider that other species such as Gdm^+ and Cl^- also as possible neighbors and choose distance-wise first four neighbors of a central water molecule, then in a concentrated Gdmcl solution, all the four neighbors will not be water (as some of water neighbors are now replaced by other species). Now for calculating $<q_4>$, if we consider only n (≤4) water neighbors that are within the first four neighbors, then $<q_4>$ value does not

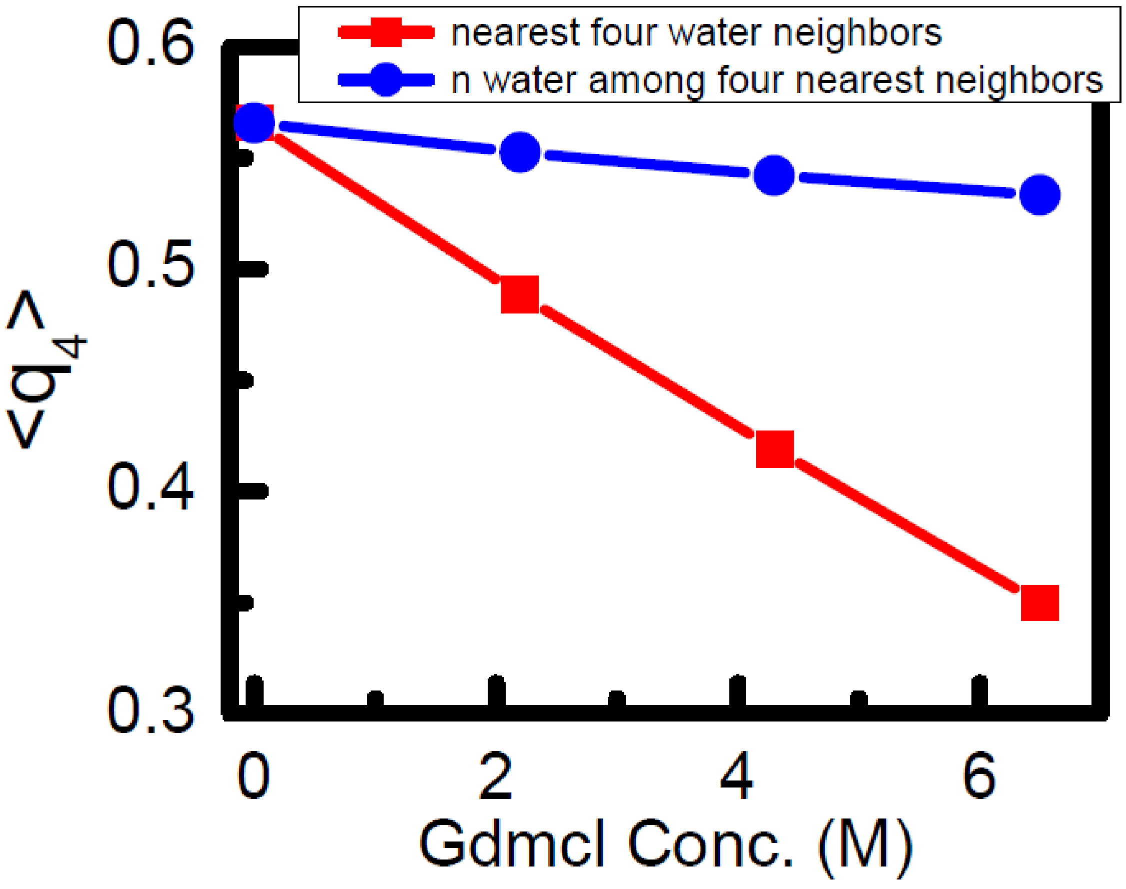

Figure4.b.11.b Same as in Figure 4.b.10.a for Tip3p water model.

significantly decrease with Gdmcl concentration (see blue line in Figure 4.b.11.a 4.b.11.b).In this case, when n<4, we have used proper normalization (see chapter-2 for details). So, the rapid decrease in $<q_4>$ as a function of Gdmcl concentration that has been observed earlier[51] should not be attributed to breaking of tetrahedral network of water but, on the contrary, it is due to selection of wrong water neighbours. Those water molecules residing in the second shell of a central water molecule contribute to the decrease in $<q_4>$. Since we are using TIP4P/2005 water model and Mandal et al.[307] used TIP3P model in their study, we have also calculated relevant structural quantities by using TIP3P water model. The results obtained from the TIP3P model also show similar trend as those obtained from the TIP4P/2005 water model. Even when we choose correct water neighbors, a slight decrease in $<q_4>$ is observed (see blue line in Figure 4.b.11.a and 4.b.11.b). Similar behaviour has been observed in case of aqueous solution of urea also in chapter 4a. The reason for this slight decrease in $<q_4>$ with concentration has been attributed to change in proportion of n-hydrogen bonded molecules (with *n=1,4*) in water as a function of solute concentration in chapter -4a.

Hydrogen Bonding Structure: As stated in the Model and Methods Section, hydrogen bonding angle (θ_{HB}) is the angle between the line joining oxygen atoms of the two neighboring water molecules and the O-H bond of any one of the two water molecules. In order to check how first 5 nearest neighbors are hydrogen bonded to the central water molecule, the distribution of θ_{HB}, $P(\theta_{HB}$) for first five "water neighbors" are shown in Figures 4.b.12(a)-(e). As earlier, in this case we have considered only water as neighbors (without considering Gdm and chloride ions as probable neighbors while choosing the neighbors). It is interesting to observe that the distribution does not change much for 1st and 2nd neighbors, but for 3rd and 4th neighbors(see Figures 4.b.12(c) and (d)), it changes significantly giving rise to a new peak at around 55-60° at higher Gdmcl concentration. It is interesting to observe that for the 5th nearest neighbor, the main peak is at 55-60°. In fact, we have calculated (not shown here) distributions for 6th, 7th and 8th neighboring molecules also and found that they all look like the 5th neighbor's distribution, indicating that the 55-60° peak is probably characteristic of second shell water molecules. It is also evident from the distributions of the pure water. For pure water (red curves) up to 4th nearest neighbors, there is no change in the peak positions. But for the 5th neighbor the distribution has the major peak

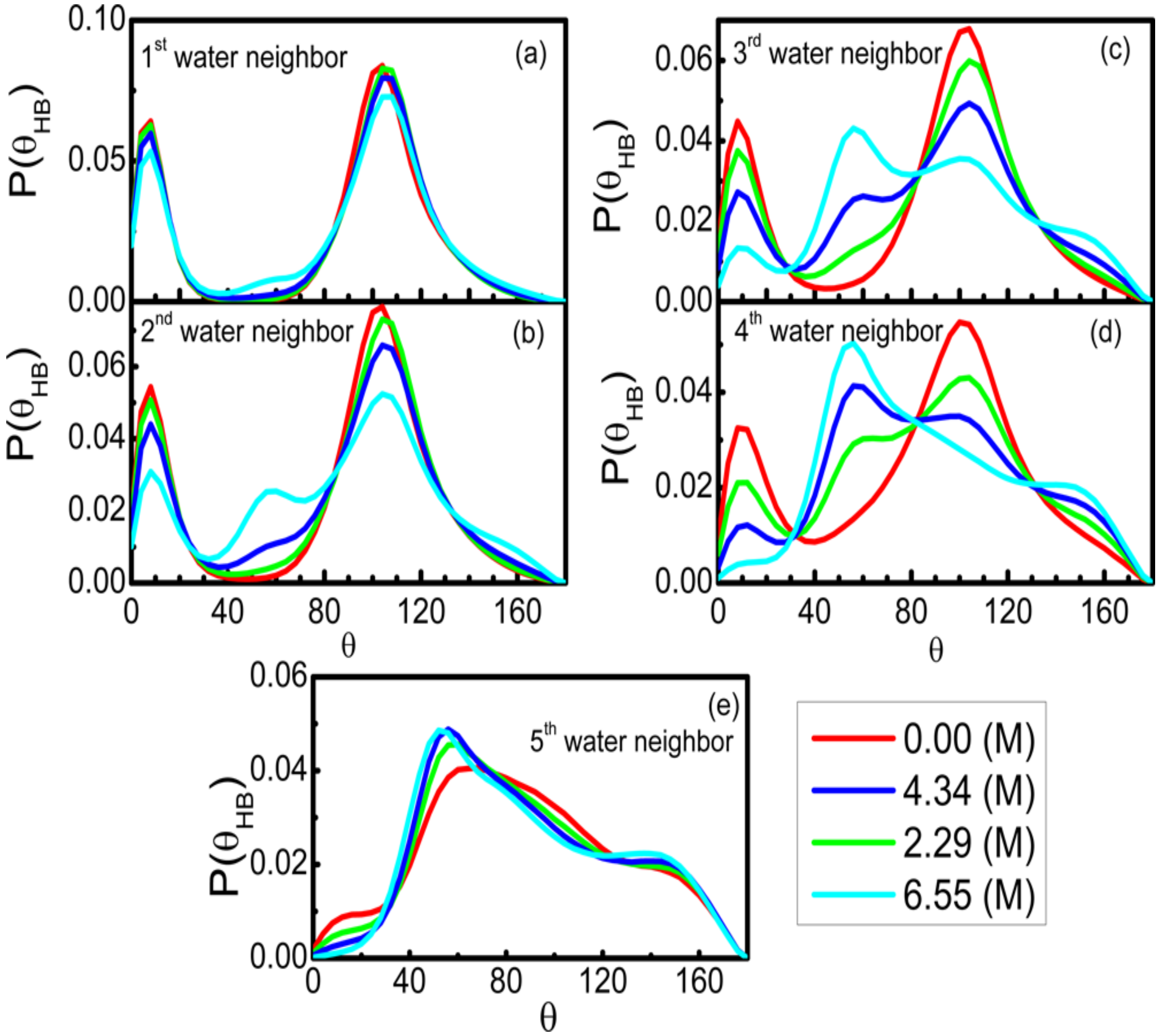

Figure 4.b.12.a. Distributions $P(\theta_{HB})$ of the hydrogen-bonding angle formed by a reference water molecule and one of its neighbors. Hydrogen bonding angle θ_{HB} is the angle formed by the line joining the two oxygen atoms and the OH bond vector. In panels (a)−(e) distributions for five nearest water neighbors are shown. In this case, species from GdmCl molecules are not considered to be a probable neighbor.

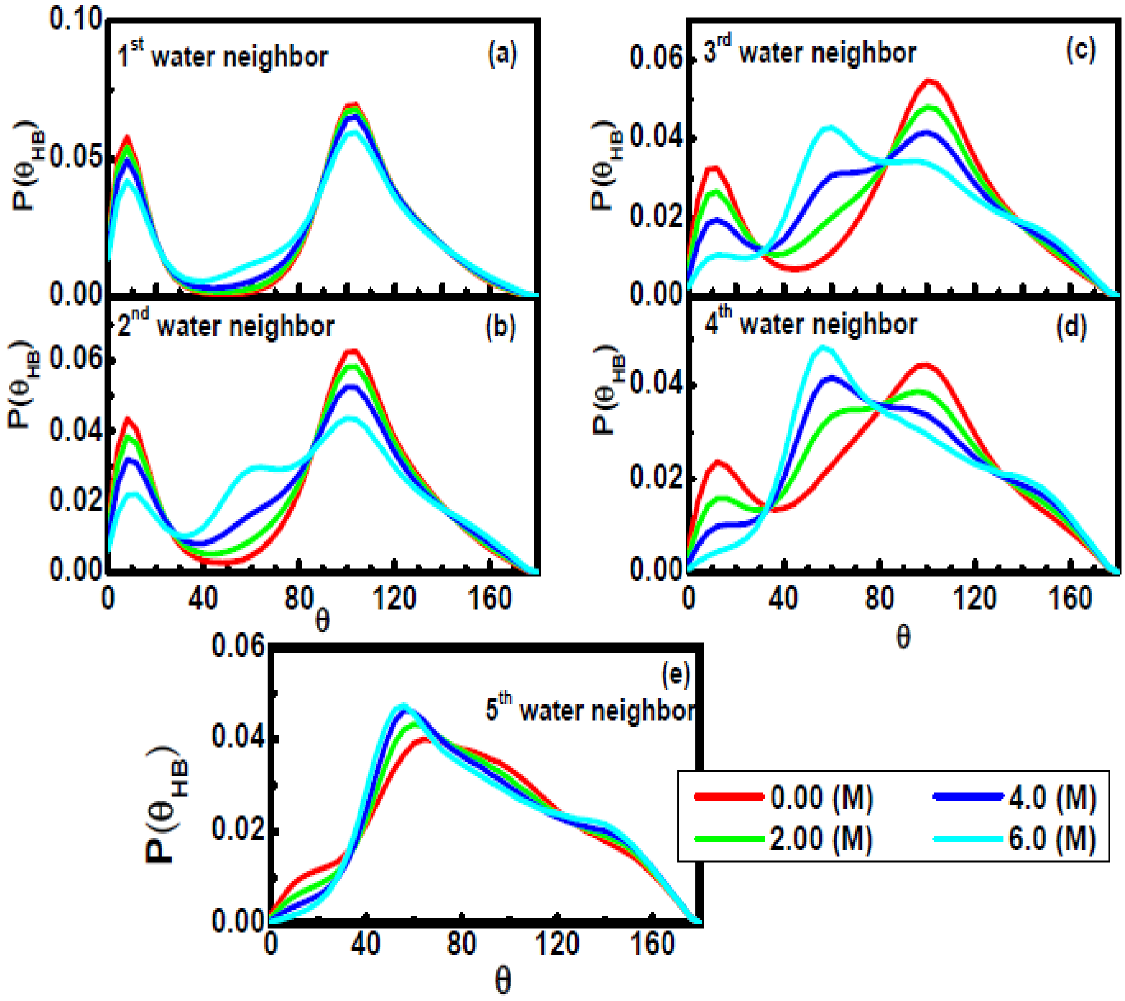

Figure4.b.12.b Same as in Figure 4.b.12.afor Tip3p water model

at 55-60°. The same trend has been observed from our simulations using TIP3P water model also. (see fig 4.b.12.b). However, from the HB distributions presented by Mondal et al.[307], who used TIP3P water model, it is seen that even in pure water (with no Gdmcl) the distribution of the fourth neighbor is different (in terms of positions of the peaks) from those of 1st, 2nd and 3rd neighbors and it is the same as that of the 5th neighbors (see Figure 4.b.8 of Mondal et al.[51]). However, it is very unlikely; as in pure water, in the first solvation shell of water molecule there are on an average 4 nearest neighbors. Therefore, all first four neighbors should behave in the same way. In our simulation with TIP3P, we however observed that all the four neighbors in pure water behave in the same way and this behavior is different from that of the fifth neighboring molecule.

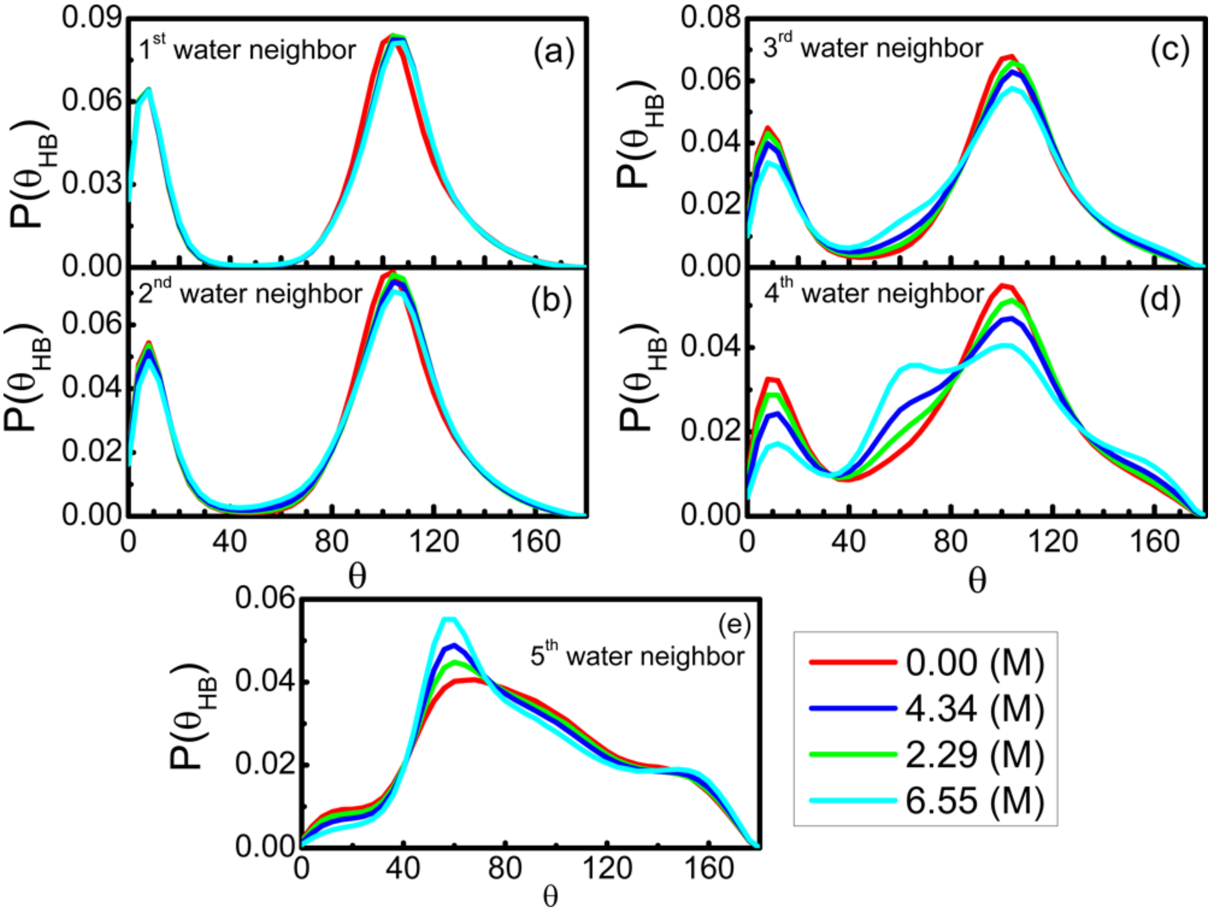

Figure 4.b.13.a.. Same as in Figure 4.b.11.a, except that now we choose five nearest neighbors irrespective of whether it is any species of GdmCl or water and then calculate the required hydrogen-bonding angle between the reference water molecule and the water neighbor, which is within the first five (distance-wise) neighbors.

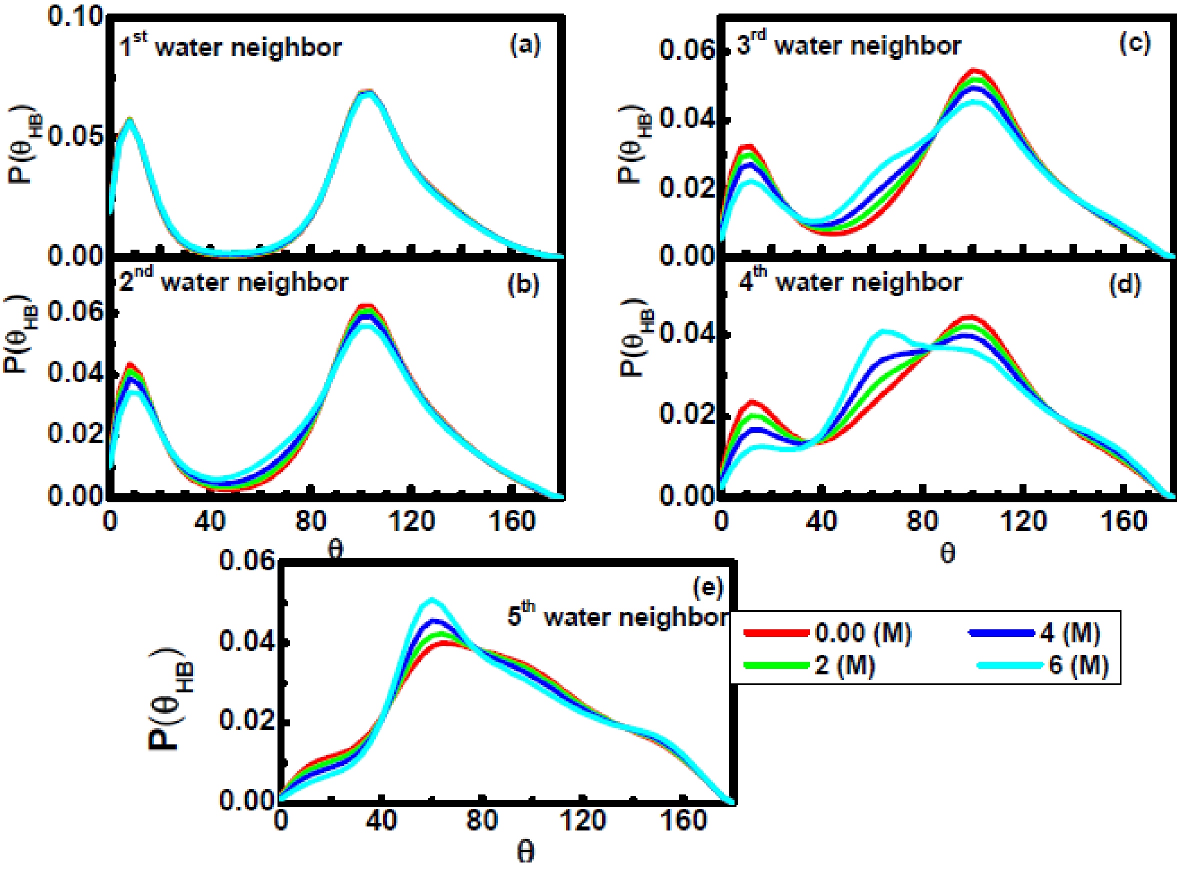

Figure4.b.13.b Same as in Figure 4.b.13.afor Tip3p water model.

The emergence of 55-60° for the 3rd and the 4th "water neighbors" (see Figures 4.b.12.a(c) and (d)), is probably because some of the water neighbors that we have assigned as 3rd and 4th neighbors are actually not within the first four nearest neighbors (not within first solvation shell) if we allow other species (Gdm^+ and Cl^-) also to be probable neighbors.As we have seen in case of tetrahedral order parameter calculation, if we now correctly choose neighbors by considering Gdm and chloride ions also to be probable neighbors, and consider only those water molecules that are within the first four neighbors, then the $P(\theta_{HB})$ distribution for the first three nearest neighbors are almost identical with almost no distortion (see Figures 4.b.13.a and 4.b.13.b) with increasing Gdmcl concentration. However, the distribution for the fourth neighbor still shows a small peak near 55-60°at higher Gdmcl concentration. Thus, it can be concluded that fourth neighbor may not be perfectly hydrogen-bonded to the central water molecule at higher Gdmcl concentrations.

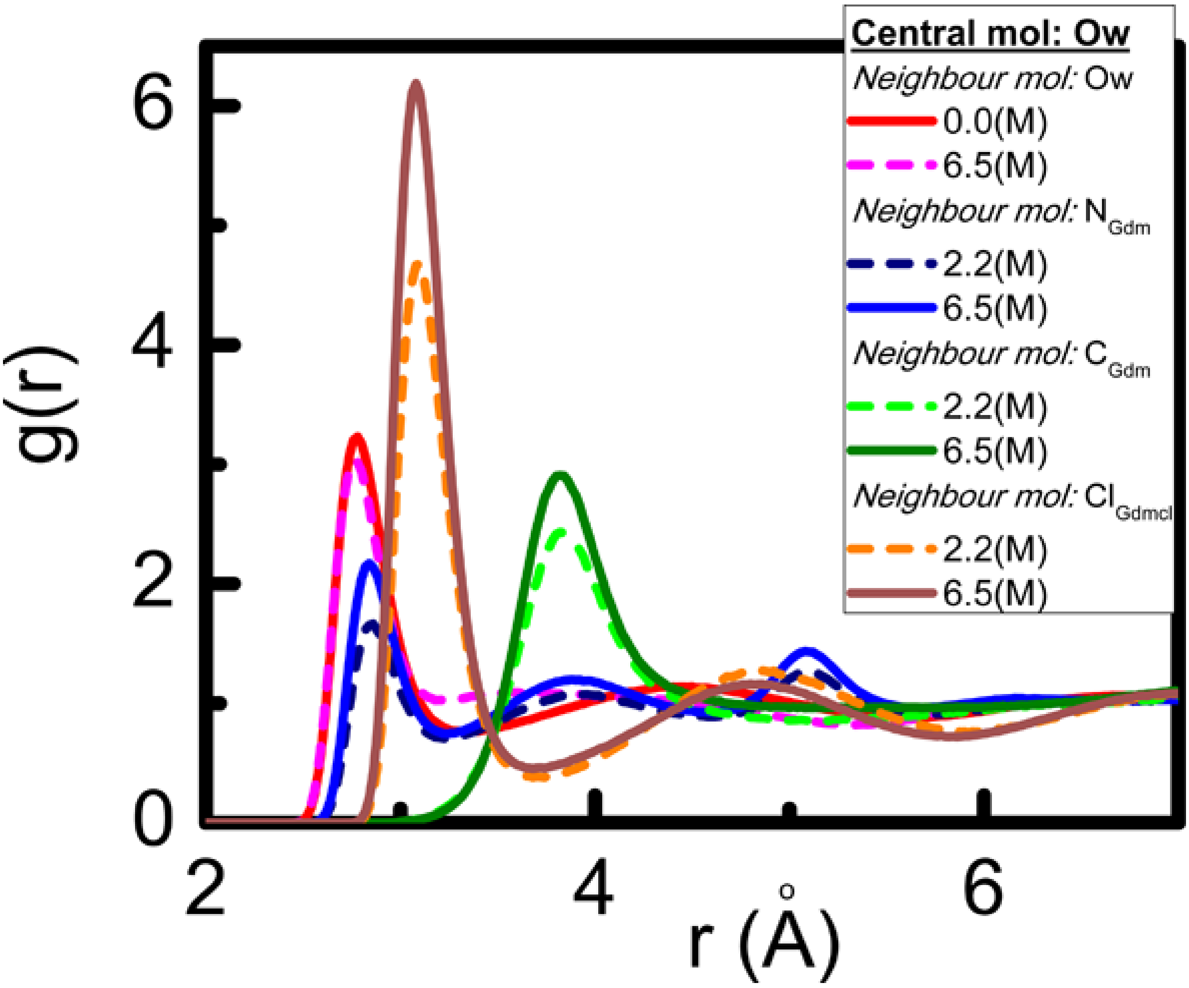

Figure 4.b.14. Radial distribution functions of O_w of water, nitrogen and carbon atoms of the guanidinium moiety and chloride ions around the O_w of water. Different color codes are described in the legend on the Figure.

In order to investigate further about the origin of the 55-60° peaks in the θ_{HB} distributions of 3rd and 4th neighbors at higher Gdmcl concentrations, we need to get idea about average relative positions of different species around a central water molecule. For that we have calculated related RDFs and these are shown in Figure 4.b.14 for two different (lowest and highest) Gdmcl concentrations considered here. It is interesting to observe that carbon atom of the Gdm$^+$(green curves) ion stays relatively far away from the central water oxygen in comparison to chloride ion, O_w of another water molecule and nitrogen atom of Gdm ion. The O_w of water and N of Gdm$^+$ are almost in the same position (see red and blue sets of curves). This is because both can form hydrogen bonds with the central water molecule. Chloride ions also stay in the first solvation shell of water probably because of strong ion-dipole interaction. As far as concentration dependence is concerned, there is not much change with respect to peak position in all the cases.

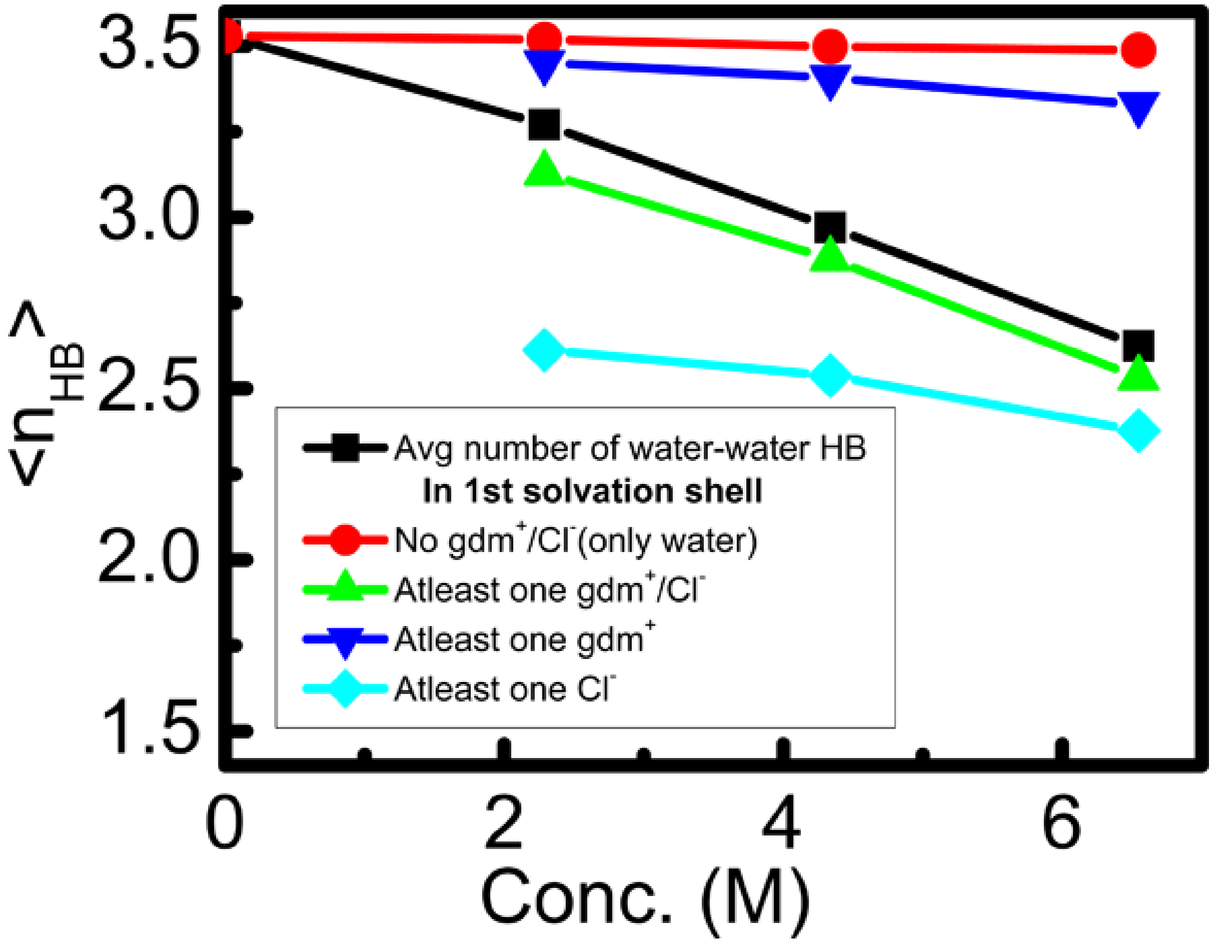

Figure 4.b.15. Average number of water−water hydrogen bonds ⟨n_{HB}⟩ as a function of concentration of GdmCl at different conditions (stated in the figure legend; also see the text).

As we have seen in Figure 4.b.13.a that other than O_w of neighboring water, chloride ion and nitrogen of Gdm$^+$ ion can also stay in the 1st solvation shell of a central water molecule, it is important to know how their presence in the first solvation shell influences average number of water-water hydrogen bonds. We have, therefore, calculated average number$<n_{HB}>$ of water-water hydrogen bonds as a function of guanidinium chloride concentration. The average number of water-water hydrogen bonds (see black line in Figure 4.b.15) steadily decreases with Gdmcl concentration. Therefore, it supports the result of Figure 4.b.13.a in which an additional peak (at around 55-60°) in the distribution of HB angles forthe 4thnearest neighbour appeared at higher Gdmcl concentration. Now, in order to get an idea about how this distortion in HB network originates, we have further calculated $<n_{HB}>$ by choosing water molecules with various restrictions. In one case, we have chosen all those water molecules that do not contain any Gdm^+ or Cl^- ions in their first solvation shells (i.e. all four nearest neighbours are water). In this case (see red line in Figure4.b.16) we have found negligible change in $<n_{HB}>$ as a function of Gdmcl concentration. However, if we consider only those water molecules with at least one Gdm^+ or Cl^- ions in their first solvation shell, we find (see green line) profound decrease in the average number of HB (almost the same as the black line). Now, if we choose only those water molecules with atleast one Gdm^+ ion(no Cl^-ions) in the first solvation shell, the decrease in $<n_{HB}>$ with Gdmcl concentration (see blue line) is not so drastic (much above the average black line). However, if at least one chloride ion is present in the first solvation shell, then $<n_{HB}>$ decreases more rapidly than the average value given by the black line. Therefore, the noticeable distortion in the HB network at high Gdmcl concentrations (see Figure 4.b.13(d) and black line in Figure 4.b.15) arises from the presence of the Cl^- ion in the first solvation shell of a water molecule.

Although we have shown by calculating average number of water-water HB that the presence of chloride ion in the first solvation shell induces distortion in the water-water HB network, whether appearance of the 55-60° peak in the distribution of θ_{HB} (as shown in Figures 4.b.12.a(d) and (e)) is related to the presence of chloride ion in the first solvation shell is yet to be ascertained. For that purpose, we have now calculated the distribution P(θ_{HB}) in three different ways by imposing three different conditions viz. considering only those water molecules that have (a) no Gdm$^+$/Cl$^-$ ions in the first solvation shell (i.e. all four neighbors are water) (b) no chloride ion (but Gdm$^+$ and O_w can be there) in the first solvation shell and (c) no Gdm$^+$ ions but at least one Cl$^-$ in the first solvation shell. As shown in Figure 4.b.16 (a) that if we choose condition (a), the two characteristic peaks of P(θ_{HB}) appears. It indicates that if a water molecule is surrounded by only water molecules in the first solvation

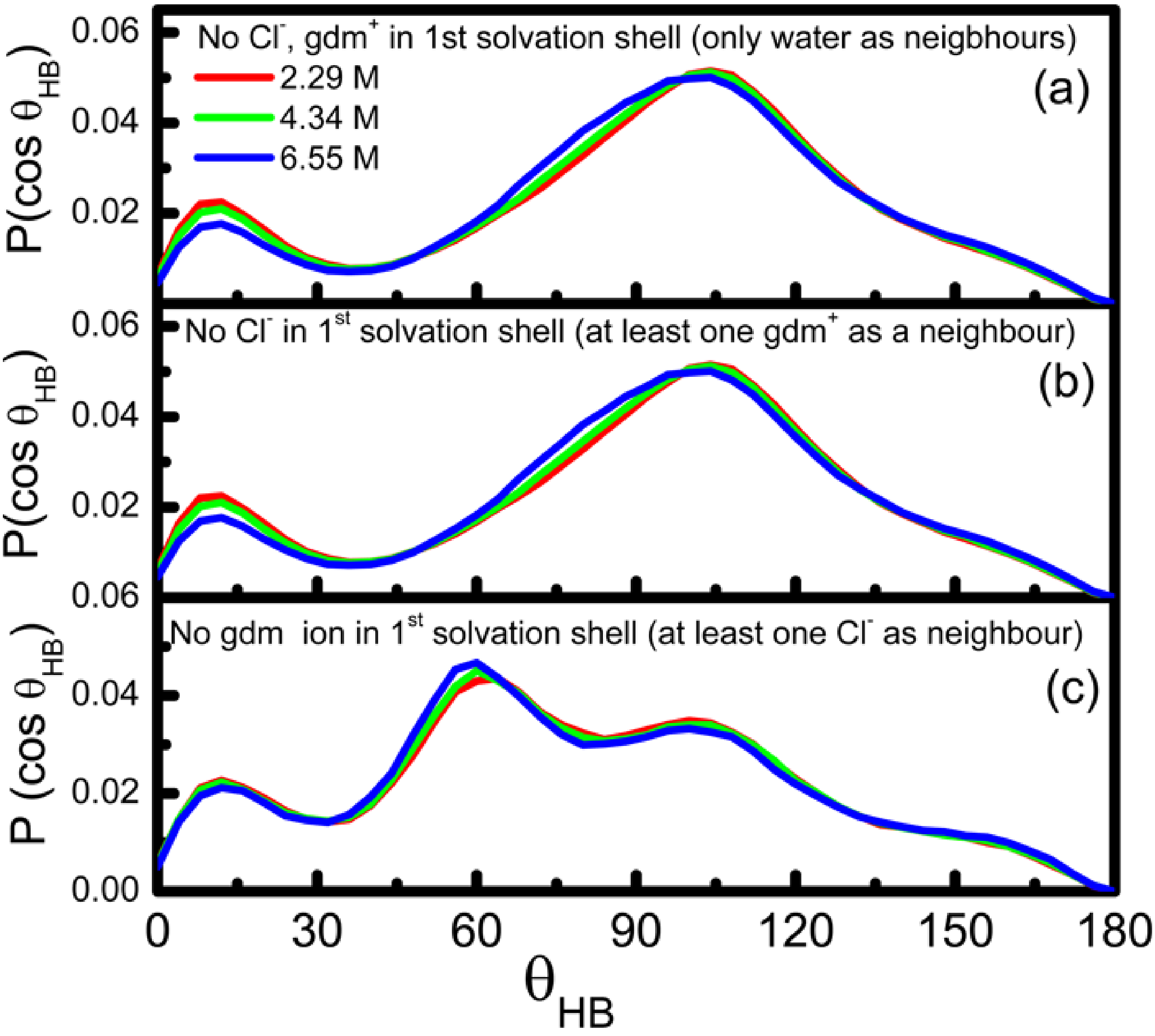

Figure 4.b.16 Distributions P(θ_{HB}) of the hydrogen-bonding angle calculated by imposing three different conditions (see figure legend and also see the text).

shell, no change in HB network. If we now consider condition (b) stated above, then also the characteristic shape of the P(θ_{HB}) distribution does not change considerably. However, if at least one chloride ion is present in the first solvation shell (condition (c) above), then a new peak at around 55-60° appears in the P(θ_{HB}) (see Figure 2.b.16(c)). Thus, it is confirmed that the new peak at 55-60° in Figure 2.b.13.(d) is due to presence of chloride ion in the first

4.B.3.1.c: An Arginine-rich Peptidein the Aqueous Solution of Gdmcl

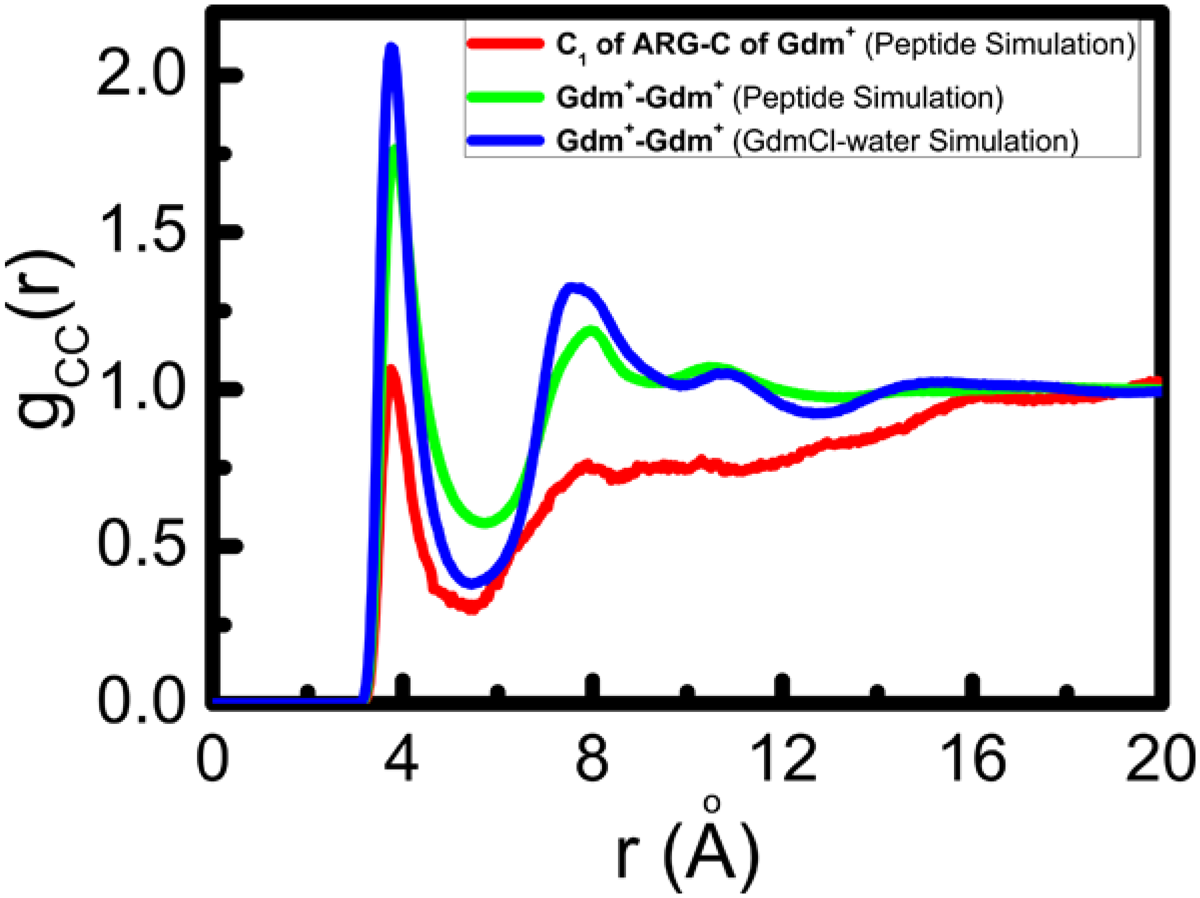

Figure 4.b.17. Radial distribution functions of the carbon atom of the Gdm$^+$ moiety of GdmCl around the C1 carbon atom (see Figure 1B) of the ARG side chain of the protein (red line) in protein−GdmCl−water system, carbon atom of the Gdm$^+$ moiety of GdmCl around the same of other GdmCl molecule in the protein−GdmCl−water system (green line), and carbon atom of the Gdm$^+$ moiety of GdmCl around the sameof other GdmCl molecules in the GdmCl−water (without protein)system (blue line).

solvation shell of water. It is to note that this 55-60° peak in the P(θ_{HB}) distribution can also appear if a water molecule chosen as a neighbor is actually in the second solvation shell of the central water molecule.

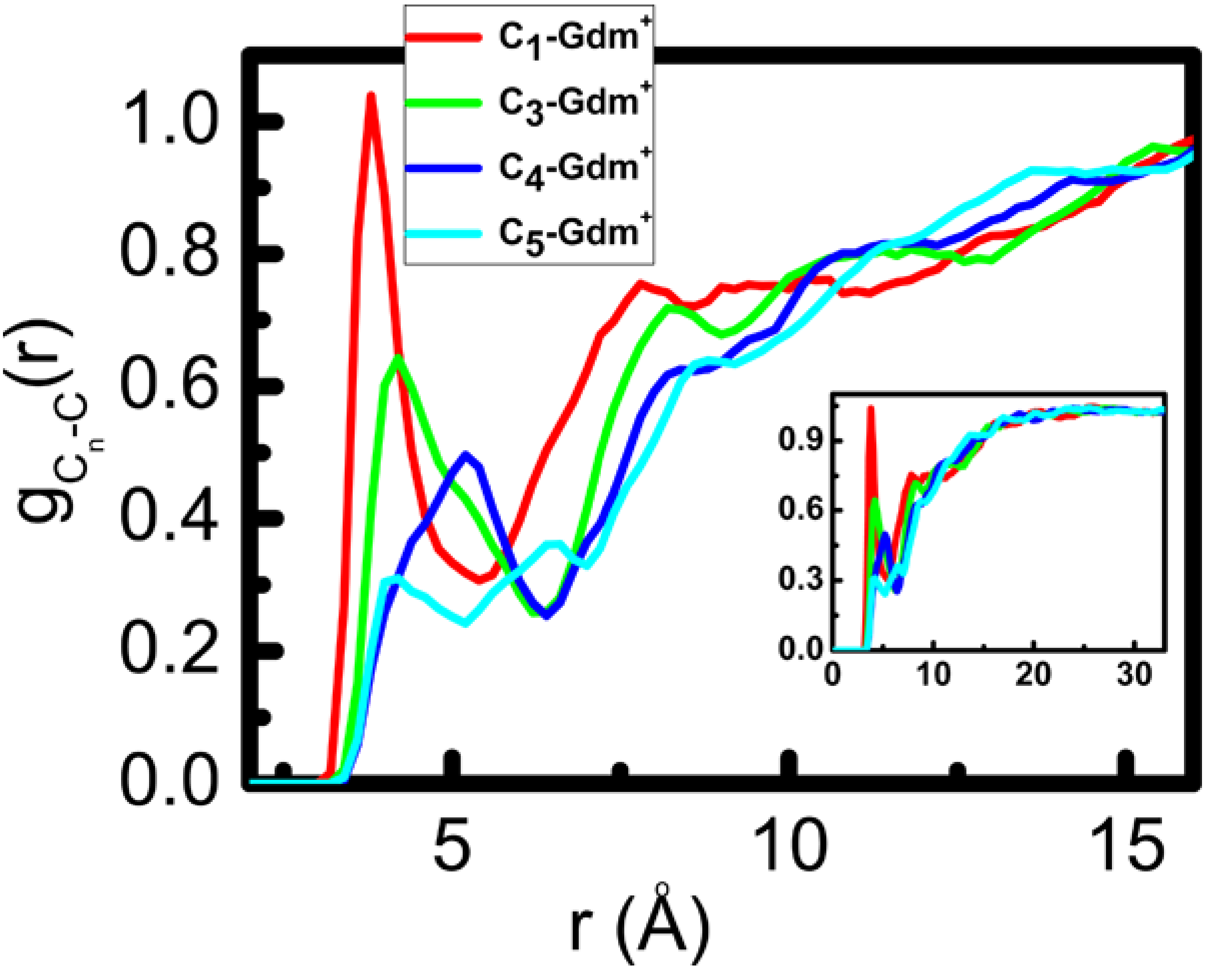

Figure 4.b.18. Radial distribution functions of the carbon atom of the Gdm$^+$ moiety of GdmCl around the C1 carbon atom of the ARG side chain (red line), C3 carbon atom of the ARG side chain of the protein (green line), C4 carbon atom of the ARG side chain of the protein (blue line),and C5 carbon atom of the ARG side chain of the protein (cyan line) in the protein−GdmCl−water system (see Figure 1B for ARG bal and stick model). In the inset, same plots with longer range are shown.

As already mentioned the aggregation of Gdm$^+$ ions and its parallel stacking can have implications in the mechanism of unfolding of an arginine-rich protein or peptide. The arginine (ARG) side chain of a protein peptide has a similar moiety as guanidinium ion (see the C1 carbon along with N2, N9, N10of ARG in Figure 4.b.1.B). Therefore, there is a possibility that the Gdm^+ moiety will attack the similar moiety of ARG and in this case also Gdm^+ will be stacked in parallel to the ARG moiety. As already stated, in order to check this hypothesis, we have simulated an arginine-rich peptide(PDB ID: 2MIA) in a 6 M Gdmcl solution. We have shown the results for ARG-Gdm^+ and Gdm^+-Gdm^+ radial distribution functions as obtained from the peptide simulation in Figure 4.b.17. In the same figure, we have also shown the Gdm^+-Gdm^+ RDF obtained from aqueous solution of Gdmcl (without peptide). The first peak of the g(r) in all these three cases is in the same position indicating ARG-Gdm^+ pair are forming similar aggregates as the Gdm^+-Gdm^+ aggregates in aqueous salt solution. In the peptide solution, the first peak of Gdm^+-Gdm^+ RDF is smaller than that of ARG-Gdm^+ RDF, indicating that most of the Gdm ions in the peptide solution are in the close vicinity of the peptide. This fact is further supported by the depletion region beyond the first solvation shell seen (see green curve in Figure 4.b.17) in the Gdm^+-Gdm^+ RDF of the peptide solution. Similar phenomenon have been observed in case of a small tetra-arginine peptide.[299]

The guanidinium moiety formed by the N2, C1, N9 and N10 atoms of the ARG is separated by three carbon atoms (C3, C4, and C5 (see Figure 4.b.1,B)) from the α carbon of the peptide main chain. In order to further pin-point that the Gdm^+ moiety of the Gdmclsalt comes close to the guanidinium moiety (C1 atom) of the ARG, we have further calculated the RDFs of Gdm^+ around different carbon atoms (C1, C3, C4, and C5 atoms) of the ARG side chain and are shown in Figure 4.b.18. As expected, the Gdm^+ ion of the salt comes closer to the C1 carbon atom of ARG as compared to other carbon center of ARG. The peak height in this case (around C1 atom) is also larger than that corresponding to other carbon centers.

Thus, it clearly indicates that Gdm$^+$ ion attacks the guanidinium moiety (C1 carbon center) of the ARG.

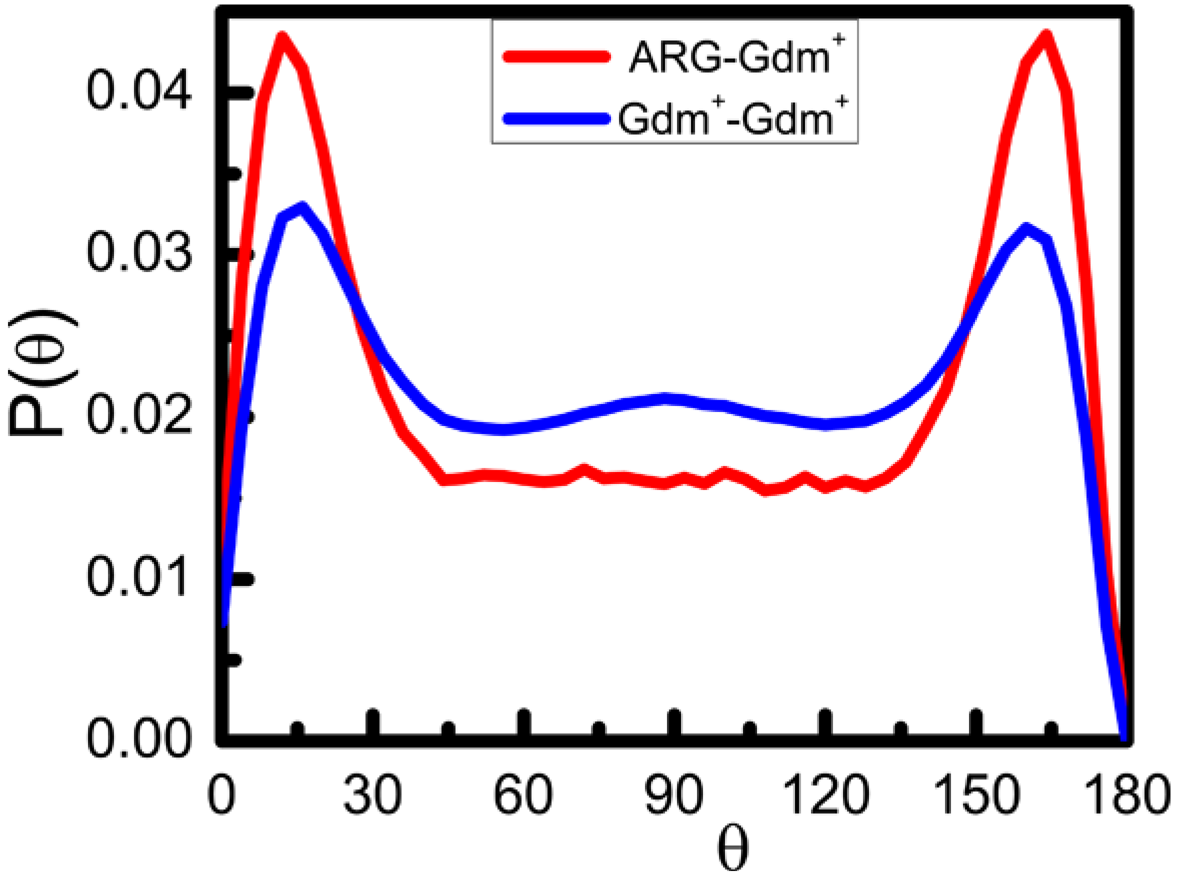

Figure 4.b.19. Distributions P(θ) of the angles θ made by the perpendiculars drawn from the molecular plane formed by carbon and three nitrogen atoms of Gdm$^+$ moiety in the GdmCl and the molecular plane of the guanidinium moiety formed by C1, N2, N9, and N10 atoms of the ARG side chain of the protein (see Figure 4.b.1B).

In order to further investigate the possibility of parallel stacking between the Gdm$^+$ and ARG moieties, we have calculated the probability distribution of the angle made by the Gdm$^+$ plane and the ARG plane (where ARG plane is defined by the C1-N2-N9-N10 (see Figure 4.b.1A) atom centers of ARG side chain). The calculated probability distributions for ARG-ARG and Gdm$^+$-Gdm$^+$ planes as obtained from the peptide simulation are shown in

Figure 4.b.19. In both the cases parallel orientations are observed. Thus it is demonstrated that the Gdm^+ moiety of the Gdm ion not only attacks the guanidinium moiety of the ARG side chain, but also forms a parallel stacking configuration with the same.

4.B.3.2: Effect of Gdmcl Concentration on Translational Dynamics of Water

Translational diffusivities of the different species in solution can be calculated from the respective mean squared displacements (MSD) using Einstein relation viz.,

$$D = \frac{1}{2d} \lim_{t\to\infty} \frac{\langle \Delta r^2 \rangle}{\Delta t} = \frac{1}{2d} \lim_{t\to\infty} \frac{\langle |\mathbf{r}(t) - \mathbf{r}(0)|^2 \rangle}{\Delta t}, \qquad (4.b.5)$$

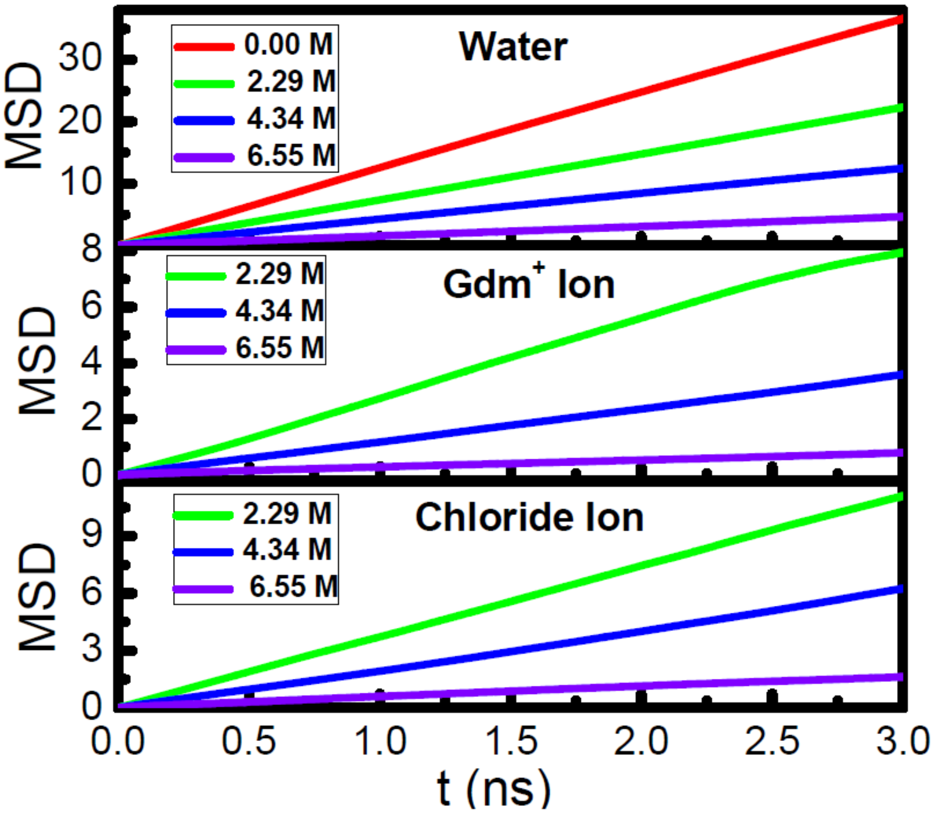

Figure 4.b.20. Mean squared displacements of water, Gdm+ ions and Chloride ions in the Gdmcl-water solutions of different concentrations.

where$<\Delta r^2>$ is the mean squared displacements averaged over number of particles and time origins. In the above equation, **r**(t) is the position vector at time t and d is the dimensionality of the system. The MSD of water, Gdm+ ions and chloride ions at three different concentrations are displayed in Figure 4.b.20. The MSD decreases with increasing concentration of Gdmcl for all the species including water in the solution. The diffusivity values calculated from the slope of the MSD plots at different concentrations for the three different species are shown in Table 4.b.2. The pure water diffusion coefficient is calculated to be 2.04 $\times 10^{-5}$ cm^2/s and a similar value has been obtained earlier.[52]Diffusivity values for all the species decrease considerably with increasing Gdmcl concentration (see Table 4.b.2).

Table 4.b.2:

System	**Conc. (M)**	**D (Water)** (10^{-5} **cm^2/s**)	**D (Gdm$^+$)** (10^{-5} **cm^2/s**)	**D (Cl$^-$)** (10^{-5} **cm^2/s**)
1G	0.00	2.040 ± 0.147		
2G	2.29	1.259 ± 0.035	0.396 ± 0.158	0.595± 0.065
3G	4.34	0.683± 0.019	0.202± 0.007	0.370 ± 0.044
4G-1	6.55	0.257± 0.002	0.046 ± 0.010	0.087±0.001

4.B.4: Summary and Conclusions

In order to elucidate the effect of Gdmcl concentration on the extent of like-charge Gdm$^+$-Gdm$^+$ ion pair formation and on the local structure of water, we have performed molecular dynamics simulations of aqueous Gdmcl solutions of different concentrations ranging from 0 M to 6.50 M. The analyses of carbon-carbon (of Gdm moiety) radial distribution function reveal the like-charge ion pairing with a clear existence of contact-pair and solvent-separated states. It is stated[295,297] that the driving force behind this type of like-charge ion-pair formation arises due to collapse of weakly hydrated planar Gdm$^+$ moieties.

As the concentration of Gdmcl increases, although the height of the first peak decreases and that of the second peak of $g_{CC}(r)$ increases, actual numbers of Gdm^+ ions in both the contact-pair and solvent-separated states increase. Since the individual $g_{CC}(r)$ profile is normalized with respective bulk concentration, the peak height in RDF actually signifies the relative density of the species at the peak position as compared to bulk (away from the centre) density. Thus, although peak heights of $g_{CC}(r)$ decreases with increase in concentration, the absolute number of Gdm^+ ions in both the contact and solvent separated states increase with increasing concentration of the Gdmcl solution (see inset of Figure 4.b.1). The position of the first peak in the $g_{CC}(r)$ (see Figure 4.b.2) at 3.7 Å excludes side-wise association and indicates possible parallel stacking of the Gdm^+ moieties. Indeed, appearance of two peaks at around 0° and 180° in the distribution of angle between two Gdm planes (as shown in Figure 4.b.6) corroborates parallel stacking of the Gdm^+ moieties.

Existence of such like-charge ion pair stacking in its aqueous solution has two faceted implications. As Gdmcl at sufficiently high concentration denatures proteins, the like-charge ion-pair formation indicates the tendency of the Gdm^+ moieties to stack against the structurally similar arginine moieties in proteins. In order to test this hypothesis we have simulated an arginine-rich peptide in an aqueous solution of 6 M Gdmcl. The analyses of the results clearly demonstrate that Gdm^+ ions stack against ARG side chain of the peptide. In fact, Gdm^+ ion attacks the Guanidinium moiety of the ARG and it is also shown that the stacking is in parallel orientation. Thus, it supports a direct mechanism of chemical denaturation of a protein by guanidinium chloride. In fact, many other studies[223,235,249,305,306] have advocated direct preferential interaction mechanism of protein denaturation by Gdmcl. On the other hand, the like-charge ion association in aqueous solution also signifies that due to this affinity, during protein folding, arginine and other similar moieties will come close to each other. In fact, from the structural analyses of proteins it has been observed that arginine and other similar group stack together and the orientation of the guanidinium group of arginine is parallel to the side chains of aromatic amino acid residues.[287,312,313]The temperature dependence of the distribution of orientation angles between two Gdm^+ molecular planes shows decreasing orientational preferences with increasing temperature, and it is consistent with the temperature induced denaturation of proteins.

As already stated, apart from direct mechanism, indirect effect of breaking water structure by the Gdmcl at higher concentrations has also been suggested[12,223,235,249,248,264,304-308] by many researchers. The results presented in the previous section highlighted the effect of presence of Gdmcl at higher concentrations on the radial, tetrahedral and hydrogen bonding structure of water. It is shown that if nearest neighbors are chosen properly by allowing Gdm^+ and Cl^- ions also to be possible neighbors (other than water molecules) of a central water molecule, radial and tetrahedral structures remain intact even at as high as a concentration of 6.55 M of Gdmcl. In an earlier study we have demonstrated the same for aqueous solution of urea as well in chapter-4a.However, in case of hydrogen bonding structure, it is surprising to notice that at high enough Gdmcl concentration, the distributions of hydrogen bonding angles made by 3rd and 4th neighbors to the central molecules get distorted. Also the average number of hydrogen bonds decreases steadily with increasing concentration. But in case of another denaturant urea, it is shown in chapter 4a that even hydrogen bonding structure of urea is not broken at as high concentration as 9M. Further analyses show (Figures 4.b.14 and 4.b.15) that the decrease in average number of HB and the uncharacteristic peak at θ_{HB}=55-60° in the distribution of θ_{HB} (as seen in Figure 4.b.13.a) arise due to presence of chloride ion in the solvation shell of the water.

As mentioned in the beginning of this Chapter that the behaviour of interfacial water depends on the length scale of the interface. Manifestation of various properties of water at a nanoscopic or larger interface formed by water and a nanoscopic or large surface is dramatically different from the same at the molecular level interface. It has a huge significance in terms of bio-macromolecular stability and protein folding if the interface is made up of nanoscopic or larger hydrophobic objects and water. In fact, for a nanoscopic or larger hydrophobic solute in water, a new interaction, the so called hydrophobic interaction originates and it is thought that the hydrophobic interaction is responsible for self-assembly and aggregation/folding of many bio-macromolecules**.**[19,30] However, measuring hydrophobicity of such a nanoscopic interface using the conventional method of measuring contact angle is rather difficult and therefore defining new order parameters to estimate hydrophobicity at the nanoscale is essential. Therefore, in the next Chapter characterization of hydrophobicity at the nanoscale will be discussed.

Chapter 5

Characterizing Hydrophobicity at the Nanoscale

5.1: Introduction

Hydrophobicity[314, 315] is considered as one of the most sought-after concept that provides rationale for apparently confusing phenomenon of assembly of hydrophobic groups in water and demixing of oil and water. Proximity of water to a hydrophobic surface dictates[316] its behavior and is thus fundamental to the so-called hydrophobic effect. Although its reason as well as definition is disputed, its importance in a variety of fields ranging from chemistry, biology, material science, and chemical engineering is beyond doubts.

The concept of hydrophobicity[314,315,113,114] has long been used to explain many natural and synthetic phenomena and processes such as dissolution of inert gases in water, protein folding, colloidal stability, micelle formation, nano particle aggregation, etc. At the macroscopic level, degree of hydrophobicity is generally assessed by measuring droplet contact angle.[115] In this conventional view, hydrophobicity is often characterized by an obtuse contact angle of water on a surface. In other words, water on a hydrophobic surface forms droplets in the form of beads, whereas it spreads on a hydrophilic surface. However, this view becomes obscure and sometimes ambiguous or untenable when translated into the molecular or even macromolecular domains. It is therefore a challenge[116, 117] to define an unambiguous descriptor of hydrophobic solute water interface at the nanoscopic length scales such as those involving proteins, micelles, nanoparticles, nanotubes, etc., where defining a droplet is not possible. Sensitivity of hydrophobicity to solute-water dispersion interaction[30,118,317 –319] and topography[29,216,320] poses additional challenge to define it.

It is well known that in smaller lengthscales[321–325] involving dissolution of inert gases in water, although molecular density distribution of water around the solute is quite high as compared to the bulk, a simple hard sphere modelcaptures[321, 324] hydration thermodynamics and the effects of temperature,[326,327] pressure,[328] and added salt[329–331] quite successfully. At larger length scale, however, water density distribution changes significantly from its molecular counterpart and generally for hard sphere model or purely repulsive model of the nanoscopic solutes, water recedes[332, 323] from the solute surface, forming a thin vapor layer around the surface. When two such macroscopic hydrophobic surfaces approach each other, below a critical distance cumulative effect of the fluctuations[334] of the individual surfaces leads to dewetting[19,333] of the intersolute region and this intersolute dewetting is thought[19] to be the origin of hydrophobic interaction that leads to self-assembly of hydrophobic groups as observed in the core of a protein or a micelle. At the nanoscopic and larger length scales, theory[333, 335] and many simulations[30,214,215,218,317,318, 336–455] have captured this picture. It was also demonstrated[446] that hydration free energy of a hydrophobic solute scales with volume at small length scales and with surface area at larger length scales and the crossover between the two occurs at the nanometer length scale.

Apart from thermodynamic conditions, behavior of hydrophobic hydration and interfacial water dynamics are also dependent on solute-water dispersion interaction. It has been thoroughly demonstrated[30,217,218, 338, 339, 347] how dispersion interaction changes hydration behavior as well as thermodynamics Several recent studies[29, 216, 284,342] have shown that surface topography has so significant influence on the hydration behavior that only by controlling the topography of the solute surface, one can create dry, wet, or oscillatory (with time) wet-dry state of the intersolute region. Therefore, understanding hydrophobicity has been a challenge of multidimensional nature in the space of parameters such as thermodynamic conditions, length scale, solute-water dispersion interaction, solute topography, etc.[348, 349]Recent studies[350] have analyzed contributions of these different parameters on the manifestation of hydrophobicity by separating geometry or topography from chemistry that determines hydrophobic/hydrophilic nature of an engineered protein surface. It has also been shown[351] that surface hydrophobicity can be enhanced by suitably coupling polarity of the surface with its topography. As far as understanding the molecular mechanism of protein folding is concerned, two limiting views have so far emerged.[350, 352] In one case, the traditional view is that the density of water is gradually reduced in the intersolute region in a manner concerted with their spatial approach toward each other. Thus water evacuation here is a gradual process. In the alternative scenario, due to thermodynamic instability, expulsion of all the water from the intervening space between large hydrophobic domains leads to cavitation and then follows the so-called hydrophobic collapse.[19,333, 336] In the later case, the process of self-assembly is a two steps process. Recent discussion and analyses as summarized from available protein folding studies however suggest[352] that the two step cavitation pathway is not the actual pathway in most of the cases, rather water has involvement in almost all the stages of the folding landscape. On the other hand, cavitation may play an important role in experimentally observed[353–355] long-ranged attraction between two hydrophobic surfaces when they are put into water. However, the range of attraction as observed in these experiments is much more than what most of the theoretical[333] and computational[318] studies have predicted on the basis of even idealized hard body model.

Recent studies of Berne and co-workers with BphC,[347]melittin tetramer,[320] and many other proteins[343] in water have clearly demonstrated how sensitive is this dewetting or cavitation to the nature of protein surface in terms of geometry, chemistry, and presence of specific residue. In case of BphC, no cavitation was observed in the interdomain region where water can sterically access the region. However, by turning off the electrostatic interactions between the protein and the water, dewetting did result. On the other hand, for melittin tetramer cavitation was observed even with usual electrostatic interactions, but it disappeared by altering the geometry through specific mutations. Actually this mutation altered the surface topography by removing protruding hydrophobic side chains. All these studies have pointed out the subtleness of defining hydrophobicity at the nanoscale.

One convenient way of predicting hydrophobicity from molecular dynamics simulation is through calculation of(molecular level) local density of water as calculated by averaging over all the relevant configurations. A fundamental question arises in this case that whether such an averaged out picture of the local density can provide a true and quantitative measure of hydrophobicity of a realistic surface. Given the fact that microscopic fluctuations are inherent[30] to such a hydrophobic interface, characterization of hydrophobic solute-water interface in terms of local density, which cannot capture these fluctuations, is not enough. Very recently Chandler and co-workers[356, 357] and Garde and co-worker[358, 348] have addressed this issue nicely and have come up[116, 117] with some descriptors based on water density fluctuations to characterize hydrophobic, nanoscopic solute-water interfaces. The newly developed approach of Chandler and co-workers[356,357] for capturing water density fluctuations near an interface has demonstrated that water near an extended hydrophobic surface are sitting "on the edge" of the liquid-vapor phase transition. Garde and co-workers have demonstrated[117] that local density description is ambiguous in many cases, and free energy of hydration of small solutes near the surface, position dependent as well as average solvation shell compressibility and solvent induced solute-water potential of mean force (PMF) can be used to characterize a hydrophobic solute-water interface.

In the present investigation, we extend this idea by examining suitability of these already developed order parameters and proposing many other descriptors such as hydrogen bond distribution, orientational orders of the water molecules in the second shell of a central molecule, distributions of various orientational vectors of the water molecule with respect to the solute plate, tetrahedrality parameter, fraction of hydrogen bonded neighbor of a solvation shell water, etc. to characterize hydrophobic solute-water interfaces. All these new as well as already developed[117,348] descriptors have been tested in the present investigation to characterize a simple, model, nanoscopic, planar, and hydrophobic solute-water interface. In the present investigation, instead of considering more realistic hydrophobic plates[344, 345] the planar plates are constructed by arranging five paraffin molecules side by side. Plates with varying hydrophobicity have been created just by varying the affinity of these molecule for water through the modification of the dispersion interaction between the water oxygen and surface carbon atoms. Our main aim here is to examine how the existing as well as new descriptors respond to the change in the degree of hydrophobicity as achieved by tuning only the van der Waals interaction between water oxygen and the carbon atoms of the solute plate.

Generally, a nanoscopic or larger hydrophobic solute dewets its immediate vicinity at the Angstrom lengthscale. But when two such hydrophobic solutes are immersed in water, as already mentioned, at a certain critical intersolute distance dewetting induced collapse of the two solutes occurs. This is one of the most sought-after[19,332,333,] plausible pathways for protein folding. In the present investigation, we have therefore investigated whether interplate dewetting exists between any such pair of plates. We found dewetting in almost all the cases, but critical distance for dewetting depends on the degree of hydrophobicity. In what follows, we describe simulation model and method along with a brief description for various analyses in Sec. 5.2. Results and discussions have been presented in Sec. 5.3 and a few concluding remarks in Sec. 5.4.

5.2: Models and methods

We consider a planar model of solute consisting of paraffin-like molecules by placing a number of *n*-$C_{18}H_{38}$molecules arranged in parallel in such a way that all the carbon atoms are lying on the same plane. For the alkane molecule, the united atom OPLS (OPLSUA) force field[58] has been used. In this description, both CH_3 and CH_2 groups are modelled as uncharged spherical sites with Lennard-Jones (LJ) interactions, with no explicit consideration of the hydrogen atoms. The LJ parameters for the CH_3 group according to the OPLSUA force-field are $\sigma_{CH_3-CH_3}$ =3.905 Å and $\in_{CH_3-CH_3}$= 0.7322 kJ/mol and those for CH_2 group are $\sigma_{CH_2-CH_2}$ =3.905 Å and $\in_{CH_2-CH_2}$=0.4937 kJ/mol. In order to prepare various plates of different degree of hydrophobicity, we have varied $\in$values through a parameter λ such that site site interaction between CH_3 or CH_2 group and water oxygen follows

$$u(r) = 4 \in \left[\left(\frac{\sigma}{r}\right)^{12} - \lambda\left(\frac{\sigma}{r}\right)^{6}\right] \qquad (5.1)$$

where λ = 1 corresponds to the original OPLSUA parameters. We have used a paraffin-like plate of roughly the dimension (center to center distance) of 20 Å × 21 Å. Water has been modeled by the standard SPC/E (Ref. 51) potential in which there are one LJ center and three charge centers coinciding with the three atoms of the water molecule. For solute water interaction, the cross parameters for the LJ potential were obtained from the Lorentz-Berthelot mixing rule. One solute plate was placed in the middle of a water box with the plane of the plate parallel to the *xy*-plane of the box. All the water molecules from the immediate vicinity of the plate were removed followed by a steepest decent minimization.

The simulations were performed in isothermal isobaric ensemble with molecular dynamics extended system approach of Nose and Anderson.[10] Periodic boundary conditions were applied in all three directions and Ewald method was applied to compute electrostatic interactions among all the water molecules. The bonds and the angle of the water molecule were constrained by using RATLE algorithm.[10]The solute plates were kept rigid and fixed during the simulation run. Equations of motion were integrated using velocity Verlet algorithm with 2 fs time step. All the simulations were carried out at a target temperature of 298 K and a target pressure of 1 atm. Each of the simulation runs was 2 ns or longer.

To study the spatial structure such as one-particle density distribution, and hydrogen-bond distribution around the solute plate, we have considered only those water molecules residing within a rectangular box of the dimensions of the solute plates in *x* and *y*-directions and of the size of the simulation box in *z*-direction. For the analysis of fluctuations as well as compressibility as calculated from the pressure dependence of the local density, we considered a rectangular slab of water molecules at different values of *z* (corresponding to different perpendicular distances from the plate) with the size of the slab considered to be the size of the solute plates in *x*- and *y*-direction and a width of 1 Å in *z*-direction. For calculation of compressibility, we have first calculated density of water at different slabs using simulation trajectories at different pressures P = 1, 150, 300, 500, 1000, and 2000 bars. Finally position dependent compressibility, $\chi T(z)$ is calculated[7]from the derivative of density, $\rho(z)$ with respect to pressure, P, viz.,

$$\chi_T(z) = \frac{1}{\rho(z)}\left(\frac{\partial\rho(z)}{\partial P}\right)_{\Delta,\ T} \qquad (5.2)$$

where *z* is the location of the center of the slab and $\Delta$is the slab thickness. We have calculated the derivative from

the fitting[116, 359] of the density vs. pressure data to a second order polynomial. For the calculation of density fluctuations, we used normalized fluctuations[334] in the number of water molecules within a specific volume, viz.,

$$\kappa_N = \frac{[\langle N^2\rangle - \langle N\rangle^2]}{\langle N\rangle} \qquad (5.3)$$

where$\langle \dots \rangle$denotes ensemble average.

5.3: Result and discussion

5.3.1. Hydration characteristics of single plate

As stated earlier, in this investigation, we have considered various model paraffin-like plates differing from each other only in the Lennard-Jones interaction with the oxygen of water according to Eq. (1) with different λ values. Decreasing values of λ correspond to increasing degree of hydrophobicity of the plate. In Fig.5.1, plots of normalized single-particle distributions of water oxygens, $g_{SO}(z)$ $(=\rho(z)/\rho_0)$ as a function of the distance, z from the plate for various values of λ are shown. Here the values of λ considered are 0.0, 0.25, 0.50, 0.75, and 1.0, in which $\lambda = 1.0$ corresponds to the ϵ parameter of the OPLSUA force-field. The variation of the nature of the density distributions with the parameter λ as obtained in the present study resembles that obtained by Patel *et al.*[356] for similar type of interfaces. It is clearly seen that for $\lambda = 0.0$, water recedes from the interface and the density profile looks like that of a liquid-vapor interface. This is in agreement with many previous theoretical and computational investigations,333 in which it is demonstrated that a thin vapor layer exists in the vicinity of the hydrophobic solute in water. So for a purely repulsive solute, we have also found that there is a depletion zone surrounding the solute plate and the width of the depletion layer, as obtained from the distance of the mid-density plane from the plate, is around 3 Å in the present case. As the value of λ is increased from 0 to 0.25, which corresponds to considering a very small attraction in the interaction between solute atom and the oxygen of water, the density profile is pulled closer to the plate surface slightly, although the overall nature of the density profile still resembles that of a liquid-vapor interface. In this case, the width of the depletion region is reduced and it is around 2.5 Å. For $\lambda = 0.5$, increased attraction changes the nature of the plot and now the sigmoidal nature of the density plot as observed in case of $\lambda = 0.0$ or 0.25, which are reminiscent of liquid vapor interface, has been changed to a liquid like density profile with peaks and troughs defining solvation layers. For λ = 0.75 and 1.0, there are pronounced peaks and troughs in the density profile and the first density peak adjacent to the wall is as enhanced as about twice that of the bulk density and it appears that the paraffin surface with these parameter sets are hydrophilic. Thus, by changing the parameter λ from 0 to 1, we are able to create various paraffin-like plates that behave like hydrophobic to hydrophilic as far as local density distribution of water is concerned. However, as mentioned in the Introduction, ensemble averaged density distribution may not bring out actual nature of the interface and thus further analyses are necessary.

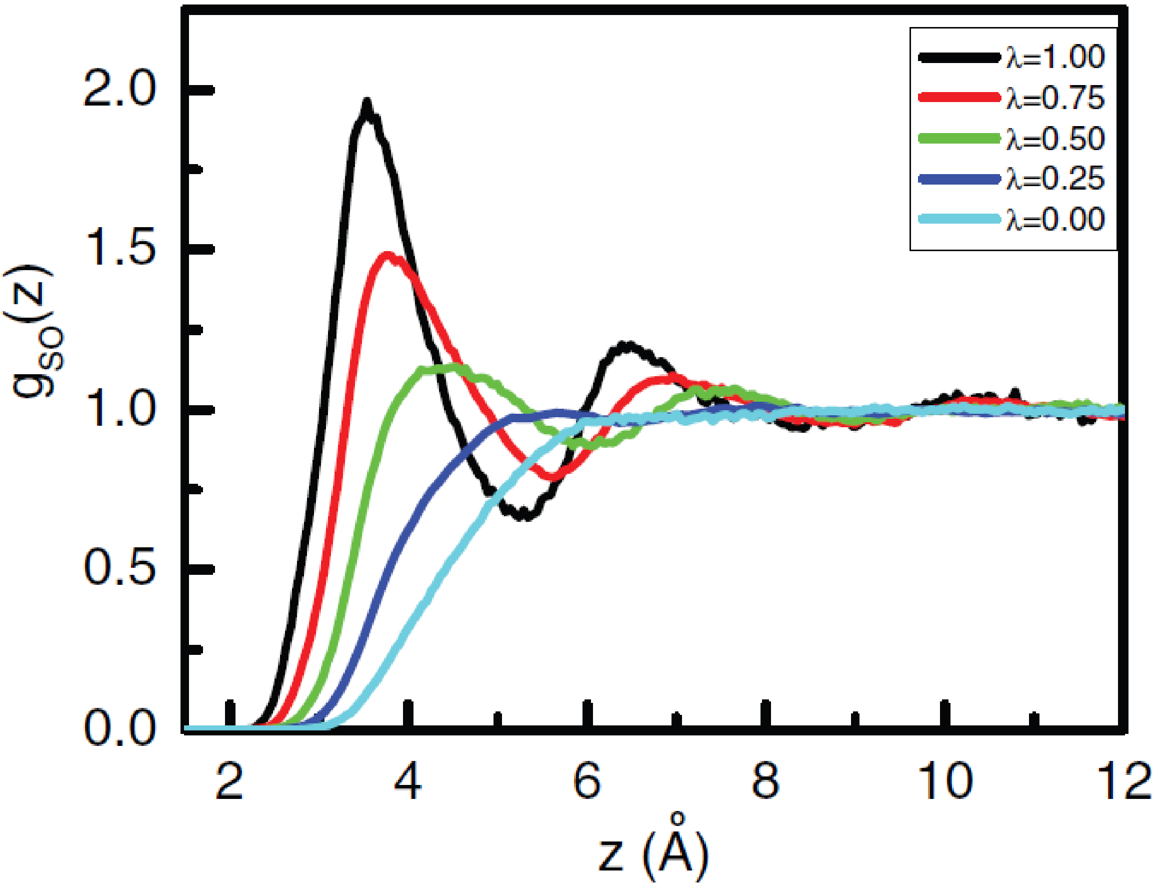

***Figure.5.1.** The normalized single particle density $g_{SO}(z)$ of water oxygen as a function of distance z from the model paraffin plate for different values of λ.*

As evident from the local density distribution of water around the plate, water experiences different forces from different plates (with different λ values). One can thus represent the density distribution plots in terms of PMF between the plate and a water molecule $W_{SO}(z)$ by calculating it using the relation

$$W_{so}(z) = -K_B T ln g_{so}(z)$$
$$= U_{so}(z) + \ w_{ind}(z) (5.4)$$

Where $k_B$is the Boltzmann constant, T is temperature, $U_{SO}(z)$ is the direct interaction energy between water and the plate and $\omega_{ind}(z)$ is the solvent induced contribution to the overall PMF. The solvent induced contribution $\omega_{ind}(z)$ is a measure of the indirect effect of all the other water molecules. As it is displayed in Fig.5.2(a), the PMFs for λ = 0.0 is repulsive throughout the whole separation range, whereas for λ = 0.5 or 1.0 there are regions of plate-water separations (z values) for which PMF is negative, manifesting attraction. The corresponding solvent induced PMFs $\omega_{ind}(z)$ show interesting behavior as a function of λ. For λ = 0.0, i.e., when the paraffin wall is purely repulsive, the solvent induced contribution $\omega_{ind}(z)$ shows a barrier at around z = 4 Å, below which the value is negative. As the value of λ is increased to 0.25 and then to 0.5, the barrier height at z = 4 Å decreases, but another barrier is formed at around 6 Å. As the value of $\lambda$is increased further to 0.75 and then to 1.0, a broad shoulder region is formed with a steep barrier height starting from 6 Å downwards till 4 Å. Thus addition of attractive interaction in the interaction potential between solute site and water surprisingly makes the solvent induced contribution positive. Thus water molecule in the hydration shell prevents the test molecule from entering into it from the bulk. This has already been observed[62] in case of hydration of methane and fullerenes of different sizes. The barrier in induced PMF on approaching the plate can be understood by assuming $\omega_{ind}(z)$ as correction to the huge increase in density in the vicinity of the solute plate due to attractive interaction according to the Boltzmann response, $g_{SO}|\lambda=0 \exp[-U_{tt}^{SO}/KBT]$. Therefore as the value of λ increases, attractive interaction increases and therefore density at the contact should increase to a very high value according to the above equation, but increased positive $\omega_{ind}(z)$ value at high λ corrects the excess density probably by forming a repulsive core packing due to solvation shell waters and/or hydrogen bonding constraints.[6]

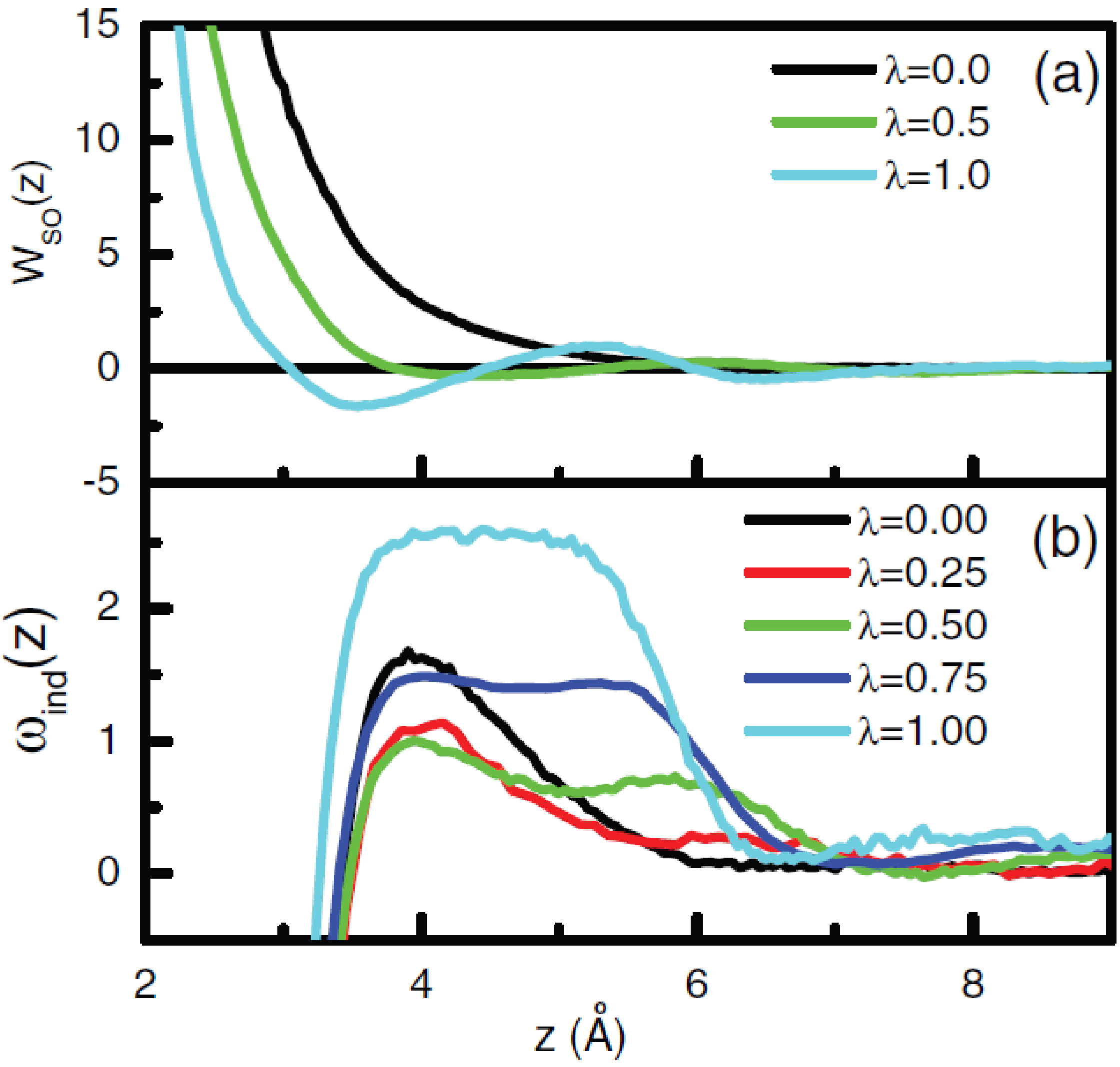

Figure.5.2. The normalized single particle density $g_{SO}(z)$ of water oxygen as a function of distance z from the model paraffin plate for different values of λ.(a) Solute-water potential of mean force $W_{SO}(z)$ of a water molecule as a function of distance z from the model paraffin solute (plate) for values λ = 0, 0.5, and 1. (b) Solvent induced PMF $\omega_{ind}(z)$ for values of λ = 0, 0.25,0.5, 0.75, and 1.

In order to investigate the average orientational preference of water near the surface, we have considered a rectangular slab of water molecules of the dimensions of the solute in x- and y-directions and of width around 6 Å corresponding to the size of the 1st hydration shell in the z-direction and calculated orientational distributions of the three orientational vectors of the water molecule, namely, dipole moment vector (μ), OH bond vector, and a vector perpendicular to the molecular plane of the water molecule. The angles made by the vectors μ, OH, and the vector perpendicular to the plane of the water molecule (i.e., plane vector) with outward (solute) plate normal vector are represented by θ, ψ, and φ, respectively. These orientational distributions are shown in Fig.5.3. The distribution for the dipole moment vector $P_{\mu}(\cos\theta)$ vs. Cosθ as shown in Fig.5.3(a) shows a broad distribution around $\cos\theta = 0$ and does not show considerable change with change in λ or attractive interaction of the solute. In case of OH bond vector, we observe (see Fig.5.3(b)) a noticeable change in the intensity of the distribution $P_{OH}(\cos\psi)$, but positions of the peaks of the distribution remain almost unchanged with λ. There is an increase in peak height at around $\cos\psi = -0.25$ indicating a preferred orientation of OH bond pointing the paraffin plate at large λ value. Similar distribution of the OH of water has been observed[344, 345] over graphene-CH_3 and graphene-COOH surfaces. The distribution of the molecular plane vector $P\perp(\cos\varphi)$ of the water molecule also does not change much with the change in λ, except that intensity changes at two values of θ viz., 0° and 180°. Thus, it seems that orientational distributions of water are not so sensitive to the degree of hydrophobicity of the plate. However, these distributions have been obtained by considering all the water molecules residing in the first hydration shell of the respective solute plate and thus provide an averaged out picture. In order to get further insight into the nature of the orientational distributions, we have calculated average of the cosine of the orientational angel (i.e., θ, ψ, and φ) as a function of z. The average value of the cosine of the angle ($\langle\cos\theta\rangle$) made by the dipole moment vector with the outward normal to

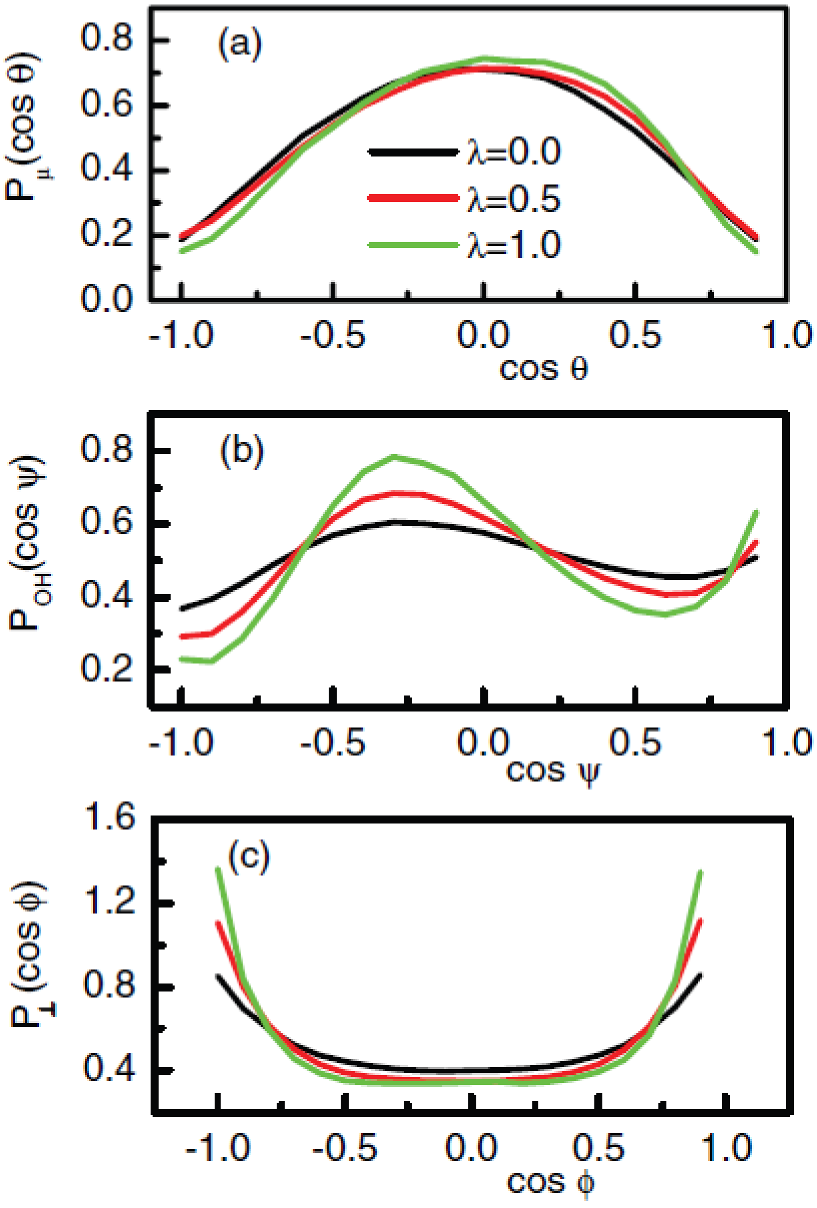

Figure.5.3. Orientational distribution functions of the (a) dipole moment vector $P\mu(\cos\theta)$ vs. $\cos\theta$(b) OH bond vector $P_{OH}(\cos\psi)$ vs. $\cos\psi$, and (c) $P_\perp(\cos\varphi)$ vs. $\cos\varphi$of the water molecules for different values of λ.

the solute plate is shown in Fig.5.4(a) for three different solute plates with $\lambda = 0$, 0.5 and 1. It is now clearly seen that at smaller values of z, the $\langle\cos\theta\rangle$vs. z profile changes considerably with the change in the λ value, i.e., degree of plate water affinity. We have shown in Fig.5.4(b) average values of the cosines of the angles ($\langle\cos\psi\rangle$) made by OH bond vector with the outward normal to the (solute) plate as a function of perpendicular distance, z from the surface. In this case, we also find considerable changes in the average value of cosψat lower z values with the changes in the λ values. The average values of the cosine of the angle ($\langle\cos\varphi\rangle$) made by molecular plane-perpendicular vector are close to zero (see Fig.5.4(c)) at all values of z. This is because two exactly opposite orientations of the the molecular plane of the water molecule with respect to the plate are equally probable. In summary, although average orientation profiles of the dipole moment vector of the water molecules in the entire solvation shell do not show much sensitivity to the parameter λ, position dependence of the average orientational angle shows a considerable change with λ, i.e., degree of plate-water attractiveness.

Histograms of hydrogen bond (H-bond) distribution of the water molecule having nH-bonds are displayed inFigs.5.5(a)–5(f). The fraction of molecules having nH-bonds f_n^{HB} are shown as a function of number of H-bonds n$_{HB}$. These are calculated for water molecules residing in a 1 Å wide slab parallel to the solute plate at a distance 3.5 Å from the plate and the slab dimension in x and y-directions are the same as the dimensions of the solute plate. For λ = 0.0 plate (Fig.5.5(a)), almost 50% of the water molecules have 2 Hbonds and 35% have 3 H-bonds. As the value of λ increases from 0 to 0.25 (Fig.5.5(b)), the fraction of molecules having 2 H-bonds decreases where as that having 3 H-bonds increases and at λ = 0.5 (see Fig.5.5(c)), population having 3 H-bonds f_3^{HB}3 crosses over to that (f_2^{HB}) having 2 H-bonds. Along with this, fraction having 4 H-bonds also increases marginally. As we go on increasing λ further, fraction of molecules having 3 H-bonds increases whereas that having 2 H-bonds decreases and f_3^{HB} reaches almost 50% at λ = 1. If this result is compared with the same for bulk (see Fig.5.5(f)), we find that in the bulk, almost 50% of the molecules have 4 H-bonds and 35% have 3 H-bonds. Thus even for the plate having maximum degree of hydrophilicity (λ = 1) as considered here, fraction of molecules having 4 H-bonds are quite

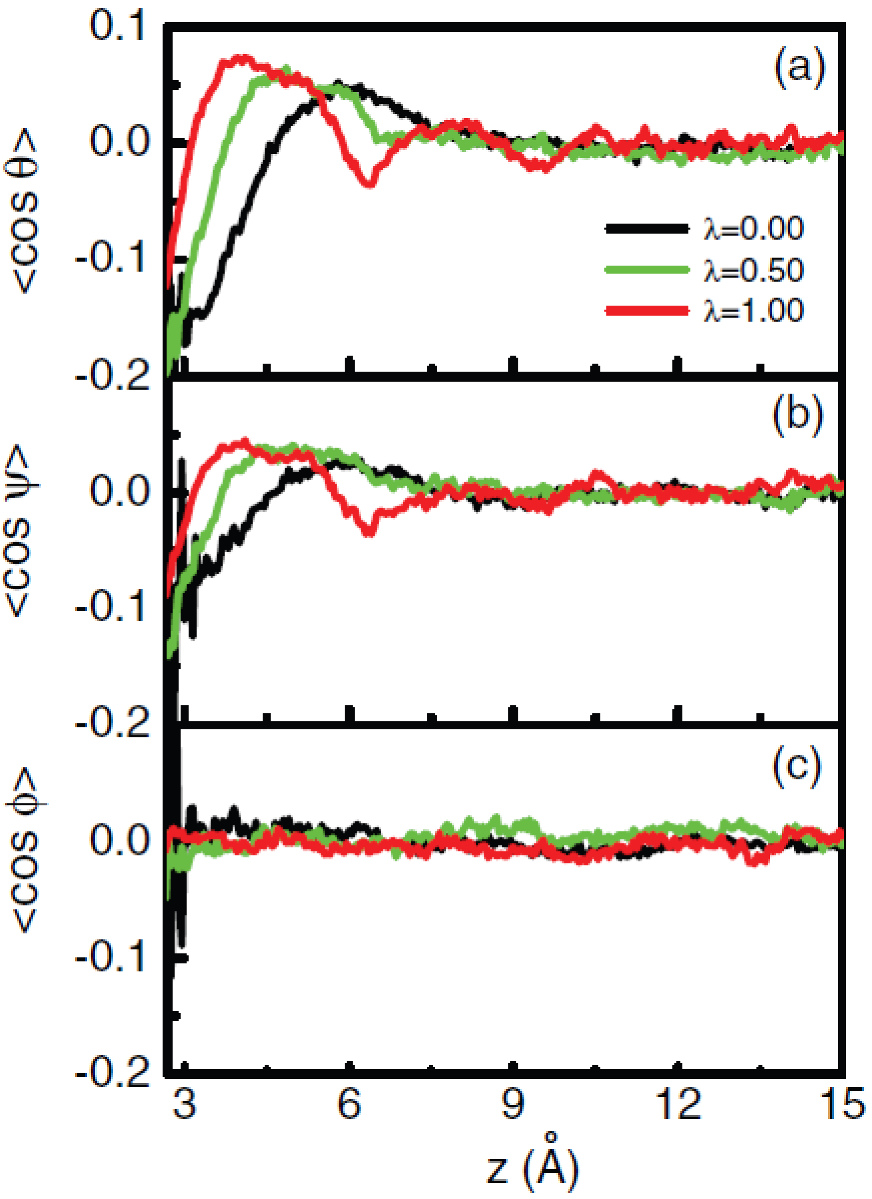

***Figure.5.4.**Average values of the cosines of the angles made by (a) dipole moment vectors, (b) OH bond vectors, and (c) plane-perpendicular vectors of the water molecules with outward normal to the solute plate as a function of perpendicular distance from the solute plate with different values of λ.*

less (20%)as compared to the bulk. Thus the presence of the solute plate in one side of the water slab introduces geometric frustration and reduces the number of molecules having 4 H-bonds. We have also calculated average coordination number $\langle n_{CN} \rangle$defined as the number of water molecules within a radius of 3.5 Å of a central water molecule and average number of H-bonds $\langle n_{HB} \rangle$ as a function of perpendicular distance from the plate. It is observed (see Fig.5.6(a)) that average coordination number of water, $\langle n_{CN} \rangle$is in the range of 2.3–3at the closest distance of approach depending on the value of λ and it increases with z slowly and finally reaches to the bulk value at around z = 6 Å. At a particular value of z near the plate, $\langle n_{CN} \rangle$of water near λ = 0 plate is less as compared to the same near plates with greater λ values. In case of hydrogen bonds also, it is observed (see Fig.5.6(b)) that far away from the plate where water behaves like bulk water, average no of H-bonds are about 3.5 and from around 6 Å and below, number of H-bonds decreases and reaches the value of 2–2.5 at around $z = 2 - 2.5$ Å from the plate depending on the λ values. In case of λ = 0.0, the depletion zone ends around 8.5 Å. On the other hand, minimum distance at which n_{HB}goes to zero is more for λ = 0 plate as compared to the other two plates. Like average coordination number, average number of hydrogen bonds also shows the same trend with λ. At a particular z near the plate, the average value $\langle n_{HB} \rangle$increases with increasing λ values or increasing hydrophilicities. However, fraction ($\langle n_{HB} \rangle / \langle n_{CN} \rangle$) of the nearest neighbors that are hydrogen bonded as a function of perpendicular distance from the interface, z shows (see Fig.5.6(c)) that the fraction of neighbors that are hydrogen bonded is more at lower λ values as compared to the the same at higher λ values. Similar results have been obtained by Garde and co-workers[63] for a model octane-water interface. Thus, water near hydrophobic plates are surrounded by larger fraction of neighbors that are hydrogen bonded than those near hydrophilic plates. This increasing correlation among the solvation shell water molecules at the hydrophobic solute-water interface has been further illustrated through the calculation of in-plane oxygen-oxygen g(r) and discussed later (see Fig.5.9 and associated discussions).

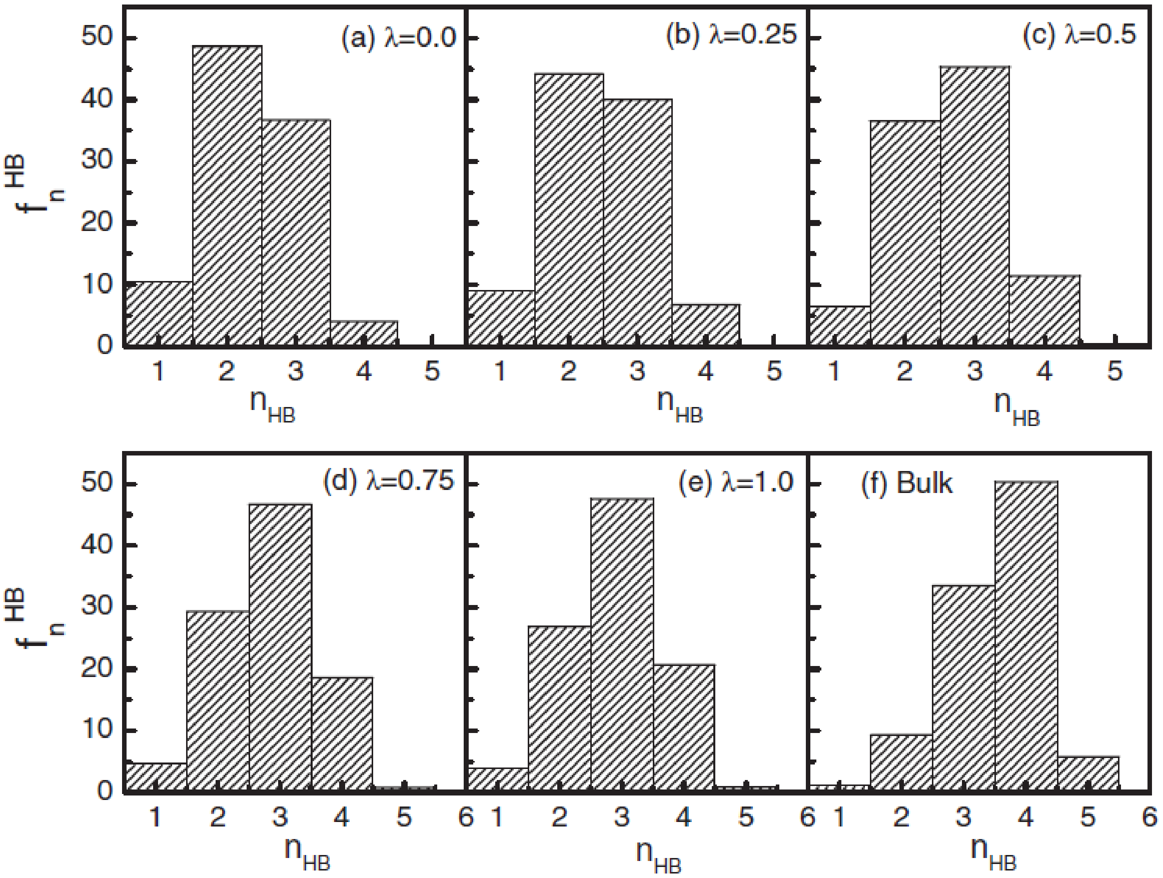

Figure.5.5.Histograms of water molecules with n hydrogen bonds $f_3^{HB}$for water in plate-water systems with λ = 0, 0.25, 0.5, 0.75, 1, and bulk.

Another quantity which may be a yardstick to measure hydrophobicity is the isothermal compressibility[117] of water inthe vicinity of the solute surface. In order to calculate this quantity, we have simulated a systems with a particular value of λ at different pressures as mentioned in Sec. II and from the simulation trajectory we have calculated density of water in a slab of width 1 Å placed at various positions parallel to the plate. From the pressure dependence of the density(cf. Eq.(2)), $\chi(z)$ is calculated. As shown in Fig.5.7,the

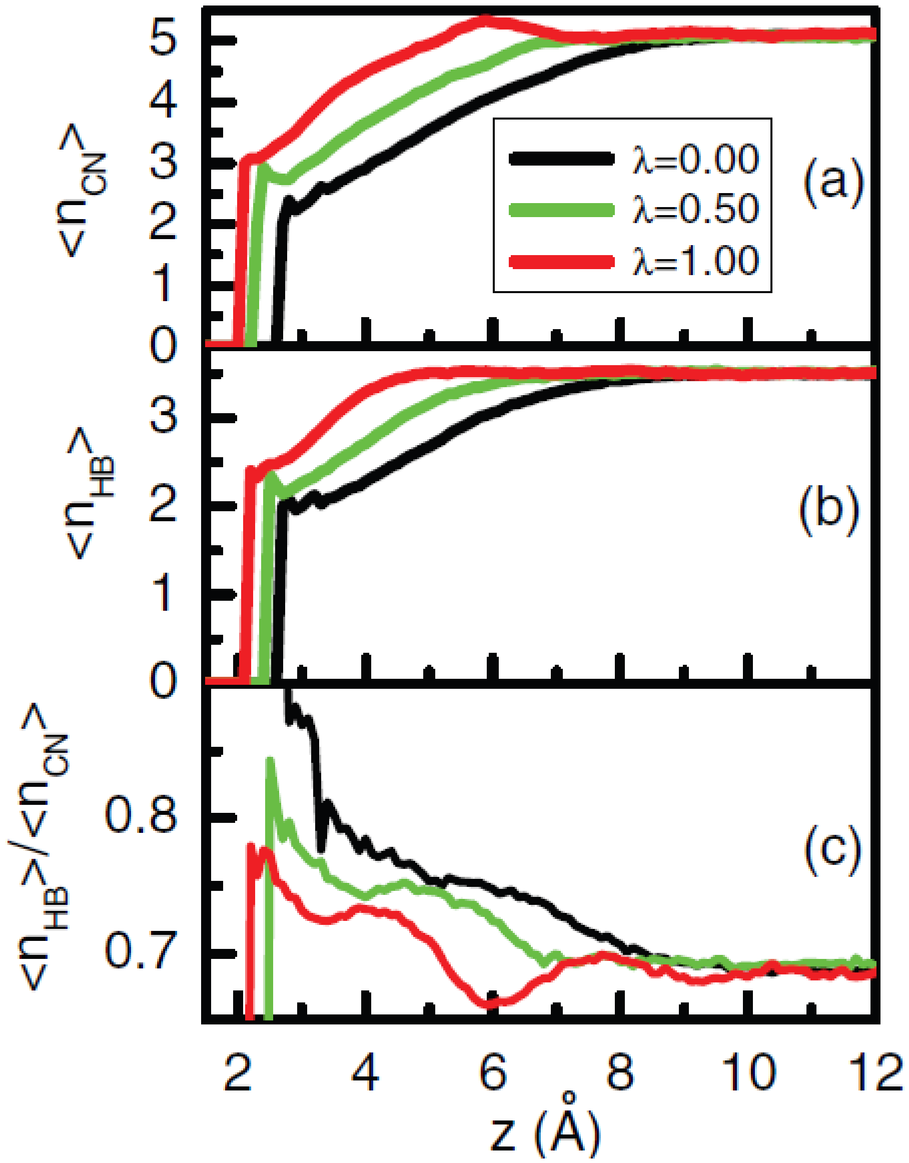

Figure.5.6. (a) Average coordination number ($\langle n_{CN} \rangle$) of water, (b) average number of hydrogen bonds ($\langle n_{HB} \rangle$) per water molecules, and (c) fraction ($\langle n_{HB} \rangle / \langle n_{CN} \rangle$) of nearest neighbors that are hydrogen bonded as a function of perpendicular distance z from the solute plate for different paraffin-like plates (with different values of λ).

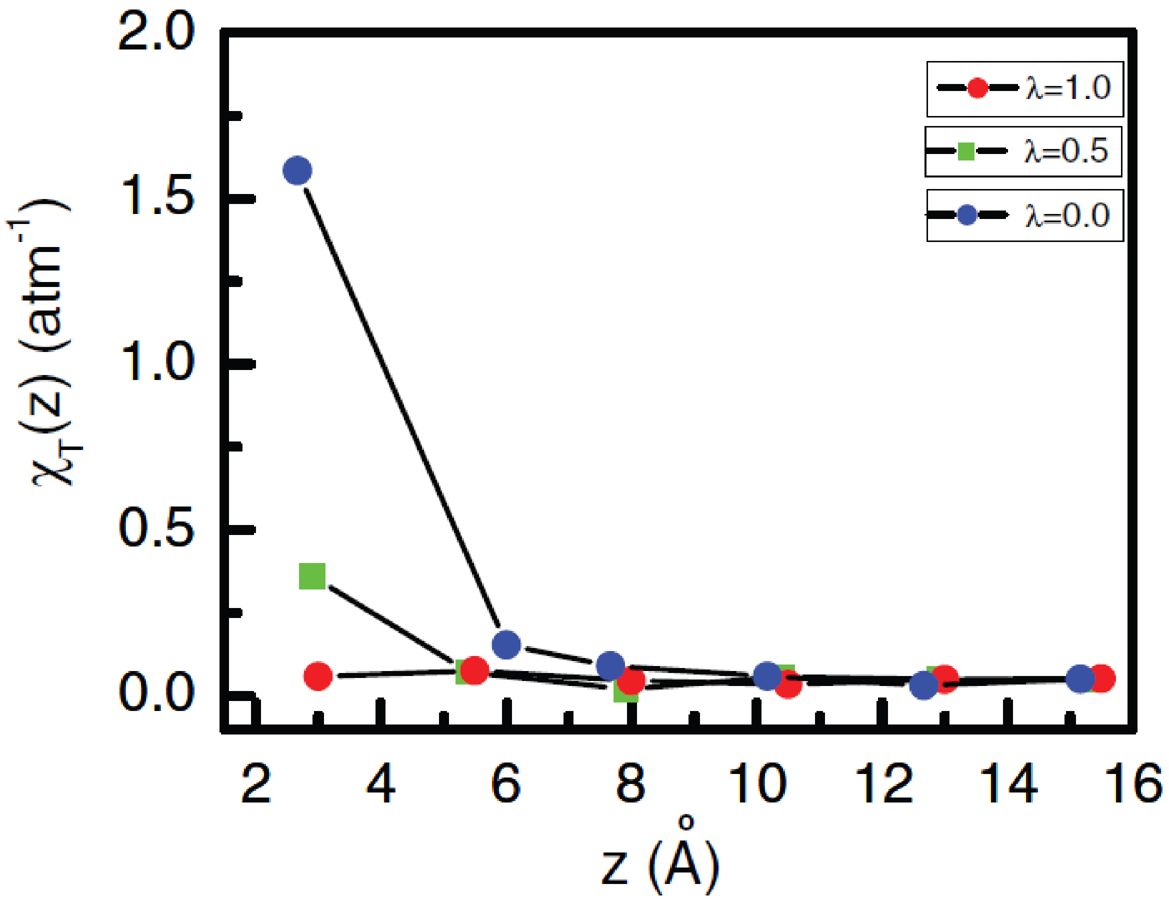

Figure.5.7. Local compressibility $\chi_T(z)$ of a slab of water of width 1 Å at different locations along the perpendicular direction of the plate for different values of λ.

compressibility value of the system with λ = 1.0 and 0.5 are very low everywhere, whereas that for plate with λ = 0.0 is very high near the surface. The increase in compressibility of water near a hydrophobic surface has already been observed for self-assembled monolayer-water, protein-water interfaces.[116, 117]Thus compressibility is a good descriptor of hydrophobic solute-water interface. However, calculation of compressibility through this route is computationally demanding as one requires to simulate the system at various pressures. An alternative to this compressibility could be the water density fluctuations as calculated by the variance in the number of water molecules normalized by mean in a specific slab volume at a particular distance from the plate surface (cf. Eq. (3)). In the macroscopic

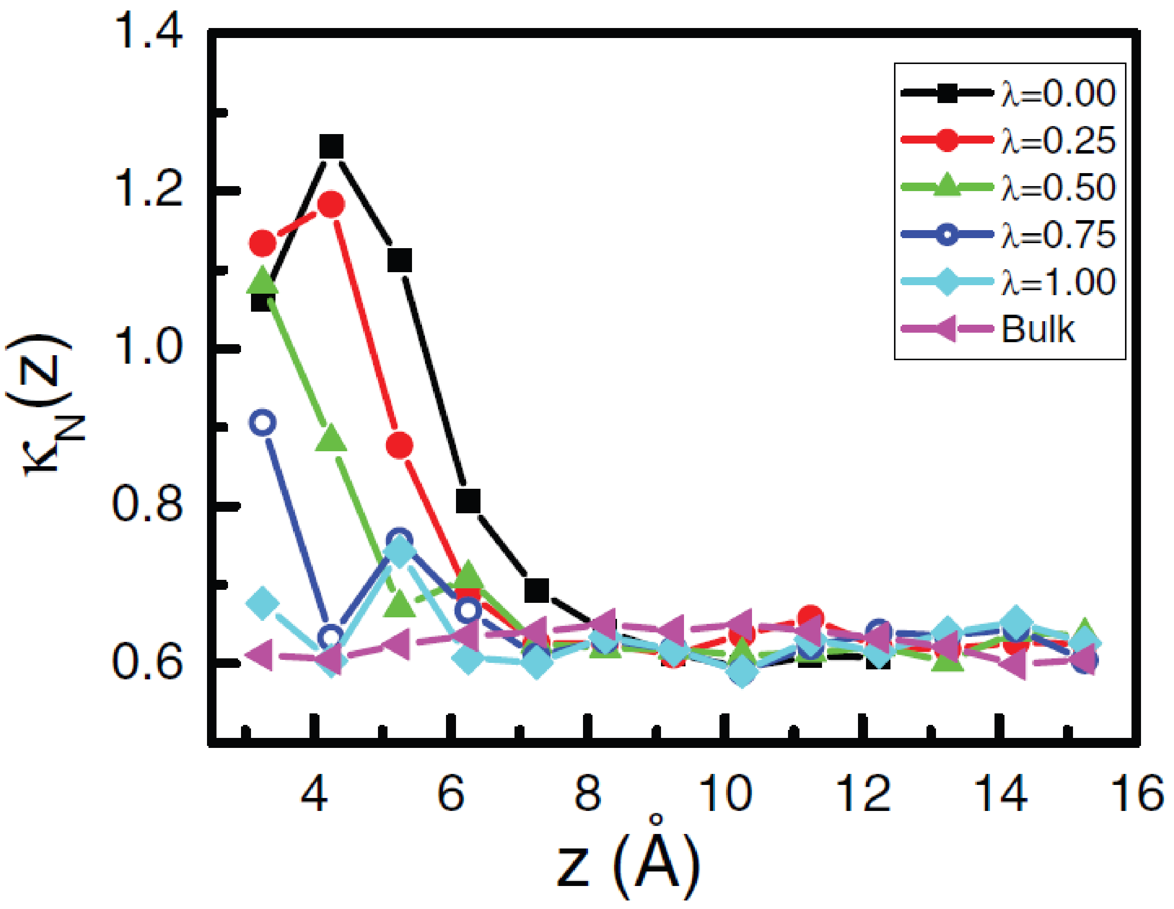

Figure.5.8. Normalized fluctuations $K_N(z)$ of a slab of water of width 1 Å at different locations along the perpendicular direction of the plate for different values of λ and for bulk water.

limit, in an open system this ratio κ_N approaches $\rho k_B T \chi_T(z)$. The κ_N values as a function of slab distances from the solute plate is shown in Fig.5.8. It is seen that fluctuations for $\lambda = 1.0$ are just like bulk fluctuations. For $\lambda = 0.75$, only at $z = 3.5$ fluctuations are more, while for other values of z, these are the same as the $\lambda = 1.0$ case. Fluctuations are at the maximum in case of plates with $\lambda = 0.0$, i.e., for the most hydrophobic plate. This quantity at distances (upto 3.5 Å) close to the surface shows considerable fluctuations even for $\lambda = 0.5$ case, and is in contrast to the χ_T variation. This is because the average number of water molecules $\langle N \rangle$ at low z is very small and since it appears in the denominator of Eq. (3), the normalized fluctuations become quite high. However, at $z = 4.0$ Å, the variation of κ_N is of the same nature as that of

χ_T. The calculation of κ_N is computationally not expensive and therefore easier to use. The value of κ_N for the repulsive plates with λ values 0.0 and 0.25 exceed the ideal gas limit of 1 and this super-Poissonian statistics may be due to contributions from weak clustering to the density fluctuations.[334]A structural measure, sensitive to the degree of hydrophobicity of the solute (value of λ here) is the water-water correlation as obtained from the radial distribution function of the oxygen atoms of water, $g_{OO}(r)$ in a 1 Å wide slab parallel to the plate. It is clearly seen from Fig.5.9(a) that the two particle correlation, $g_{OO}(r)$ shows nice variation with the surface hydrophobicity (i.e., with λ). When λ is large, i.e., degree of hydrophobicity of the surface is less, peak in the correlation is smaller as compared to the same when λ is small, i.e., when degree of hydrophobicity of the surface is more. It is important to note that even the peak height for the least hydrophobic plate considered here (λ = 1.0) is more than that of the bulk and thus the plate with λ = 1.0 also has considerable signature for hydrophobicity. Similar correlation has also been observed for intermolecular oxygen-hydrogen correlation as calculated through $g_{OH}(r)$ within the slab. Plots of $g_{OH}(r)$ for different λ values are shown in Fig.5.9(b). For comparison, the same is shown for bulk water. There is enhanced correlation in the intermolecular oxygen-hydrogen correlation among the water molecules in the slab for water near plate with higher degree of hydrophobicity. Thus, the water correlation within a narrow slab parallel to the solute plate also can be used to characterize hydrophobic solute-water interface. However, as the change in the peak height is gradual with the increase in λ it is difficult to identify the crossover between hydrophobic and hydrophilic surfaces.

Water is a network forming liquid with tetrahedral configuration of the water molecules. In order to quantify the degree of tetrahedrality various order parameters have been proposed and used[71,75,362] for bulk water. In the vicinity of a hydrophobic plate, it is expected that the tetrahedral structure of water will be disrupted and therefore an order

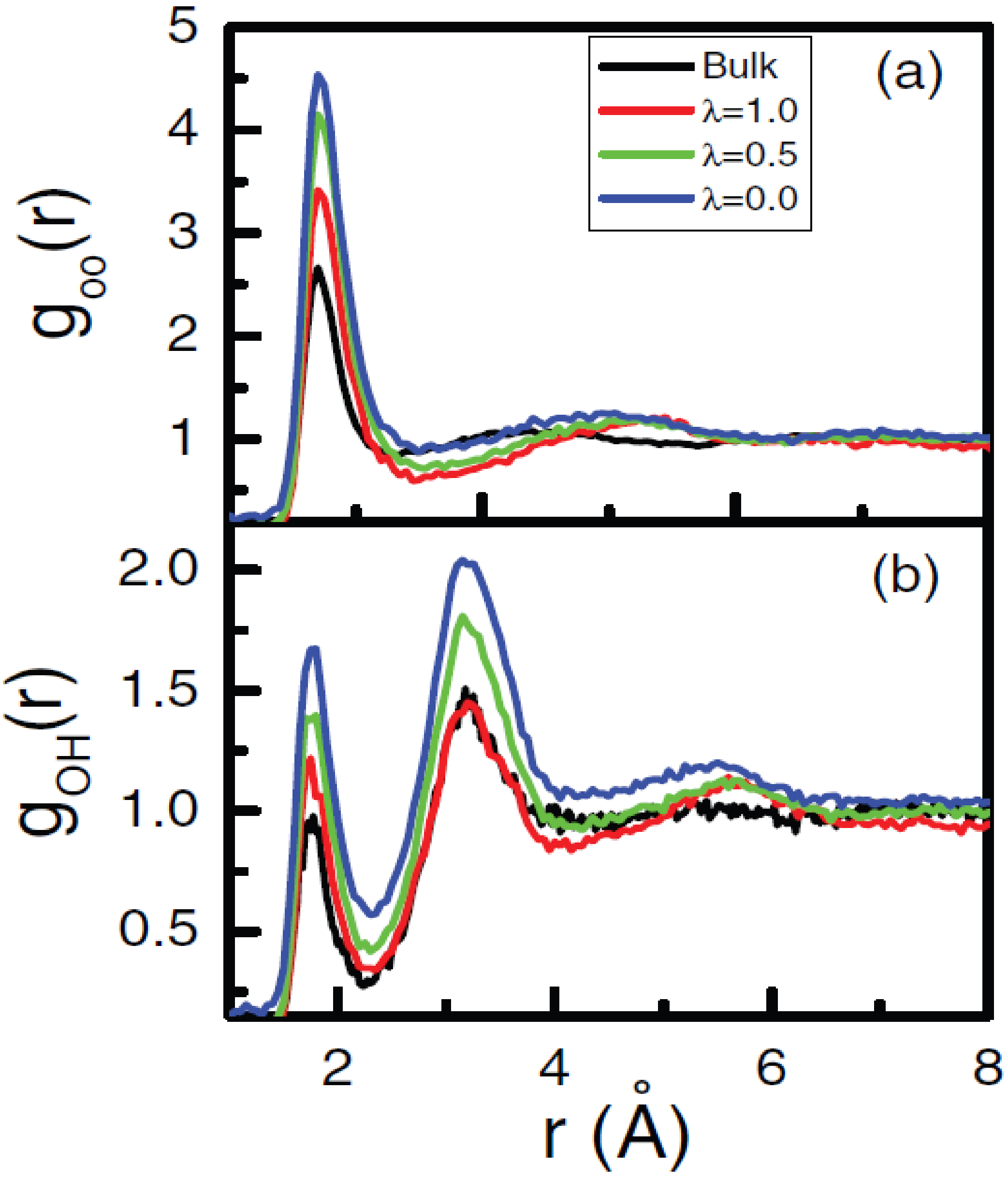

Figure.5.9.Water-water correlations at different interfaces with different λ values as calculated through intermolecular water (a) oxygen-oxygen pair correlation function $g_{OO}(r)$ and (b) oxygen-hydrogen pair correlation function $g_{OH}(r)$ near the paraffin plate measured in a 1 Å thick slab placed parallel to the interface located at the half density plane of water.

parameter measuring tetrahedrality of water as a function of distance from the solute plate will be a good predictor for hydrophobicity. Here the order parameter corresponding to the central water molecule i is defined[362, 71] as

$$q_i = 1 - \frac{3}{8}\sum_{j=1}^{3}\sum_{k=j+1}^{4}\left[\cos\theta + \frac{1}{3}\right]^2 \quad (5.5)$$

Where θ_{jik} is the angle formed between neighbors j and k and the central molecule i. The average value for a given set of molecules

$$q_4 = \frac{1}{N}\langle\sum_{i=1}^{N} q_i\rangle \qquad (5.6)$$

quantifies the tetrahedral order of the system. When we calculate this parameter in the vicinity of the plate, we extend the above definition and consider that the four nearest neighbors of the central molecules may be water or a solute carbon atom. In the above expression N_s is the number of central molecules considered in the given set. This definition is a slightly modified version of the parameter introduced in Ref. 362. In an ideal gas the value of the q_4 is zero and for a perfect tetrahedral network q_4= 1. Thus, q_4 measures the degree of tetrahedrality in the distribution of four nearest neighbors around a central water oxygen atom. In the present case, we have calculated q_4 for (central) water molecules residing in a slab of width 1 Å parallel to the plate and of the dimensions of the plate in the other two directions. In Fig.5.10(a), the plots of q_4 as a function of the distance of the center of the slab from the plate, z for different values of λ are presented. In all the cases q_4 values near the surface are small and as the distance of the plate increases q_4 value increases and eventually reaches steady bulk value. The distance from the plate at which q_4 reaches the bulk value

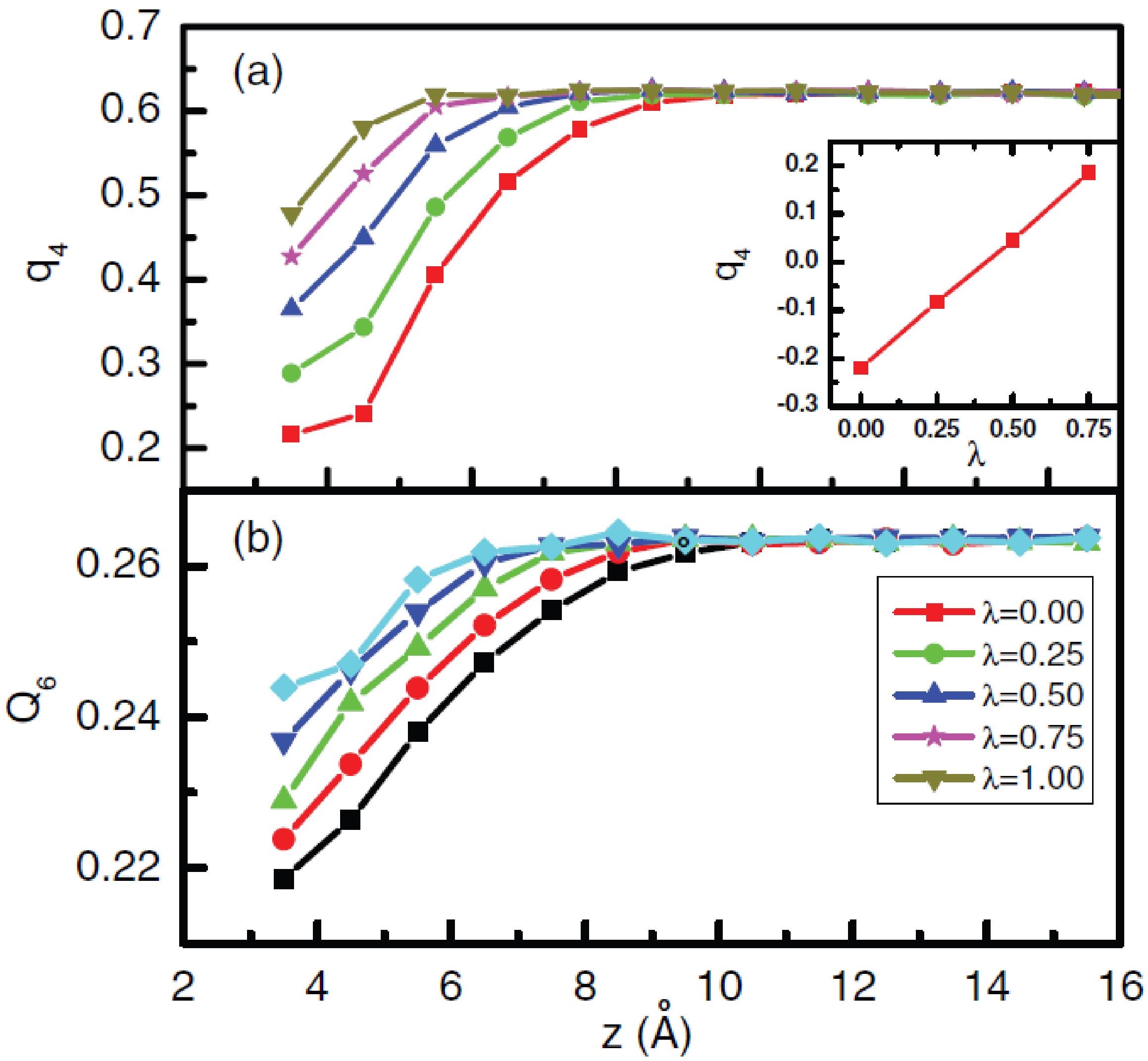

Figure.5.10.(a) First shell tetrahedral order parameter, q_4 (Bottom to top:λ= 0.0, 0.25, 0.50, 0.75, 1.00) and (b) second shell orientational order parameter Q_6 for water at different slabs parallel to the surfaces as a function of distance from the plate for different plates of varying λ values. In the inset of panel (a), q_4 as a function of λ is shown.

depends on the degree of hydrophobicity of the plate (i.e., on the value of λ). For the most hydrophobic plate ($\lambda = 0$), effect of the plate on the tetrahedrality extends upto 8.5 Å, whereas for the least hydrophobic plate (plate with $\lambda = 1$), it extends only upto 5 Å. Near the plate deviation from tetrahedrality is more as compared to the same away from the plate. At around 2.5 Å, the q_4 value is as low as −0.2 for the most hydrophobic plate (i.e., $\lambda = 0.0$) and it increases to 0.27 for the least hydrophobic plate (i.e., $\lambda = 1.0$) considered here. In the inset of

Fig.5.10(a), we have shown the q_4 values for the slab of water adjacent to the solute plate as a function of degree of hydrophilicity λ and it shows that with the increase of λ, q_4 increases steadily.

In case of a hexagonal crystal, the second shell forms an *hcp* structure and therefore an orientational order parameter for the second shell molecule around the central molecule *i*, Q_{6i}, which quantifies the extent to which the central molecule *i* and 12 of its second shell neighbors form a *hcp, fcc,* or *bcc* structure is defined. In order to compute Q_{6i}, we first define[66] 12 bonds connecting the central molecules with its 12 next neighbors in the second shell and compute for each bond its azimuthal and polar angles (θ, φ). Next we calculate $\bar{Y}_{lm}(\theta,\varphi)$, the average of the spherical harmonics over 12 bonds of the central molecule *i*. From this $\bar{Y}_{lm}(\theta,\varphi)$, finally the function

$$Q_{li} = \left[\frac{4\pi}{2l+1}\sum_{m=-l}^{m=l}|\bar{Y}_{lm}|^2\right]^{1/2} \qquad (5.7)$$

is calculated. For $l = 6$, the average value for a set of N_s central molecules

$$Q_6 = \frac{1}{N_s}\sum_{i=1}^{N_s} Q_{6i} \qquad (5.8)$$

quantifies the orientational order of the set of molecules in the second shell around the central molecule. This parameter is large for most crystals and for perfect *hcp, bcc,* and *fcc* structures Q_6 values are 0.485, 0.511, and 0.574, respectively. Figure 5.10(b) shows the Q_6 parameters as calculated by taking all the central molecules residing in the slab of width 1 Å parallel to the plate as a function of the position of the slab with respect to the plate, *z*. As in the case of *q*4, the value of Q_6 also is very low in the vicinity of the surface and increases with the increase of the distance from the plate surface, and saturates to the bulk value at sufficiently large distances. The influence of the plate on this orientational parameter is also maximum for the most hydrophobic plate (λ = 0.0) and the least for the least hydrophobic plate (λ = 1.0). At around z = 2.5 Å, value $Q6$ for λ = 0.0 is the minimum and increases gradually as the value of λ increases, i.e., degree of hydrophobicity decreases. However, the change of the Q_6 with λ in the vicinity of the plate is not as much as change in q_4.

5.3.2. Interplate dewetting

In order to investigate dewetting in the interplate region, we have considered two plates immersed in water. We considered all five plates with λ values 0.0, 0.25, 0.5, 0.75, and 1.0. In Fig.5.11(a), the one-particle density of water in and around the two-plates system is shown for the most hydrophilic, i.e., λ = 1.0 plate-water system at an interplate distance of 7.5 Å. A very sharp peak in the middle of the two plates as well as at the outside surfaces of the plate shows hydrophilic nature of the plates and there is no dewetting in the middle. In this inter particle distance geometrically only one layer of water molecules can be accommodated. The same for λ = 0.75 plate-water system is shown in Fig.5.11(b)). When interpolate distance, r0 is increased from 7.5 Å to 10 Å, there is no density peak of water in the middle, i.e., there is no water in the middle of the two plates (see black plot of Fig.5. 11(b)). It is important to mention that although there is no density peak in the middle, the density peaks adjacent to outside surfaces of the plates are high and sharp indicating wet interfaces. This indicates that even when each of the individual plates is wet, combined fluctuations of the two plate-water interfaces in the inter solute region induce dewetting. However, when the distance between the two plates is increased to 12 Å, water enters into the middle as evidenced by the two distinct peaks in the middle (see red lines in the same plot). Thus for λ = 0.75 plate, the critical distance for dewetting is around 10 Å.

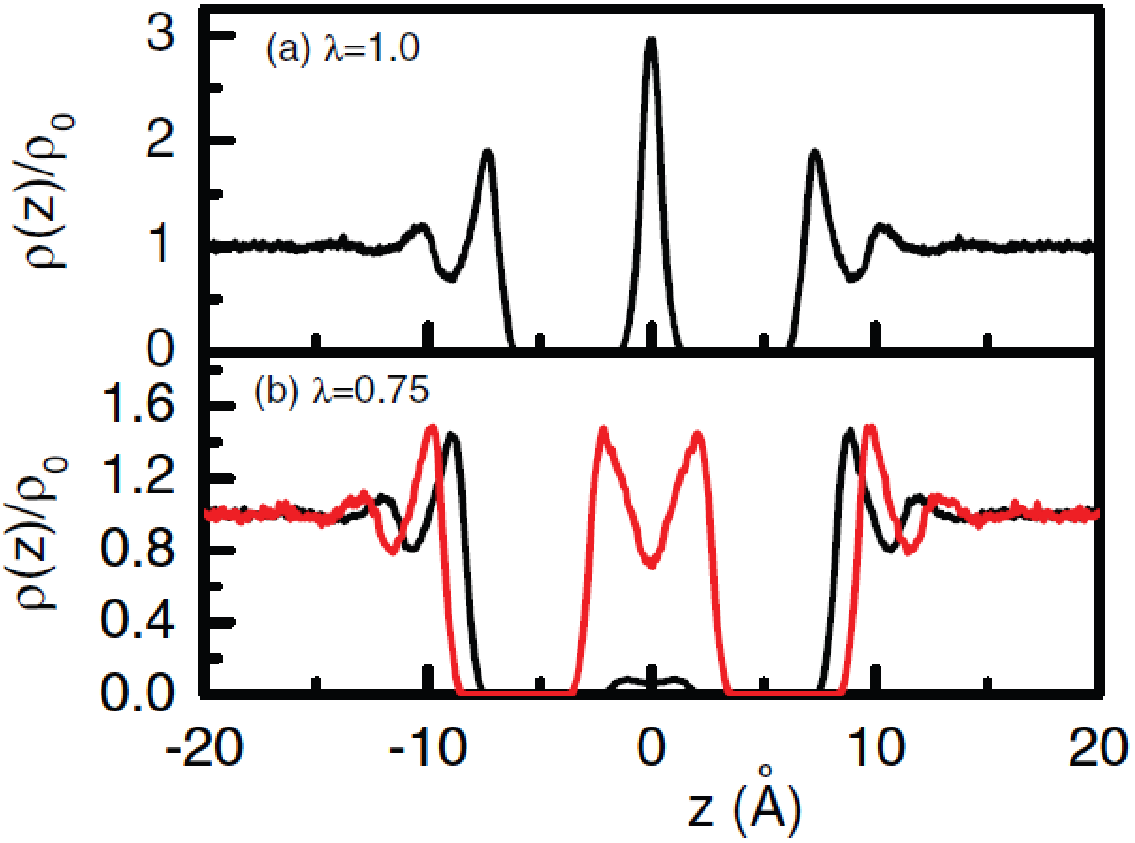

Figure.5.11. Normalized one-particle density profile, $\rho(z)/\rho_0$ as a function of perpendicular distance from the plate, z (a) for λ = 1.0 and (b) for λ = 0.75 plate-water systems. The red lines in (b) is for plates with interplate distance,r_0= 12 Å and the black line is for the same with r_0= 10 Å.

In Fig.5.12, we have shown density profiles of water for λ = 0.5 and λ = 0.0 plates. In case of λ = 0.5 plates (Fig.5.12(a)), the space between the two plates is dewetted upto interpolate distance r_0 of 12 Å. When the interplate distance is changed to 14 Å, there are density peaks in the middle (see the red graph in Fig.5.12(a)). Although not so sharply defined, there are almost three peaks in the middle, indicating that the inter solute space is enough to accommodate three water layers. However, a slight decrease of r0 value dewets the inter plate

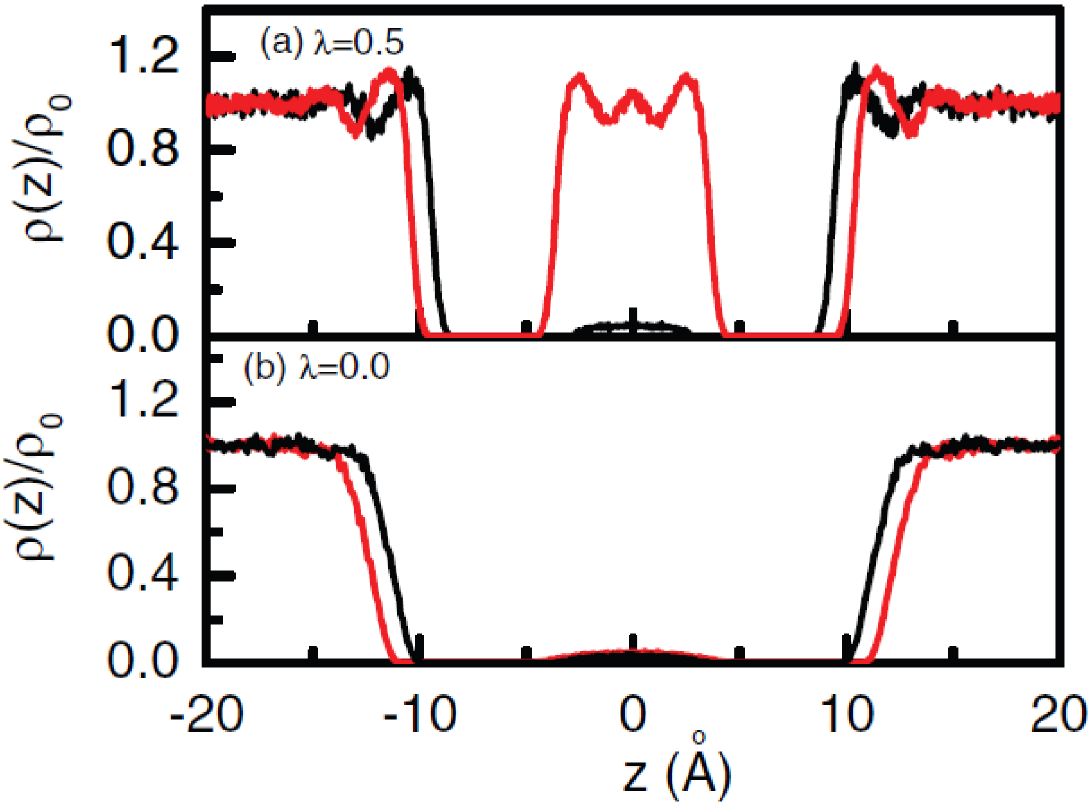

Figure.5.12. Normalized one-particle density profile, $\rho(z)/\rho_0$ as a function of perpendicular distance from the plate, z for (a) λ = 0.5 and for (b) λ = 0.75 plate-water systems. The red lines are for plates with interplate distance, r_0= 14 Å and the black line is for the same with r_0 = 12 Å.

region and there is no existence of two- or one-layer water between the plates. For λ = 0.0 plates, however, we always found dewetted interplate region upto interplate distance of r_0 = 16 Å (see Fig.5. 12(b)). It is interesting to observe that in this case, density peaks adjacent to two outside surfaces are also flat and sigmoidal in shape, which is reminiscent to the liquid-vapor interface. Thus, we found that except λ = 1.0 plate, which is completely hydrophilic, all other plates show dewetting at some critical distance.

5.4: Summary and Conclusions

In order to characterize a hydrophobic solute-water interface at the nanoscale, we have calculated various structural and thermodynamic quantities related to water structure and thermodynamics in the vicinity of hydrophobic surfaces. At the nanoscale, it is difficult to use the macroscopic contact angle criterion to characterize such an hydrophobic interface. Here we varied the hydrophobicity of the plate by changing the energy parameter of the solute-water non-bonded LJ interaction through a parameter λ (see Eq. (1)). It is already demonstrated[317] that the non-bonded energy parameter is a good tuning parameter, variation of which can create wet, dry, or intermittent wet-dry state in the intervening region between two nanoscopic plates. In the present study, we have calculated various structural quantities such as single-particle density of water and average number of H-bonds as a function of distance from the surface, three different orientational distributions of water, H-bond histogram, isothermal compressibility as calculated through the pressure derivative of the water density, water number fluctuations, in-plane radial distribution of water, tetrahedral and Q_6 orientational order parameters, etc. and a thermodynamic quantity, namely, the potential of mean force of a water molecule with the hydrophobic surface. Although average dipole orientational structure of water in the solvation shell does not depend much on the surface hydrophobicity, distance dependent average cosines of the orientational angles show considerable variation with degree of hydrophobicity of the solute plate. Other quantities also show considerable variation with respect to degree of hydrophobicity of the plate. The solvent induced contribution to the PMF of a water molecule with the plate shows unusual behavior in that addition of attraction to the plate-water interaction although decreases the barrier height, widens the width of the barrier. This is observed till $\lambda = 0.75$ and when the attractive interaction is further increased the barrier height as well as width increases beyond that of the $\lambda = 0.0$ case. In the cases of tetrahedral order parameter and Q_6 orientational parameter also a clear distinction appears for water near the hydrophobic and hydrophilic plates. The dewetting between two plates has also been investigated and it is found that the critical distance for dewetting varies with the degree of hydrophobicity of the plate as described by the parameter λ.

All these structural and thermodynamic parameters can respond to the degree of hydrophobicity of the plate, but no distinct demarcation exists between the hydrophobic and hydrophilic solute-water interfaces. It is important to note that different hydrophobic plates used in this study are nonpolar in nature and just the increase of the plate(solute)-water Lennard-Jones interaction parameter changes the nature of the plate from hydrophobic to hydrophilic and visa versa. It is to note that the $\lambda = 1$ in the present study corresponds to solute water interaction of the well-known OPLS-UA force field and these forcefield values are not very far from the same from any other well-known force fields. The hydrophilic nature of the $\lambda = 1$ plate as demonstrated in the present study therefore raises a question about applicability of these force field parameters in modelling hydrophobic interfaces. Since it is well known that manifestation of hydrophobicity is length scale dependent, it is also important to know how these quantities vary with the length scale of the hydrophobic solutes and investigation in this direction is in progress.

In all these investigations as described in Chapters 2-5, we were involved in the modelling at the atomistic length scale. In many cases, where we deal with extended solid-water interfaces such as nanomaterial-water interfaces, modelling at the atomistic lengthscale may be computationally expensive and therefore use of a coarse-grained (CG) description might be beneficial. In this context, a spherically symmetrical two-length scale potential[134-137] has been found to reproduce almost all the anomalies of liquid water. In the next Chapter, we have used this coarse-grained description to study the hydration behaviour of one of the very important nanomaterial C_{60}.Using molecular dynamics simulation using CG potentials it is demonstrated how solvation characteristics of C_{60}change with the changes in the degree of attractiveness in the interaction between the atoms of the C_{60} and CG water.

Chapter 6

Effect of Temperature, Solvent Density and Hydrophobicity on the Solvation of Fullerene: A Coarse-Grained Description

6.1: Introduction

In recent years carbonaceous nanomaterials have found a wide range of applications in different areas as diverse as chemistry, chemical engineering, material science, nanotechnology etc. Among various carbonaceous nanomaterials, fullerenes and carbon nanotubes (CNTs) have found huge attention due to their many interesting physical and chemicalproperties[363-372] and wide applications in different fields ranging from nanoelectronics to nanotribology.It is proposed that fullerenes can be used in inhibiting HIV protease,[373,374]DNAcleaving,[375]and drug delivery.[370] Recently, applications of fullerenes in biomedicalimaging and bio-sensing are also gaining momentum.It is interesting to note that application of C_{60} in material science has also been considered recently. For example, incorporation of C_{60} into various materials such as polymers,[376]inorganic porous materials,[377]and organic supermolecules[378,379] has modified the structures and improved mechanical and other properties ofthese materials.

Applications of C_{60} in nanotechnology and nano-biotechnology are limited by inadequate knowledge of the hydration behaviour of C_{60} in physiological condition. It is a well-known problem that C_{60}forms aggregates in aqueous and many non-aqueous solvents and that poses a serious challenge in its applicability in physiological condition. It is well recognized that solvent behaviour at the fullerene-water interface determines solvation behaviour, knowledge of which, in turn, holds the key to understand the aggregation behaviour. As C_{60} is comprised of non-polar carbon atoms and of nanoscopic dimension, it is usual to consider C_{60}as a nanoscopic hydrophobic object and therefore understanding hydrophobic hydration and dewetting in aqueous solution of hydrophobic nanomaterial will shed light on the hydration of C_{60}. There are many investigations in the literature to understand hydrophobic hydration and dewetting phenomena at the nanoscopic length scale [19,114,380,314,381-385].In a series of investigations Choudhury and Pettitt[30,318,339] and Choudhury

[29,216,284] have shown how minute factors like solute-water van der Waals interaction, surface morphology and other related factors affect hydrophobic hydration behaviour. The hydration behaviour of C_{60} and potential of mean force between a pair of C_{60} in water has also been investigated recently[213-215]. Most of the above mentioned investigations are based on atomistic molecular dynamics (MD) simulations. Because of higher computational requirements in the atomistic MD simulation, these simulation studies were restricted to smaller lengthscales and shorter timescales. However, in order to understand aggregation behaviour properly, simulations with larger lengthscales and longer timescales are essential. A coarse-grained simulation, which can access larger lengthscale and longer timescale is a viable alternative. In a recent simulation study, coarse-graining of the fullerene in atomistic water is considered and it is shown to produce encouraging results.[213]In order to achieve computational economy further, simplification of the atomistic water model by a CG water model is required.

Water is an anomalous liquid and a good model of water should reproduce the anomalous properties of water. Most of the three-site atomistic water models do not reproduce these anomalies correctly. The reason for the anomalous properties of water is not clear till date and thus generated intense debate till recently.[42,78,88-93,260,386-388] Although water is a network forming liquid with tetrahedral local structure, a spherically symmetric two-lengthscale potential has been shown to reproduce anomalous properties of water quite well. Long back in 1970, Hemmer and Stell[134] first designed a pair potential by combining Lennard-Jones potential with a Gaussian peak to show that water like anomalies in two-dimension can be obtained from such a two-lengthscale potential, commonly referred to as core-softened (CS) potential. Since then, a large number of studies have been devoted to understand water-like anomalies in three-dimensions. Jagala[138,389,390] successfully developed a discontinuous ramp potential, which is able to describe water-like anomalies in three-dimensions. Using discontinuous potential in MD simulation is problematic and hence sincere effort has been devoted to develop a continuous version of the core-softened potential. After that, many continuous versions of the core-softened potential have been developed. Barbosa and co-workers[390] have used the same form of the CS potential as that of the Hemmer and Stellpotential with a suitable set of parameters and this potential is found to reproduce water-like anomalies. Using atomistic SPC/E model[51]of water, Errington*et al.*[71]have found a cascade of anomalies involving structural, thermodynamic, and dynamic quantities. The Hemmer-Stell model with a suitable parameterization as shown by Barbosa and coworkers[391,392,393] is also able to reproduce the same cascade of anomalies.

As all these CG water models are simpler and also can reproduce water-like anomalies quite well, their use in understanding solvation behaviour of various solute-solvent systems is desirable. In fact, recently many studies have been reported in the literature showing that these CG water model can capture some of the salient features of confined fluids[391], fluids in nanopores[392] etc. In the present work we intend to study the hydration behaviour of C_{60} fullerene in this CG water.

6.2: Models and methods

In the present work, we represent water by a spherically symmetric model potential of the form of Hemmer and Stell[134] potential, which is described by the combination of Lennard-Jones and Gaussian functions. The form of this model potential in dimensionless form can be given as,

$$U(r) = 4\left[\left(\frac{\sigma}{r}\right)^{12} - \left(\frac{\sigma}{r}\right)^{6}\right] + a\exp\left[-\frac{1}{c^2}\left(\frac{r-r_0}{\sigma}\right)^2\right], \qquad (6.1)$$

where, *a* and *c* respectively are dimensionless parameters associated with the height and width of the Gaussian part of the potential. The parameter σ in the above equation is the usual size parameter. This form of potential with a soft core is usually referred to as core-softened potential. We have considered a=5.0, c=1.0 and r_0/σ=0.7, which represents a two length scale potential, with a shoulder. This potential of water represents most of the structural, dynamic and thermodynamic anomalies of real water.[363,364] The C_{60} fullerene molecule is however described by atomistic model in which a C_{60} molecule consists of sixty carbon atoms. Each carbon atom of the C_{60}molecule is modelled as uncharged sp^2 carbon atom of the AMBER forcefield. The interaction potential $U_{uv}(r)$ between the particles of the solute and the solvent is modelled by

$$U_{uv}(r) = 4\left[\left(\frac{\sigma}{r}\right)^{12} - \lambda\left(\frac{\sigma}{r}\right)^{6}\right], \tag{6.2}$$

using Lennard-Jones interaction with variable attractive interaction. Here the parameter λ tunes the attractive interaction between the atoms of the C_{60} with the CG water and thus dictates hydrophobicity of the C_{60}molecule. The solute-solvent potential $U_{uv}(r)$ with λ=0 represents a purely repulsive C_{60}-water system with maximum hydrophobicity and that with λ=1 corresponds to full van der Waals dispersion interaction corresponding to AMBER force filed parameter for sp^2 carbon atom and SPC/E model of water oxygen atom. The solvent-solvent interaction potential $U_{vv}(r)$ and the solute-solvent interaction potential $U_{uv}(r)$ with λ=0 and λ=1 are shown in Figure.6.1 (a) and (b) respectively. First, a box of solvent molecules corresponding to a particular density ρ* is simulated in NVE ensemble and the temperature of the system is fixed by velocity scaling method. During simulation, periodic boundary conditions and minimum image conventions have been employedin *x*-, *y*- and *z*-directions. In each simulated system, the velocity scaling is performed in the first 50000 steps and after that velocity scaling is removed. After the equilibration of a cubic solvent box of a particular density ρ* at a particular temperature T*, the C_{60} molecule was inserted at the middle of the box. All the overlapping solvent molecules were removed. The C_{60} molecule is rigid and has been held fixed at the middle of the box. The composite C_{60}-solvent system was equilibrated in the same way as mentioned above. A snapshot of the simulation system is shown in Figure. 6.2. Finally, a production run of 600000 steps were performed.

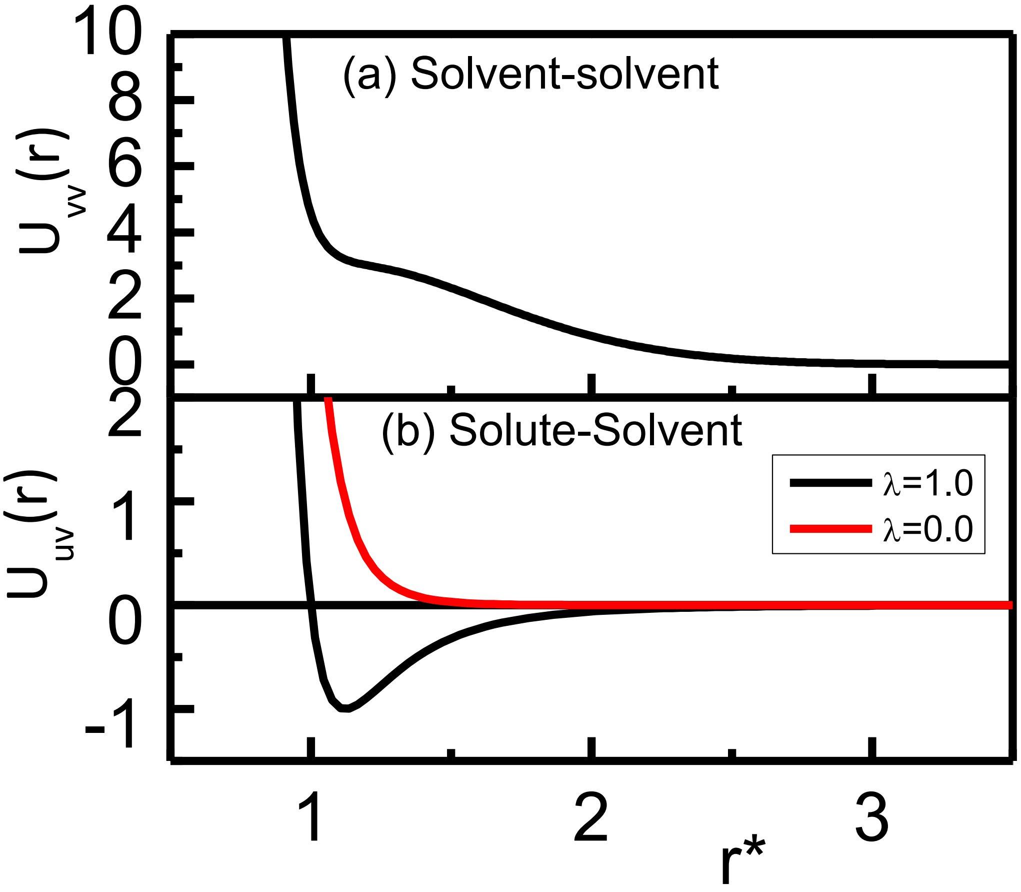

Figure. 6.1. Interaction potential between (a) two CG water molecules interacting with core-softened model potential [cf. Eq.(6.1)] and (b) a carbon atom of C_{60} and the CG water molecule [cf. Eq. (6.2)].

In these works, all the quantities are expressed in reduced units. The reduced quantities for distance, potential energy, temperature, pressure, density of particles and time step respectively are defined as follows,

$$r^* = r/\sigma_{vv}, U^* = U/\varepsilon_{vv},$$
$$T^* = k_B T/\varepsilon_{vv}, P^* = P\sigma_{vv}^{\ 3}/\varepsilon_{vv},$$
$$\rho^* = \rho\sigma_{vv}^{\ 3}, dt^* = dt\left(\frac{\varepsilon_{vv}}{m_{vv}\sigma_{vv}^{\ 2}}\right)^{1/2},$$

where the symbols with subscript *vv* represent solvent parameters.

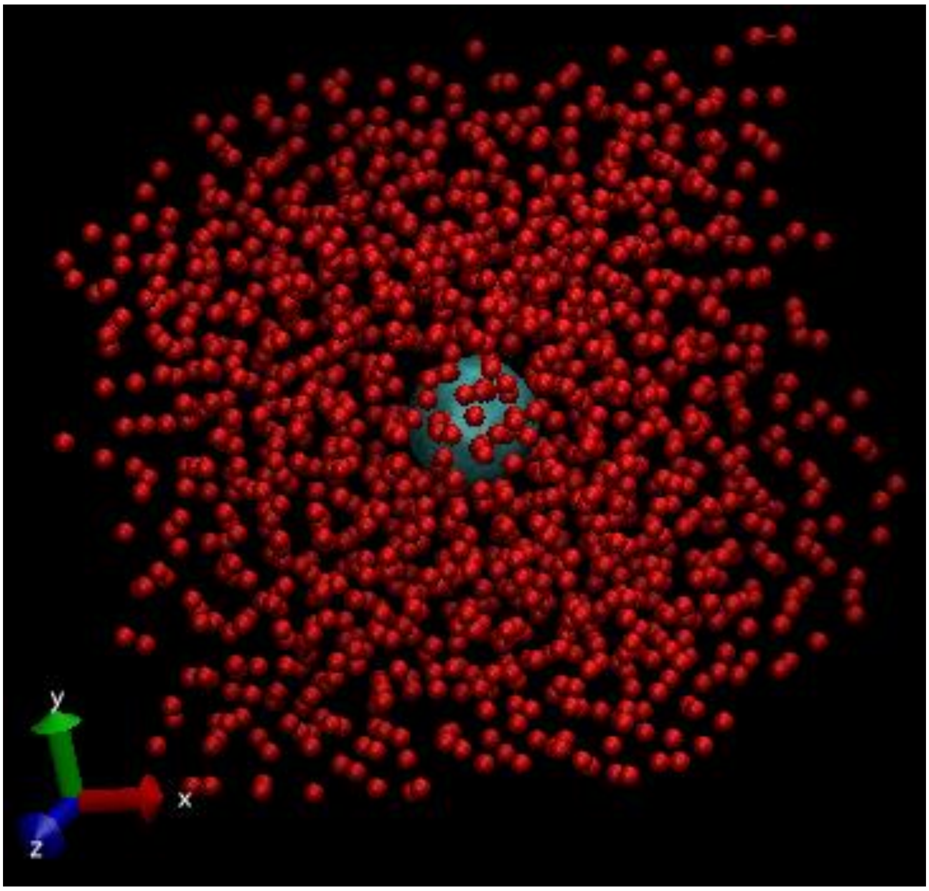

Figure. 6.2. Snapshot of a typical configuration of a box of CG water with a C_{60} molecule in it.

6.3: Result and discussion

In this study, we are concerned about the solvation of a nonpolar molecule C_{60}molecule in coarse-grained water. The local radial density of the solvent around the solute C_{60} is estimated by calculating radial distribution $g_{C60\text{-}water}(r)$ of the solvent molecules around the solute C_{60}. First, we shall discuss the case of, in which the interaction between the atoms of the C_{60} and the CG water is taken to be LJ interaction corresponding to the cross parameters obtained by combining parameters of SPC/E oxygen (for CG water) and Girifalco parameterized[393] sp^2 C atom of the C_{60} molecule using Lorentz-Berthelot mixing rule. In Figure.6.3, we have shown the radial distribution functions (RDFs) of CG water molecules around the C_{60} molecule i.e. $g_{C60\text{-}water}(r)$ at four different temperatures viz., T*=0.25, 0.5, 2.5, 3.0 and four different solvent densities namely, ρ*=0.07, 0.12, 0.16, 0.24 at each temperature.

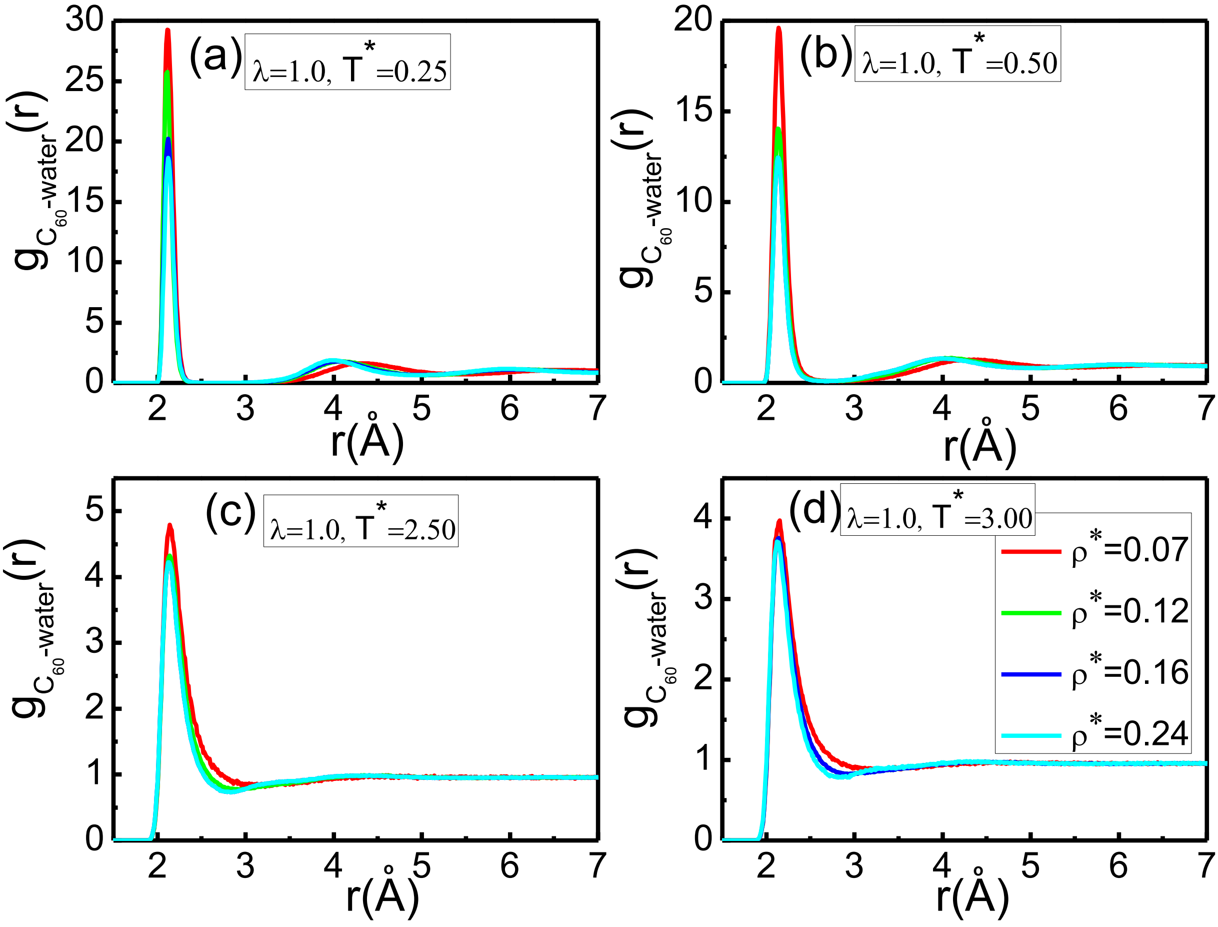

Figure. 6.3. Radial distribution of CG water around the C_{60} molecule at four different temperatures and at different densities.

It is interesting to observe (see Figure. 6.3(a)) that at lowest temperature considered here i.e. T*=0.25for all thefour bulk solvent densities considered, there is a region of “zero water density" between the first and the second peaks of the density profile. So, there exists a region between the first and the second solvation shells where average solvent density is zero. It suggests a solid like behavior. At this bulk density, the density of water at the surface of the C_{60} is almost 30 times as large as that of the bulk density. When the temperature is slightly increased from T*=0.25 to T*=0.50, the RDFs follow (see Figure. 6.3(b)) the same trend as in case of T*=0.25. However, now the first peak is wider and the peak heights are smaller as compared to the T*=0.25 cases. Also, the zero density region between the first and the second peaks of the RDF has been reduced. When the temperature is significantly increased from T*=0.50 to T*=2.5 and 3.0, a distinct change in the appearance of the RDF is observed (see

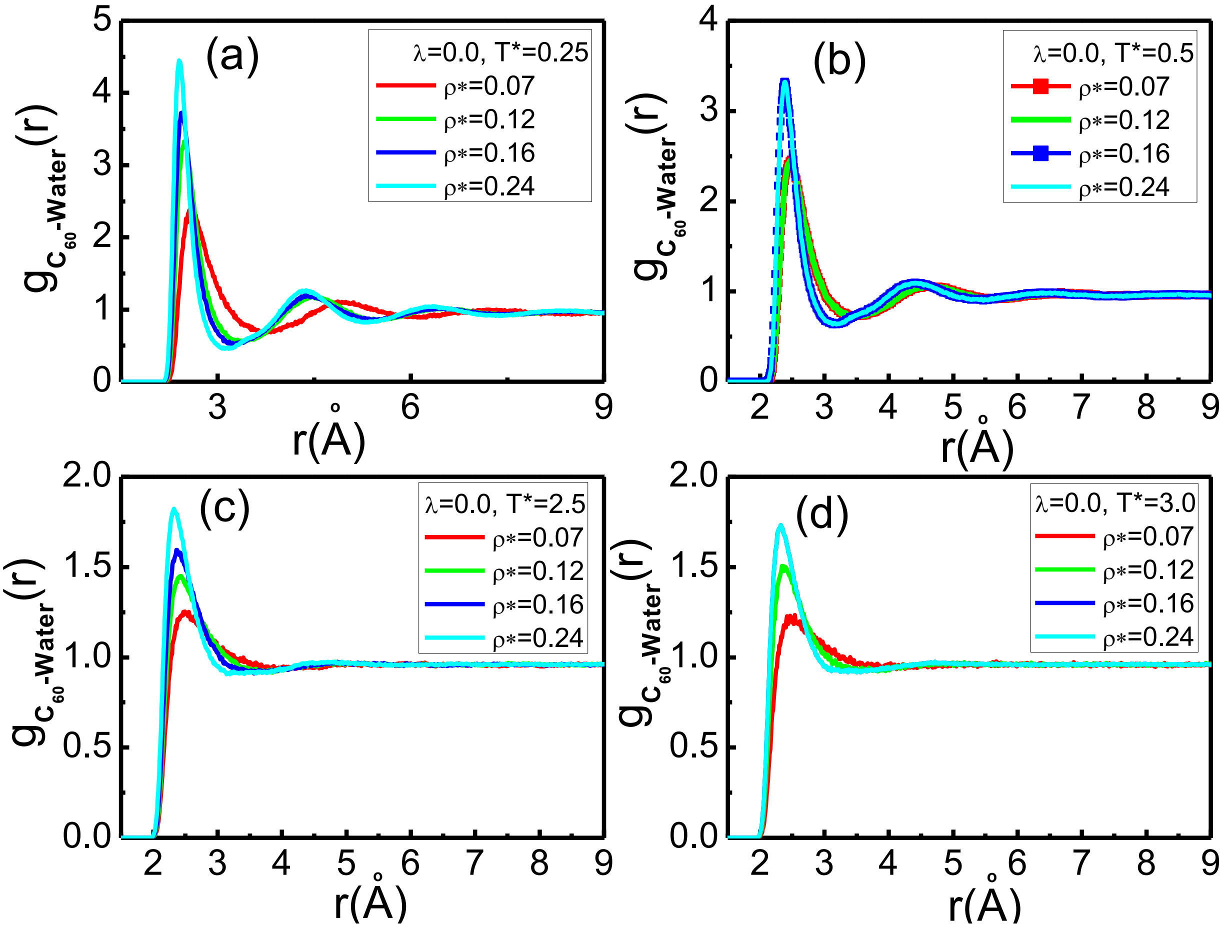

Figure 6.4.Radial distribution functions of CG water around the C_{60} molecule at four different temperatures and at four different densities for repulsive solute (λ=0 case).

Figure.6.3(c) and (d)). Now the trough between the first and the second peak of the RDF has non-zero density and the nature of the RDF is like that of a liquid. Except ρ*=0.07 case, in all other densities, the RDFs are almost coincident. It is important to notice that at all temperatures, as the bulk density of the solvent is increased, the height of the first peak of the C_{60}-water RDF decreases.

In order to check how solvent particles are distributed around a purely repulsive solute (λ=0), we have again estimated the RDF of water around the repulsive C_{60} solute from our simulation of repulsive C_{60} in water. We have shown in Figure. 6.4, the RDFs at four different temperatures and different densities as above but for the C_{60}-water interaction to be purely repulsive [cf. Equation (6.2) with λ=0]. Here all the RDFs are showing normal liquid-like characteristic with the trough between the first and the second peaks being nonzero. At lower temperatures, oscillations in the RDF representing locally ordered structure are more pronounced as compared to those at higher temperatures. The most striking difference of these RDFs with those in Figure6.3 is that in the first (λ=1) case, first peak of the RDF was decreasing with increasing bulk densities, whereas in case of λ=0 exactly the opposite trend is observed.

From this opposing trend in the peak heights of the RDFs for λ=0 and λ=1 cases, it may appear that as the bulk solvent density is increasing, the accumulation of water around the C_{60} is increasing the case of attractive solute (λ=1), whereas it is decreasing in case of repulsive solute. In order to verify that, we have calculated from the simulation trajectory the average number $\langle N \rangle_{\text{1st shell}}$ of water molecules in the first solvation shell for both λ=1 and λ=0 cases and these are shown in Figure. 6.5 as a function of bulk density ρ* for different temperatures. Here it is found that in both the cases at all temperatures, average number of solvent molecule in the 1st solvation shell is increasing with increasing bulk density of the solvent. It is easy to understand that an RDF in normalized with respect to individual bulk density and $< N >_{1stshell} = 4\pi\rho_0 \int_0^{r_0} g(r)\, r^2 dr$, where r_0 is the outer boundary of the first solvation shell and ρ_0 is the bulk solvent density. Therefore a smaller peak in RDF can produce larger N due to larger value of bulk density. At a particular solvent density as expected, average number of the solvation shell molecules is decreasing with the increase in temperature.

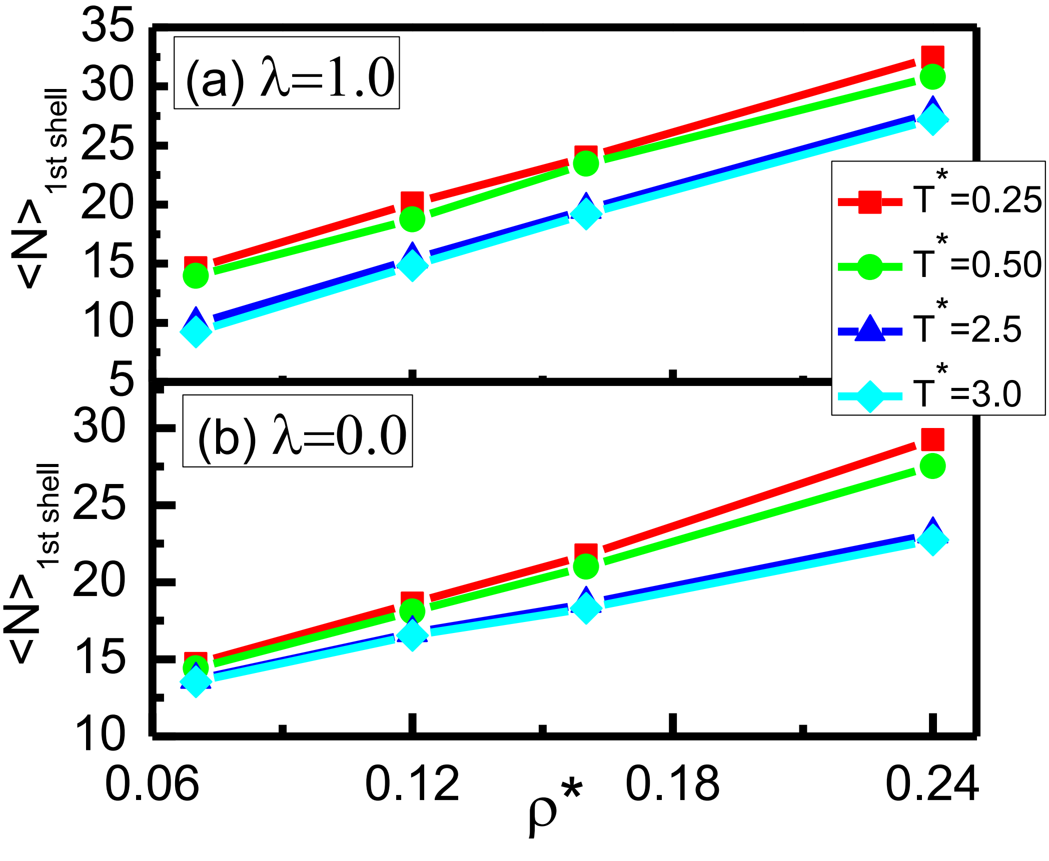

Figure 6.5.Average number $<N>_{1st\ shell}$ of solvent molecules on the first solvation shell of C_{60} for (a)λ=1 and (b) λ=0.

Another quantity which may be important in such an analysis is the nature of fluctuation of the number of molecules in the first solvation shell, κ, calculated as $\kappa = \left[\frac{< N^2 > - < N >^2}{< N >}\right]$,

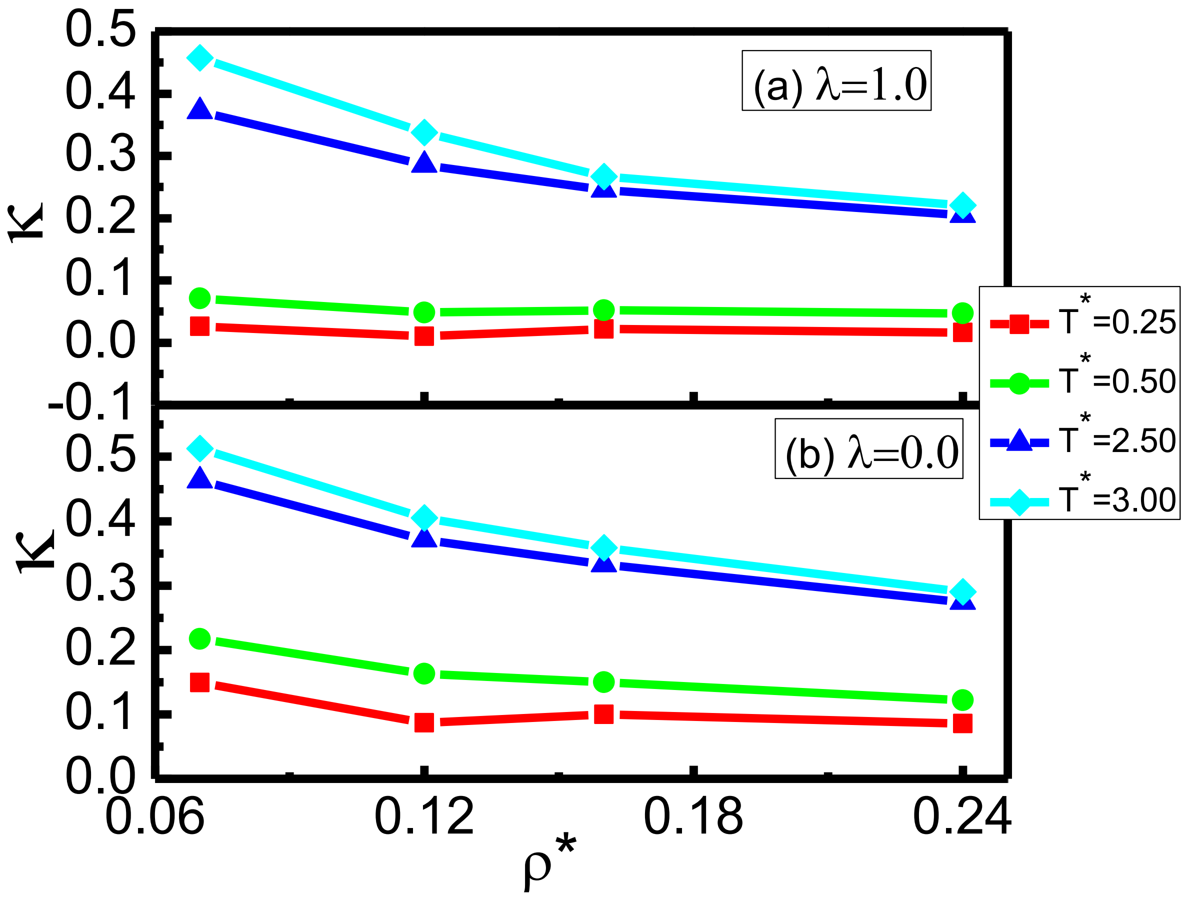

Figure 6.6. Fluctuations in the number of solvent molecules in the first solvation shell of C_{60} for (a)λ=1 and (b) λ=0.

where N is the number of particles in the 1st solvation shell an angular bracket denotes ensemble average. In Figure. 6.6, we have plotted this quantity as a function of density for different temperatures and for λ=1 and λ=0. A careful look at the fluctuation values shows that in general the fluctuation is more (see lower panel of Figure. 6.6) around the repulsive (λ=0) solute as compared to that around an attractive ((λ=1) solute. This nature is consistent with more hydrophobic nature of the solute with repulsive interaction. In both the λ=1 and λ=0 cases, at a particular density fluctuation at lower temperatures is less as compared to the same at higher temperatures. It is also interesting to note that the change in fluctuation due to change in temperature is more at lower densities as compared to the same at higher densities.

At a particular T*, as the density is increased, fluctuation decreases. This behavior is prominent at higher temperatures. Similar behaviour of fluctuations near large hydrophobic surfaces has been studied by Hummer et. al.

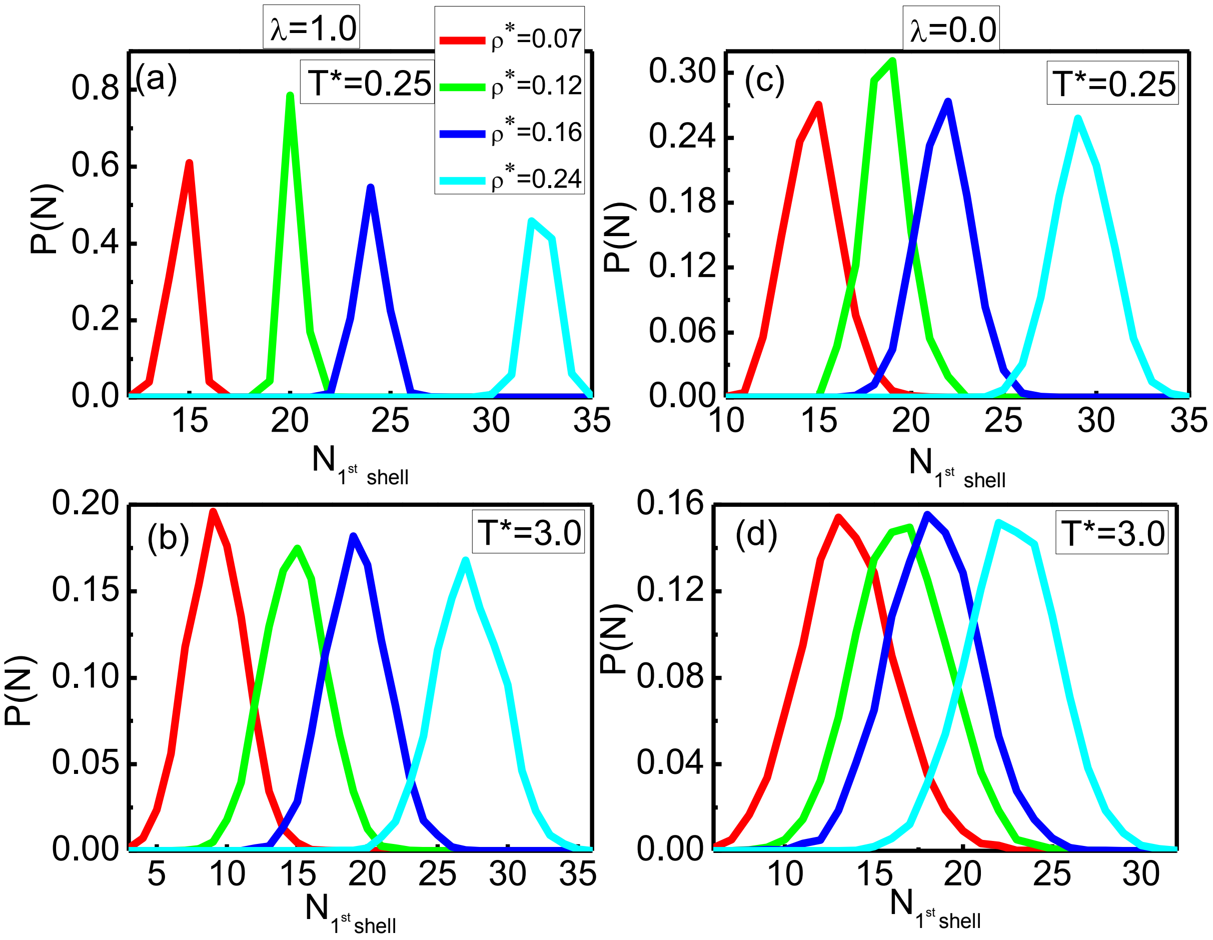

Figure 6.7.Distributions of solvent molecules in the first solvation shell of C_{60}. In left panel distribution is shown for λ=1 at (a) T*=0.25 and (b) T*=3.0. In the right panel the same is shown for λ=0 at (c) T*=0.25 and (d) T*=3.0.

The distribution of the number of particles in the 1^{st} solvation shell also gives us idea about fluctuation. In Figure. 6.7, the probability distribution of occupying N number of solvent particles in the 1^{st} solvation shell for λ=1 and λ=0 at two different temperatures T*=0.25 and T*=3.0 are shown. It is evident from the width of the distribution that the fluctuation for λ=1(i.e. attractive solute-water interaction) cases is more than that of λ=0 (right panel) cases. For the lowest density ρ*=0.07, for λ=1, fluctuation is small as compared to the same for λ=0.

Now the question remains why the first peak height is decreasing with bulk density in case of λ=1 but it is increasing with bulk density in case of λ=0 (see Figures. 6.4 and 6.5). The RDFs presented in the Figures. 6.3 and 6.4 are the distribution ($\rho(r)\sigma^3$) of solvent particles normalized by bulk density ρ_0. If we look at the un-normalized g(r) or $\rho(r)\sigma^3$ at T*=0.25 for the minimum and the maximum bulk densities (ρ*=0.07 and 0.24) considered here it is evident that for both λ=0.0

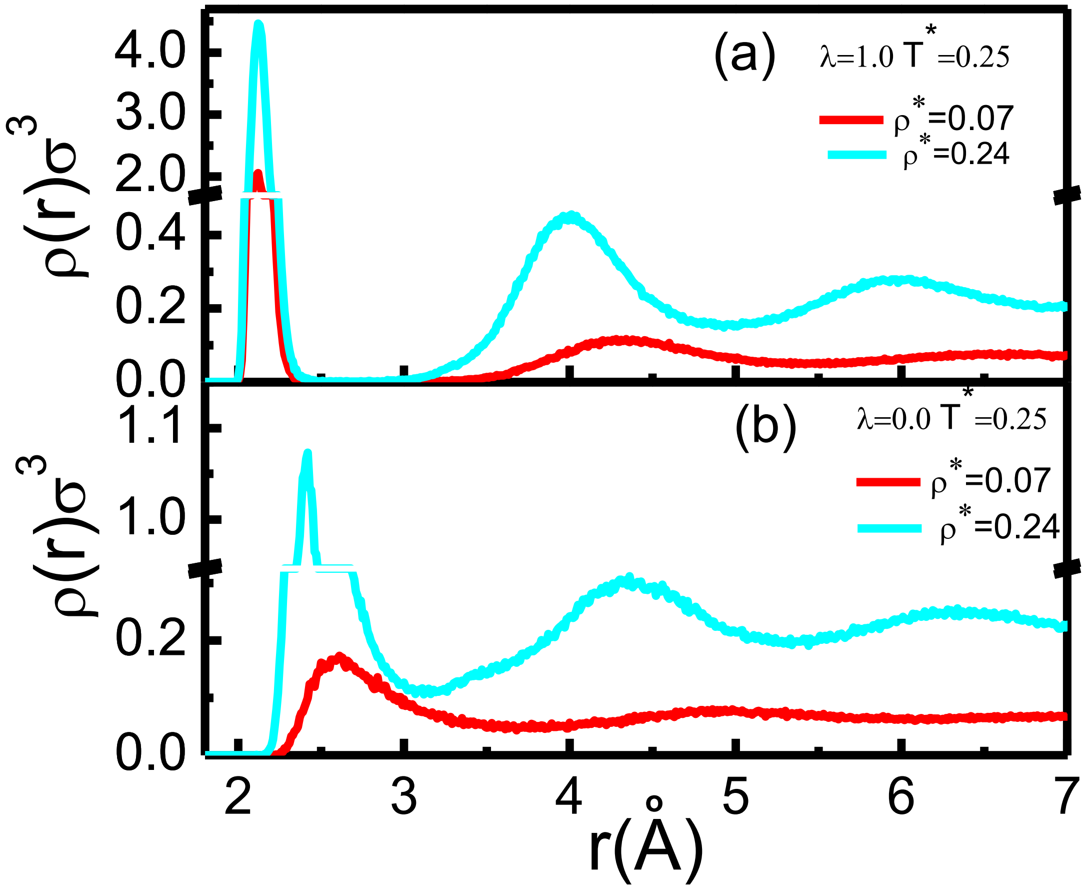

***Figure 6.8.**Density distributions $\rho(r)\sigma^3$or the un-normalized $g_{C60\text{-}water}(r)$ of solvent molecules around the solute C_{60} at T*=0.25 and at two different bulk densities ρ*=0.24 and 0.07.Top panel is for λ=1 and the bottom panel is for λ=0.*

and 1.0 [see Figure. 6.8(a) and (b)] the peak height of the actual distribution ($\rho(r)\sigma^3$) increases with increasing bulk density. Now if we look at the ratio of the peak heights at this two densities for λ=1, we find it to be ~4.5/2.0=2.25, whereas the corresponding bulk density ratio is 0.24/0.07=3.43. Thus the proportion in which bulk density is increased, the solvent density around the solute is not increasing in the same proportion. Hence, while normalizing by bulk density to get $g_{C60\text{-}water}(r)$ the trend becomes opposite (i.e. peak height decreases with bulk density). Now if we look at the Figure 6.8(b) which is for λ=0, the ratio of the peak heights is 1.07/0.17=6.3, but the ratio of the bulk densities is 3.43.Thus by dividing with bulk density in $g_{C60\text{-}water}(r)$ we do not find any change in trend (i.e. peak height increases with increase in bulk density) with the increase in bulk density.

Second question that arises from the careful observation of $g_{C60\text{-}water}(r)$ as shown in Figure. 6.3 and 6.4 is that why in case of λ=1, and at lower temperatures, a region exists between the first and the second solvation shells where no solvent molecules exist. In order to explain it we first observe that the RDF in the first peak region is very sharp and narrow in these cases and also the fluctuations in number of solvent particles in these low temperature cases are also very small signifying that almost same number of particles occupying almost the same spatial region around the C_{60} molecule throughout the simulation time, i.e. almost a solid-like layer is formed around the C_{60} molecule. Now if we look at the solvent-solvent g(r) distribution of particles

6.4: Summary and Conclusions

In this work, we have presented molecular dynamics simulation results on different aspects of solvation behaviour of a C_{60} molecule in CG water. Two cases with different C_{60}-water interactions have been considered here. In one case (λ=0) the interaction between an atom of $C_{60}$and the CG water molecule is considered to be purely repulsive and in another case (λ=1)the interaction is considered to be Lennard-Jones interaction consisting of repulsive and attractive van der Waals interactions. We observed distinct features of the hydration behaviour of C_{60} in these two cases. The effects of temperatures and pressures have also been investigated. For λ=1, it is found that the height of the first peak of the C_{60}-water RDF is decreasing with increasing bulk density and on the contrary for λ=0, the peak height is increasing with the increasing bulk density. It is somewhat surprising. However when we checked the average number of solvent molecules in the first solvation shell of the C_{60}, it is found that the number of neighbors are increasing with the increase in density irrespective of the value of λ. Further analysis of the un-normalised radial distribution function also shows that the density peak is actually increasing with the increase of bulk density in both the cases. The reversal of the peak heights in case of λ=1 is due to the fact that the proportion in which bulk density is increased, the local density near the fullerene surface is not increasing in that proportion. Most likely, in this case, since the first solvation layer is very close to the C_{60} surface with very less positional fluctuations due to C_{60}-water attractive interaction, accommodation of more number of solvent molecules in the first solvation shell due to increase in bulk density is somewhat restricted. On the other hand, in case of λ=0, where the first solvation shell has higher radius and more positional fluctuations, with the increase of bulk density more and more water molecules are pushed into the first solvation shell. It is observed that at lower temperatures, fluctuations (κ) in the number of molecules in the first solvation shell is small and as the temperature is increased κ increases. At lower temperatures, with the increase of bulk density, fluctuations almost remain the same, but at higher temperatures, fluctuations decreases with increase in bulk density. Further studies in progress to calculate the potential of mean force between two C_{60} molecules in the CG water.

Chapter 7

Summary and Future Directions

Water is an intriguing liquid and it becomes more interesting when it meets an interface. Many of the interesting phenomena originate from the mysterious interfacial waters and understanding such phenomena requires adequate knowledge of various structural and dynamical characteristics of bulk water. It is well known that water has many anomalous properties and it is important to note that even after a tremendous amount of research on understanding the anomalous properties of bulk water, many of its anomalous behaviors are either ill understood or remain debatable.[78,386-388,395,396]Our main focus in this thesis is to understand manifestation of various properties of water in three different situations, namely (i) water in bulk (ii) water in contact with molecular interfaces and (iii) water at nanoscopic interfaces. Details of the issues covered in different chapters of this thesis are described below.

In **Chapter1**, the present thesis starts with a very general introduction about the importance and application of water in numerous fields. This chapter clearly points out the importance of studying different microscopic variables of water both structurally and dynamically which actually governs macroscopic properties of water. Molecular dynamics simulation has been used as a theoretical tool for the entire studies. This chapter also covers a small description of classical statistical mechanics. Combination of these two subjects makes enable one to gauge thermo-physical, structural and dynamical properties of fluids in various state points. Finally, in the last part of the Chapter 1, the nature and scope of the present thesis is discussed.

Enormous application and colossal importance of water in almost all the fields of science and technology are strongly correlated with it’s number of anomalous properties. Among these, density anomaly is the most well known one. Significant work has been devoted to understand the origin of density anomaly. However, contradictory observations and predictions about this exploration have made this field ever challenging. **Chapter 2** of this thesis deals with the investigation of structural aspects of liquid water at ambient pressure to understand the origin of its density anomaly. The computed results for various structural parameters and properties as a function of temperature as obtained from different atomistic water models are found to be significantly different which is one of the major hurdles in said investigation. In this chapter, a new yardstick (average number of hydrogen bonds), which is able to correlate apparently disparate results from all these water models has been established. On the basis of this newly defined yardstick, a new definition of 1st solvation shell of a water molecule in the bulk water has been introduced. This work clearly demonstrates the fact that competitive effects of thermal expansion and contraction due to angular distortion are the deciding factors to exhibit density anomaly of water. The present work clearly illustrates the fact that density anomaly of water at ambient pressure can be explained without invoking the concept of structural and density inhomogeneity of water. The same yardstick has been explored to correlate dynamical properties too. However, similar correlation among the results on dynamical properties of water arising from different water models in terms of average number of hydrogen bonds has not been observed.

Heavy water is an important material in view of its relevance in nuclear, chemical, medical and pharmaceutical industries. Theoretical predictions about properties of heavy water at ambient and extreme condition by using Molecular dynamics simulation is restricted by the absence of a suitable atomistic model of heavy water. A three-site SPC/HW heavy water model has been proposed earlier. Although this model is shown to reproduce properties of heavy water at ambient condition quite accurately, its applicability has never been tested beyond the ambient condition. In **Chapter 3**, the applicability of this model has been checked in the range of 223K to 360K at ambient pressure by calculating various thermophysical properties and comparing them with the available experimental or literature values. The comparative study shows that, the SPC/HW model although reproduces experimental data for heavy water at room temperature appreciably well, however it largely fails at lower range of temperatures. A comparative study of different thermophysical and structural properties of D_2O (SPC/Hw) and H_2O (SPC/E) has also been presented. Finally, the effect of various potential parameters such as molar mass and partial charges on atoms on the results has been estimated and the findings can act as a guide for further development of a new model for heavy water.

The interface may arise due to solvation of different solute molecules in water or due to physical contact of water with a large extended solid surface. The physical or chemical environment around water molecules differs appreciably than that of bulk water. Hence, structure, dynamics and thermodynamic properties are considerably modified in the vicinity of interfaces. In the case of molecular interfaces, it is interesting to know whether structural integrity of water will be retained or not in presence of such molecular interfaces. In this connection, structural information of two molecular interfaces namely that of urea-water and guanidinium chloride (GdmCl)-water are extremely important as these two interfaces are relevant to protein denaturation. The **Chapter 4** of this thesis deals with the structural and dynamical aspects of these interfaces and its relevance in elucidating role of water in the underlying mechanism of protein denaturation. This chapter is divided into two parts. In **Part A**, various structural and dynamical properties of water in the urea-solution have been investigated at different concentration. By calculating various order parameters that gauge the structural integrity of water, it has been demonstrated that tetrahedral and hydrogen bonding structure of water remain unaffected at least up to the concentration of 9M urea. Exploration of the dynamical features of the aqueous urea solution reveals that with increasing concentration of urea, translational diffusivity decreases considerably, whereas the rotational dynamics remains almost unaltered with the increasing urea concentration.

The **Part B** of this chapter has dealt with another molecular interface created due to solvation of guanidinium (Gdm) chloride, another very useful chemical denaturant of protein, in water. The In **Part B,** primarily the effect of increasing concentration of guanidinium chloride (GdmCl) on the structural and dynamical properties of water has been vividly investigated. The two major issues, one dealing with the staked ion-pair formation of the Gdm moieties and the other on the influence of guanidinium ion on the tetrahedral and hydrogen bonding structures of water in the aqueous solution of GdmCl, have been explored. This study clearly illustrates that water structure is not significantly perturbed by the presence of GdmCl. The finding from this study supports the so-called direct mechanism of protein denaturation according to which Gdm moieties of the denaturant directly attacks the similar (arginine) moieties of the protein in parallel-staking orientation. In order to confirm the above observation, one polypeptide has been introduced into the aqueous solution of Gdmcl and the outcome clearly confirms the existence of such staking between the Gdm ion and the arginine moiety of the peptide. This study also shows that such parallel staking orientations (of the arginine moieties) can be observed in case of temperature denaturation of an arginine based peptides. Apart from these, various dynamical properties at different concentrations of the GdmCl have also been calculated as a function of concentration.

Manifestation of various properties of water at a nanoscopic or larger interface formed by water and a large surface is dramatically different from the same at the molecular level interface. Hydrophobic interaction originates when water comes in the vicinity of hydrophobic substance. Hydrophobicity plays a significant role in terms of bio-macromolecular stability and protein folding. However, measuring hydrophobicity of such a nanoscopic interface using the conventional method of measuring contact angle is rather difficult and therefore defining new order parameters to estimate hydrophobicity at the nanoscale is essential. The **Chapter 5** of this thesis deals with the characterization of hydrophobicity at the nanoscale. For this, a nanoscopic paraffin like plates dipped into water has been simulated and its hydrophobicity has been tuned by altering the attractive part of plate-water dispersion interaction. The changes on various structural parameters have been estimated as a function of degree of hydrophobicity. In this work, few order parameters, each one of which can be a promising descriptor to gauge the hydrophobicity at the nanoscale are identified.

Chapters 2-5, atomistic lengthscale models have been used for md study. In many cases, where one needs to estimate extended solid-water interfaces such as nanomaterial-water interfaces, modelling at the atomistic lengthscale may be computationally expensive and therefore use of a coarse-grained (CG) description might be economical one. In this context, a spherically symmetrical two-lengthscale potential has been found to reproduce almost all the anomalies of liquid water. **Chapter 6** of this thesis deals with the coarse-grained description to understand the hydration and dewetting behaviour of a very important nanomaterial C_{60}. Using molecular dynamics simulation, it is demonstrated how solvation characteristic changes with the changes in the degree of attractiveness in the interaction between the atoms of the C_{60} and CG water.

Water is one of the most important compounds on earth due to its innumerable uses in our daily life. Its extensive uses as solvents in numerous industrial and technological processes, as heating, cooling and cleaning agents make water an invaluable substance. From environmental point of view, water in seas, lakes and rivers acts as heat reservoirs and the evaporated water from these water bodies in the form of humidity largely controls the climate on the earth. On the other hand, existence of life in any form is intimately associated with water. In fact, the list describing importance of water is rather endless. As we have already mentioned in our previous chapters that remarkable properties of liquid water which make it such a versatile liquid must be interconnected to its local structure and dynamics. Hence exploration of water to understand its microscopic features is not a matter of choice but a necessity to appreciate and if possible to exploit various processes of nature. More we understand microscopic details of water, better we can predict, control or exploit various physical and chemical processes. In the last few decades a tremendous amount of research effort has been dedicated to understand microscopic behaviour of water in different bio-chemical and chemical processes. In the present scenario, with the advent of many sophisticated experimental tools and newer theoretical tools along with high performance super-computing machines, a marriage between experimental and theoretical research has become a reality. All these efforts will help us to comprehend water in a new light and if so, it will definitely lead us to a better world than where we are today.

The present thesis explored behavior of water in bulk and at different interfaces. Manifestation of different properties of water also changes when confined in nanoscopic channels and pores. The present work can be further extended towards understanding behavior of water and other fluids in nano-porous medium. Various structural and dynamical aspects of polar and non-polar fluids confined in a nanotube or nanopores can be studied.

Apart from water, which is used as solvent almost universally, now-a-days room temperature ionic liquids (RTIL) are also increasingly used as solvents in green chemistry. RTIL is comprised of organic molecules, each of which consists of a polar head group and a nonpolar alkyl chains. Depending on the length of the alkyl chain, theses RTIL can have structural micro-heterogeneity leading to many unique properties. It has the unique property of solvating both polar and nonpolar molecules. Currently we are investigating the solvation behavior of different polar and non-polar molecules in the RTIL and its correlation with the structural heterogeneity of the RTIL.

In Chapter 6, we have shown that a coarse-grained spherically symmetric model of water can be used to explore the solvation of nanoscopic solutes in water. In this description, we have considered atomistic description of fullerene along with CG water. This study can be further extended to include a coarse-grained description of fullerene in the CG water in one hand. On the other hand this CG description can further be extended to study flow of fluids through nanochannels and nanopores.

References

1. van Gunsteren, W. E.; Berendsen H. J. C. *Angew. chem. Int. Ed. Engl,* **1990***, 29*, 992-1023.
2. Karplus, M.; McCammon, J. A. *Nat. Struct. Biol*, **2002**, *9*, 646-652.
3. Nagaoka, M.; Okuno, Y.; Yamabe; T. *J. Phys. Chem.*, **1994**, *98*, 12506–12515.
4. Wang, J.; Hou, T. *J. Chem. Theory Comput.,* **2011**, *7* , 2151–2165.
5. Karplus, M.; Peetsko, G. A. *Nature,* **1990***, 347*, 631 – 639.
6. Palmer, J. C.; Debenedetti, P.G. *AIChE*, **2015**, *61*, 370-383.
7. Elliott, J. A. *Int. Mater. Rev*, **2011**, *56*, 207-225.
8. Andriantahina, F.; Liu. X.; Huang, H. *Acta Oceanologica Sinica*, **2015**, *34*, 59-65.
9. Nakata, H.; Kannan, K.; Nasu, T.; Cho. H.S.; Sinclair. E.; Takemurai, A. *Environ Sci Technol.* **2006,** *40*, 4916-4921.
10. Allen, M. P.; Tildesly, D. J. C*omputer simulation of Liquids* (Oxford Science, Oxford, **1987**).
11. Jorgensen, W. L.; Tirddo-Rives, J. *J. Am. Chem. Soc.*, **1988**, *110*, 1657-1666.
12. Franks, F. In *Water: A Comprehensive Treatise*; Plenum: New York, 1973; Vol. 2, pp 1-54.
13. http://www.cuchd.in/elibrary/resource_library/University%20Institutes%20of%20Sciences/Fundamentals %20of%20Biochemistry/Chap-02.pdf
14. Dill, K.; Truskett, T.; Vlachy, V.; Hribar-Lee, B. *Annu. Rev. Biophys. Biomol. Struct*., **2005**, *34,* 173−199.
15. Pradeep, K. *Phd Thesis*: *Anomalies of bulk, nanoconfined and protein-hydration water,* **2001**, Boston University.
16. Ball, P. *Chem. Rev*. **2008**, *108*, 74−108.

17. Bellissent-Funel. *Hydration Processes in Biology*, (M. M.C. IOS Press: Amsterdam, Netherlands, **1999**.)
18. Franks, F. *Water Science Review 3* (Cambridge University Press, Cambridge, **1985**.)
19. Chandler, D. *Nature*, **2005**, *437*, 640-647.
20. Hilser, V. J. *Nature*, **2011**, *469*, 166-167.
21. Rand, R. P.; Trans, R. P. *R. Soc. Lond*. **2004**, *359*, 1277–1285.
22. Bevendge, D. L.; Jorgensen, W. L. *Ann. N. Y Acad. Sci.*, **1986**, *482*, 269-286.
23. McCammon, J. A.; Harvev, *S* .C. *Cellular Regulation by Protein Phosphorylation.* (Spinger –verlag, Berlin, **1991**).
24. van Gunsteren, W. F.; Weiner, P. K. *Computer Simulation of Bio-molecular System.* (Escom, Leiden **1989)**.
25. Tarek, M.; Tobias, D. J. *Biophys. J* .**2000**, *79*, 3244–3257.
26. Bagchi, B. *Water in Biological and Chemical Processes: From Structure and Dynamics to Function* (Cambridge Molecular Science, **2014**).
27. Vogler, E. A. .*Adv Colloid Interface Sci*., **1998**, *74*, 69-117.
28. Ataka, K.; Yotsuyanagi, T.; Osawa, M. *J. Phys. Chem.*, **1996**, *100*, 10664–10672.
29. Choudhury, N. *J. Phys. Chem. B*, **2008**, *112*, 6296–6300.
30. Choudhury, N.; Pettitt, B. M. *J. Am. Chem. Soc.*,**2005**, *127*, 3556-3567.
31. Boecker, J.; Brickmann, J.; Bopp, P. *J. Phys. Chem.*, **1994**, *98*, 712–717.
32. Sorenson, J.M.; Hura, G.; Glaeser, R.M.; Head-Gordon, T. *J. Chem. Phys*., **2000**, *113*, 9149-9161 .
33. Soper, A.K. *Chem. Phys*., **2000**,*258*, 121-137.

34. Wilson. K.R.; Tobin, J.G.; Ankudinov, A.L.; Rehr, J.J.; Saykally, R. J. *Phys. Rev. Lett*., **2000**, *85*, 4289-4292.
35. Odelius, M. *J. Phys. Chem. A,* ***2009****,113,* 8176-8181.
36. Sturchio, N.C.; Chiarello, R. P.; Cheng, L.; Lyman, P. F.; Bedzyk, M.J.; Qian, Y.; You, H.; Yee, D.; Geissbuhler, P.; Sorensen, L. B. *Geochimicaet Cosmochimica Acta*, **1997**,*61*, 251-263.
37. Bosio, L.; Teixeira, J.; Stanley, H.E. *Phys. Rev. Lett*.,**1981**,*46* , 597-600.
38. Bosio, L.; Teixeira, J.; Bellissent-Funel. M.C. *Phys. Rev. A*, ***1989***, *39*, 6612-6613.
39. Clark. G.N.I.; Cappa. C. D.; Smith. J. D.; Saykally. R. J.; Head-Gordon. T. *Mol. Phys*, **2010**, *108*, 1415–1433.
40. Winsberg, E. *Philosophy of Science*,**2003**,*70*, 105–125.
41. Frenkel. D.; Smit. B. *Understanding Molecular Simulation* (Academic Press, **1996**).
42. Alder, B.J.; Wainwright, T. E. *J. Chem. Phys.* **1957**, *27*, 1208–1209.
43. Alder, B.J.; Wainwright, T. E. *J. Chem. Phys*, **1959**, *31*, 459-466.
44. Rahman, A. *Phys. Rev.*,**1964**, *136*, A405-A411.
45. Cornell, W. D.; Cieplak, P.; Bayly, C.I.; Gould, I.R.; Merz, K.M.; Ferguson, D. M.; Spellmeyer, D. C.; Fox, T.; Caldwell, J. W.; Kollman, P. A. *J. Am. Chem. Soc.,* **1995**,*117*, 5179–5197.
46. Mackerell, A. D.; Wiorkiewiczkuczera. J.; Karplus. M. *J. Am. Chem. Soc.,* **1995**, *117*, 11946-11975.
47. Jorgensen. W. L.; Maxwell. D. S.; Tiradorives, J. *J. Am. Chem. Soc.,* **1996**, *118*, 11225–11236.

48. Jorgensen, W. L. ; Chandrasekhar, J. ; Madura, J. D. ; Impey, R. W; Klein, M. L. *J. Chem. Phys*, **1983**, *79*, 926-935.
49. Neria, E.; Fischer, S.; Karplus, M. *J. Chem. Phys*., **1996**, *105*, 1902−1921.
50. Vanderploeg, P.; Berendsen, H.J.C. *J. Chem. Phys*., **1982**, *76*, 3271-3276
51. Berendsen, H. J. C.; Grigera, J. R.; Straatsma, T. P. *J. Phys. Chem*., **1987**, *91*, 6269-6271.
52. Abascal, J. L. F.; Vega, C. A *J. Chem. Phys*., **2005**, *123*, 234505-1−234505-12.
53. Mahoney, M. W.; Jorgensen, W. L. *J. Chem. Phys*., **2000**, *112*, 8910−8922.
54. Pollock, E. L.; Alder, B. J. *Physica*, **1980**, *102*, 1-21.
55. Ewald, P. .*Ann. Phys.,***1921**, *369*, 253–287.
56. Ewald, P. *Ann. Phys.,***1921**,*64*, 253-287.
57. Darden, T.; York, D.; Pedersen, L. *J. Chem. Phys.,***1993**, *98*, 10089–10092.
58. Verlet, L. *Phys. Rev*., **1967**, *159*, 98-103.
59. Hockney, R. W. *Meth. Comput. Phys.,***1970**, *9*, 136–211.
60. Forester, T. R.; Smith, W. *J. Comp. Chem.*, **1998**, *19*, 102–111.
61. Hess, B.; Bekker, H.; Berendsen, H. J. C.; Fraaije, J. G. E. M. *J. Comp. Chem.*, **1997**, *18*, 1463–1472.
62. Berendsen, H. J. C.; Postma, J. P. M.; van Gunsteren, W. F.; DiNola, A.; Haak, J. R. *J. Chem. Phys.*, **1984**, *81*,3684.
63. Bussi, G.; Donadio, D.; Parrinello. M. *J. Chem. Phys*., **2007**, *126*, 014101-(1-8).
64. Nose, S. *Molec. Phys.*, **1984**, *52*,255–268.
65. Parrinello, M.; Rahman, A. *J. Appl. Phys*., **1981**, *52*, 7182-7190.
66. McQuarrie, D. A. *Statistical Mechanics* (University Science book, **1975**).

67. Hansen, J. P.; McDonald, I. R. *Theory of Simple Liquids*, 2nd ed. (Academic, London, **1986)**.
68. Bassez, M. P.; Lee. J.; Robinson, G. W. *J. Phys. Chem.*, **1987**, *91*, 5818–5825
69. http://www1.lsbu.ac.uk/water/water_anomalies.html.
70. Mallamace, F.; Branca, C.; Broccio, M.; Corsaro, C.; Chung-Yuan, M.; Chen, S. *Proc. Natl. Acad. Sci. U.S.A.*, **2007**, *104*, 18387–18391.
71. Errington, J. R.; Debenedetti, P. G. *Nature*, **2001**, *409*, 318-321.
72. Mishima, O.; Stanley, H. E. Water. *Nature*, **1998**, *396*, 329–335.
73. Kumar, P.; Buldyrev, S. V.; Stanley, H. E. *Proc. Natl. Acad. Sci. USA.*, **2009**, *106*, 22130-22134.
74. Giovambattista, N.; Stanley, H. E.; Sciortino. F. *Phys. Rev. E,* **2005**,*72*, 031510(1-12).
75. Yan, Z.; Buldyrev, S. V.; Kumar, P.; Giovambattista, N.; Debenedetti, P. G.; Stanley, H. E. *Phys. Rev. E,* **2007**, *76*, 051201.
76. Matsumoto, M. *Phys. Rev. Lett.,* **2009**, *103*, 017801 (1-4).
77. Nayar, D.; Agarwal, M.; Chakravarty, C.*J. Chem. Theory Comput.*, **2011**, *7*, 3354–3367.
78. Debated waters, editorial, *Nat. Mater.*, **2014**, *13*, 663.
79. Pi, H. L.; Aragones, J. L.; Vega, C.; Noya, E. G.; Abascal, J. L. F.; Gonzalez, M. A. McBride. C. *Mol. Phys.*, **2009**, *107*, 365–374.
80. Horn, H. W.; Swope, W. C.; Pitera, J. W.; Madura, J. D.; Dick, T. J.; Hura, G. L.; Head-Gordon, T. *J. Chem..Phys.*, **2004**, *120,* 9665 (14).
81. Russo, J.; Romano, F.; Tanaka, H. *Nat. Mater.*, **2014**, *13*, 733-739.
82. Jensen, F. *Introduction to Computational Chemistry*. (press: JOHN WILEY & SONS, **1999**)

83. Shevchuk, R.; Prada-Gracia, D.; Rao, F. *J. Phys. Chem. B,* **2012**, *116,* 7538-7543.

84. Poole, P.; Sciortino, F.; Essmann, U.; Stanley, H. E. *Nature,* **1992**, *360,* 324–328.

85. Speedy, R. *J. Phys. Chem*., **1982**, *86,* 982–991.

86. Stanley, H. E.; Teixeira, J. *J. Chem. Phys.,* **1980**, *73*, 3404–3422.

87. Soper, A. K.; Ricci, M. A. *Phys. Rev. Lett*., **2000**, *84, 2881–2884.*

88. Huang, C.; Wikfeldt, K. T.; Tokushima, T.; Nordlund, D.; Harada, Y.; Bergmann, U.; Niebuhr, M.; Weiss, T. M.; Horikawa, Y.; Leetmaa, M.; Ljungberg, M. P.; Takahasi, O.; Lenz, A.; Ojamae, L.; Lyubartsev, A. P.; Shin, S.; Pettersson, L. G. M.; Nilsson, A. *Proc. Natl. Acad. Sci. U.S.A.,* **2009**, *106*, 15214−15218.

89. Clark, G. N. I.; Hura, G. L.; Teixeira, J.; Soper, A. K.; Head- Gordon, T. *Proc. Natl. Acad. Sci. U.S.A.,* **2010**, *107*, 14003−14007.

90. Head-Gordon, T. *Proc. Natl. Acad. Sci. U.S.A.,* **1995**, *92,* 8308-8312.

91. Sedlmeier, F.; Horinek, D.; Netz, R. R. *J. Am. Chem. Soc.,* **2011**, *133,* 1391–1398.

92. Cuthbertson, M. J.; Poole. P. H. *Phys. Rev. Lett.,* **2011**, *106*, 115706 (1-4).

93. English, N. J.; Tse, J. S. *Phys. Rev. Lett.,* **2011**, *106*, 037801(1-4).

94. Overduin, S. D.; Patey, G. N. *J. Phys. Chem. B,* **2012**, *116*, 12014−12020.

95. Xu, L; Kumar, P.; Buldyrev, S. V.; Chen, S-H; Poole, P. H.; Sciortino, F.; Stanley, H. E. *Proc. Natl. Acad. Sci. USA,* **2005**, *102*, 16558–16562.

96. Stillinger, F. H. *Science,* **1980,** *209*, 451-457.

97. Grigera, J. R. *J. Chem. Phys*., **2001**, *114,* 8064- 8065.

98. Soper, A. K.; Benmore, C. *J. Phys. Rev. Lett*., **2008**, *101,* 065502(1-4).

99. Simpson, A. J.; Kingery, W. L.; Shaw, D. R.; Spraul, M.; Humpfer, E.; Dvortsak, P. *Environ. Sci. Technol*., **2001**, *35,* 3321-3325.

100. Finney, J. L.; Hallbrucker, A.; Kohl, I.; Soper, A. K.; Bowron, D. T. *Phys. Rev. Lett.*, **2002**, *88,* 225503(1-4).

101. Gardner, J. L.; Turner, S. M.; Bautista, A.; Lindwall, G.; Awada, M.; Hellerstein, M. K. *Am. J. Physiol. Gastrointest. Liver Physiol.* **2007**, *292,* 1695-1704.

102. Zeidler, A.; Salmon, P. S.; Fischer, H. E.; Neuefeind, J. C.; Simonson, J. M.; Lemmel, H.; Rauch, H.; . Markland, T. E. *Phys. Rev. Lett.*, **2011**, *107,* 145501.

103. Guzzi, R.; Arcangeli, C.; Bizzarri, A. R.; *Biophys. Chem*., **1999**, *82*, 9-12.

104. Mills, R. *J. Phys. Chem.,* **1973**, *77,* 685-688.

105. Vidulich, G. A.; Evans, D. F.; Kay, R. L. *J. Phys. Chem*. **1967**, *71*, 656-662.

106. Cioni, P.; Strambini, G. B. *Biophysics. J*., **2002**, *82*, 3246-3253.

107. Wu, Y.; Tepper, H. L.; Voth, G. A. *J. Chem. Phys.,* **2006**, *124*, 024503 (1-12).

108. Jorgenson, W. L.; Jenson, C. *J. Comput. Chem.,***1998**, *19,* 1179-1186.

109. Tanford, C. *J. Am. Chem. Soc*. **1962**, *84,* 4240−4247.

110. Kandasamy, S. K.; Larson, R. G. *Biophys. J.*, **2006**, *90*, 2326–2343.

111. Koishi, T.; Yasuoka, K.; Ebisuzaki, T.; Yoo, S.; Z. X. Cheng *J. Chem. Phys*., **2005**, *123,* 204707(1-7).

112. Pratt, R.; Pohorille, A. *Chem. Rev*., **2002**, *102*, 2671-2692.

113. Ashbaugh, H. S.; Pratt, L. R. *Rev. Mod. Phys*., **2006**, 78, 159-178.

114. Ben-Naim, *Hydrophobic Interactions,* (Plenum, New York, **1980**).

115. Werder, T.; Walther, J. H.; Jaffe, R. L.; Halicioglu, T.; Koumoutsakos, P. *J. Phys. Chem. B***, 2003,** *107*, 1345-1352.

116. Acharya, H.; Vembanur, S.; Jamadagni, S. N.; Garde, S. Faraday Discuss., **2010**, *146,* 353-365.

117. Godawat, R.; Jamadagni, S. N.; Garde, S. *Proc. Natl. Acad. Sci.U.S.A.*, **2009**, *106*, 15119-15124.

118. Ashbaugh, S.; Paulaitis, M. E. *J. Am. Chem. Soc.,* **2001**, *123*, 10721-10728.

119. Marcus, Y. *Pure Appl. Chem*., **2010**, *82*, 1889–1899.

120. Hribar, B.; Southall , N.; Vlachy , V.; Dill, K. A. *J. Am. Chem. Soc.,* **2002**, *124*, 12302–12311.

121. Nozaki, Y.; Tanford, C. *J. Biol. Chem.,***1963**, *238*, 4074–4081.

122. Brandts, J. F.; Hunt, L. *J. Am. Chem. Soc.,* **1967**, *89*, 4826.

123. Yancey, P. H.; Clark, M. E.; Hand, S. C.; Bowlus, R. D.; Somero, G. N. *Science,* **1982**, *217*, 1214−1222.

124. Alonso, D. O. V.; Dill, K. A. *Biochemistry,***1991**, *30*, 5974−5985.

125. Watlaufer, D. B.; Malik, S. K.; Stoller, L.; Coffin, R. L. *J. Am. Chem. Soc.,* **1964**, *86*, 508-514.

126. Tanford, C.; Kawahara, K.; Lapanje, S. *J. Biol. Chem.,***1966**, *241*, 1921−1923.

127. Hammes, G. G.; Schimmel, P. R. *J. Am. Chem. Soc*., **1967**, 89, 442–446.

128. Tanford, C.; Aune, K. C. *Biochemistry,* **1970**, *9*, 206−211.

129. Greene, R. F.; Pace, C. N. *J. Biol. Chem.,* **1974**, *249*, 5388−5394.

130. Pfeil, W.;Privalov, P. L. *Biophys. Chem*., **1976**, *4*, 33−40.

131. Makhatadze, G. I.; Privalov, P. L. *J. Mol. Biol.,* **1992**, *226*, 491−505.

132. Bennion, B.; Daggett, V. *Proc. Natl. Acad. Sci. U.S.A.,* **2003**, *100*, 5142−5147.

133. Vanzi, F.; Madan. B.; Sharp, K. *J. Am. Chem. Soc*., **1998**, *120*, 10748−10753

134. Hemmer, P. C.; Stell, G. *Phys. Rev. Lett*., **1970**, *24*, 1284-1287.

135. Jagla, E. A. *Phys. Rev. E,* **1998**, *58*, 1478-1486.

136. de Oliveira, A. B.; Netz, P. A.; Colla, T.; Barbosa, M. C. *Europhys. Lett*, **2009**, *85*, 36001(P1-P6).

137. Pant, S.; Gera, T.; Choudhury, N. *J. Chem. Phys*., **2013**, *139*, 244505 (1-9).

138. Ludwig, R. *Angew Chem. Int. Ed.,* **2001**, *40*, 1808-1827.

139. Angell, C. A.; Shuppert, J.; Tucker, J. C. *J. Phys. Chem.,* **1973**, *77*, 3092–3099.

140. Kell, G. S. *J. Chem. Eng. Data.,* **1975**, *20*, 97–105.

141. Saul, A.; Wagner, W. *J. Phys. Chem. Ref. Data.,* **1989**, *18*, 1537–1564.

142. Speedy, R. J.; Angell, C. A. *J. Chem. Phys.*, **1976**, *65*, 851–858.

143. Angell. C. A.; Bressel, R. D.; Hemmati. M.; Sare, E. J.; Tucker, J. C. *Phys. Chem. Chem. Phys.,* **2000**, *2*, 1559–1566.

144. Wernet, Ph.; Nordlund, D.; Bergmann, U.; Cavalleri, M.; Odelius, M.; Ogasawara, H.; Naslund, L. Å.; Hirsch, T. K.; Ojamae, L.; Glatzel, P.; Pettersson, L. G.; M. Nilsson, *Science*, **2004**, *304*, 995-999.

145. Smith, J. D.; Cappa, C. D.; Wilson, K. R.; Messer, B. M.; Cohen, R. C.; Saykally, R. J. *Science,* **2004**, *306*, 851-853.

146. Eaves, J. D.; Loparo, J. J.Fecko.; C. J. Roberts, S. T.; Tokmakoff, A.; Geissler, P. L. *Proc. Nat. Acad. Sci. USA,* **2005,** *102*, 13019–13022.

147. Smith, J. D.; Cappa, C. D.; Wilson, K. R.; Cohen, R. C.; Geissler, P. L.; Saykally, R. J. *Proc. Nat. Acad. Sci. USA* **2005,** *102*, 14171–14174.

148. Luzar, A.; Chandler,D. *Phys. Rev. Lett.,* **1996**, *76*, 928-931.

149. Head-Gordon,T.; Johnson, M. E. *Proc Natl. Acad. Sci. USA*., **2006**, *103*, 7973-7977.

150. Limmer, D. T.; Chandler D.*J. Chem. Phys.,* **2011,***135*, 134503(1-10).

151. Rocchi, C.; Bizzarri, A. R.; Cannistraro, S.; *Phys. Rev. E*, **1998**, *57*, 3315-3325.

152. Kumar, P.; Han, S.; Stanley, H. E. *J Phys-condens Mat.*, **2009**, *21*, 504108(1-9)

153. Dinga, Y. ; Hassanalia, A. A.; Parrinello, M. *Proc Natl. Acad.Sci.,* **2014**, *111*, 3310–3315.

154. Mallamace, F.; Corsaro, C.; Stanley, H. E. *Proc Natl. Acad.Sci.,* **2013**, *110*, 4899–4904.

155. Netza, P. A.; Starr, F.; Barbosac, M. C.; Stanley, H. E. *Braz. J. Phys.,* **2002**, *34*,24-31.

156. Van Der Spoel, D.; Lindahl, E.; Hess, B.; Groenhof, G.; Mark, A. E.; Berendsen, H. J. C. *J. Comput. Chem.***2005**, *26*, 1701−1718. Hess, B.; Kutzner, C.; van der Spoel, D.; Lindahl, E. *J. Chem. Theory Comput.,* **2008**, *4*, 435-447.

157. Huggins, D. J. *J. Chem. Phys.,* **2012,** *136*, 064518(1-13).

158. Gallo, P.; Sciortino, F.; Tartaglia, P.; Chen, S. H. *Phys. Rev. Lett.,* **1996**, *76,* 2730-2733.

159. Starr, F.W.; Sciortino, F.; Stanley, H. E., *Phys. Rev. E*, **1999**, *60*, 6757-6758.

160. Starr, F. W.; Harrington, S. T.; Sciortino, F.; Stanley, H. E., *Phys. Rev. Lett*., **1999**, *82*, 3629-3332.

161. Sciortino, F.; Geiger, A.; Stanley, H. E., *J. Chem. Phys*., **1992**, *96*, 3857-3865.

162. Baez, L. A.; Clancy, P. *J. Chem. Phys.,* **1994**, *101*, 9837-9840.

163. Harrington, S.; Poole, P. H.; Sciortino, F.; Stanley, H. E., *J. Chem. Phys*., **1997**, *107*, 7443-7450.

164. Sciortino, F.; Gallo, P.; Tartaglia, P. , Chen, S. H.;, *Phys. Rev. E*, **1996**, *54*, 6331-6346.

165. Chen, S. H.; Gallo, P.; Sciortino, F.; Tartaglia, P. , *Phys. Rev. E*, **1997**, *56*, 4231-4243.

166. Rami Reddy, M.; Berkovitz, M. *J. Chem. Phys*., **1987**, *87*, 6682-6686.

167. Sciortino, F.; Geiger, A.; Stanley, H. E., *Nature,* **1991**,*354*, 218-221.

168. Sciortino, F.; Fabbian, L.; Chen, S. H.; Tartaglia, P. *Phys. Rev. E*, **1997**, *56*, 5397-4504.

169. Scala, A.; Starr, F. W.; Nave, E. La.; Sciortino, F.; Stanley, H. E., *Nature,* **2000**, *406*, 166-169.

170. Netz, P. A.; Starr, F.W.; Stanley, H. E.; M.C. Barbosa, *J. Chem. Phys*, **2001**, *115*, 344-348.

171. Bagchi, K.; Balasubramanian, S.; Klein, M.L. *J. Chem. Phys*., **1997**, *107,* 8561-8567.

172. Jonas, J.; DeFrieas, T.; Wilbur, D.J. *J. Chem. Phys*., **1976**, *65*, 582-601.

173. Prielmeier, F.X.; Lang, E.W.; Speedy, R.J.; LOudemann, H.D. *Phys. Rev. Lett.,* **1987**, *59,*1128-1131.

174. Gruwald, E. *J. Am. Chem. Soc.,* **1986**, *108*, 5719-5726.

175. Geiger, A.; Mausbach, P.; Schnitker, J.; Neilson, G.W.; Enderby, J.E. *Water and Aqueous Solutions (*Adam Hilger, Briston, **1986**.)

176. Jorgenson, W. L.; Jenson, C. *J. Comput. Chem.,* **1998**, *19,* 1179-1186.

177. Svishchev, I. M.; Kusalik, P. G. *J. Chem. Phys***., 1993,** *99*, 3049-3058.

178. Poole, P. H.; Sciortino, F.; Grade, T.; Stanley, H. E.; Angell, C. A. *Phys. Rev. Lett*., **1994**, *73,* 1632-1635.

179. Tomberli, B.; Benmore, C. J.; Egelstaff, P. A.; Neuefeind, J.; Honkimaki, V. *J. Phys.: Condens. Matter.*, **2000**, *12,* 2597-2612.

180. Guillot, B.; Guissani, Y. *Fluid Phase equil.* **1998**, *150-151***,** 19-32.

181. Miller, T. F.; Manolopoulos, D. E. *J. Chem. Phys***.,** **2005**, *123,* 154504(1-10).

182. Paesani, F.; Voth, G. A. *J. Phys Chem***., 2008.** *112C*, 324-327.

183. Pena, L. H.; Kusalik, P. G. *J. Chem. Phys.,* **2006**, *125,* 054512(1-10).

184. Steinbach, P. J.; Brooks, B. R. *Proc. Natl. Acad. Sci. USA*., **1993**, *90*, 9135-9139.

185. Matubayasi, N. *J. Am. Chem. Soc*., **1994.** *116,* 1450-1456.

186. Shiga, M.; Shinoda, W. *J. Chem. Phys*., **2005**, *123,* 134502(1-7).

187. Herrero, C. P.; Ramirez, R. *J. Chem. Phys*., **2011**, *134,* 094510(1-10).

188. Noya, E. G.; Vega, C.; Sese, L. M.; Ramirez, R. J. *Chem. Phys*., **2009**, *131,* 124518 (1-5).

189. Habershon, S.; Markland, T. E.; Manolopoulo, D. E. *J. Chem. Phys***., 2009**, *131*, 24501(1-11).

190. Pena, L. H.; Kusalik, P. G. *J. Chem. Phys***., 2004,** *121*, 5992-6002.

191. Kuharski, R. A.; Rossky, P. J. *J. Chem. Phys.,* **1985,** *82*, 5164-5177.

192. Wallqvist, A.; Berne, B. *J. Chem. Phys. Lett*., **1985**, *117,* 214-219.

193. Paesani, F.; Zhang, W.; Case, D. A; Cheatham, T. E.; Voth, G. A. *J. Chem Phys*., **2006**, *125,* 184507(1-11).

194. Paesani, F.; Iuchi, S.; Voth, G. A.; *J. Chem. Phys***., 2007,** *127*, 074506(1-14).

195. Guillot, B.; Guissani, Y. *J. Chem. Phys.,* **1998,** *108***,** 10162-10174.

196. Lobaugh, J.; Voth, G. A. *J. Chem. Phys.*, **1997**, *106*, 24-34.

197. Smirnova, N. N.; Bykova, T. A.; Van Durme, K.; Van Mele, B. *J. Chem. Thermodynamics*., **2006**, *38,* 879–883.

198. Andersen, H. C. RATTLE: *J. Comput. Phys.,* **1983**, *52,* 24–34.

199. Svishchev, I. M.; Kusalik, P. G. *Phys. Rev. Lett*., **1994**, *73*, 975-979.

200. Liu, D.; Zhang, Y.; Chen, C. C.;   Mou, C. Y.; Poole, P. H.; Chen, S. H. *Proc. Natl. Acad. Sci. USA.,* **2007**, *104*, 9570-9574.

201. Chandra, A. *Phys. Rev. Lett*., **2000,** *85*, 768-771.

202. Dave, S. M.; Sadhukhan, H. K.; Novaro, O. A. *Heavy water: properties, production and analysis* (Quest, **1997**)

203. Vega, C.; Conde, M. M.; McBride, C.;. Abascal, J. L. F.; Noya, E. G.; Ramirez, R.; Sese, L. M. *J. Chem. Phys.,* **2010**, *132*, 046101(1-2)**.**

204. Crabtree, A.; Sman-Tov, M. *ORNL/TM-12322*. May-**1993**

205. Angell, C. A.; Ogunl, M.;. Slchlna, W. J. *J. Phys. Chem.,* **1982,** *86*, 998-1002.

206. Braibanti, A.; Fiscicaro, E.; Ghiozzi, A.; Compari, C. *Thermochim. Acta*., **1996.** *286*, 51-56.

207. Nakamura, M.; Tamura, K.; Murakami, S. *Thermochim. Acta.,* **1995**, *253*, 127-136.

208. Walser, R.; Mark, A. E.; van Gunsteren, W. F. *Biophys. J.,* **2000**, *78*, 2752-2760.

209. Motakabbir, K. A; Berkowitz**,** M**.** *J. Phys. Chem.,* **1990,** *94,* 8359-8362.

210. Millero F. J.; Lepple, F. K. *J. Chem. Phys.,* **1971**, *54*, 946-949.

211. Aragones, J. L.; MacDowell, L. G.; Vega, C. *J. Phys. Chem*., **2011,** *A115*, 5745-5758.

212. Smith, P. E.; vanGunstern, W. F. *J. Chem Phys*., **1994,** *100,* 3169-3174.

213. Choudhury, N. *J. Chem. Phys.,* **2006**, *125*, 034502(1-7).

214. Choudhury, N. *J. Phys. Chem.* C, **2007**, *111*, 2565-2572.

215. Choudhury, N. *J. Phys. Chem. B,* **2007**, *111*, 10474-10480.

216. Choudhury, N .*J. Chem. Phys.,* **2009**, *131*, 014507(1-8).

217. Schellman, J. A. *Biophys. Chem.,* **1990**, *37,* 121-140.

218. Bruning , W; Holtzer, A. *J. Am. Chem. Soc.,* **1961**, *83*, 4865–4866.

219. Schick, M. J. *J. Phys. Chem.,* **1964,** *68,* 3585–3592.

220. Kallies, B. *Phys. Chem. Chem.Phys.,* **2002**, *4*, 86−95.

221. Mountain, R. D.; Thirumalai, D. *J. Phys. Chem. B,* **2004**, *108*, 6826−6831.

222. Felitsky, D. J.; Record, M. T. *Biochemistry.,***2004**, *43*, 9276−9288.

223. Batchelor, J. D.; Olteanu, A.; Tripathy, A.; Pielak, G. J. *J. Am. Chem. Soc.,* **2004**, *126*, 1958−1961.

224. Zou, Q.; Habermann-Rottinghaus, S. M.; Murphy, K. P. *Proteins: Struct.;Funct. Genet.,* **1998**, *31*, 107−115.

225. Wallqvist, A.; Covell, D. G.; Thirumalai, D. *J. Am. Chem. Soc.,* **1998**, *120*, 427−428.

226. Felitsky, D. J.; Record, M. T. *Biochemistry,* **2003**, *42*, 2202−2217.
227. Tobi, D.; Elber, R.; Thirumalai, D. *Biopolymers,* **2003**, 68, 359−369.
228. Klimov, D. K.; Straub, J. E.; Thirumalai, D. *Proc. Natl. Acad. Sci. U.S.A.,* **2004**, *101,* 14760−14765.
229. O'Brien, E. P.; Dima, R. I.; Brooks, B.; Thirumalai, D. *J. Am. Chem. Soc.,* **2007**, *129,* 7346−7353.
230. Das, A.; Mukhopadhyay, C. *J. Phys. Chem. B,* **2008**, *112*, 7903−7908.
231. Hua, L.; Zhou, R.; Thirumalai, D.; Berne, B. J. *Proc. Natl. Acad. Sci. U.S.A.,* **2008**, *105,* 16928−16933.
232. Stumpe, M. C.; Grubmüller, H. *Biophys. J.,* **2009**, *96*, 3744− 3752.
233. Zangi, R.; Zhou, R.; Berne, B. J. *J. Am. Chem. Soc.,* **2009**, *131*, 1535−1541.
234. Canchi, D. R.; Paschek, D.; García, A. E. *J. Am. Chem. Soc.*, **2010**, *132*, 2338−2344.
235. Ma, L.; Pegram, L.; Record, M. T.; Cui, Q. *Biochemistry.,* **2010**, *49*, 1954−1962.
236. Berteotti, A.; Barducci, A.; Parrinello, M. *J. Am. Chem. Soc.,* **2011**, *133*, 17200−17206.
237. Guinn, E. J.; Pegram, L. M.; Capp, M. W.; Pollock, M. N.; Record, M. T. *Proc. Natl. Acad. Sci. U.S.A.,* **2011**, *108*, 16932−16937.
238. Zhou, R.; Li, J.; Hua, L.; Yang, Z.; Berne, B. J. *J. Phys. Chem. B,* **2011**, *115*, 1323−1326.
239. England, J. L.; Haran, G. *Annu. Rev. Phys. Chem.,* **2011**, *62*, 257−277.
240. Schellman, J. A. *Biopolymers,* **1975**, *14*, 999−1018.
241. Schellman, J. A. *Biopolymers,* **1987**, *26*, 549−559.
242. Muller, N. *J. Phys. Chem.,* **1990**, *94*, 3856−3859.
243. Graziano, G. *Phys. Chem. Chem. Phys.,* **2011**, *13*, 17689−17695.
244. Yang, Z.; Xiu, P.; Shi, B.; Hua, L.; Zhou, R. *J. Phys. Chem. B,* **2012**, *116*, 8856−8862.

245. Pazos, I. M.; Gai, F. *J. Phys. Chem. B*, **2012**, *116*, 12473−12478.
246. Canchi, D. R.; García, A. E. *Biophys. J.,* **2011**, *100*, 1526−1533.
247. Rezus, Y. L. A.; Bakker, H. J. *Proc. Natl. Acad. Sci. U.S.A.,* **2006**, *103*, 18417−18420.
248. Frank, H. S.; Franks, F. *J. Chem. Phys.,* **1968**, 48, 4746−4757.
249. Wei, H.; Fan, Y.; Gao, Y. Q. *J. Phys. Chem. B,* **2010**, *114*, 557−568.
250. Caballero-Herrera, A.; Nordstrand, K.; Berndt, K. D.; Nilsson, L. *Biophys. J.,* **2005**, *89*, 842−857.
251. Das, A.; Mukhopadhyay, C. *J. Phys. Chem. B,* **2009**, *113*, 12816−12824.
252. Guo, F.; Friedman, J. M. *J. Phys. Chem. B,* **2009**, *113*, 16632−16642.
253. Zhang, Y.; Cremer, P. S. *Annu. Rev. Phys. Chem.,* **2010,** *61*, 63−83.
254. Kokubo, H.; Roesgen, J.; Bolen, D. W.; Pettitt, B. M. *Biophys. J.*, **2007**, *93*, 3392−3407. Kokubo, H; Pettitt B. M. *J. Phys. Chem. B.,* **2007**, *111*, 5233-5242.
255. Shimizu, A.; Fumino, K.; Yukiyasu, K.; Taniguchi, Y. *J. Mol. Liq.,* **2000**, *85*, 269−278.
256. Funkner, S.; Havenith, M.; Schwaab, G. *J. Phys. Chem. B,* **2012**, *116*, 13374−13380.
257. Sharp, K. A.; Madan, B.; Manas, E.; Vanderkooi, J. M. *J. Chem. Phys.,* **2001**, *114,* 1791−1796.
258. Sharp, K. A.; Vanderkooi, J. M. Water *Acc. Chem. Res*., **2010**, *43*, 231−239.
259. Kuffel, A.; Zielkiewicz, J. *J. Chem. Phys.,* **2010**, *133*, 035102(1-8).
260. Soper, A. K.; Teixeira, J.; Head-Gordon, T. *Proc. Natl. Acad. Sci. U.S.A.,* **2010**, *107*, E44-1.
261. Walrafen, G. E. *J. Chem. Phys.,* **1966,** *44*, 3726-3727**.**
262. Sacco, A.; Holz, M. *J. Chem. Soc.; Faraday Trans.,* **1997**, *93*, 1101-1104.
263. Chen, X.; Sagle, L. B.; Cremer, P. S. *J. Am. Chem. Soc.,* **2007**, *129,* 15104–15105.
264. Soper, A. K.; Castner, E.W.; Luzar, A. *Biophysical Chemistry,* **2003**, *105,* 649–666.

265. Hayashi, Y.; Katsumoto, Y.; Omori, S.; Kishii, N.; Yasuda, A. *J. Phys. Chem. B,* **2007,** *111,* 1076-1080.
266. Carr, J. K.; Buchanan, L. E.; Schmidt, J. R.; Zanni, M. T.; Skinner, J. L. *J. Phys. Chem. B,* **2013,** *117*, 13291–13300.
267. Tsai, J.; Gerstein, M.; Levitt, M. *J. Chem. Phys.,* **1996,** *104*, 9417-9430.
268. Berkowitz, M. L.; Vaisman, I. I. *J. Am. Chem. Soc.,* **1992**, *114*, 7889–7896.
269. Aastrand, P.-O.; Wallqvist, A.; Karlstroem, G. *J. Phys. Chem.,* **1994**, *98*, 8224–8233.
270. Weerasinghe, S.; Smith, P. E. *J. Phys. Chem. B,* **2003**, *107*, 3891–3898.
271. Mehrotra P. K.; Beveridge, D. *J. Am. Chem. Soc.,* **1980**, *102*, 4287-4294.
272. Kuharski, R. A.; Rossky, P. J. *J. Am. Chem. Soc.,* **1984**, *106*, 5786-5793.
273. Almarza, J.; Rincon, L.; Bahsas, A.; Brito, F. *Biochemistry,* **2009**, *48*, 7608–7613.
274. Stumpe, M. C.; Grubmuller, H. *J. Phys. Chem. B,* **2007**, *111*, 6220-6228.
275. Chitra, R.; Smith, P. E. *J. Phys. Chem. B,* **2002**, *106*, 1491-1500.
276. Yamazaki, T.; Kovalenko, A.; Murashov, V. V. ; Patey, G. N. *J. Phys. Chem. B*, **2010**, *114*, 613–619.
277. Idrissi, A.; Gerard, M.; Damay, P.; Kiselev M.; Puhovsky, Y.; Cinar, E.; Lagant, P.; Vergoten, G. *J. Phys. Chem. B,* **2010**, *114*, 4731–4738.
278. Essmann, U.; Perera, L.; Berkowitz, M. L.; Darden, T.; Lee, H.; Pedersen, L. G. *J. Chem. Phys.*, **1995**, *103*, 8577–8592.
279. Pearlman, D. A.; Case, D. A.; Caldwell, J. W.; Ross, W. S.; Cheatham III, T. E.; DeBolt, Steve; Ferguson, D.; Seibel, G.; Kollman, P. *Comput. Phys. Commun.,* **1995**, *91*, 1-41.
280. Sokoli, F.; Idrissi, A.; Perera, A. *J. Chem. Phys.,* **2002**, *116*, 1636-1646.

281. Sarma, R; Paul, S. *J. Phys. Chem*. B, **2013**, *117*, 9056–9066.

282. Horinek, D; Netz, R. R. *J. Phys. Chem.* A, **2011**, *115*, 6125–6136.

283. Booth, J.; Abbott, S.; Shimizu, S. *J. Phys. Chem. B*, **2012**, *116*, 14915−14921.

284. Choudhury, N. *J. Chem. Phys.,* **2010**, *132*, 064505 (1-5).

285. Guinn, E. J. et al. *J. Am. Chem. Soc.,* **2013**, *135*, 5828−5838.

286. Priyakumar, U. D.; Hyeon, C.; Thirumalai, D.; MacKerell, A. D. Jr. *J. Am. Chem. Soc.,* **2009**, *131*, 17759–17761.

287. Tsumoto, K.; Umetsu, M.; Kumagai, I.; Ejima, D.; Philo, J. S.; Arakawa, T.*Biotechnol. Prog.,* **2004**, *20*, 1301-1308.

288. Arakawa, T.; Tsumoto, K. *Biochemical and Biophysical Research Communications*, **2003**, *304*, 148–152.

289. Reddy, R. C.; Lilie, K. H.; Rudolph, R.; Lange, C. *Protein Science*, **2005**, *14*, 929–935.

290. Pednekar, D.; Tendulkar, A.; Durani, S. *Proteins,* **2009,** *74*, 155-163.

291. Kameda, A. T.; Arakawa, T.; Shiraki, K. *J. Phys. Chem. B,* **2010**, *114,* 13455–13462.

292. Arakawa, T.; Ejima, D.; Tsumoto, K.; Obeyama, N.; Tanaka, Y.; Kita, Y.; Timasheff, S. N. *Biophy. Chem.,* **2007**, *127*, 1–8.

293. Bogan, A. A.; Thorn,K. S. *J. Mol. Biol.,* **1998**, *280*, 1-9.

294. Boudon, S.; Wipff, G.; Maigret, B. *J. Phys. Chem.,* **1990**, *94*, 6056-6061.

295. Vazdar, M.; Vymetal, J.; Heyda, J.; Vondrasek, J.; Jungwirth, P. *J. Phys. Chem. A,* **2011**, *115,* 11193-11201.

296. Soetens, J. C.; Millot, C.; Chipot, C.; Jansen, G.; Ángyán, J. G.; Maigret, B. *J. Phys. Chem. B,* **1997**, *101*, 10910-10917.

297. Vazdar, M.; Uhlig, F.; Jungwirth, P. *J. Phys. Chem. Lett.,* **2012**, *3,* 2021-2024.

298. Shih, O.; England, A. H.; Dallinger, G. C.; Smith, J. W.; Duffey, K. C.; Cohen, R. C.; Prendergast, D.; Saykally, R. J. *J. Chem. Phys.*, **2013**, *139*, 035104-1 - 035104-7.
299. Kubickova, A.; Krizek, T.; Coufal, P.; Wernersson, E.; Heyda, J.; Jungwirth, P. *J. Phys. Chem. Lett.*, **2011**, *2*, 1387- 1389.
300. Wernersson, E.; Heyda, J.; Vazdar, M.; Lund, M.; Mason, P. E.; Jungwirth, P. *J. Phys. Chem. B*, **2011**, *115*, 12521–12526.
301. Shortle, D.; Chan, H. S.; Dill, K. A. *Protein Sci.*, **1992**, *1*, 201-215.
302. Ohtaki, H.; Radnai, T. *Chem. Re*v., **1993**, *93*, 1157-1204.
303. Soper, A. K.; Luzar, A. *J. Phys. Chem.*, **1996**, *100*, 1357-1367.
304. Akhtar, Md. S.; Ahmad, A.; Bhakuni, V. *Biochemistry*, **2002,** *41*, 3819-3827.
305. Kuharski, R. A.; Rossky, P. J. *J. Am. Chem. Soc.*, **1984**, *106*, 5794-5800.
306. Godawat, R.; Jamadagni, S. N.; Garde, S. *J. Phys. Chem. B*, **2010**, *114*, 2246-2254.
307. Mandal, M.; Mukhopadhyay, C. *Phys. Rev. E***2013,** *88*, 052708-1-052708-10.
308. Lim, W. K.; Jorgrosgen, S.; Englander, W. *Proc. Natl. Acad. Sci. U.S.A.***2009**, *101*, 2595–2600.
309. Mason, P. E.; Neilson, G. W.; Dempsey, C. E.; Barnes, A. C.; Cruickshank, J. M. *Proc. Natl. Acad. Sci. USA*, **2003**, *100*, 4557-4561.
310. Mason, P. E.; Neilson, G. W.; Enderby, J. E.; Saboungi, M. L.; Dempsey, C. E.; MacKerell, A. D.; Brady, J. W. *J. Am. Chem. Soc.*, **2004**, *126*, 11462-11470.
311. Casu, F.; Duggan, B. M.; Hennig, M. *Biophys. J.*, **2013**, *105*, 1004-1017.
312. Flocco, M. M.; Mowbray, S. L. *J. Mol. Biol.*, **1994**, *235*, 709-717.
313. Mitchell, J. B. O.; Nandi, C. L.; McDonald, I. K.; Thornton, J. M.; Price, S. L. *J. Mol. Biol.*, **1994**, *239*, 315-331.

314. Tanford, C. *The Hydrophobic Effect: Formation of Micelles and Biological Membranes* (Wiley, New York, **1973**).
315. Kauzmann, W. *Adv. Protein Chem*., **1959**, *14*, 1-63.
316. Granick, S.; Bae, S. C. *Science*, **2008**, *322*, 1477-1478.
317. Choudhury, N.; Pettitt, B. M, *J. Am. Chem. Soc*., **2007**, *129*, 4847-4852.
318. Huang, X.; Margulis, C. J.; Berne, B. J. *Proc. Natl. Acad. Sci. U.S.A*., **2003,** *100*, 11953-11958.
319. Choudhury, N.; Pettitt, B., in *Modelling Molecular Structure and Reactivity in Biological Systems* (RSC Publishing, **2006**), *31*, 49–57.
320. Liu, P.; Huang, X.; Zhou, R.; Berne, B. J, *Nature (London)*, **2005**, *437*, 159-162.
321. Pratt, L.R.; Chandler, D. C. *J. Chem. Phys*., **1977**, ***67***, 3683-3704.
322. Pangali, C.; Rao, M.; Berne, B. J. *J. Chem. Phys*., **1979**, *71*, 2975-2985.
323. Smith, D. E.; Haymet, A. D. J. *J. Chem. Phys*., **1993**, *98*, 6445-6454.
324. Hummer, G.; Garde, S.; Garcia, A. E. ; Pohorille, A.; Pratt, L.R, *Proc. Natl. Acad. Sci. U.S.A*., **1996,** *93*, 8951 -8955.
325. Southall, N. T.; Dill, K.A. *Biophys. Chem*., **2002**, *101*, 295-307.
326. Guillot, B.A.; Guissani, Y.A. *J. Chem. Phys*., **1993**, *99*, 8075-8094.
327. Garde, S.; Garcia, A. E.; Pratt, L.R, Hummer, G. *Biophys. Chem*., **1999**, *78*, 21-32.
328. Hummer, G.; Garde, S.; Garcia, A. E.; M. E. Paulaitis.; Pratt, L.R , *Proc.Natl. Acad. Sci. U.S.A.* , **1998**, *95*, 1552-1555.
329. Smith, P.E.; *J. Phys. Chem. B***, 1999,** *103*, 525-534.
330. Kalra, A.; Tugcu, N.; Cramer, S. M.; Garde, S. *J. Phys. Chem. B* **, 2001,** *105*,6380 -6386.
331. Choudhury, N, *J. Chem. Eng. Data***, 2009,** *54*, 542-547.

332. Stillinger, F. H.; *J. Solution Chem.*, **1973**, *2*, 141-158.

333. Lum, K.; Chandler, D.; Weeks, J. D. *J. Phys. Chem. B,* **1999***, 103*, 4570-4577.

334. Mittal, J.; Hummer, G.; *Proc. Natl. Acad. Sci. U.S.A.*, **2008**, *105*, 20130-20135.

335. Truskett, T. M. ; Debenedetti, P. G.; Torquato, S.; *J. Chem. Phys*., **2001**, *114*,2401-2418.

336. Wallqvist, A.; Berne, B. J, *J. Phys. Chem.,* **1995***, 99*, 2893-2899.

337. Hummer, G.; Rasaiah, J. C.; Noworyta, J. P. *Nature (London),* **2001***, 414*, 188-190.

338. Ashbaugh, H. S.; Pratt, L.R.; Paulaitis, M. E.; Clohecy, J.; Beck, T.L. *J. Am. Chem. Soc*., **2005**, *127*, 2808-2809.

339. Choudhury, N.; Pettitt, B. M. *J. Phys. Chem*., **2006,** *110*, 8459-8463.

340. Choudhury, N.; *J. Chem. Phys*., **2005**, *125*, 034502(1-7).

341. Hotta, T.; Kimura, A.; Sasai, M. *J. Phys. Chem. B.,* **2005,** *109*, 18600-18608.

342. Choudhury, N.; *J. Chem. Phys*., **2010**, *133*, 154515 (1-8).

343. Hua, L.; Huang, X.; Liu, P.; Zhou, R.; Berne, B. J, *J. Phys. Chem. B,* **2007***, 111,* 9069-9077

344. Li, X.; Li, J.; Eleftheriou, M.; Zhou, R. *J. Am. Chem. Soc*., **2006**, *128*, 12439-12447.

345. Li, J.; Liu, T.; Li, X.; Ye, L.; Chen, H.; Fang, H.; Wu, Z.; Zhou, R. *J. Phys. Chem. B*, **2005**, *109*, 13639-13648.

346. Rajamani, S.; Truskett, T. M. ; Garde, S.; *Proc. Natl. Acad. Sci. U.S.A.*, **2005**, *102*, 9475-9480.

347. Zhou, R.; Huang, X,; C. J. Margulis, and Berne, B. J, *Science*, **2004**, *305*, 1605-1609.

348. Sarupria, S.; Garde, S. *Phys. Rev. Lett*., **2009**, *103*, 037803(1-4) .

349. Jamadagni, S. N.; Godawat, R.; Garde, S. *Ann. Rev. Chem. Biomol. Eng*., **2011**, *2*, 147-171.

350. Giovambattsta, N.; Lopez, C. F.; Rossky, P. J.; Debenedetti, P. G. *Proc. Natl. Acad. Sci. U.S.A.*, **2008**, *105*, 2274-2279 .
351. Giovambattsta, N.; Debenedetti, P. G.; Rossky, P. J. *Proc. Natl. Acad. Sci. U.S.A.*, **2009**, *106*, 15181-15185 .
352. Levy, Y.; Onuchic, J. N. *Annu. Rev. Biophys. Biomol. Struct.*, **2006**, *35*, 389-415.
353. Christenson, H. K.; Claesson, P. M. *Science*, **1988**, *239*, 390-392.
354. Christenson, H. K. in *Modern Approaches to Wettability: Theory and Applications*, edited by M. E. Schrader and G. Loeb (Plenum, New York, **1992**).
355. Pashley, R. M.; McGuiggan, P. M.; Ninham, B.W.; Evans, D. F. *Science*, **1985**, *229*, 1088–1089.
356. Patel, A. J.; Varilly, P.; Chandler, D. *J. Phys. Chem. B*, **2010**, *114*, 1632-1637.
357. Patel, A. J.;, Varilly, P.; Jamadagni, S. N.; Hagen, M.; Chandler, D.; Garde, S. *J. Phys. Chem. B***, 2012,** *116*, 2498-2503.
358. Jorgensen, H. J. C.; Madura, J. D.; Swenson, C. J.; *J. Am. Chem. Soc*., **1984**, *106*, 6638-6646.
359. Garde, S. private communication (**2011**).
360. Athawale, M. V.; Jamadagni, S. N.; Garde, S. *J. Chem. Phys*., **2009**, *131*, 115102(1-9) .
361. Patel, H. A.; Nauman, E. B.; Garde, S. *J. Chem. Phys.*, **2003,** *119*, 9199-9206.
362. Chau, P.L.; Hardwick, A. J. *Mol. Phys*., **1998**, *93*, 511-518.
363. Dai, H.; Hafner, J. H.; Rinzler, A. G.; Colbert, D. T.; Smalley, R. E. *Nature*, **1998,** *384,* 147–150.
364. Dresselhaus M. S.; Dresselhaus, G.; Eklund, P.C. *Science of Fullerenes and Carbon Nanotubes* (Academic, New York, **1996**).

365. Wong, E.W.; Harper, J.D.; Lansbury, P.T.; Lieber, C.M. *J Am Chem. Soc.*, **1998**, *120*, 603–604.
366. Wilson, L. J; Cagle, D. W.; Thrash, T. P.; Kennel, S. J.; Mirzadeh, S.; Alford, J.M.; Ehrhardt, G.J. *Coord.* Chem. Rev., **1999**, *146*, 190 – 192, 199–207.
367. Murthy, C.N.; Geckeler, K.E. *Chem Commun*, **2001**, *13*, 1194–1195.
368. Tagmatarchis, N.; Shinohara, H. *Mini Rev Med Chem*, **2001**, *1*, 339–348.
369. Ōsawa E. *Perspectives of Fullerene Nanotechnology* (Kluwer, Dordrecht,The Netherlands, **2002**).
370. Nakamura, E.; Isobe, H. *Acc. Chem. Res.*, **2003**, *36*, 807–814.
371. Szymańska, I.; Radecka, H.; Radecki, J.; Kikut-Ligaj, D. *Biosens Bioelectron*, **2001**, *16*, 911–915.
372. Da Ros, T.; Spalluto, G.; Prato, M. *Croat. Chem. Acta*., **2001**, *74*, 743–755.
373. Noon, W. H.; Kong, Y.; Ma, J. *Proc. Natl. Acad. Sci. U.S.A.*, **2002**, *99*, 6466-6470.
374. Friedman, S. H.; Decamp, D. L.; Sijbesma, R. P.; Srdanov, G.; Wudl, F.; Kenyon, G. L. *J.Am. Chem. Soc.*, **1993**, *115*, 6506-6509.
375. Tokuyama, H.; Yamago, S.; Nakamura, E.; Shiraki, T.; Sugiura, Y. *J. Am. Chem. Soc.*, **1993**, *115*, 7918-7919.
376. Minakata, S.; Tsuruoka, R.; Komatsu, M. *J. Am. Chem. Soc.*, **2008**, *130*, 1536-1537.
377. Innocenzi, P.; Brusatin, G. *Chem. Mater.*, **2001**, *13*, 3126-3139.
378. Voityuk, A. A.; Duran, M. *J. Phys. Chem. C*, **2008,** *112*, 1672-1678.
379. Bond, A. M.; Miao, W.; Raston, C. L.; Ness, T. J.; Barnes, M. J.; Atwood, J. L. *J. Phys. Chem. B*, **2001**, *105*, 1687-1695.
380. Lum, K.; Chandler, D.; Weeks, J. D. *J. Phys. Chem. B*, **1999**, *103*, 4570-4577,

381. Pratt, L. R.; Pohorille, A. *Chem. Rev*., **2002**, *102*, 2671-2692.

382. Ball, P. *Nature London*, **2003**, *423*, 25-26.

383. Pratt, L. R. *Rev. Mod. Phys*., **2006**, *78*, 159-178.

384. Huang, D. M.; Chandler, D. *J. Phys. Chem. B,* **2002***, 106*, 2047-2053.

385. Huang, D. M.; Chandler, D., *Proc. Natl. Acad. Sci. U.S.A.*, **2000**, *97*, 8324-8337.

386. Palmer, J. C.; Martelli, F. ; Liu, Y.; Car, R.; Panagiotopoulos, A. Z. ; Debenedetti, P. G. *Nature*, **2014**, *510*, 385–388.

387. Sellberg, J. A. et al. *Nature*, 2014, *510*, 381–384.

388. Angell, C. A. *Nature Mat.,* **2014***, 13*, 673-675.

389. Jagla, E. A. *J. Chem. Phys.,* ***1999****, 111*, 8980-8986.

390. Jagla, E. A., *Phys. Rev. E,* **2001**, *63*, 061501(1-7).

391. de Oliveira, A. B.; Netz, P. A.; Colla, T.; Barbosa, M. C. *J. Chem. Phys.,***2006**, *125*, 124503 (1-7).

392. Krott, L. B.; Barbosa, M. C. *J. Chem. Phys.,* **2013***, 138*, 084505 (1-12).

393. Bordin, J. R.; de Oliveira, A. B.; Diehl, A.; Barbosa, M. C. *J. Chem. Phys.,* **2012**, *137*, 084504 (1-5).

394. Girifalco, L. A. *J. Phys. Chem.,* **1992**, *96*, 858-861.

395. Slater, B.; Quigley, D. *Nature Mat.,* **2014,** *13***,** 670-671.

396. Soper, A. K. *Nature Mat.,* **2014,** *13***,** 671-673.